ABSTRACT

GALVIN, CASEY JAMES. Copolymer Synthesis and Characterization by Post-Polymerization Modification. (Under the direction of Dr. Jan Genzer).

This PhD thesis examines the physical behavior of surface-grafted polymer assemblies (SGPAs) derived from post-polymerization modification (PPM) reactions in aqueous and vapor enriched environments, and offers an alternative method of creating SGPAs using a PPM approach. SGPAs comprise typically polymer chains grafted covalently to solid substrates. These assemblies show promise in a number of applications and technologies due to the stability imparted by the covalent graft and ability to modify interfacial properties and stability. SGPAs also offer a set of rich physics to explore in fundamental investigations as a result of confining macromolecules to a solid substrate. PPM reactions (also called polymer analogous reactions) apply small molecule organic chemistry reactions to the repeat units of polymer chains in order to generate new chemistries. By applying a PPM strategy to SGPAs, a wide variety of functional groups can be introduced into a small number of well-studied and well-behaved model polymer systems. This approach offers the advantage of holding constant other properties of the SGPA (*e.g.*, molecular weight, MW, and grafting density, σ) to isolate the effect of chemistry on physical behavior.

Using a combination of PPM and fabrication methods that facilitate the formation of SPGAs with position-dependent gradual variation of σ on flat impenetrable substrate, the influence of polymer chemistry and σ is examined on the stability of weak polyelectrolyte brushes in aqueous environments at different pH levels. Degrafting of polymer chains in SGPAs exhibits a complex dependence on side chain chemistry, σ, pH and the charge fraction (α) within the brush. Results of these experiments support a proposed mechanism of degrafting, wherein extension of the grafted chains away from the substrate generates tension along the polymer backbone, which activates the grafting chemistry for hydrolysis. The implications of these findings are important in developing technologies that use SGPAs in aqueous environments, and point to a need for potential alternative grafting chemistries.

The behavior of SGPAs in vapor environments remains an underexplored phenomenon. By changing systematically the chemistry of SGPAs derived from a parent sample, the influence of side chain functional groups on the swelling of weak and strong polyelectrolyte brushes in the presence of water, methanol and ethanol vapors is explored. The extent of swelling and solvent uptake depends strongly on the chemistry in the polymer side chain and of the solvent. Despite bearing a permanent electrostatic charge in the side chain, the strong polyelectrolyte brushes exhibit no behavior typical of

polyelectrolytes in water due to no dissociation of the counterion. Of particular interest is the behavior in humid environments of an SGPA bearing a zwitterionic group in its side chain, which results in exposure of electrostatic charges without counterions. Using substrates bearing the aforementioned σ gradient of polymeric grafts, evidence of inter- and intramolecular complex formation is presented.

Finally, a method of developing SGPAs by polymerizing bulk polymer chains through surface-grafted monomers (SGMs) is described. The SGMs are incorporated onto a solid substrate using the same PPM reaction employed in the degrafting and vapor swelling experiments, highlighting the versatility of PPM. The thickness of these SGPAs is correlated to the bulk polymer chains MW, suggesting this technique can be used in existing industrial bulk polymerization processes.

Copolymer Synthesis and Characterization by Post-Polymerization Modification

by
Casey James Galvin

A dissertation submitted to the Graduate Faculty of
North Carolina State University
in partial fulfillment of the
requirements for the degree of
Doctor of Philosophy

Chemical Engineering

Raleigh, North Carolina

2014

APPROVED BY:

_____	_____
Dr. Jan Genzer Committee Chair	Dr. Orlin Velev
_____	_____
Dr. Alan Tonelli	Dr. Michael Dickey

DEDICATION

To those who have struggled, will struggle and are struggling with the challenges of life, which at some point includes us all.

BIOGRAPHY

Casey J. Galvin hails from Milwaukee, WI, and attended Marquette University High School. He graduated with a degree in Chemical Engineering from Northwestern University in Evanston, IL in 2007. While there, he worked with Prof. Randy Snurr and then-postdoc Dr. David Dubbeldam conducting molecular simulations of alkane adsorption in zeolites.

Following undergraduate studies, CJG enrolled in the graduate program of the Department of Chemical & Biomolecular Engineering at North Carolina State University, Raleigh, NC. He joined the group of Prof. Jan Genzer and has worked on projects related to the behavior of polymer chains grafted to solid interfaces that incorporate elements of chemistry and physics.

During his tenure in the Genzer group, he received an NSF EAPSI Fellowship to work with Prof. Taihyun Chang at POSTECH in South Korea, and has worked as a visiting researcher with Prof. Kookheon Char at Seoul National University in South Korea, and Dr. Jiři Šrogl at the Institute of Organic Chemistry and Biochemistry in Prague. CJG also collaborated with Prof. Svetlana Santer from the University of Potsdam during her sabbatical at NCSU.

In addition to his research, CJG served as President of the Chemical & Biomolecular Engineering Graduate Student Association and departmental Recruiting Captain. Outside of the lab (and sometimes in it), he enjoys making music, studying languages and practicing martial arts.

ACKNOWLEDGEMENTS

The person most responsible for this PhD Thesis is my partner, Lauren Dembeck, who has provided significant professional and personal support since our fairytale meeting. She heard the hypotheses and results contained in this document before anyone else, and continues to provide constructive questions, comments and looks of confusion when I am not making any sense.

I am grateful to my advisor, Jan Genzer, for letting me do a second PhD, which starts roughly at Chapter 4. You also provided my first international exposure, resulting in a fundamental shift in my world outlook and life's pursuits. Those experiences will remain relevant long after this work has faded into scientific obscurity.

The Genzer group itself has been integral to the work contained in this thesis. I must give special thanks to Drs. Young Kuk Jhon and Evren Özçam, who provided an early introduction and on-going training in scientific research. To the rest of the Genzer group alumni, current members and visitors, I extend a thank you for listening to my GM presentations, being flexible about instrument schedules and generally making day-to-day life in the lab enjoyable.

I have enjoyed a number of collaborative efforts during my PhD tenure. I had the distinct pleasure of working with Prof. Svetlana Santer during her sabbatical at NCSU. I want to acknowledge also my collaboration with Dr. Mike Dimitriou, a one-time NIST post-doc, who performed the neutron and X-ray reflectivity measurements in Chapter 4. I am similarly appreciative to Prof. J-P Maria and his students Edward Sachet and Chris Shelton for facilitating AFM measurements in Chapters 3 and 6.

Finally, as suggested above, I gained my first significant exposure to the rest of the world during my PhD. That could not have happened without Prof. Kookheon Char, Prof. Taihyun Chang and Dr. Jiři Šrogl. Likewise, I would have never discovered aspects of local culture without Drs. Hyoseon Suh, Younghyun Cho, Jinkee Hong, Adam Henke and Jakub Hyvl. I am especially indebted to Jinkee for his assistance after a missed flight out of South Korea. Finally, without pre-departure lessons in Korean from Ms. So Shin Park

TABLE OF CONTENTS

LIST OF TABLES

LIST OF FIGURES

1. Introduction and Dissertation Scope

1.1 Introduction

The behavior of surface-grafted polymer assemblies (SGPAs) has attracted significant research interest over the past two decades due to the rich physics and practical applications these systems offer[1]. These systems comprise typically polymer chains grafted to a solid substrate at one of their ends via a covalent bond. This covalent grafting leads to stable films with thicknesses ranging from a few nanometers to several hundred nanometers, depending on the method of preparation. These coatings change substantially the surface properties of the substrate, such as wettability, surface charge or elastic modulus, among others. Given this ability to tune physico-chemical properties of surfaces to which they are attached, SGPAs hold promise as a platform nanotechnology in numerous applications[2], ranging from biocidal and anti-microbial coatings[3] to chromatography[4] and separation technologies[5] to sensing and detection[6], among others.

Two approaches are generally employed to generate end-tethered SGPAs[7]. The first approach, termed "grafting to", tethers polymer chains to a substrate by one end or a segment of the polymer chain. The second approach, which is the method used extensively in this PhD Thesis, is termed "grafting from". The "grafting from" technique produces substrate-grafted polymer chains by growing the polymers directly from substrate-anchored initiating centers. To achieve this feat, an initiator molecule is first deposited onto the substrate surface, and such an initiator-modified substrate is incubated in a polymerization solution containing monomer and any necessary catalysts or other chemical agents. The surface-grafted initiator generates a polymer chain, which grows through addition of monomer in solution. SGPAs produced by "grafting from" possess typically higher grafting densities (σ) than SGPAs created by "grafting to"[1,7]. While the "grafting from" method alleviates some drawbacks of the "grafting to" technique, most notably the rather low grafting density (σ), the former method makes determination of the molecular weight (MW) and MW distribution very challenging.

The invention of controlled radical polymerization (CRP) techniques in the late 1990's brought SGPAs into a new era of understanding. The two most common of these schemes, atom-transfer radical polymerization (ATRP)[8] and reversible addition-fragmentation transfer (RAFT) polymerization[9], enabled the creation of well-defined SGPAs with relatively narrow MW distributions. The living nature of these techniques allowed for the creation of complex polymer-graft architectures, such as diblock and multiblock copolymers[10,11] and gradients in MW and grafting density (*i.e.*, chains per unit area; σ)[12–14]. These approaches were used to demonstrate the complex

behavior of SGPAs, such as the dependence of brush thickness on σ and MW and their mutual interplay.

Unfortunately, not all monomers are compatible with these CRP techniques. In the case of ATRP, which traditionally requires the use of copper salt catalysts, acidic and basic monomers can interfere with the catalyst-ligand complex. RAFT uses elevated temperatures that can degrade temperature sensitive materials. Furthermore, monomers that are particularly bulky, such as those bearing peptide-moieties, may not polymerize well due to steric hindrance. Moreover, some monomers exhibit detrimental side reactions during polymerization. A common example is the transesterification of functional groups in monomer side chains, such as those of 2-hydroxyethyl methacrylate (HEMA), which leads to chemical crosslinking of the polymer chains[15]. These and other issues apply not only to bulk polymerization, but to polymerization from solid substrates as well.

One approach to alleviating issues associated with preparing specialty polymer grafts is the application of post-polymerization modification (PPM) strategies in creating SGPAs[2,16]. This technique is also called polymer-analogous reaction in the literature, and uses small molecule organic chemistry reactions to transform chemically the repeat units of polymer chains into the desired structure. Chapter 2 of this PhD Thesis offers a detailed introduction to PPM and a review of the practical uses that SGPAs derived from PPM strategies have found. The merits of PPM are highlighted, particularly in comparison to synthesizing and characterizing new monomers. Several examples of different starting polymers and subsequent chemical reactions are discussed in the context of their applications. This section also introduces the primary reactions employed in subsequent chapters, such as quaternization and betainization.

While tremendous advancements have been achieved over the past two decades in understanding the physics of SGPAs, several fundamental questions related to the behavior of these systems remain open and relevant, especially as these systems find use outside of the polymer science community. This PhD Thesis articulates a selection of such questions, and attempts to provide answers using SGPAs derived from PPM strategies. Some questions include: How the stability of SGPAs is affected by the interplay of environmental conditions, system architecture (*e.g.*, MW and σ) and chemistry present in the polymer chains? How do SGPAs behave when exposed to solvent vapors? How does side chain chemistry influence this behavior? What avenues are available to create SGPAs using existing industrial infrastructure, such as systems capable of executing bulk, free radical polymerizations? These questions cover a wide breadth, and are tied together by the use of

the versatile monomer 2-(dimethylamino)ethyl methacrylate (DMAEMA) and the PPM reactions available to the tertiary amine present in DMAEMA's side chain.

Chapter 3 of this Ph.D. Thesis examines the role of mechanical forces generated in SGPAs in the mechanism of degrafting chains from a solid substrate. Based on a mechanism proposed in prior work[17], degrafting occurs when tension generated along a grafted chain backbone focuses on the grafting point of the chain. This focusing activates the chemistry at the polymer/substrate interface for hydrolysis by hydroxyl ions in solution. In these experiments, the tension needed for activation can originate either from electrostatic repulsion due to charging within the brush, or extension of the grafted chains away from the substrate due to crowding from neighboring chains (*i.e.*, high grafting density) or the combination of both effects. In this regard, degrafting itself represents a new example of PPM that employs elements of mechano-chemistry. Using polyanionic and polycationic brushes that express a gradient in σ, the interplay between electrostatic repulsion and σ is examined and the effect of this interplay on degrafting illustrated.

Chapter 4 examines a series of polyelectrolyte brushes created using a post-polymerization modification (PPM) strategy exposed to humid environments in order to elucidate the influence of side-chain chemistry on the swelling behavior of the brushes. Starting from a weak polycation bearing a side-chain tertiary amine, *i.e.*, polyDMAEMA (PDMAEMA), quaternization reactions introduce methyl and propyl groups into the side chain chemistry and produce simultaneously strong polyelectrolytes with iodide counterions. Similarly, a sulfopropyl group incorporated by a betainization reaction results in a polyzwitterion that exhibits charge separation, but does not bear a counterion. A combination of neutron and x-ray reflectivity and spectroscopic ellipsometry is employed to characterize the swelling and sorption behavior of these samples as a function of relative humidity.

Chapter 5 extends the work in Chapter 4 by exposing a neat PDMAEMA brush, quaternized PDMAEMA brushes and a poly(2-diethylamino)ethyl methacrylate (PDEAEMA) SGPAs, to low molecular weight alcohols. In these experiments, the length of alkyl chains in the solvent, on the tertiary amine, and from the moiety introduced through quaternization are gradually extended. These systematic variations in alkyl chain length provide insight into the role of the hydrophobic and hydrophilic groups within the brush and the solvent on swelling and sorption behavior.

Finally, Chapter 6 describes an unconventional approach to producing substrates with surface-grafted chains. Here, DMAEMA monomers are grafted using quaternization onto a halogen-

terminated monolayer deposited on a substrate. Incubating these modified substrates in a solution undergoing a bulk polymerization leads to a "grafting-through" process that incorporates the surface-grafted monomer (SGM) into the bulk chains, resulting in surface-grafted polymer chains. The resulting grafted polymer film measures up to several nanometers in thickness, is uniform over the sample area and strongly correlated to the MW of the bulk chains. By using a bulk –initiated polymerization, this method of producing surface-grafted polymer assemblies is more accessible to existing polymerization processes, and as such may be applicable in roll-to-roll processes.

1.2 References

(1) Barbey, R.; Lavanant, L.; Paripovic, D.; Schüwer, N.; Sugnaux, C.; Tugulu, S.; Klok, H.-A. *Chem. Rev.* **2009**, *109*, 5437–5527.

(2) Galvin, C. J.; Genzer, J. *Prog. Polym. Sci.* **2012**, *37*, 871–906.

(3) Huang, J.; Koepsel, R. R.; Murata, H.; Wu, W.; Lee, S. B.; Kowalewski, T.; Russell, A. J.; Matyjaszewski, K. *Langmuir* **2008**, *24*, 6785–6795.

(4) Kawai, T.; Saito, K.; Lee, W. *J. Chromatogr. B* **2003**, *790*, 131–142.

(5) Sun, L.; Baker, G. L.; Bruening, M. L. *Macromolecules* **2005**, *38*, 2307–2314.

(6) McCaig, H. C.; Myers, E.; Lewis, N. S.; Roukes, M. L. *Nano Lett.* **2014**, *14*, 3728–3732.

(7) Zhao, B.; Brittain, W. J. *Prog. Polym. Sci.* **2000**, *25*, 677–710.

(8) Matyjaszewski, K.; Miller, P. J.; Shukla, N.; Immaraporn, B.; Gelman, A.; Luokala, B. B.; Siclovan, T. M.; Kickelbick, G.; Vallant, T.; Hoffmann, H.; Pakula, T. *Macromolecules* **1999**, *32*, 8716–8724.

(9) Chiefari, J.; Chong, Y. K. (Bill); Ercole, F.; Krstina, J.; Jeffery, J.; Le, T. P. T.; Mayadunne, R. T. A.; Meijs, G. F.; Moad, C. L.; Moad, G.; Rizzardo, E.; Thang, S. H. *Macromolecules* **1998**, *31*, 5559–5562.

(10) Tomlinson, M. R.; Genzer, J. *Langmuir* **2005**, *21*, 11552–11555.

(11) Osborne, V. L.; Jones, D. M.; Huck, W. T. S. *Chem. Commun. (Camb).* **2002**, *1*, 1838–18399.

(12) Wu, T.; Efimenko, K.; Genzer, J. *J. Am. Chem. Soc.* **2002**, *124*, 9394–9395.

(13) Tomlinson, M. R.; Genzer, J. *Macromolecules* **2003**, *36*, 3449–3451.

(14) Bhat, R. R.; Tomlinson, M. R.; Genzer, J. *J. Polym. Sci. Part B Polym. Phys.* **2005**, *43*, 3384–3394.

(15) Robinson, K. L.; Khan, M. A.; de Paz Báñez, M. V.; Wang, X. S.; Armes, S. P. *Macromolecules* **2001**, *34*, 3155–3158.

(16) Günay, K. A.; Theato, P.; Klok, H.-A. *J. Polym. Sci. Part A Polym. Chem.* **2013**, *51*, 1–28.

(17) Bain, E. D.; Dawes, K.; Evren, A. O.; Hu, X.; Gorman, C. B.; Jir, S.; Genzer, J. **2012**.

2. Applications of Surface-Grafted Macromolecules Derived from Post-Polymerization Modification Reactions*

*This chapter contains material published as "Applications of surface-grafted macromolecules derived from post-polymerization modification reactions" in the journal *Progress in Polymer Science*, vol. 37, pp. 871-906, 2012,

2.1 Introduction

Arguably the most straightforward approach to the formation of specialty polymers designed for specific applications involves polymerization of monomers with desired properties. In many cases this design philosophy will prove the most efficient at achieving the end product. Given the tremendous number of monomers available readily from chemical manufacturers today, and the various synthetic methods that have been developed over the past century that enable the incorporation of a variety of functionalities into a single macromolecule, the need for additional chemical reactions that modify macromolecules after polymerization may not be apparent. Yet, this is indeed the case. This review will discuss numerous applications accomplished via modifications of polymers anchored to substrates that illustrate the power and utility of this synthetic approach.

Despite the relative simplicity of the direct synthetic approach, several problems may arise quickly at various points along the synthetic pathway. We list them here in no particular order of preference. First, the monomer may prove incompatible with the reaction conditions required to incorporate a specific functionality. In this case, time and effort will be spent on what may become an increasingly complex monomer synthesis. Furthermore, the yield of modified monomer may prove too small and too costly to produce appreciable quantities of polymer. In the event of a successful monomer synthesis, the actual polymerization may fail to produce sufficiently high molecular weights or low polydispersities. Several modern polymerization techniques can generate polymers that meet both those conditions, but even these approaches cannot handle every monomer or ones bearing bulky pendant groups, notably bioconjugates. The possibility exists that the functional groups incorporated into the original monomer are not amenable to the polymerization reaction conditions (*i.e.*, temperature, solvent, *etc.*). In cases where it is possible to protect susceptible chemical groups, the deprotection reaction may not proceed to completion, thus negating the benefit of starting with the modified monomer in the first place. These (and other non-specified) issues apply not only to bulk polymerization reactions but also to the synthesis of macromolecules tethered by at least one of its repeat units to a substrate. The entropic constraints associated with such confinement provide yet another obstacle that may prevent direct polymerization of a given monomer by surface-initiated polymerizations. With these points in mind, the need for an alternative approach to producing functionalized polymer chains is apparent.

Post-polymerization modification (PPM), also termed polymer analogous reactions, incorporates functionalities into polymer chains by decorating already-synthesized polymers with an

appropriate chemical and/or biological species. This approach is not new. In fact, several industrial processes take advantage of this methodology in bulk polymer production, such as modification of polyolefins[1]. On smaller scales, a number of single-step, high-yield reactions under mild conditions can produce modified bulk and brush polymers, as highlighted in recent reviews by Klok *et al* [2,3]. Some particularly useful examples of chemical reactions involved in PPM, including the "click" family of reactions, quaternization, betainization, reactions between hydroxyl groups and acid chlorides, and others will be discussed briefly in a following section.

This review will discuss a variety of innovative applications achieved through polymer brush modifications that illustrate the power and utility of this synthetic approach. The concept of the PPM of macromolecules anchored to flat impenetrable surfaces and a few applications of such systems are summarized in **Figure 2.1**. The ability of PPM to alter the chemical nature and architecture of the polymer is married with controlling the degree of chemical modification and spatial distribution of the newly-added modifier along the macromolecule. While the degree of "chemical coloring" is adjusted by varying the reaction conditions (*i.e.*, temperature, concentration of the chemical modifier, coupling chemistry, catalyst, solvent type), changing the co-monomer distribution of the parent and new monomers is achieved through altering the "degree of confinement" of the parent polymer by either adjusting the solvent quality or by varying the grafting density of the macromolecular graft on the substrate (*cf.* **Figure 2.1b**). It is possible to produce complex brush systems with position-dependent distributions of the chemical modifiers that can be combined to express orthogonal gradients in functionality (**Figure 2.1c** and **2.1d**). Alternatively, substrates can be prepared that contain two distinct chemical patterns of various shapes and dimensions separated by sharp boundaries (**Figure 2.1d**). Copolymers with tuned co-monomer distributions that bridge the continuum between diblock and random distributions (**Figure 2.1b**) exhibit responsive characteristics (**Figure 2.1e**). These can be employed in a wide variety of applications that rely on stimuli-responsive character of surfaces. A few examples of those are depicted in **Figures 2.1f-2.1h**.

Figure 2.1. A Schematic representing the formation (a-e, yellow background) and function (f-h, green background) of surface-anchored polymer systems generated by post-polymerization modification (PPM) protocols. In a typical PPM (**Figure 2.1a**), a parent polymer is exposed a solution of the chemical modifier; during this process a portion of the surface-tethered macromolecule is decorated with the new chemical units (blue). Additional modification is possible with another chemical agent (red). The extent of modification depends on the PPM reaction conditions, such as the reaction time and temperature, concentration of the chemical agent, type of catalyst used (if any). In addition, the extent and spatial distribution of the modification depends on the grafting density of the grafted chain on the surface and solvent quality (**Figure 2.1b**). In general, decreasing the solvent quality and/or increasing the density of the chains on the surface leads to a decrease in the degree of PPM and a non-uniform distribution of the newly-added chemical units along the parent polymer tether. The latter effect can further be tailored by varying the geometry of the substrate (not shown in **Figure 2.1**). Methods exist that enable the formation of substrate-tethered polymer assemblies with a gradual spatial variation of the density and distribution (along the chains) of the PPM agents. A few examples are illustrated in **Figure 2.1c**. Combination two of these building blocks enables the formation of complex orthogonal substrates (**Figure 2.1d**), where each spot on the substrate represents a unique combination of properties 1 and 2. In addition, substrates can be formed that comprise chemical patterns comprising either PPM-modified/PPM-unmodified patterns or patterns created by applying two separate PPM modification protocols (**Figure 2.1d**). The variation of the degree of chemical modification and the spatial extent of the modifying agents along the chains endow the grafts with the ability to change their conformation (**Figure 2.1e**) as a result to some environmental trigger (*i.e.,* temperature, pH, salt concentration, or some other external field, such as electric or magnetic). Particularly, macromolecular grafts exposed to PPM under poor solvent conditions exhibit a diblock copolymer-like character and are amenable to large conformational change. Surface-tethered systems prepared by PPM protocols can be employed in various applications ranging from "affinity-like" chromatography (**Figure 2.1f**), design of amphiphilic surfaces facilitating decreased biomass adsorption (**Figure 2.1g**) or simply changing the wettability of the substrate (**Figure 2.1h**).

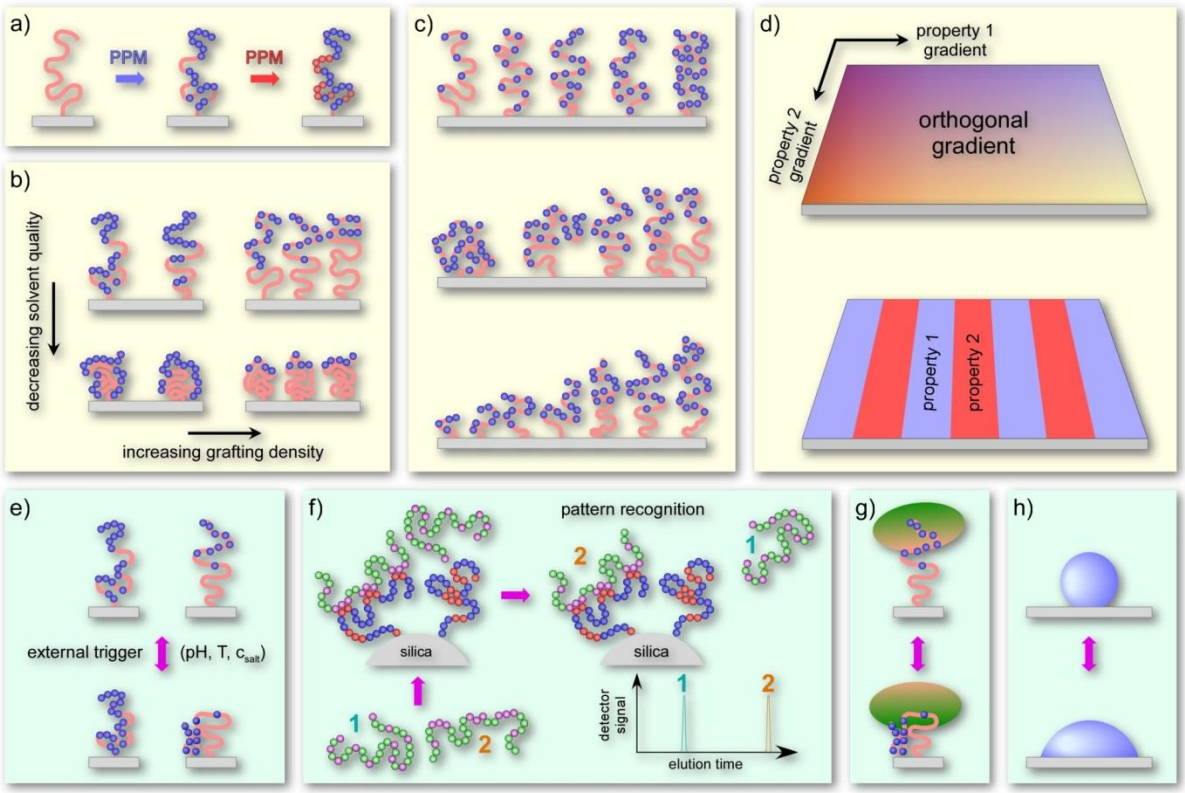
a)
PPM
PPM
b)
decreasing solvent quality
increasing grafting density
c)
d)
property 1 gradient
property 2 gradient
orthogonal gradient
property 1
property 2
e)
external trigger
(pH, T, c_salt)
f)
pattern recognition
silica
silica
detector signal
elution time
g)
h)

In the rest of this review we will provide a short overview of polymer brushes and discuss briefly a few examples of PPM chemistries that have proven particularly useful in brush modification. This latter section will not be inclusive as it has already received due attention in the reviews by Boaen and Hillmyer[1], Klok[2,3], and Pollino and Weck[4]. This review is divided into topics based on applications. These sections include: Altering Wetting Behavior (3.1), Ion Transport Barriers (3.2), Manipulating Nanoparticles (3.3), Mineralization of Protein Brushes (3.4), Incorporating Biological Moieties (3.4), Cellular Studies (3.5), and Tissue Engineering (3.6).

2.1.1 Overview of Polymer Brushes

Polymers located at an interface have attracted significant research attention over the past several decades[5] due to both academic interests and many potential industrial applications. Early work considered adsorption of polymer chains at solid and air interfaces from a liquid melt or solution. These systems produced surface coatings with a relatively low-density of polymers due to entropic barriers that prevented formation of extended and densely packed polymer chain conformations that deviated significantly from the native Gaussian shapes. While advantageous in systems where access to the surface is desirable, many applications necessitated denser chain grafting. In time, techniques have been developed that enabled the formation of densely-packed polymer assemblies on the surface, in which one end or a section of a polymer chain is tethered physically or chemically to a solid surface[2,6–34]. While these systems adopt two possible conformations, so-called mushroom or brush, they are often referred to commonly as "polymer brushes". We will commence this section by first defining a polymer brush and follow with a brief outline of the many synthetic approaches for creating such macromolecular tethers on surfaces. We will then promptly relax this definition in the remaining sections of this review in favor of inclusivity.

2.1.1.1 Structural Definition of a Polymer Brush

Brittain and Minko[35] offered a structural definition of a polymer brush based on key intrinsic parameters. Specifically, Brittain and Minko recommend the use of $\Sigma = \sigma \pi R_g^2$, where $\sigma = (h \rho N_A)/M_n$ is the brush grafting density (h is dry brush thickness, ρ is bulk density of the polymer, N_A is Avogadro's number, and M_n is the number average molecular weight). Examination of the terms in Σ reveals that it compares the area occupied by a single polymer chain (proportional to the square of the radius of gyration of the polymer, *i.e.*, R_g^2) to the number of chains per unit area of the substrate. One

would expect the brush regime to occur when the distance between chains is significantly less than R_g of the coil. Based on experimental results, the authors note that this transition occurs typically at $\Sigma \approx 5$, where systems at lower values are usually in the so-called "mushroom regime". It is important to note that this value depends on solvent quality and intra-chain interactions; *i.e.*, $\Sigma \approx 5$ is a rough estimate at best. **Figure 2.2** depicts pictorially the conformations of polymer brushes in the brush and mushroom regimes and shows the shape of a single collapsed macromolecular graft in a poor solvent. The transition from mushroom to brush regimes has been demonstrated experimentally by Wu and coworkers on a single substrate that possesses a gradient in initiator density[36]. As seen from the data in **Figure 2.3**, the polymer grafts begin to stretch away from the substrate as the density increases, eventually entering into the brush regime.

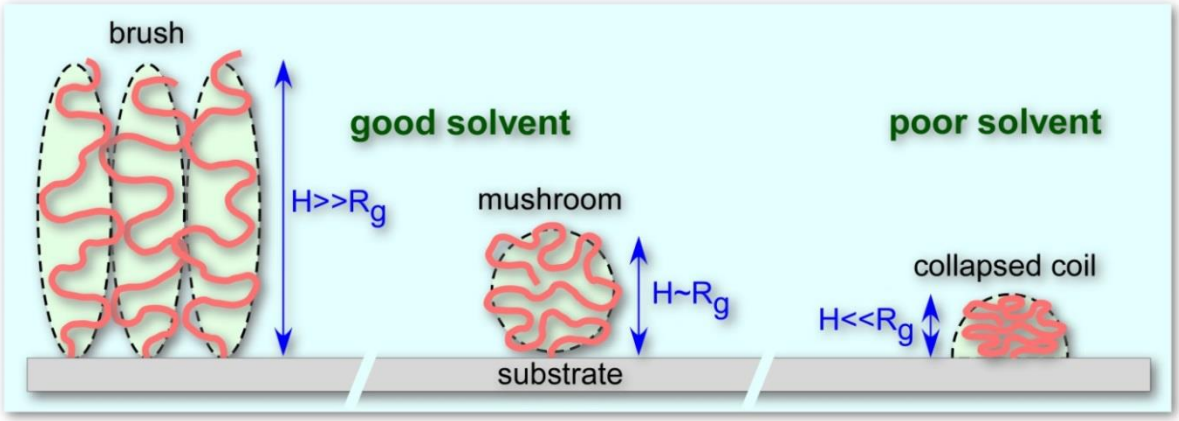

Figure 2.2. A Schematic representing conformations of surface-anchored polymers in brush (left) and mushroom (middle) regimes in a good solvent. Also shown is the conformation of surface-tethered polymer in a poor solvent.

We make this point about the structural definition of a polymer brush because many of the unique properties of these systems derive from the stretched nature of the grafted polymer chains. As mentioned previously, the properties of surface-anchored polymer assemblies depend on the density of grafts on the substrate. Therefore, for the sake of unambiguous science, Σ (or at least σ) should be reported. In this review, however, we will relax this strict definition of a polymer brush, as our focus is on the modification of these tethered polymer layers and the resulting application.

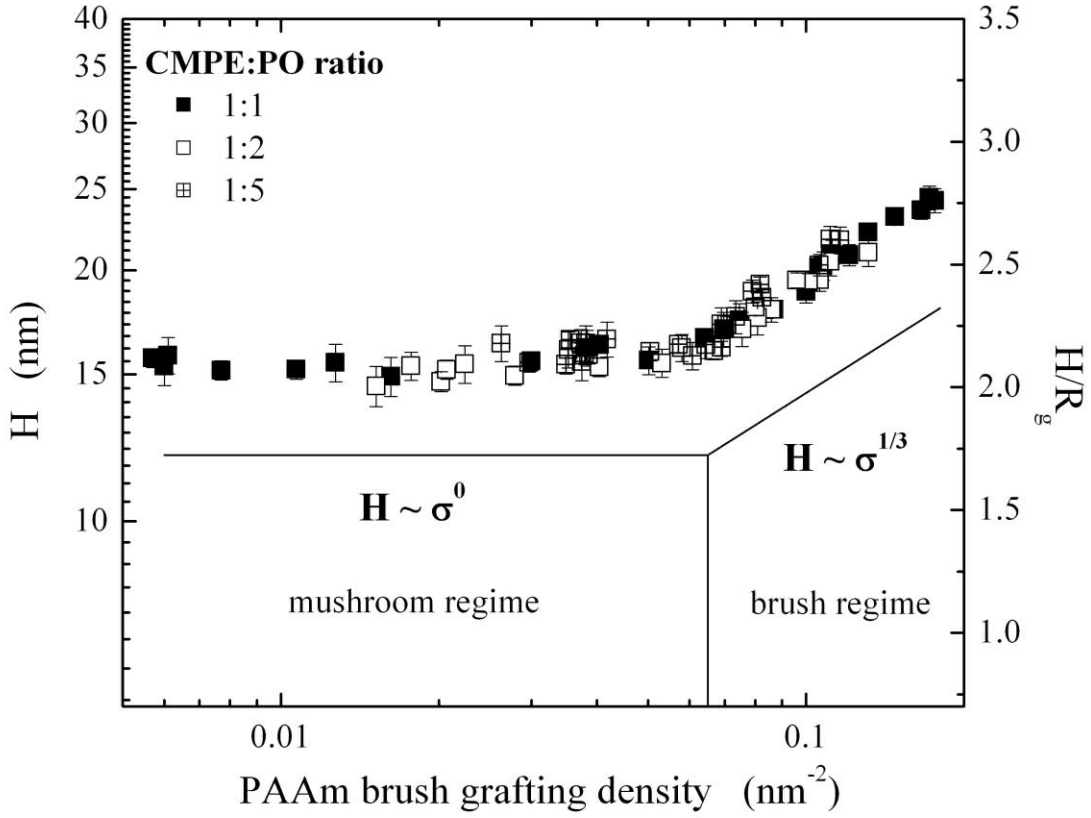

Figure 2.3. Wet thickness of the poly(acrylamide) (PAAm) brush (H) as a function of the PAAm brush grafting density. Reproduced with permission from the American Chemical Society[36].

2.1.1.2 Polymer Brush Synthesis

Functional polymer brushes have been generated from a rich library of monomer species by following either conventional free radical polymerization[37,38] or one of several controlled radical polymerization schemes, including atom transfer radical polymerization (ATRP)[34,39–53], reversible addition-fragmentation chain transfer (RAFT) polymerization[54–61], and nitroxide-mediated polymerization (NMP)[62–65]. Polymerization of chains from surfaces proceeds similarly to bulk polymerization, except that the initiator is deposited onto (and typically grafted to) the substrate surface rather than floating freely in solution. This approach has been termed "grafting from" polymerization. Alternatively, polymer in the bulk or in solution containing a specific functionality

(usually at the chain end or one block in a diblock copolymer) may adsorb onto the substrate at that functional group. Since the chains move from solution to the surface, this approach is called the "grafting to" method. The choice for one grafting technique over the other depends on the application of the brush. While the "grafting from" method produces denser brushes, the polymer chains tend to have greater polydispersity[33,66,67].

Regardless of the synthetic technique, the resulting polymer brush possesses properties that differ dramatically from the underlying substrate. Post polymerization modification provides a means to tailor these properties beyond what the original polymer brush possesses. For example, by exposing selective parts of the patterned macromolecule tether to the PPM, one can create macromolecule amphiphiles with unique physical characteristics that would be difficult to synthesize directly. In this way, PPM offers the possibility to produce next generation substrates, coatings, and devices for a wide range of technologies, as highlighted in the following sections.

2.1.2 Modification Chemistries

While the physical behavior of a polymer differs significantly from that of its building blocks, the chemistry available at the repeat units tends to be analogous to small-molecule reactions. Researchers have taken advantage of this point for decades, and a number of recent reviews summarize the options available to polymer chemists[1,3,68–70]. We will only highlight a few of the more common and versatile reactions here (*cf.* **Figure 2.4**).

One of the most popular PPM reactions to appear in the literature is the 1,3-dipolar cyclo addition reaction, better known as the “click” reaction. We note, however, that the term “click” reaction refers to a synthesis philosophy, and not a specific reaction[71,72]. Nonetheless, the reaction between an alkyne and azide in the presence of a Cu^{I} catalyst has been applied to a wide variety of polymeric systems with great success[73,74]. This reaction is noted for its mild conditions (including water) and near-quantitative conversion. The necessity of a copper catalyst does complicate its application, especially to biological systems, however. The Locklin group has recently demonstrated PPM of a polymer brush using a catalyst-free cyclo addition[75].

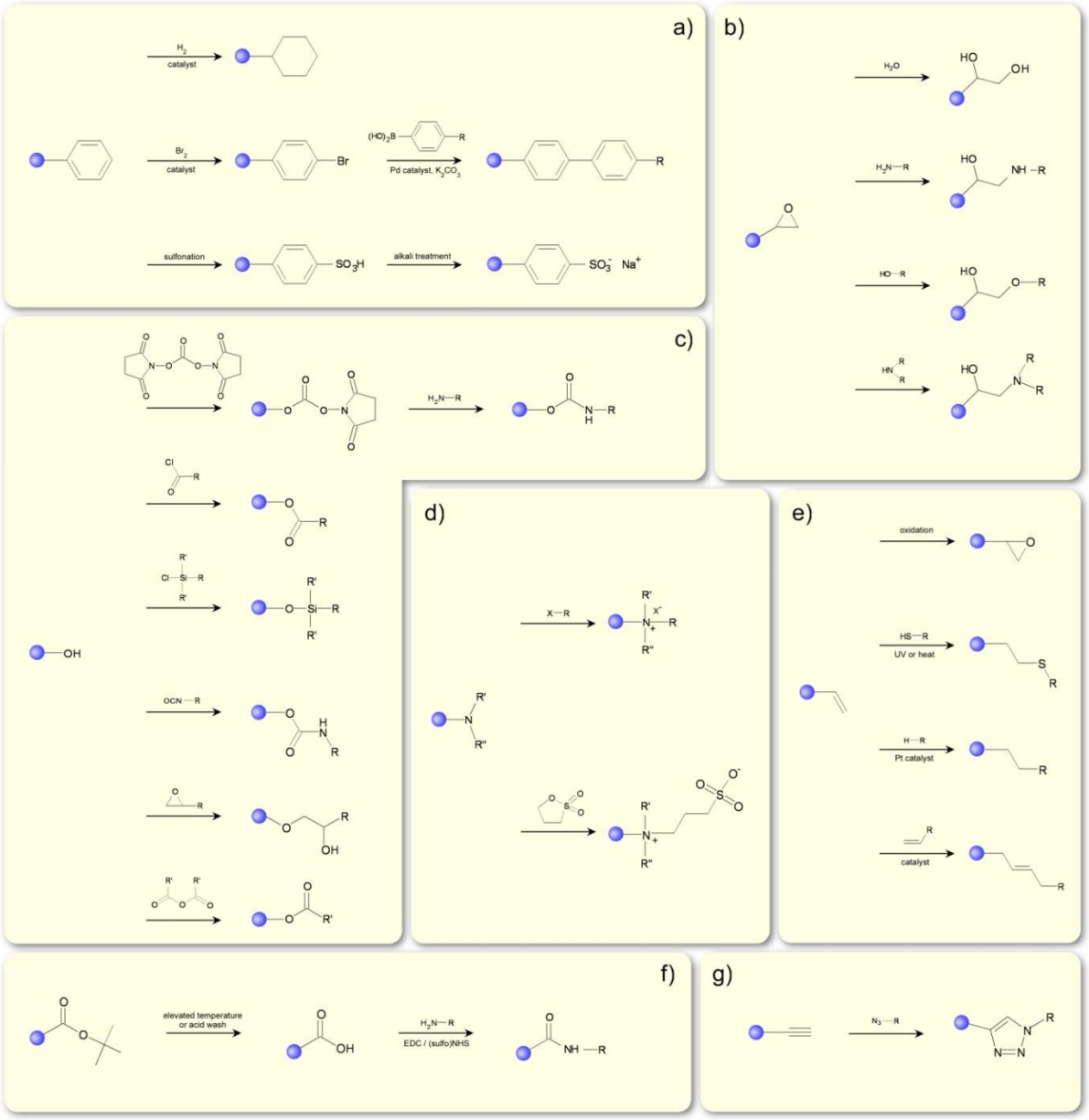

Figure 2.4. Selected coupling reactions employed in PPM processes involving coupling of various functional groups with pendent: a) phenyls, b) epoxys, c) hydroxyls, d) tertiary amines, e) vinyls, f) *t*-butyls and amino acids, g) alkynes.

The cyclo addition is not the only reaction to fall under the "click" philosophy. The Diels-Alder reaction has received due attention in polymer modification[68], as well as the thiol-ene

reaction[68,69,76,77], and the related thiol-yne reaction[77,78]. Both of these reactions proceed to high conversions, and the ease of inserting these functional groups into polymers makes them very appealing. Furthermore, the fact these reactions do not require (typically) a catalyst makes those coupling reactions particularly useful for incorporating biological moieties in polymer chains.

Another class of reactions employed in post-polymerization modification involves the quaternization of tertiary amines to quaternary ammonium groups[79]. These reactions appear often in this review to produce cations of poly(2-dimethylaminoethyl methacrylate) (PDMAEMA) and poly(2-vinylpyridine) (P2VP) and poly(4-vinylpyridine) (P4VP) (see Section 2). A general scheme is shown in **Figure 2.4**. These reactions quickly proceed to high conversions, and can introduce a number of functional groups into the polymer at mild conditions without a catalyst, as well as produce polycations. Tertiary amines are also available for betainization, which produces zwitterionic pendant groups; that is the polymer has an overall neutral net charge, but possesses two sites of opposite charge on the same pendant group (*cf.* **Figure 2.4d**). Like quaternization, this reaction proceeds typically to high conversions under relatively mild reaction conditions.

Polymers that bear aryl groups, particularly phenyl rings, can be modified by a number of addition reactions, including halogenation[80,81] and sulfonation[82], the latter of which produces polyanions, as noted in Section 2. Brominated aryl-containing groups can subsequently undergo Suzuki coupling with boronic acids to produce biaryls, whose functionality is derived by the chemical nature of the boronic acid[83,84].

In addition to the above examples, PPM reactions using isocyanate reactions[85–87] fluorination[88,89], active esters[90,91], ring opening reactions[92–94], and non-covalent interactions[4] have appeared in the literature. Furthermore, reports of polymer modification using electrochemical reduction[95], electron beams[96,97] have been published. Finally, the emerging field of mechanical modification of polymers, in which PPM is enacted by pressure changes or sonication, among others, has started to receive attention[98–101].

2.2 Stimuli Responsive Brushes

In recent years, the development of stimuli-responsive polymer brushes has emerged as a major research topic[102–109]. These systems demonstrate variation in chain conformation in response to an external stimulus (*i.e.*, temperature, light radiation, and electric and magnetic fields) that leads to variations of microscopic (*i.e.*, functional group reorientation/reorganization) and macroscopic (*e.g.*,

wettability) characteristics. While all these examples have produced notable results, here we will focus solely on pH responsive polymer brushes[23,110–115], which tend to protonate or deprotonate (*i.e.*, change chemically, which is in line with the spirit of this review) under varying pH conditions. These polymers become charged above or below a certain pH value (pK_a), producing polyanions or polycations, respectively. When the pH is adjusted back below or above the pK_a, respectively, the polymers return to their original neutral state. Polymers that undergo this type of reversible charge are called "weak" (or annealed) polyelectrolytes (WP). In contrast, polymers that possess permanent charge centers, regardless of the surrounding pH, are called "strong" (or quenched) polyelectrolytes (SP).

2.2.1 Weak Polyelectrolytes

The following examples are intended to introduce the reader to the behavior of weak polyelectrolytes. This section does not contain a comprehensive list of PPM reactions that lead to WPs. Instead, we have selected a few representative examples that illustrate the fundamental behavior of WPs and leave more recent and application-driven examples for a latter portion of this review.

An early report from Sidorenko *et al* compared[116] a mixed polystyrene (PS) and P2VP with the analogous homopolymer brushes. The authors demonstrated that the P2VP homopolymer brush swelled when exposed to a 0.1 N HCl solution, resulting from protonation of the nitrogen atom, and reverted to its original state after exposure to an alkaline solution. After exposing a mixed brush comprising 50% PS and 50% P2VP to a 0.1 N HCl solution, the top layer of the brush was 95% P2VP as determined by water contact angle. The segregation of the P2VP monomers to the surface followed their protonation, leading to an increased hydrophilicity. Exposure to toluene resulted in a top layer composition of 95% PS, confirming the solvent effect.

The above example from Sidorenko *et al* employed a polycationic WP. Similar behavior has been observed with polyanionic WPs[117,118]. Notably, Biesalski *et al* examined poly(methyacrylic acid) (PMAA) brushes exposed to different pH and ionic strengths[119]. Their findings fall in line with those seen in the previous example, except these brushes swelled at higher pH values, as the carboxylic acid groups deprotonated. Increasing ionic strength at a constant pH value of 4 led initially to an increase in brush thickness (until 0.006 M), followed by a collapse in thickness, likely due to a combination of electronic screening and solubility changes related to the hydrophilicity of the

anion. The Huck group has recently visualized this ionic strength effect directly using confocal microscopy for poly(methacryloyloxyethyl phosphate) (PMEP) brushes labeled with dye molecules via a PPM reaction[120].

2.2.2 Strong Polyelectrolytes

Many weak polyelectrolytes can be converted to strong polyelectrolytes through PPM reactions. Common examples include P4VP brushes[121] and PDMAEMA brushes quaternized with alkyl halides[122], as well as poly(styrene sulfonate) brushes produced via saponification[123] or sulfonation[82], and PMAA brushes produced via a deprotection reaction[124,125].

In the case of the P4VP brushes, Rühe and coworkers used a PPM reaction in these studies, which enabled the direct comparison of the same brush's behavior before and after quaternization with ethyl bromide[121] and methyl iodide[126] (*cf.* **Figure 2.5**). In salt-free solutions quaternization leads to an increase in the film thickness due to the increase in molecular mass of the repeating units. Furthermore, incorporation of a permanent charge center in the polymer pendant groups results in a polymer brush whose thickness does not depend on grafting density in salt-free solutions, as seen in **Figure 2.5**. This so-called "osmotic brush" results from an increased osmotic pressure within the brush caused by the addition of counterions. Biesalski and Rühe also examined the effect of charge density and ionic strength by quaternizing poly(4VP-*co*-dimethylacrylamide) brushes[127], finding a smooth transition between the swelling behavior of a polyelectrolyte and neutral brush.

Another example of a popular WP that is quenched readily into a SP is PDMAEMA. In addition to being easily quaternized on the tertiary amine terminus, it exhibits a lower critical solution temperature (LCST) at physiological temperatures, making it a doubly responsive polymer[128,129]. Its LCST behavior aside, the electrolyte aspect of PDMAEMA makes it a common feature in this review. Tran and coworkers published[130] the results of a scaling law analysis of unmodified and quaternized PDMAEMA brushes, finding behavior in good agreement with theory. Sanjuan and Tran followed this work with reports on the synthesis[124] and physical behavior[125] of weak polyampholyte brushes consisting of P(DMAEMA-*co*-MAA) and the same brushes with the DMAEMA repeat units quaternized with methyl iodide. This system and a similar one have also been examined by Ayres *et al*[131,132]. Reports have also appeared on the electrochemical characteristics and associated behavior of counterions of partially and fully quaternized PDMAEMA brushes[133–135].

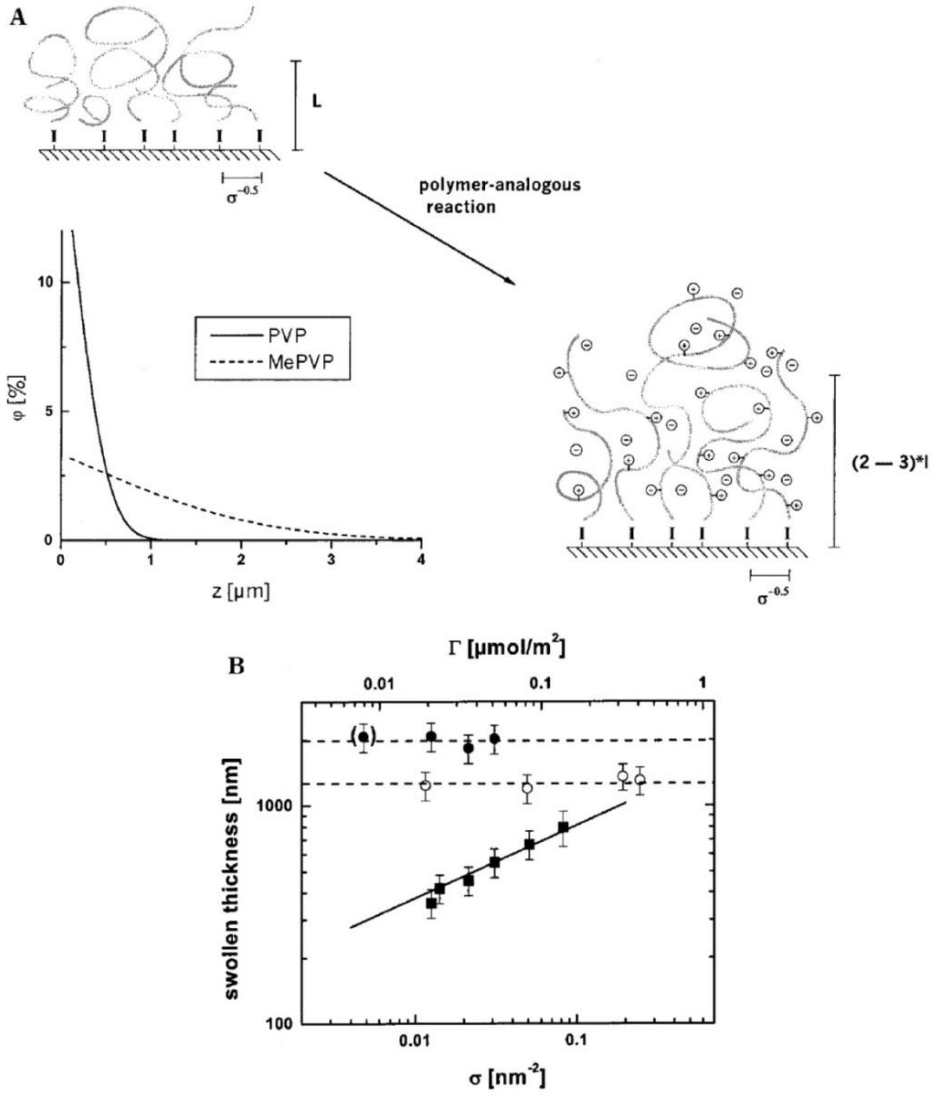

Figure 2.5. (A) Schematic depiction of the increase in swollen thickness of a polymer brush in a good solvent after the conversion of the neutral brush into the charged species due to the introduction of electrostatic forces. (B) Brush thickness as a function of graft density for neutral and charged brushes. The experimental results agree well with the predicted scaling laws, which are indicated as lines in the figure ($L \sim \sigma^{0.33}$ for the neutral brushes and $L \sim \sigma^{0}$ for the polyelectrolyte brushes). Reproduced with permission from the American Chemical Society[126].

2.3 Selected case studies involving PPM on macromolecular grafts

Polymer brushes can modify substantially properties of surfaces to which they are anchored. Very thin (only a few nm), yet active layers make great candidates as surface-bound barriers, functional coatings, and many others. PPM of grafted chains enhances greatly the functionality of the parent homopolymer brush in that it alters the chemistry of the grafted chains and in some instances also the co-monomer distribution of the original and newly added monomers. The chemical composition of the PPM grafts can be tuned by varying the degree of "chemical coloring" by controlling the reaction conditions, as was mentioned before. Adjusting the co-monomer distribution can be achieved by either varying the solvent quality or by using substrates with different curvatures. In **Figure 2.6** we demonstrate pictorially how varying the substrate geometry alters the distribution (and affects to some extent the degree of PPM) of the chemical modifiers along the grafted macromolecules.

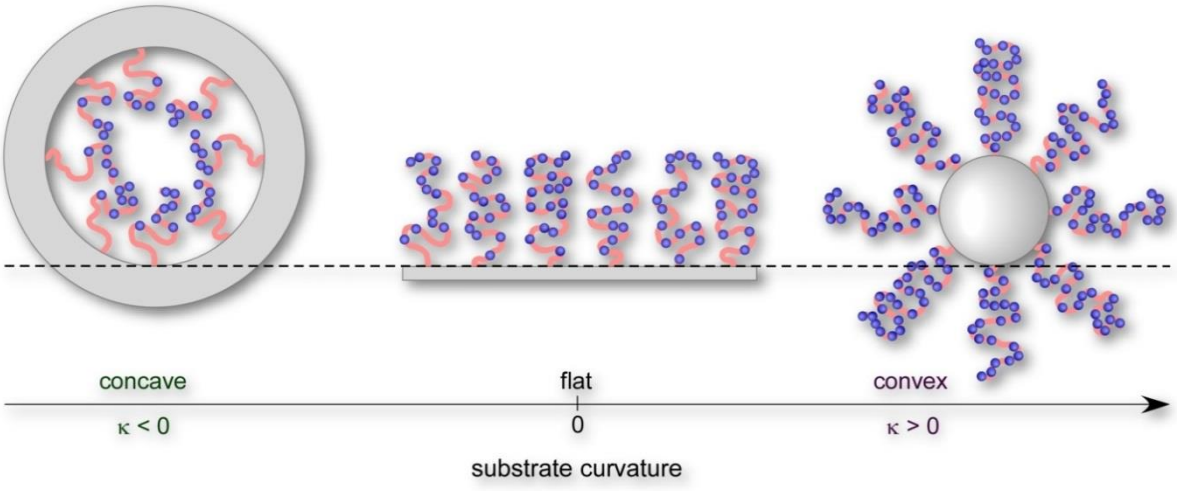

Figure 2.6. Schematic illustrating the conformations of polymer grafts in concave, and on flat and convex surfaces. The spatial distribution of the modifying agent after the PPM depends on the curvature of the substrate. The smallest degree of confinement will be present for chains grafted to substrates with large positive curvatures (κ). Decreasing κ from large positive to small positive, zero or even negative values will increase the degree of confinement. As a result, the modifying agent will only access the topmost regions of the polymeric grafts. While chains grafted to small particles can be modified nearly completely, those attached inside small pores will undergo PPM to only a limited degree.

2.3.1 Altering Wetting Behavior of Surfaces

The wettability of a surface can be tuned by an appropriate choice of the surface chemistry and surface topography. For example, hydrophobic surfaces are fabricated by introducing fluorinated compounds. Thin films of hydroxylated poly(styrene-*b*-isoprene) or poly(methyl methacrylate-*b*-2-hydroxyethylmethacrylate) modified at the pendant hydroxyl groups with perfluorinated ester or fluorinated urethane and carbonate moieties exhibited heightened hydrophobicity and oleophobicity compared to the unmodified parent polymer[85]. These properties stem from the characteristics of fluorinated compounds enriching the surface, as demonstrated by x-ray photoelectron spectroscopy (XPS). These substrates could be patterned using a laser beam to selectively degrade the fluorinated compounds resulting in selected regions of enriched hydrophobicity. Brantley, Jennings and coworkers reported on PPM of poly(2-hydroxyethylmethacrylate) (PHEMA) brushes by acylchloride-based fluorinated compounds[20,136–138]. Arifuzzaman and coworkers[139] later extended the efforts of Brantley *et al* by performing a comprehensive study aimed at modifying PHEMA brushes with fluorinated agents bearing various chemical head-groups, including acylchlorides, anhydrides, and organosilanes. Attachment of organosilanes to PHEMA was previously studied by two other groups[140,141].

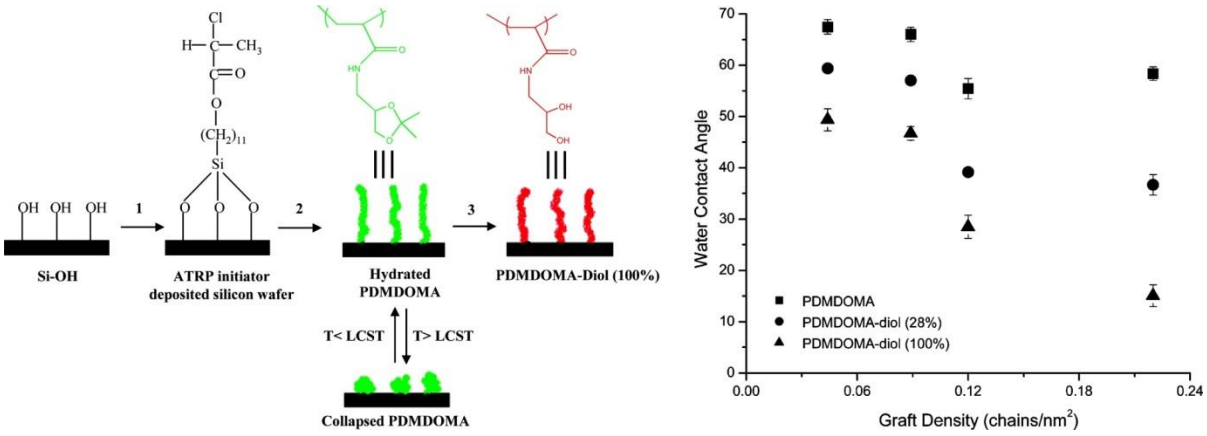

Figure 2.7. (left panel) Preparation of PDMDOMA-grafted silicon wafer via surface-initiated atom transfer radical polymerization (SI-ATRP): (1) deposition of self-assembled ATRP initiator, 11-(2-chloro)propionyloxyundecenyltrichlorosilane; (2) SI-ATRP of DMDOMA from wafer surface; (3) acidic hydrolysis of PDMDOMA brushes to obtain PDMDOMA-diol (100%) brush. (right panel) Evolution of water contact angle with increased graft density for PDMDOMA brushes with different hydrophilicity. Reproduced with permission from the American Chemical Society[142].

In another example, brushes of poly-*N*-[(2,2-dimethyl-1,3-dioxolane)methyl]acrylamide (PDMDOMA), which displays LCST behavior, were altered chemically by hydrolyzing the dioxolane groups, resulting in modified wetting behavior (*cf.* **Figure 2.7**)[142]. The authors reported on the dependence of wettability on the degree of chemical modification of the parent polymer as well as the grafting density of the brushes on the surface.

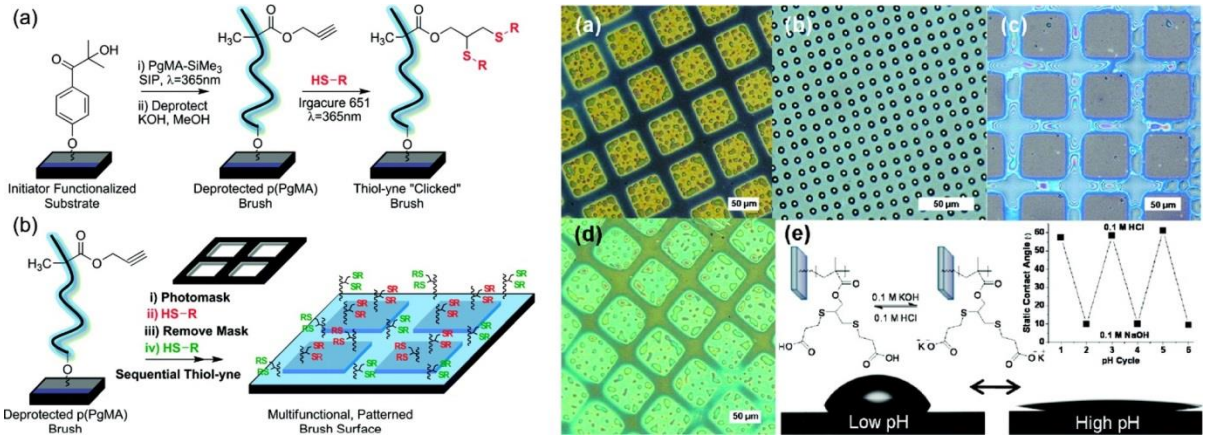

Figure 2.8. (left panel) (a) Schematic procedure of surface-initiated photopolymerization of TMS-protected propargyl methacrylate, deprotection, and subsequent thiol-yne functionalization. (b) Schematic procedure for photopatterning "yne"-containing polymer brush surfaces with sequential thiol-yne reactions. (right panel) Condensation images of sequential thiol-yne micropatterned brushes showing water droplets selectively nucleating on the hydrophilic MPA areas: (a) MPA/DDT (square/bars), 300 mesh; (b) MPA/DDT (squares/bars), 2000 mesh; (c) inverse DDT/MPA (squares/bars), 300 mesh; (d) Sunlight MPA/DDT (squares/bars); (e) static water contact angle measurements showing pH responsive reversible wettability of MPA surfaces prepared outdoors in sunlight. Note: Color variations result from thin film interference under humid conditions. Reproduced with permission from the American Chemical Society[78].

Reports on patterning regions with tuned wettability have also appeared. Taking advantage of a photoresist layer on top of a polymer brush, work from IBM demonstrated a method to produce patterns with modified wettability via the deprotection of poly(*tert*-butyl acrylate) (PtBA) films to poly(acrylic acid) (PAA) using acids generated during lithographic patterning of the resist[143]. While the unmodified PtBA regions remained hydrophobic, water droplets wetted selectively the PAA-rich surfaces, taking on the shape of the PAA water-wettable pattern. Brown *et al* have improved upon this idea by developing a monomer that produces an acid upon exposure to UV light, and creating

diblock brushes with PtBA[144], as well as using a methacrylate monomer with photocleavable *o*-nitrobenzene derivatives[145]. In a similar vein, Hensarling *et al* have modified propargyl methacrylate brushes using thiols in a UV-modulated reaction[78]. By masking certain regions during a first modification (say, to introduce hydrophobic pendant groups), then backfilling in a second modification step with hydrophilic groups, wettability patterning could be achieved like that shown in **Figure 2.8**.

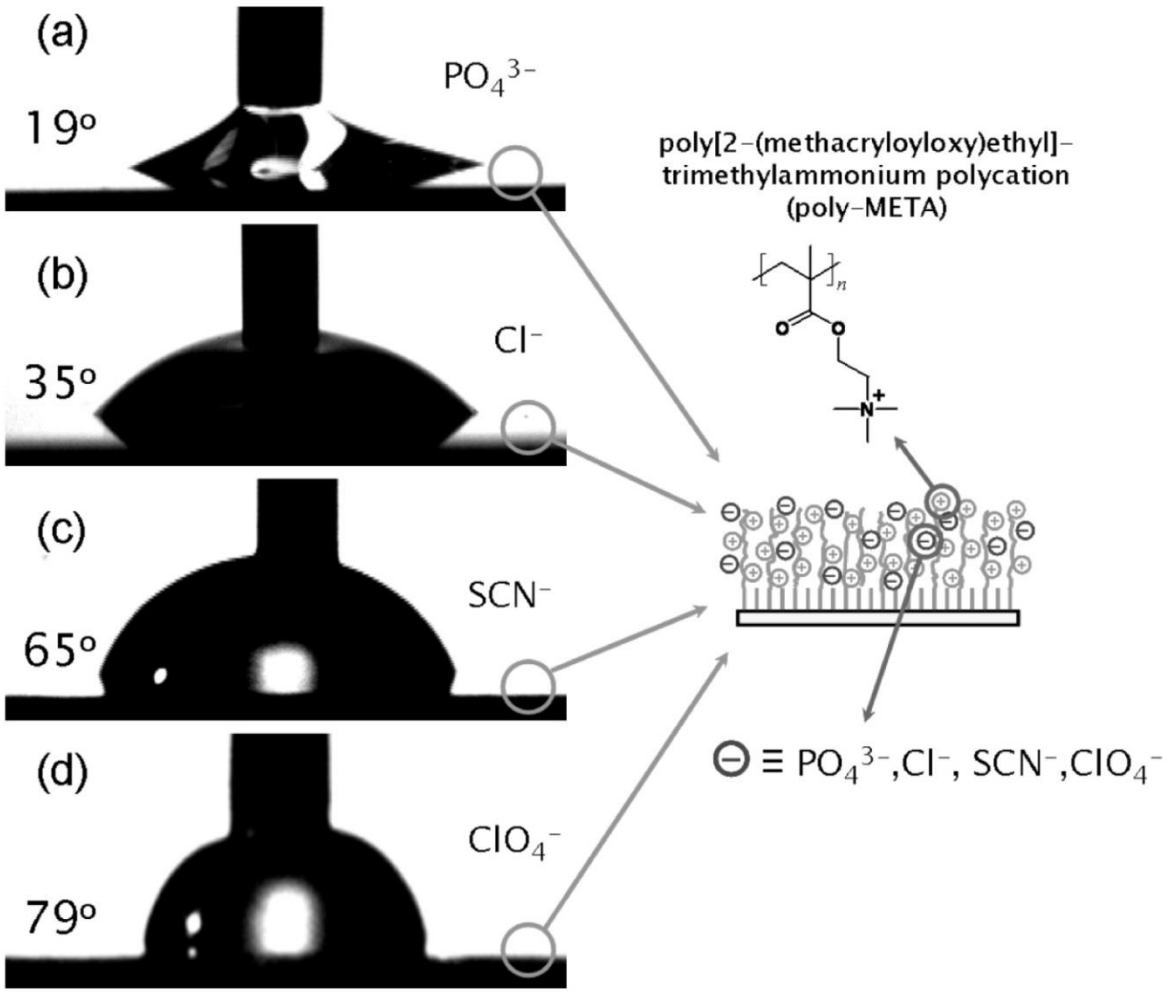

Figure 2.9. Changes in wettability corresponding to a Au surface modified with PMETAC brushes (h = 20 nm) when their corresponding counterions are: a) PO43–, Cl–,b) SCN–, and c) ClO4–. The schematic depicts the structure of the cationic polyelectrolyte brush. Reproduced with permission from Wiley[148].

Several reports on using counterions in polyelectrolyte brushes to modify surface wettability have also appeared[146,147]. To this end, Huck and coworkers have demonstrated the ability to modify the wetting behavior of polyelectrolyte brushes simply by exchanging different ions into the brush[148]. In a polycationic brush, water contact angle measurements for various counter ions went as: PO_4^{-3} = 19, Cl- = 35, SCN- = 65, ClO_4- = 79 degrees (*cf.* **Figure 2.9**). Similar results have been reported for polyanion brushes[149]. Furthermore, reduction of ferricyandide ions in a quaternized PDMAEMA brush using cyclic voltammetry led to similar control over the wetting angle[150].

The Locklin group has also used counterions to control wetting behavior in polymer brushes containing spiropyran moieties[151,152]. Upon exposure to UV light in salt solutions, the pendant spiropyran groups rearrange and form organometallic complexes. In line with the aforementioned work by the Huck group, different counterions yield different water contact angles, though the spiropyran system reverts back to its original water contact angle upon exposure to light wavelengths in excess of 500 nm. Importantly, the various counterions also produced different color changes in the brush, suggesting these compounds hold promise as metallic ion sensors.

2.3.2 Ion Transport Barriers

The Jennings group has explored ion transport through fluorinated brushes thoroughly[136,137]; the researchers established that -CF_3 groups decorating PHEMA brushes and enriched the surface after 25% conversion. The authors employed electrochemical impedance spectroscopy (EIS) to monitor ion transport and noted that resistance increased sharply up to 25% conversion of the HEMA units before leveling off. While this finding demonstrated how important the top few nanometers of a surface are to the properties of a substrate, impedance decreased rapidly until ≈60% conversion, indicating that the entire brush plays a role in governing ion barrier properties. In a similar examination, Brantley *et al* illustrated[138] a method to modify reversibly PHEMA brushes modified with pentafluorobenzoyl chloride (FBZ). A basic solution hydrolyzes the ester linkages formed by FBZ, recovering the original PHEMA brush. By taking advantage of diffusion, the authors tuned the thickness of the FBZ layer, then modified the recovered PHEMA brush with a second moiety, including alkyl and fluoroalkyl chains, or FBZ. The hydrophobicity and resistance of the film increased as F7/FBZ > H7/FBZ > FBZ/FBZ > PHEMA/FBZ.

While the low surface energy of fluorinated compounds lends itself well to resistive surface properties, the high cost of fluorine-based compounds has motivated research to seek less expensive

alternatives. The Jennings group developed[153] an effective ion transport barrier based on PM-COOH films that exhibited pH-dependent resistivity, where PM refers to poly(methylene). At lower pH values, the carboxylic group was in a protonated state, effectively blocking ion transport. With increasing pH deprotonation occurred and the charged brush facilitated ion transport. In a next step[154], the authors converted the carboxylic groups to amine-terminated groups, resulting in barrier properties that acted in the opposite direction to the original PM-COOH brushes. That is, at low pH values the amine compound was protonated, enabling ion transport, while at high pH values it was neutral and acted as a barrier. Bai *et al* have also investigated related behavior in brushes with amine side chains[155].

In some cases, membranes that always facilitate ion transport are desired, such as polyelectrolyte membranes in fuel cells. With this goal in mind, Jennings' group sulfonated polynorborene (PNB) brushes grown on Au-coated substrates[156]. One notable feature of these brushes is that they grow to a thickness of 120 nm in only fifteen minutes, enabling the rapid synthesis of thick polymer brushes. The neat PNB films show a three order of magnitude increase in resistivity over the original Au substrate. Subsequent sulfonation leads to only a one order of magnitude increase over the substrate, indicating improved ion transport.

Huck's group has also carried out studies on the transport of ions through polymer brushes modified by PPM reactions. Brush types included the aforementioned PDMAEMA[133], as well as poly(ethyleneimine) (PEI) brushes modified with ferrocene moieties using a 1,3-dipolar cyclo addition reaction[157]. In the latter report, it was noted that the redox activity of the polymer brushes depended on the brush thickness, conformation of brush as a function of salt concentration, and distance of the ferrocene groups from the electrode surface (*i.e.*, located at the terminus of the brush chains, or along the side chain).

Minko and Katz have taken advantage of this control over ion transport using pH responsive polymer brushes in their development of biocomputing technologies, which use logic gates based on biological moieties like enzymes. Specifically, they have prepared assemblies of mixed polymer brushes of P2VP and PAA[158,159], which have very different pK_a values. Changing the solution pH beyond either of the pK_a boundary values leads to the selective swelling of one of the polymer species, enabling the discerning passage of anionic or cationic species in solution (*cf.* **Figure 2.10**). A similar report controlling P2VP and PDMS mixed brushes using exposure to air (PDMS selective) or submersion in water (P2VP selective) has also appeared[160].

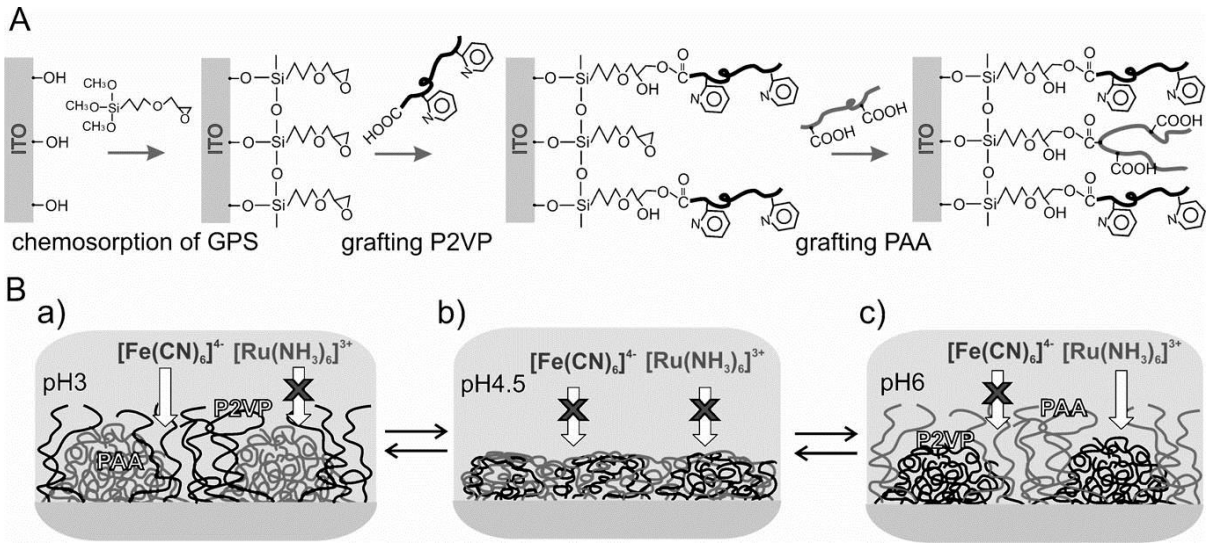

Figure 2.10. (A) Stepwise covalent modification of the ITO electrode surface to yield the mixed polymer brush composed of P2VP and PAA. (B) The polymer brush permeability for the differently charged redox probes controlled by the solution pH value: a) the positively charged protonated P2VP domains allow the electrode access for the negatively charged redox species; b) the neutral hydrophobic polymer thin-film inhibits the electrode access for all ionic species; c) the negatively charged dissociated PAA domains allow the electrode access for the positively charged redox species. Reproduced with permission from Wiley[158].

In another example, applying an electrochemical potential that reduces oxygen in the vicinity of an unmodified P4VP polymer brush results in a local pH change (the bulk buffer solution pH does not change)[161]. By choosing a bulk pH above the pK_a of P4VP, so that the brush is in the "off" state, the application of the reducing potential turned the brush to the "on" state, allowing the flow of anions present in the solution. Removing the potential and stirring, so that the localized pH in the brush equilibrated with the bulk pH, returned the brush to the "off" state. This polymer brush switch provides an excellent example of applying the swelling behavior described at the start of this section.

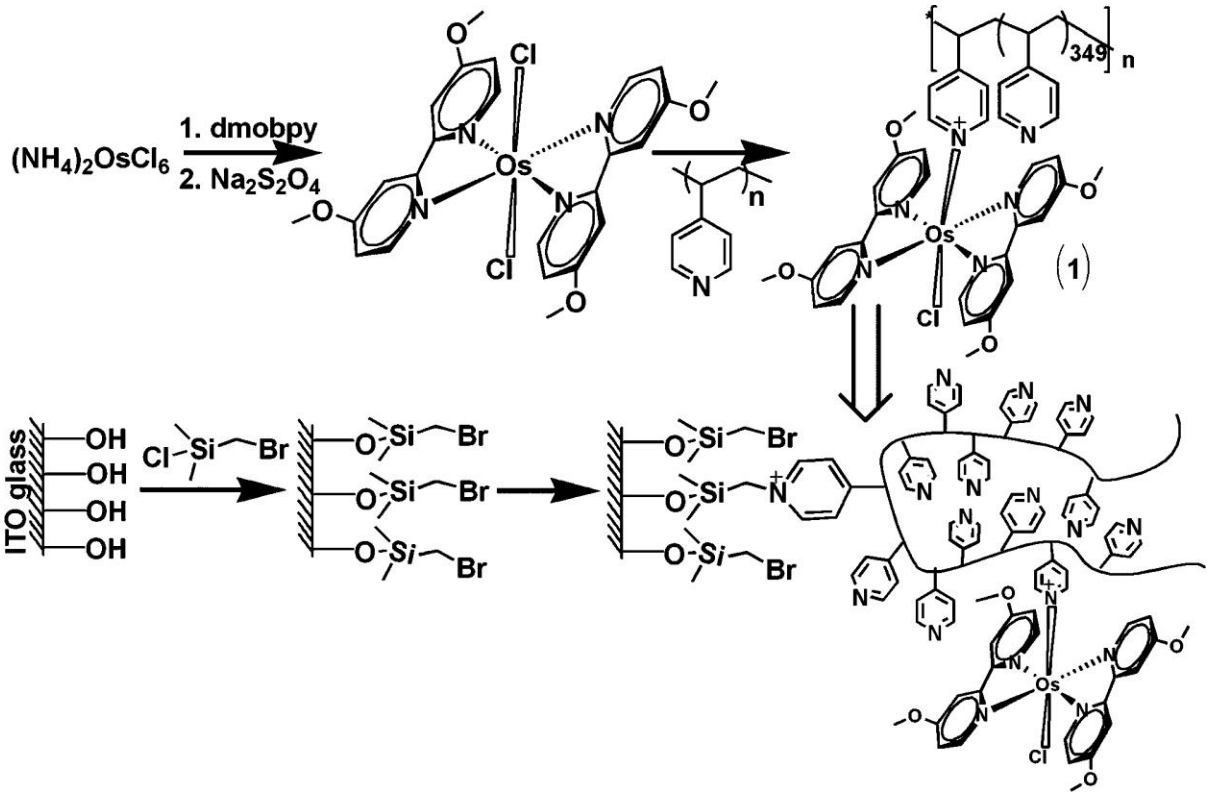

Figure 2.11. Functionalization of poly(4-vinyl pyridine) (P4VP) with the pendant redox groups and modification of the ITO electrode with the resulting redox polymer. Reproduced with permission from the American Chemical Society[162].

The Minko and Katz groups have also developed a bioelectrocatalytic interface based on P4VP functionalized with an Os-complex that acts as a redox agent[162,163]. The resulting bulk polymer was "grafted to" an ITO coated glass electrode through a quaternization reaction, forming a polymer brush that would collapse above a pH of 6, and expand below a pH of 4 (*cf.* **Figure 2.11**). When in an expanded state, electrons generated by the Os-complex redox activity can reach the electrode, as demonstrated using cyclic voltammetry illustrated in **Figure 2.12**. In the collapsed state, however, there is only negligible current for all voltages. Therefore, it is possible to think of the expanded brush below pH 4 as the "on" state, and the collapsed above pH 6 as "off". A simple system based on this concept was constructed that used the P4VP bound Os-complex to mediate electron transfer to the ITO electrode during the oxidation of glucose by glucose oxidase (GOx). To switch between the "on" and "off" states, esterase (Est) and urease (Ur) were introduced into solution with glucose and

GOx. Starting in the off state (pH > 6), addition of ethyl butyrate leads to the production of butyric acid, catalyzed by Est, lowering the pH to below 4. This state corresponds to the b curve in the cyclic voltammogram in **Figure 2.12**, indicating the electrons reach the electrode. Adding urea to the system results in the production of ammonia, catalyzed by urease, and raising the pH above 6. Trace c in the voltammogram in **Figure 2.12** reveals that the system is now off and no electrons reach the electrode. From these two states, it is possible to construct a simple logic system, demonstrating the basis of a biochemically controlled device.

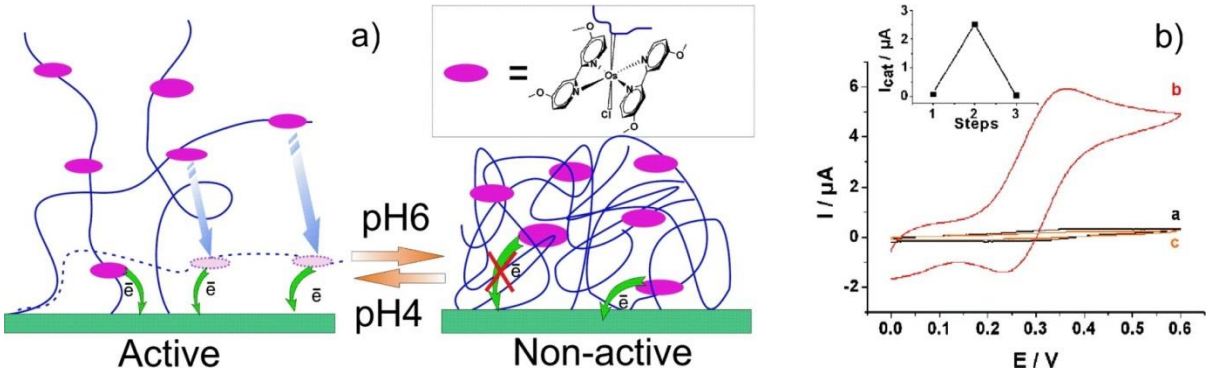

Figure 2.12. (a) Reversible pH-Controlled Transformation of the Redox-Polymer Brush on the Electrode Surface between Electrochemically Active and Inactive States. (b) Cyclic voltammograms obtained for the switchable bioelectrocatalytic glucose oxidation when the system is (a) in the initial OFF state, pH ca. 6.5; (b) enabled by the ethyl butyrate input signal, pH ca. 3.8; and (c) inhibited by the urea reset signal, pH ca. 7.5. Scan rate, 10 mV s−1. Inset: Switchable bioelectrocatalytic current: (step 1) initial OFF state, (step 2) enabled ON state, (step 3) reset to the OFF state. Reproduced with permission from the American Chemical Society[162].

In this example we see multiple uses of post-polymerization modification. The first change, which links the Os-complexes to the P4VP chains, is chemical in nature. By tethering the complex to a P4VP homopolymer, as opposed to incorporating it into a monomer and attempting to produce a copolymer, the steps to produce the functional polymer are much less ambiguous. Attempting to produce the copolymer directly would necessitate: 1) synthesizing the monomer and 2) determining reaction conditions under which the appropriate number of Os-complexes appeared in the chain. Adopting a PPM approach avoids both of these difficulties. Attaching the modified P4VP chains to the ITO surface is the second example, which is also chemical in nature. The decision to "graft to"

the surface instead of "graft from" stems from the need for a diffuse polymer brush that will accommodate the Os-complexes. Finally, the third example of PPM in this report involves the reversible protonation of the P4VP moieties, which leads to the collapse or expansion of the polymer brush. Ultimately, it is this modification that introduces an "on" and "off" state into the system. Without the ability to alter physically a component of the system (*i.e.*, the thickness of the polymer brush), the device would not possess a logical character.

Schepelina and Zharov used[122] PDMAEMA grafted to silica spheres to examine metal-complex transport through a polyelectrolyte brush. Silica particles assembled in a hexagonal closed-packed formation on a Pt electrode had a PDMAEMA or quaternized PDMAEMA coating. At a neutral pH value with neat PDMAEMA, the limiting current of $Ru(NH_3)_6^{3+}$ decreased 30-40%, while $Fe(CH_2OH)_2$ fell only 10%, a result that stems from the electrostatic repulsion in the brush. The Ru ion responded strongly to changes in pH, with the brush effectively blocking transport at lower pH values, while the Fe compound only weakly depended on pH. However, following quaternization both compounds could not transport through the brush, suggesting the strong polyelectrolyte suppresses all ion transport regardless of charge or character.

A cationic selective gate has been reported that consists of mesoporous silica modified with poly(methacryloyl-L-lysine) (PML) brushes[164]. These brushes contain a primary amine and carboxylic group. Above the pK_a of the carboxylic group (pH > 5), the walls of the silica pore and the polymer brush are negatively charged, allowing the selective passage of cations in solutions. Below a pH value of 5, however, the silica wall remains anionic, but the amine protonates and becomes cationic. As a result, both cations and anions are repelled from the pore. Similar pH sensitive gates have been reported using P4VP[165] and phosphate-bearing polymer brushes[166].

2.3.3 Manipulating Nanoparticles

Nanoparticles have presented the possibility of many innovative applications in several diverse fields, including (but not limited to) catalysis, gas separation, or drug delivery agents. While the high surface area to volume ratio of these particles facilitates many of their practical properties, it also makes preventing aggregation and flocculation challenging. Polymers adsorbed to the surface of particles have offered one means of stabilizing particles due to the steric interactions of the polymer chains that maintain a large enough interparticle distance to prevent flocculation. In some instances, these polymers allowed further PPM to tailor particle properties[167]. As the understanding of science

at the nanoscale has grown, so has the possibility of using polymer brushes on nanoparticles for more than just preventing aggregation.

Research topic combining nanoparticles and polymers is broad and voluminous. As such, we have attempted to limit the scope of this section to representative and recent examples that heavily feature PPM of polymer brushes. For further reading beyond this review, the reader is directed to a number of previously published reports on related topics[168–173].

2.3.3.1 Particle Supports

Recently, a new approach to the problem of preventing nanoparticles aggregation has used polyelectrolyte brushes as a matrix to synthesize nanoparticles from metallic counter ions in the brush, including silver[174–176], gold[177,178], palladium[179,180], various metal oxides[180–182], and quantum dots[182–184]. While the typical matrix is a spherical polyelectrolyte brush on a polystyrene colloid, examples of embedded brushes on flat substrates[174,183], TiO_2 nanowires[180] and carbon nanotubes[182] have also appeared. One innovative approach was reported by Liu *et al*, who grew quaternized PDMAEMA brushes from a cotton substrate, then exchanged and reduced Pd-based counterions to produce Pd NPs[185]. The resulting fabric comprised a conductive metal/cotton yarn that was durable enough to withstand multiple washing cycles without loss of properties (*cf.* **Figure 2.13**).

As a highlight of the application of these NP embedded brushes, Proch *et al* reported the efficiency of quaternized PDMAEMA spherical brushes loaded with Pd NPs in catalyzing Heck and Suzuki coupling reactions[186]. Their findings demonstrated that these catalyst systems are insensitive to air and moisture, and capable of recycling without loss of activity. Another example reported a spherical polyelectrolyte brush with embedded Au-Pt alloy nanoparticles[187]. By exchanging only a fraction of the ions originally present in the brush with $[AuCl_4]^-$, sites still existed for further exchange with $[PtCl_6]^{-2}$ ions. From here, reduction of the ions leads to bimetallic Au-Pt nanoparticles. The alloy nature of the particles was proven by TEM as shown in **Figure 2.14**.

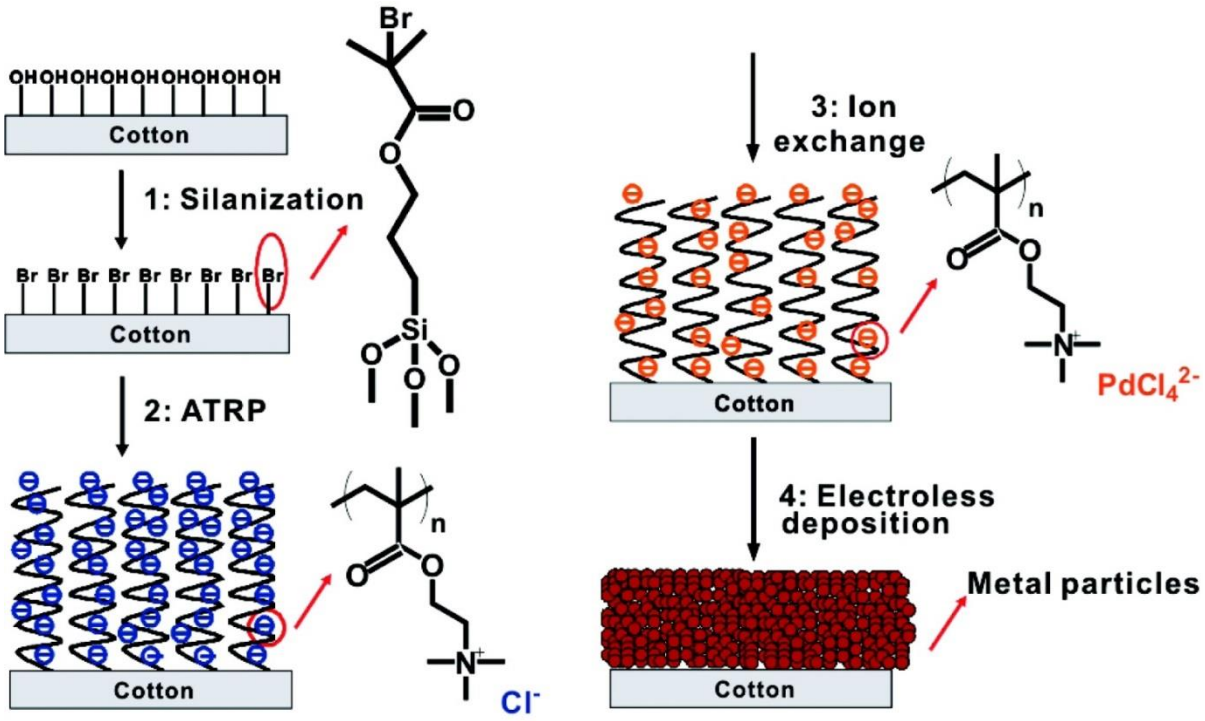

Figure 2.13. Schematic illustration of the process of preparing conductive cotton yarns. The dimension is not drawn to scale. Reproduced with permission from the American Chemical Society[185].

While the particles form, the brush thickness decreases drastically, possibly due to negative charges on the nanoparticle surface interacting with the cationic brush. This interaction results in very stable systems without the need for a stabilizing ligand on the particle, improving catalytic reactivity, and no detectable leaching of heavy metals. The catalytic activity of the embedded particles was tested for the conversion of alcohols to ketones and aldehydes. Many conversions proceeded to completion, particularly for aryl compounds, which possess a high affinity for the metal surface. Aliphatic compounds showed markedly less reactivity.

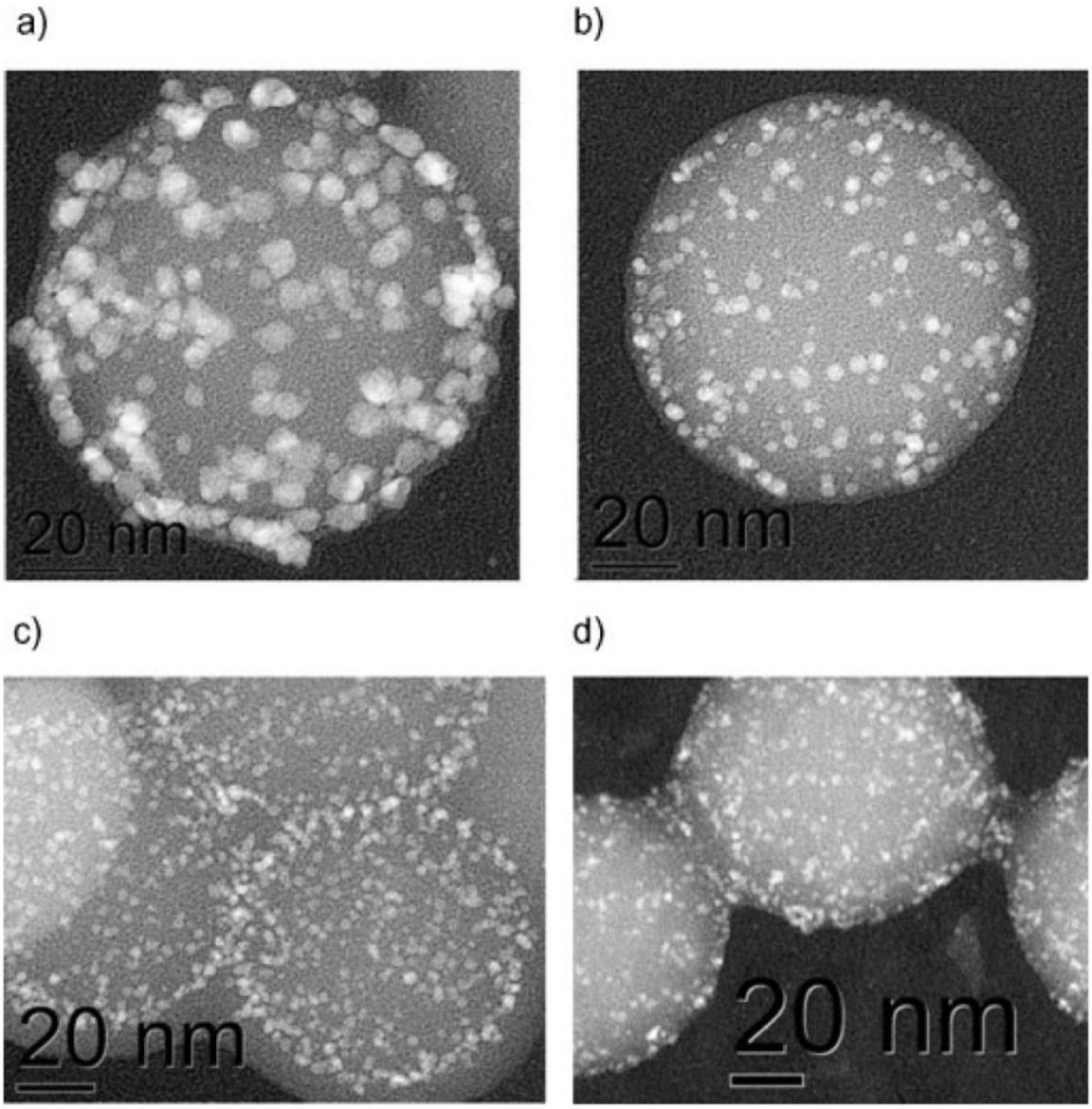

Figure 2.14. TEM images from samples a) Au73Pt27, b) Au55Pt45, c) Au45Pt55, and d) Au25Pt75. For sake of clarity the contrast has been inverted. Reproduced with permission from Wiley[187].

A field related to *in situ* particle formation is mineralization of polymer brushes. PDMAEMA brushes quaternized with bromoethane, then ion exchanged with fluorine ions provided a suitable substrate for silicification[188]. Incubating the modified PDMAEMA brushes in a monosilicic acid solution resulted in the formation of a rough silica film. In this case, PDMAEMA served as a

synthetic substitute of naturally occurring, amine-bearing peptides that induce silicification. Next, fluorinated silanes were deposited on the silica film, creating a super hydrophobic surface that demonstrated a water contact angle of 160°, compared to 15° for the silica surface.

The Klok group reported the effect of polymer brushes on the mineralization of calcium carbonate ($CaCO_3$)[189]. Homopolymer brushes of PMAA were grown with varying grafting densities and exposed to a supersaturated $CaCO_3$ solution. Low density brushes produced calcite crystals, while high density brushes resulted in the formation of an amorphous carbonate layer. Interestingly, the water contact angle behavior of the brushes and $CaCO_3$ layers mimicked each other at a given brush density (*cf.* **Figure 2.15**).

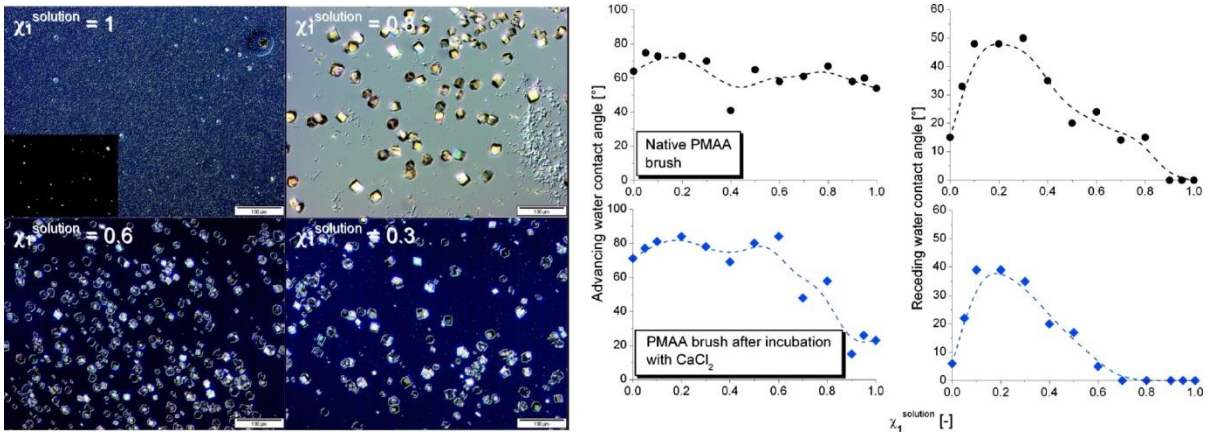

Figure 2.15. (left panel) Differential interference contrast (DIC) micrographs of mineralized PMAA brushes of varying grafting density. The insert in the image of the brush generated from a surface modified with $\chi_1^{solution} = 1.0$ was taken between crossed polarizers and illustrates the amorphous nature of the deposited $CaCO_3$ layer. (right panel) Advancing and receding water contact angles on PMAA brushes with varying grafting densities before and after incubation with aqueous 10 mM $CaCl_2$ solution. Polymerizations were carried out at 25°C and pH 9 for 30 min using the following polymerization conditions: NaMA/CuBr/$CuBr_2$/bipy/water = 200:2:0.4:5:1400. Reproduced with permission from the American Chemical Society[189].

2.3.3.2 Patterning Nanoparticles

The previous examples aimed to keep nanoparticles from coming together. In other situations, the goal is to create regions of high nanoparticle density on a surface. Given their ability

to modify surface properties and chemistries, polymer brushes offer one way to achieve efficient, well-controlled patterning of colloidal particles.

Tokareva *et al* reported an early example of P2VP brushes with citrate capped Au NPs adsorbed to the brush layer. By modulating the pH (*cf.* Section 2.1), the brushes collapsed or swelled, altering the distance between the NPs. This change in distance could be detected as a shift in the surface plasmon resonance signal, providing the basis of a pH sensitive sensor[190]. A similar approach has been used with Ag NPs on planar brushes[191]. The brushes maintained pH responsiveness due to their charged state; the authors used UV-Vis to determine changes in conformation as a function of pH. Similarly, Au NPs adhered to a neutral polymer brush[192] detected brush conformational changes due to solvent quality using UV-Vis. Finally, Au NPs adsorbed on temperature responsive PNIPAAm brushes used as temperature sensors have been reported[193].

While the above examples attempted to confine nanoparticles homogeneously to a polymer brush, it is possible to produce spatially heterogeneous NP patterns using PPM reactions[194]. Bhat and coworkers have investigated the interplay between gold nanoparticles and different parameters of the polymer brush, specifically the grafting density (σ), molecular weight (MW), and functional groups of the polymer chains[195]. In order to probe a wide range of parameter space, orthogonal gradients were prepared that varied in MW and σ, thereby creating a continuous range of data points on a single sample. Citrate-capped gold nanoparticles, which were previously shown to interact through the combination of hydrogen bonding and electrostatic interactions with the amine group in PDMAEMA, adsorbed to the brush with increasing density as MW and σ increased. The work points out that the size of the particles will affect behavior in the brush system, and that the relatively large particles (16 nm) do not penetrate into the brush, hence a monotonic increase in adsorption relative to both MW and σ. Smaller particles are expected to demonstrate a maximal value at an intermediate σ value, after which point the osmotic pressure in the brush negates the favorable chemical interactions. The experimental findings were in accord with the theory of Kim and O'Shaughnessy, who predicted that the depth inside the brush into which the nanoparticles penetrate depends on the interplay among the particle size, σ, and MW of the chains in the brush[196].

The previous example aimed to explore the effects σ and MW have on nanoparticle adsorption; it also demonstrates a facile post-polymerization patterning method. Since the concentration of adsorbed nanoparticles follows the polymer brush gradient, then a gradient in nanoparticle concentrations has also been created. The polymer phase thus acts as a molecular

template for the nanoparticles. While physical properties of the polymer brush do provide a means for assembly, chemical functionality in the pendant or terminal groups governs particle adsorption within specific sites in the brush. Building on this idea, Diamanti *et al* used a post-polymerization reaction combined with microcontact printing to produce arbitrarily shaped regions on a polymer brush that would preferentially adsorb nanoparticles[197]. Brushes of PHEMA were grown on a silicon wafer via ATRP, then activated with N,N'-disuccinimidyl carbonate (DSC) following the scheme in **Figure 2.16**. Subsequent coupling reactions with amino terminated molecules incorporated PEG50, PEG20, C16, or C8F15 into the brush, where the number indicates the number of ethylene glycol repeat units in the PEG moieties, or atomic composition of the alkyl and fluoroalkyl moieties. The location of these coupling reactions was controlled using a patterned PDMS stamp. Exposure to 30 nm citrate-capped Au nanoparticles proved that regions of heightened (PEG50 > PEG20 > PHEMA) and depressed (PHEMA > C16 > C8F15) adsorption could be created as shown in **Figure 2.16**. Incorporating a second reactant into the unpatterened (*i.e.*, unreacted) regions through a backfilling reaction provides a means to create confined regions of high nanoparticle density.

Finally, Yu *et al* used block copolymer brushes of P2VP-*b*-PAA to incorporate a pH control over sulfonated PS nanoparticle adsorption[183,198] using the principles of PPM of weak polyelectrolytes discussed previously. Since the sulfonated particles are strong polyelectrolytes, their negative charges are always present regardless of pH and in the absence of external salt. The researchers adjusted the net charge of the polymer brushes by controlling the solution pH. Incubation of the brushes in NP solutions with pH values of 1.5 and 11 revealed that the particle adsorbed readily in the acidic solution, but not the basic solution. Since the sulfonated PS NPs are anionic, this result is explained readily by considering the cationic charges present in the P2VP block at acidic pH values, and the anionic charges in the PAA block at basic pH values.

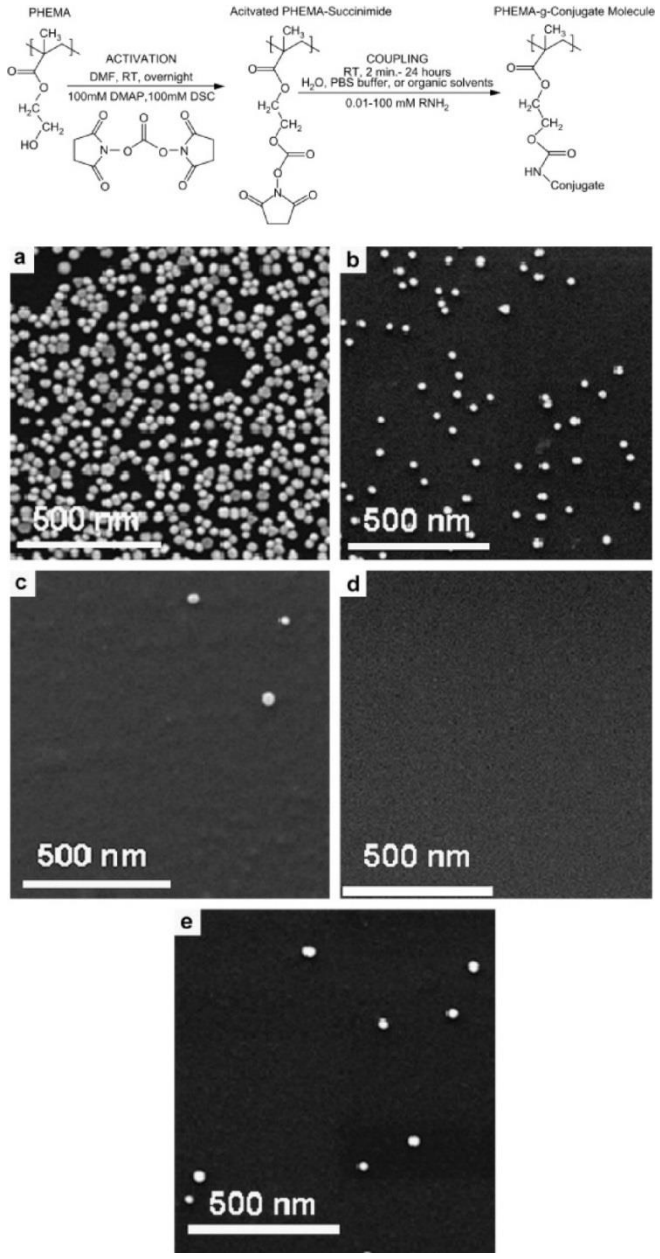

Figure 2.16. (top panel) Functionalization of PHEMA side chain using DSC activation and subsequent amination. (bottom panel) Relative affinity of post-functionalized PHEMA brushes to adsorption of 30 nm citrate-capped Au nanoparticles. (a) PHEMA-g-PEG50 (130±15 NP/mm^2); (b) PHEMA-g-PEG20 (41±6.8 NP/mm^2); (c) PHEMA-g-C16 (0.8±0.2 NP/mm^2); (d) PHEMA-g-C8F15 (0 NP/mm^2); (e) pristine PHEMA (3.2±1.8 NP/mm^2). Reproduced with permission from Elsevier[197].

2.3.4 Incorporating Biological Moieties into Polymer Brushes

Post-polymerization modification presents an attractive avenue to incorporate biomolecules into a polymer brush. This approach avoids the need to produce exotic monomers and leads to high densities of the incorporated biological groups. A number of different types of compounds have been inserted into tethered polymer systems in this manner, including proteins and peptides, enzymes, and nucleosides, to name a few. This is a very rich and active research field. The following sections are meant to illustrate the various activities rather than provide a comprehensive overview of the entire field.

2.3.4.1 Peptide/Protein Immobilization

Tethering proteins to synthetic macromolecules has received due attention in a number of recent reviews[199–204]. PPM reactions play a pivotal role in this technology because the bulkiness of proteins makes it impossible to polymerize protein-modified monomers. Furthermore, while most immobilizations occur on flat surfaces or spherical brushes[205,206], fibers[94,207,208], and star-shaped, cross-linked coatings, which outperformed their linear brush analog[86] have also been reported. A number of different tethering pathways are possible, including those outlined below.

In the realm of protein chromatography a glycidyl methacrylate (GMA) polymer backbone has proven versatile for modifying column packing[94], allowing the incorporation of a variety of functional groups (*cf.* **Figure 2.17**) that act as tethering points for proteins. Ito *et al* used a GMA-based brush and modified the pendant epoxy rings with diethylamino groups with served to bind bovine serum albumin (BSA). They demonstrated that polymer brushes bound more BSA than a gel network in a chromatography system[208]. Bayramoglu *et al* also used a spherical GMA brush and modified it with hydrazine to attach the enzyme *Invertase*[205].

Modifying polymer brushes with 1-Ethyl-3-[3-dimethylaminopropyl]carbodiimide hydrochloride (EDC) and N-hydroxysuccinimide (NHS) to create an activated ester is a common approach to tethering proteins, depicted in **Figure 2.18**. For example, researchers modified a PHEMA brush grown from an alumina substrate using the EDC/NHS coupling chemistry to incorporate a Cu complex that bound BSA[209]. Jain *et al* employed a similar approach with PHEMA and poly(2-(methacryloyloxy)ethyl succinate) (PMES) brushes[210]. Another common platform for tethering proteins involves brushes made with poly(oligo(ethylene glycol) methacrylate) (POEGMA). By activating the hydroxyl-terminal groups using either carbonate[211] or carbodiimide[212] derivatives in

conjunction with dimethylaminopyridine (DMAP), proteins can be tethered to these brushes without affecting the non-fouling nature of the native EG groups.

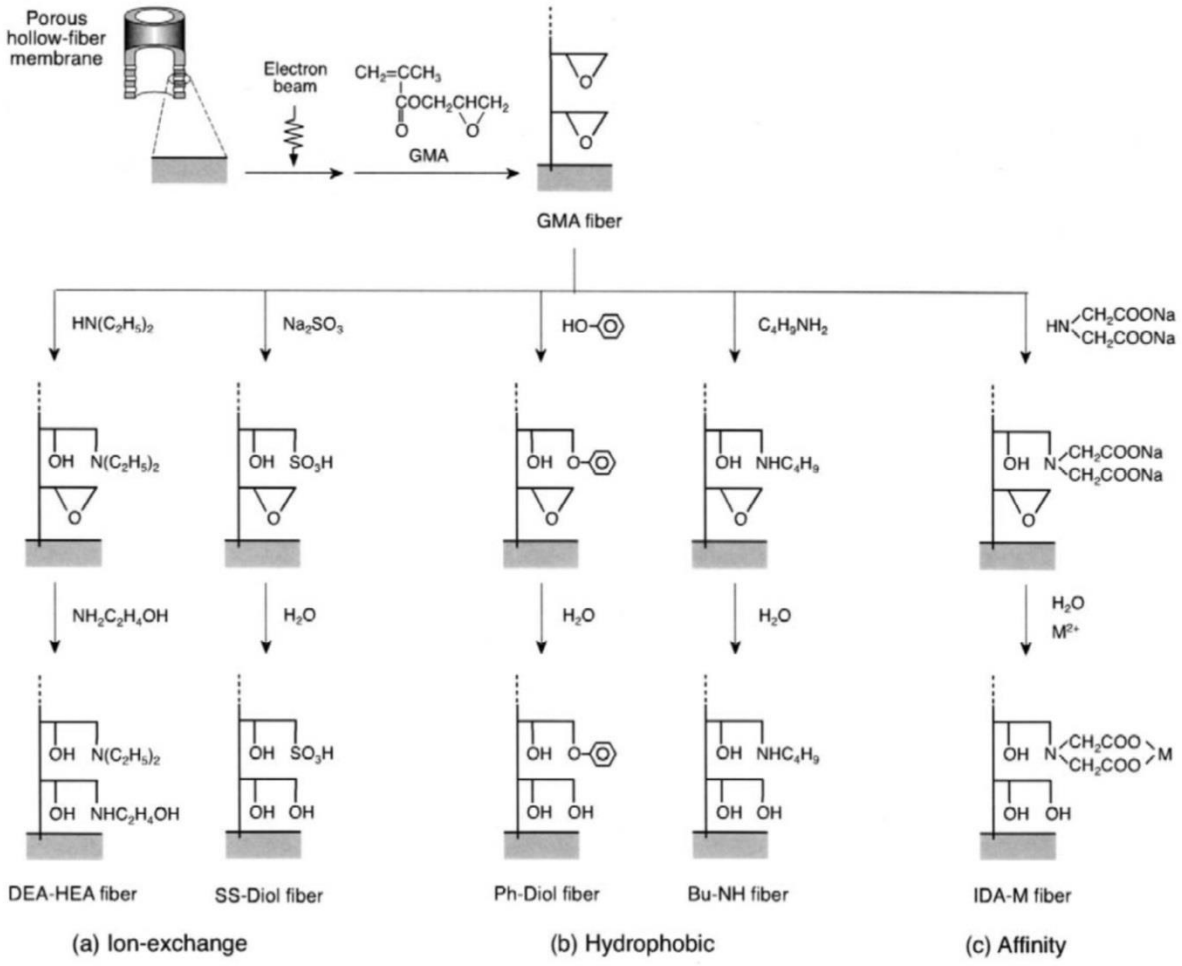

Figure 2.17. Preparation scheme of functional polymer brush grafted onto the pore surface of a porous hollow-fiber membrane. Reproduced with permission from Elsevier[94].

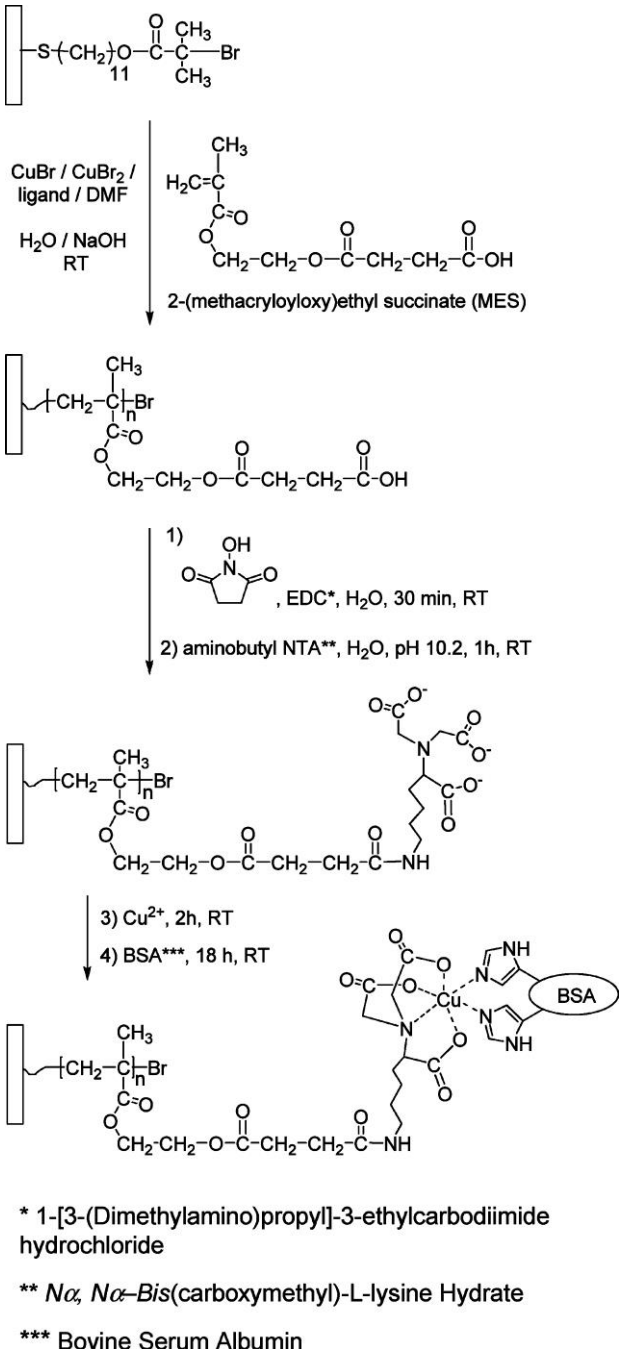

Figure 2.18. Synthesis of protein-binding poly(MES) brushes on Au surface. Reproduced with permission from the American Chemical Society[209].

The 1,3-dipolar cycloaddition between an azide and alkyne group (the so-called "click" reaction, *cf*. **Figure 2.4**) has also served to immobilize proteins, as well as DNA, to the terminal groups of polymer brushes. Chen *et al* demonstrated this approach by spin-coating solutions of appropriately modified DNA onto end-modified polymer brushes[213]. The authors controlled the grafting density simply by changing the concentration of the DNA solution. They also noted that more hydrophilic polymers tended to have higher immobilization efficiencies, and better non-specific adsorption performance (*cf*. **Figure 2.19**).

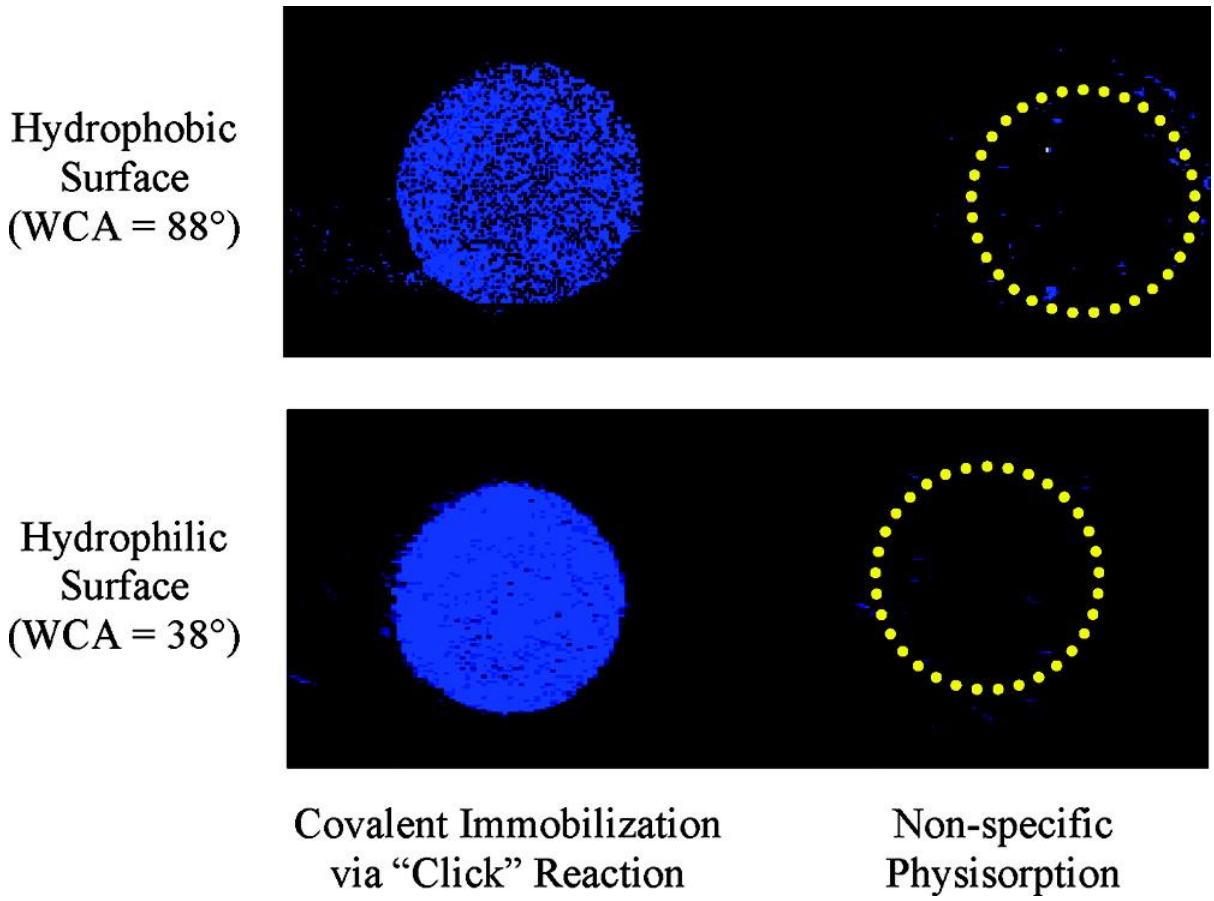

Figure 2.19. Scanned fluorescence images of DNA (N3-20mer-FAM) immobilization on hydrophobic (top) and hydrophilic (bottom) surfaces via "click" reaction (left) and nonspecific physisorption (right). The spin-coating solution concentration is 0.5%. Reproduced with permission from the American Chemical Society[213].

Electrostatics also offers a means to immobilize proteins onto polymer brushes. In this case, charged patches on the surface of the protein interact with the opposite charges present in a polyelectrolyte brush. Henzler *et al* demonstrated this mechanism using PAA spherical brushes and β-*glucosidase*, as well as suggesting the use of isothermal titration calorimetry (ITC) to determine enzyme activity in polymer brushes[206]. Reichhart and Czeslik established that lysozyme, BSA, α-lactalbumin, and insulin do not denature upon adsorption into PAA brushes[214]. The authors also found that low ionic strength favored protein adsorption regardless of the proteins net charge. Furthermore, de Vos *et al* examined the role of ionic strength, pH, and protein concentration on adsorption in a planar PAA brush[215]. Recently, Ballauff's group has shown that adsorption in the low ionic strength case leads to a release of a counterion, resulting in entropy as a driving force for adsorption[216].

2.3.4.2 Protein Microarrays

Microarrays offer a convenient platform to quantify protein concentration and interactions over a wide range of parameter space and with limited sample[217]. Polymer brush-based protein microarrays offer the advantages of high functional group density and reduced steric hindrance relative to monolayers, and in some cases, innate non-fouling properties to minimize non-specific adsorption[218].

A number of research groups have used the POEGMA activation approach to create micropatterned, protein-tethered polymer brushes. Notably, Tugulu *et al* created microarrays of polymer brushes functionalized on the side chain[219], while Waichman *et al* modified the terminal groups of a PEG-based brush[220]. Trmcic-Cvitas *et al* created similar arrays and demonstrated the efficiency of a number linker groups added at the hydroxyl group used to immobilize streptavidin[221], with the results summarized in **Figure 2.20**.

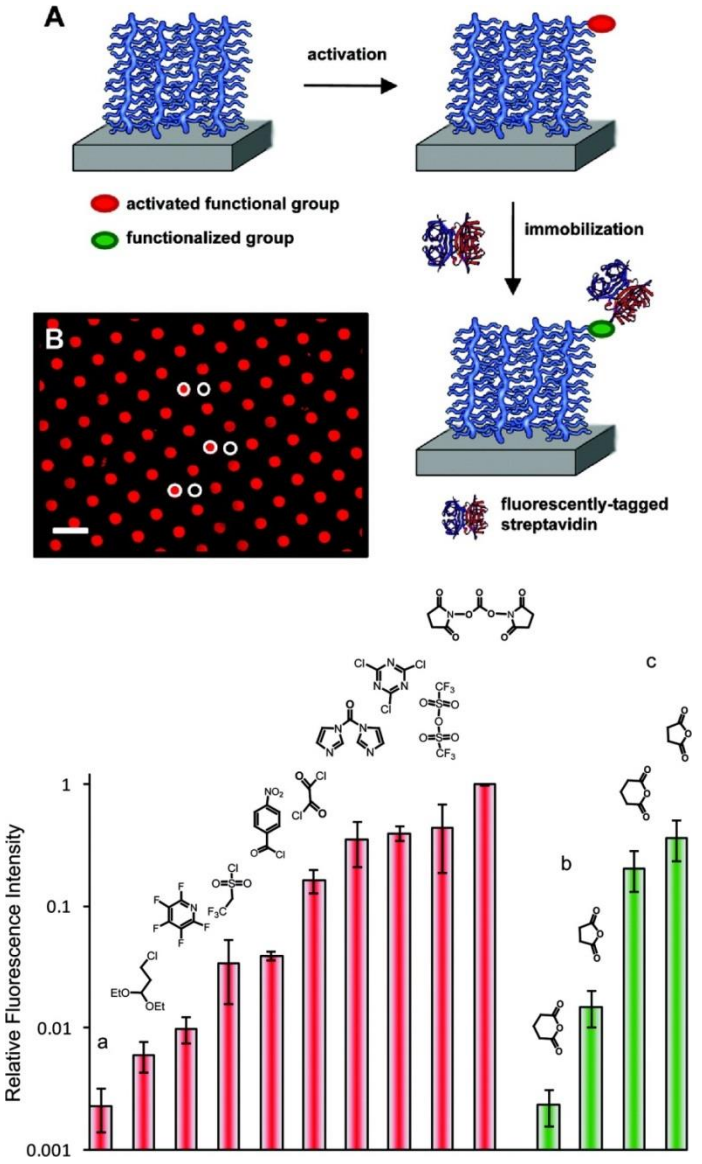

Figure 2.20. (top panel) (A) Direct immobilization of proteins on polymer brushes in a two-step process. (B) Protein (SA bearing a fluorescent tag, chromeon 546 nm) immobilization levels were determined by fluorescence assay. The average fluorescence intensity in zones delimited by the white rings was measured for a brush coated area and a bare gold area. Scale bar: 50 μm. (bottom panel) SA immobilization levels (determined by fluorescence assay) on POEGMA-360 brushes using a range of coupling agents. Red bars: hydroxyl-terminated brushes were directly activated with the corresponding coupling agents depicted (a, no coupling agent) before incubation for 18 h in a SA solution. Green bars: hydroxyl-terminated brushes were first functionalized with glutaric or succinic anhydride and incubated with SA (b) without NHS/EDC activation and (c) with NHS/EDC activation. Error bars represent standard deviations for n = 3. Reproduced with permission from the American Chemical Society[221].

Alternatively, Yun *et al* surface grafted poly(tetrafluoro ethylene) (PTFE) surfaces with a polymer brush based on a 2-(2-diazo-3-oxo-butyrloxy)ethyl methacrylate (DOBEMA) monomer[222]. This monomer contains a diazoketo group that undergoes a Wolff rearrangement upon UV irradiation, generating a carboxyl group[223]. The location of these carboxyl groups is controlled using a mask during UV irradiation. Subsequent modification of the carboxyl groups with an amine-functionalized biotin, which acts as a protein binding site for streptavidin. The high lateral resolution of the features fabricated by this method is apparent from the images shown in **Figure 2.21**.

Finally, Zou *et al* used a polymer brush of poly-*N*-(2,3-dihydroxypropyl) acrylamide (PDHPA) in combination with photolithography and chemical etching to produce patterned regions of aldehyde-functionalized brushes[224]. These regions were then functionalized with streptavidin. The unmodified PDHPA regions demonstrate good prevention of non-specific adsorption.

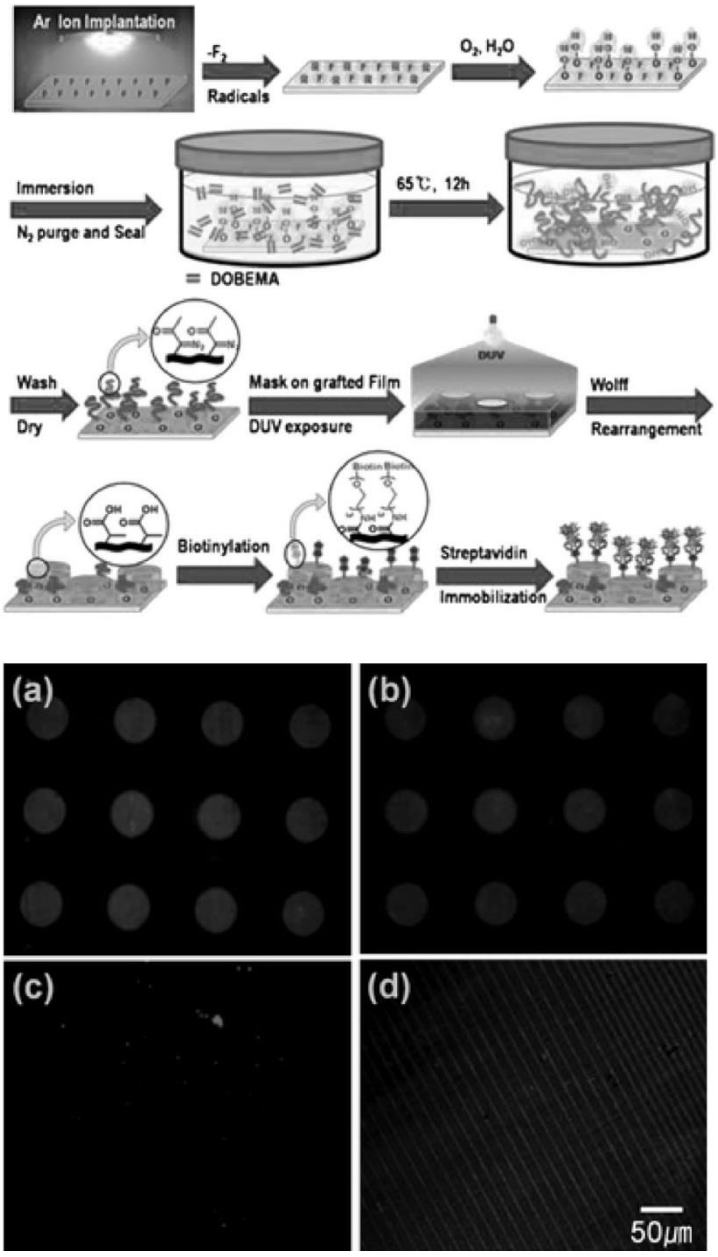

Figure 2.21. (top panel) Illustration of graft polymerization, UV exposure, and protein immobilization. (bottom panel) Confocal fluorescence images of SAv-Rh immobilized on biotinylated region of 12 h graft-polymerized PTFE films prepared under different ion-irradiation conditions; circle patterns (50 μm) (a) at 5×10^{14} ions/cm^2, (b) 1×10^{15} ions/cm^2, (c) 5×10^{15} ions/cm^2, and (d) finer line (5 μm) patterns at 5×10^{14} ions/cm^2. Reproduced with permission from the Royal Society of Chemistry[222].

2.3.4.3 Enzymatic Activity

Enzymes represent a special class of proteins that catalyze biochemical reactions. Incorporation of these molecules into polymer brushes represents a promising platform for catalytic technologies. As the examples below show, polymer brushes offer high rates of loading and protection from denaturation relative to monolayers of enzymes.

Goto *et al* described a hollow-fiber, polyethylene system grafted with GMA that was either unmodified, or modified with diethylamine (DEA) groups or hydroxyl groups (*cf.* **Figure 2.17**, which depicts a similar procedure)[207]. The authors then immobilized *Lipase* on the polymer brushes. An esterification reaction between lauric acid and benzyl alcohol tested the activity of the immobilized enzymes. The researchers found that hydroxyl-modified GMA fibers demonstrated the highest enzymatic activity (compared to free lipase), and retained the majority of this activity over three batch reaction cycles (24 hours each). The authors noted that water retained in these modified brushes protected the *Lipase* from the organic solvent, and activated its enzymatic activity. While DEA-modified brushes retained more water, their ionic character led presumably to denaturing of the enzyme.

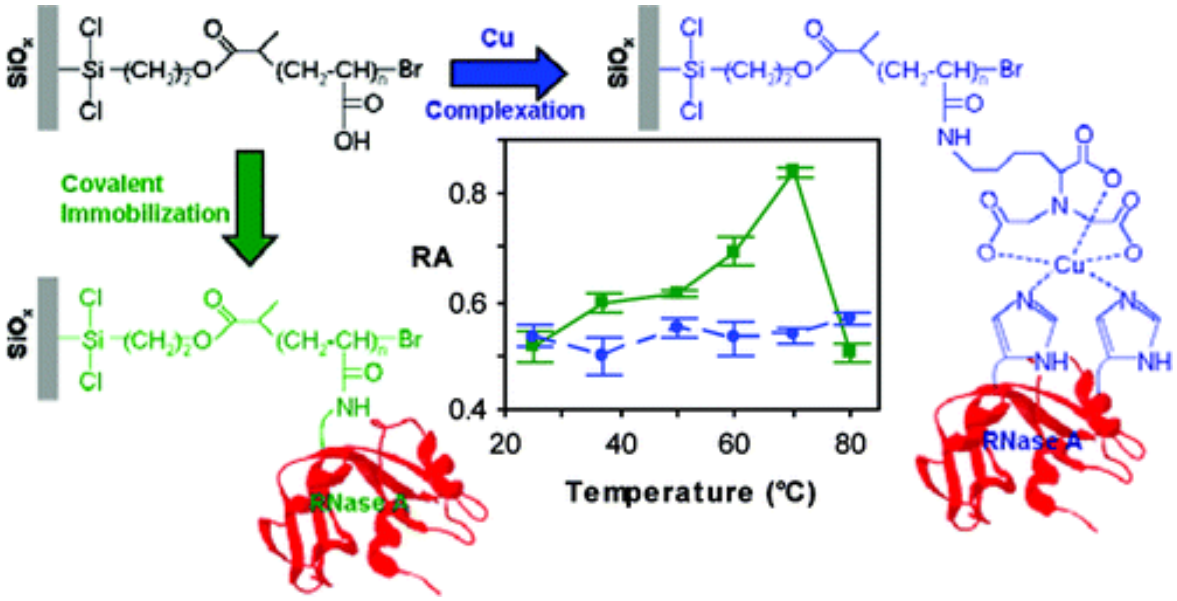

Figure 2.22. Polymeric brushes as functional templates for immobilizing Ribonuclease A. Reproduced with permission from the American Chemical Society[225].

As stated in the protein immobilization section above (Section 3.4.1), a number of methods can be employed to bind a protein to a polymer brush, *i.e.*, including hydrophobic interactions, ionic and metal complexing, and standard covalent bonding. Cullen *et al* explored the effect of the latter two on enzyme activity by immobilizing *RNase A* using the familiar EDC/NHS combination with a PAA brush, followed by direct covalent attachment or by a copper complex[225]. The authors note that if the histidine residues that create the copper complex lie in the active site of the enzyme, its activity will diminish. As shown in **Figure 2.22**, the metal-complexed enzyme exhibits essentially no temperature dependence, whereas the covalently-bound enzyme does (the researchers note it is similar to the free enzyme). It is apparent from this result that the method of immobilization plays an important role in protein-modified brushes. In a separate report[93], Cullen *et al* developed a facile immobilization route that used a ring-opening reaction in a poly(2-vinyl-4,4-dimethylazlactone) brush to covalently attach enzymes. They reported positive results regarding immobilization amount and retained activity.

Immobilized enzymes have also formed the basis of sensors. Zhang *et al* reported the development of a glucose sensor that consisted of a GOx and ferrocene-modified polymer brush on an ITO substrate[226]. In this system, when the GOx moieties are exposed to glucose, it leads to the reduction of the ferrocene moieties, which results in an increased current. The group compared brushes with two different spatial arrangements. The first had the GOx containing portion of the brush adjacent to the ITO substrate, and the ferrocene-modified portion grown above it. The second case possessed the reverse arrangement. The authors report that the latter case proved more sensitive to glucose, which makes physical sense given the sequence of events that lead to a signal.

2.3.4.4 Antibody Immobilization

Iwata *et al* used brushes composed of 2-methacryloyloxyethyl phosphorylcholine (MPC) and GMA as substrates to immobilize Fab' fragments[227]. Modification of the GMA units incorporated a disulfide linkage that served as the immobilization site of the antibodies. The authors found that antigen recognition occurred better in brushes containing MPC units (which are biocompatible), than brushes composed solely of GMA. The MPC-bearing brushes also performed better during non-specific adsorption tests. In a follow up report, Iwasaki *et al* grew the same brush system on silicone nanofilaments and smooth Si wafers[228]. The report found approximately 65x higher loading of Fab' fragments in the nanofilament samples compared to the smooth samples.

2.3.4.5 Peptide Separations

The Zauscher and Dyer groups produced a "nanosponge" system to separate peptides of opposite charges (buccalin and bradykinin)[229]. The sponge consisted of a polymer brush composed of 70% poly(N-isopropyl acrylamide) (PNIPAAm) and 30% PMAA. Under pH neutral and basic conditions, some of the PMAA monomers deprotonated, which led to swelling the brush due to electrostatic repulsion. At that point, exposing a solution of bradykinin (cationic at pH 7) and buccalin (anionic at pH 7) led to the adsorption of bradykinin by the anionic brush. The fractionation of the two peptides took approximately one minute, and the separation was confirmed by matrix-assisted laser desorption/ionization – mass spectrometry (MALDI-MS) analysis (*cf.* **Figure 2.23**). Exposing the brush to 10% formic acid solution (pH ≈1.9) caused the PMAA monomers to protonate, and the neutral brush collapsed while expelling the adsorbed bradykinin, which was confirmed by MALDI-MS. This process took approximately one minute. A clean separation of the two peptides took two minutes, compared to an hour when using commercially available high-performance liquid chromatography (HPLC) protocols.

2.3.4.6 Carbohydrate Containing Polymer Brushes

Ayres *et al* have reported on the synthesis of a polymer brush analog of sulfonated glycosaminoglycan (S-Glc) [230]. Starting from a monomer bearing protected hydroxyl groups, the researchers grew brushes from Si wafers, followed by a deprotection step to generate the Glc functional groups. Next, a sulfonation reaction resulted in the final product with S-Glc side chains (*cf.* **Figure 2.24**). Standard *in vitro* assays demonstrated the improved blood compatibility of the sulfonated sugar compared to the unmodified sugar.

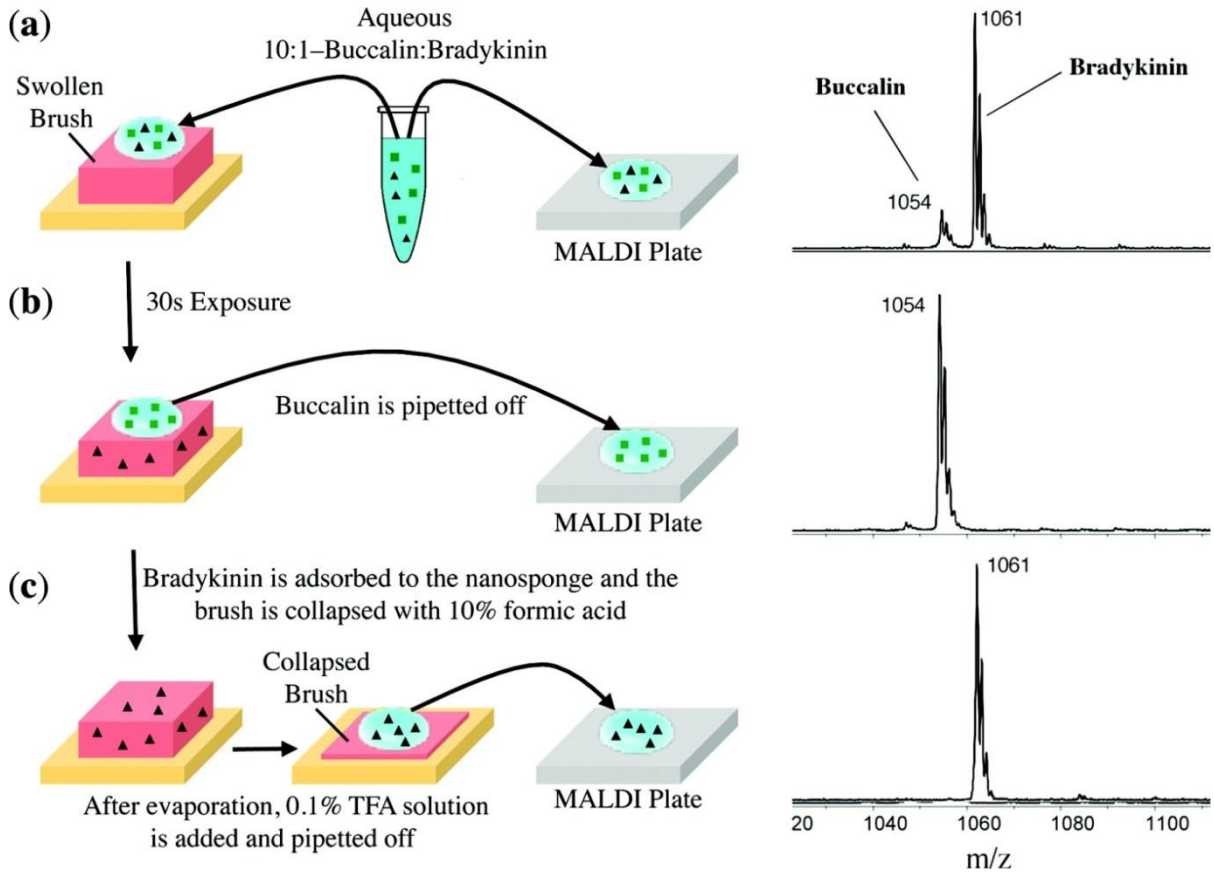

Figure 2.23. (a) A mixture of bradykinin (+ charge at pH 7) and buccalin (− charge at pH 7) is placed on a brush nanosponge-coated gold surface (w/copolymer **1**) and on a conventional MALDI plate. Since buccalin has reduced ionization efficiency in the presence of bradykinin it has a weak MALDI signal even though there is a 10-fold excess of buccalin to bradykinin in solution. (b) After 30 s exposure, the bradykinin has been adsorbed by the nanosponge brush and the eluent is removed and placed onto a conventional MALDI plate; only buccalin is detected. (c) The nanosponge is then 'squeezed' by treating with a drop of 10% formic acid, which collapses and neutralizes the brush and releases the bradykinin for subsequent MALDI analysis. Reproduced with permission from the American Chemical Society[229].

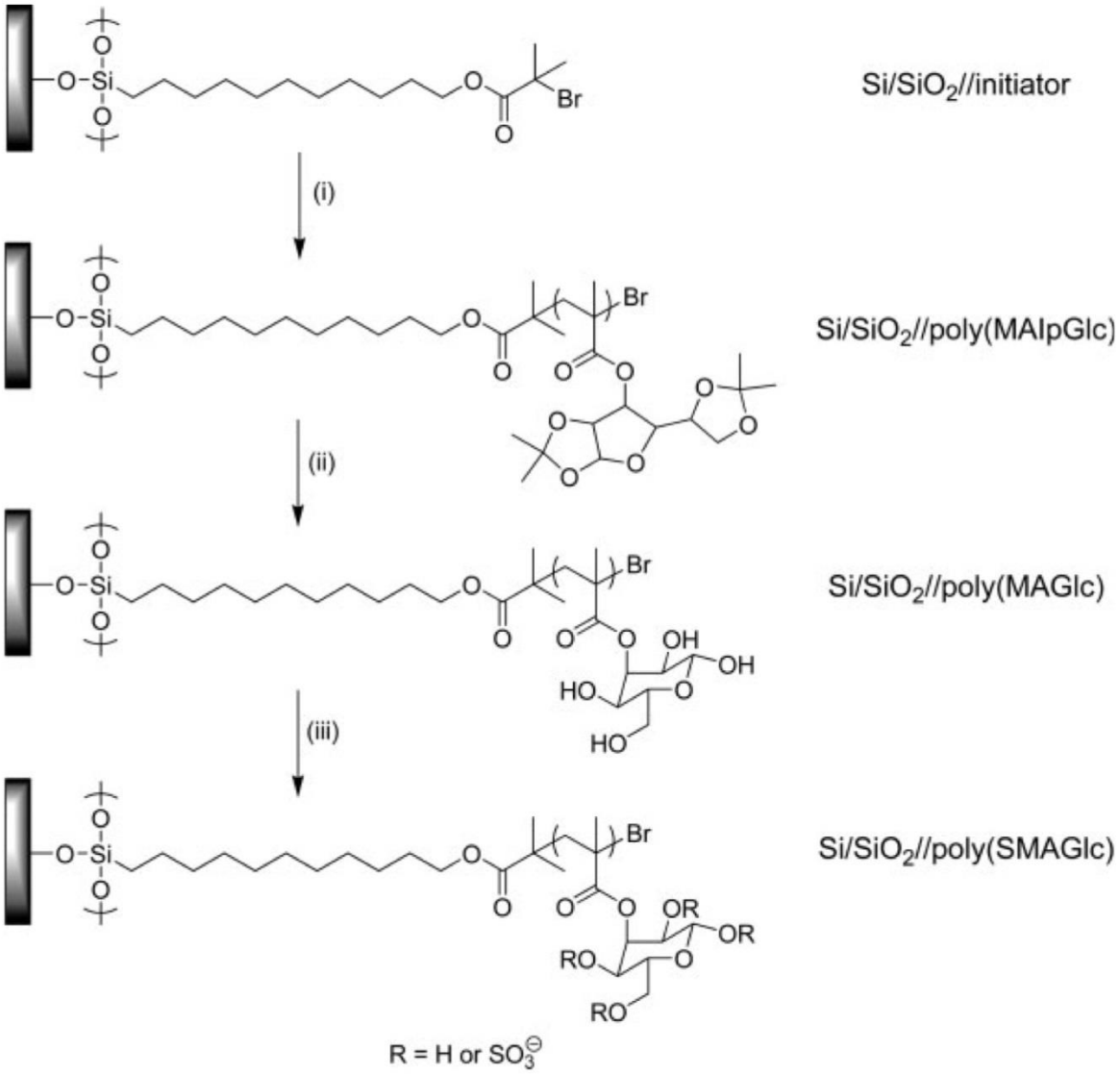

Figure 2.24. Synthetic ATRP strategy for the preparation of Si/SiO2//poly(SMAGlc) polymer brush. (i) 10/3 v/w monomer solution in veratrole, DP_{theo}=200, 12 h, 85 °C; (ii) 80% TFA solution, 30 min, RT; (iii) 0.2 M SO_3·py solution in anhydrous pyridine, 2 h, 85 °C, sat. $NaHCO_3$ solution. Reproduced with permission from Wiley[230].

2.3.5 Cellular Studies

Physical and chemical properties of an interface influence the behavior of cells both *in situ* and *ex situ*. Polymer brush coatings offer the possibility of modifying both of these properties, and as highlighted below, can lead to substrates designed to kill or grow cellular organisms.

2.3.5.1 Biocidal Surfaces

One important area of research in the field of polymer brushes concerns sterile and sterilizing surfaces[231,232]. By introducing appropriate chemical functionalities into a polymer brush, significant levels of biocidal activity occur. Ag nanoparticles and ions have been noted for their use as biocidal agents. Ramstedt *et al* synthesized brushes of poly(3-sulfopropylmethacrylate) on Si surfaces, then ion exchanged Ag^+ ions into the brush. As seen in **Figure 2.25**, the Ag^+ loaded brushes prevented effectively bacterial growth. One aspect of using ions as a killing agent that must be considered is their ability to leach out of the brush[233,234]. While this phenomenon does create a zone of inhibition around the substrate that might be useful in some applications, and can be controlled by using different types of silver compounds, other situations will call for a well-controlled area of biocidal activity. In these cases, biocidal agents other than ions must be used.

Quaternary ammonium groups display high levels of biocidal activity, and significant research has examined their use as sterilizing coatings. Huang *et al* used the "grafting to" approach to produce copolymer brushes of DMAEMA and 3-(trimethyoxysilyl)propyl methacrylate (TMSPMA)[235]. The biocidal activity increased with increasing quaternary ammonium density, but not with polymer-brush chain length. Interestingly, for the same density of QA groups, the "grafting to" approach resulted in higher cell death rates than "grafting from", though "grafting to" cannot produce as high of densities (*cf.* **Figure 2.26**). A method to produce high densities using "grafting to" would prove more compatible for a high-throughput industrial coating process, as it obviates the need for a sequential polymerization step.

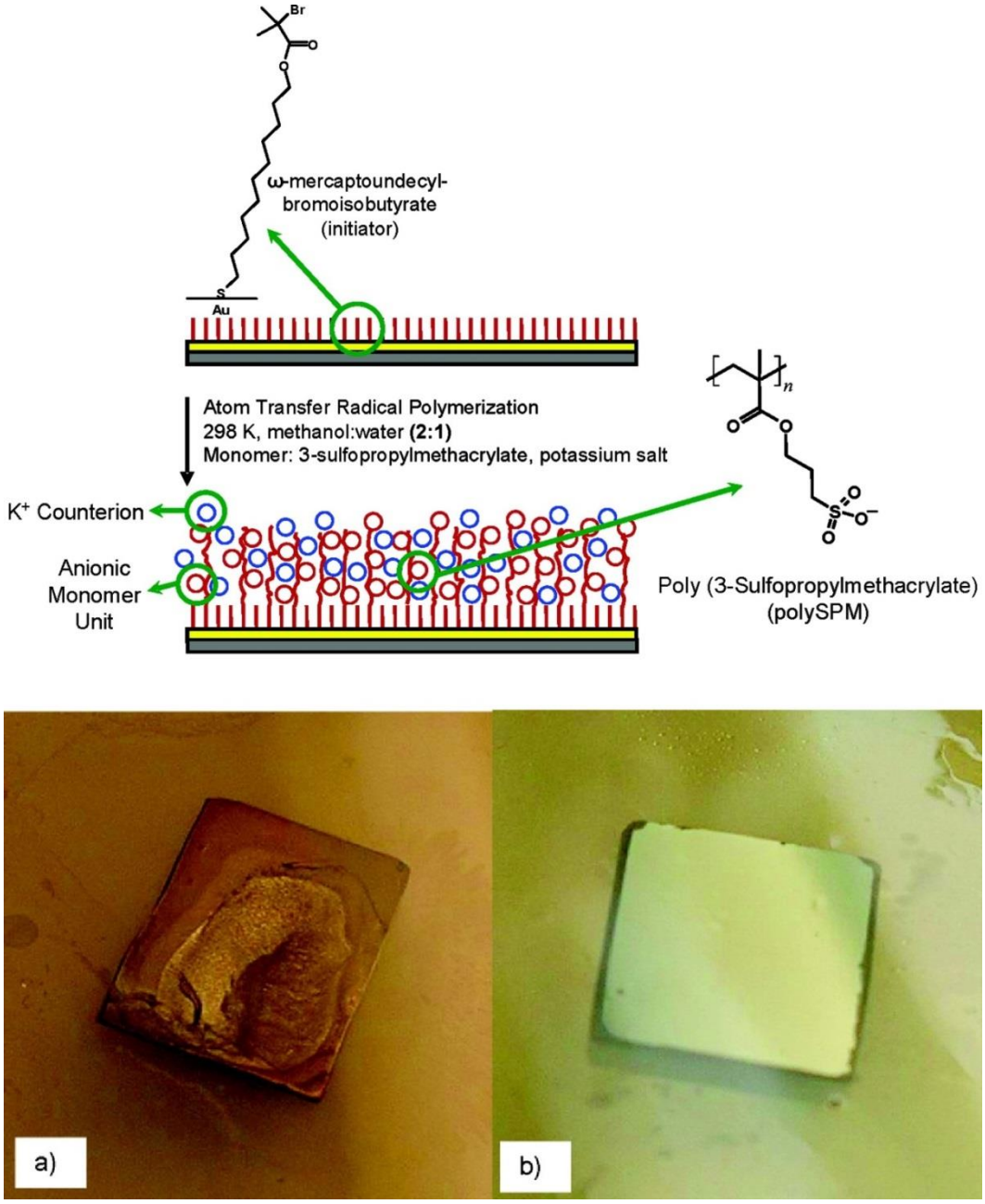

Figure 2.25. (top panel) Schematic description of the synthesis of polySPM (sulfonate brush). (bottom panel) a) Growth of *S. aureus* on a piece of silica wafer covered with sulfonate brush. (b) Absence of growth of *S. aureus* on a silica wafer covered with silver-loaded sulfonate brushes. Both images represent wafer pieces positioned in a Petri dish and covered with growth agar. Reproduced with permission from the American Chemical Society[233].

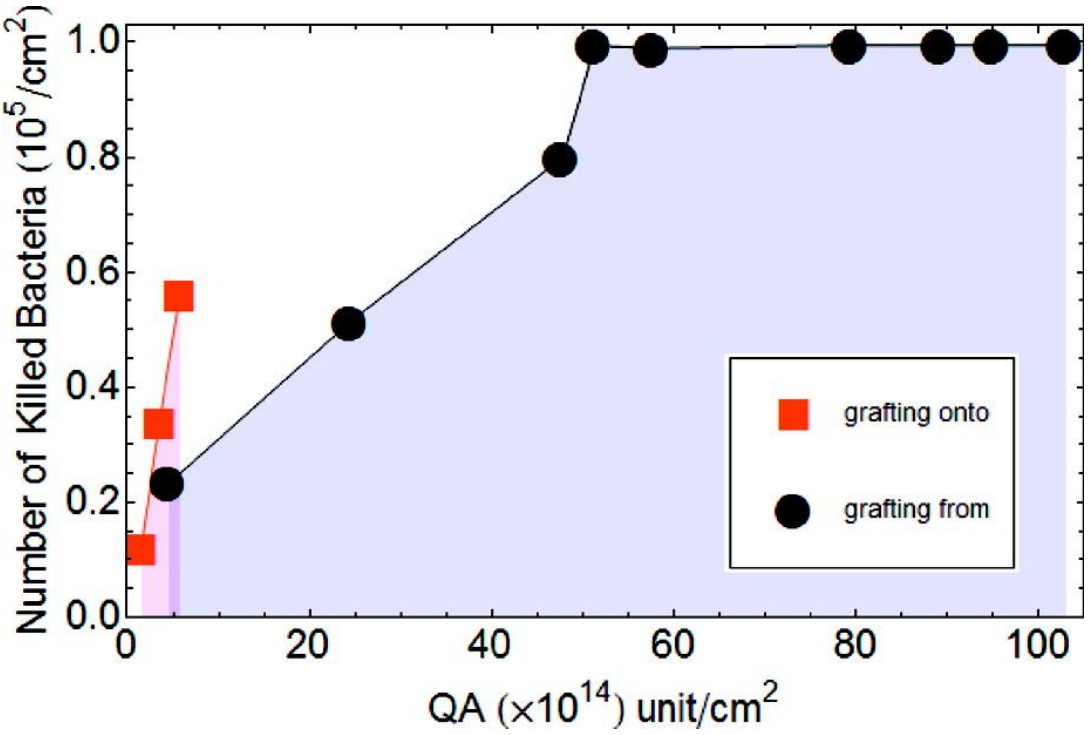

Figure 2.26. Dependence of the biocidal activity of the surfaces prepared by "grafting onto" and by "grafting from" on the average density of QA groups. Reproduced with permission from the American Chemical Society[235].

Madkour *et al* reported on another route to biocidal activity using butoxycarbonyl aminoethylmethacrylate (Boc-AEMA) brushes[236]. After growth, removing the Boc group activated the polymer to its quaternary derivative. Brushes with thicknesses between 3 and 50 nm, and a broad range of grafting densities killed 100% of *E. Coli* and *Staphylococcus* bacteria exposed to the biocidal surface. Such a wide range of thicknesses and grafting densities illustrates the effectiveness of the quaternary ammonium group. It also suggests that the killing mechanism does not involve the polymer brush piercing the cell wall, as a 3 nm thickness could not readily achieve that task. Unfortunately, serial exposure of the bacteria to the same substrate reduced effectiveness quickly. The authors investigated the possibility of the quaternary ammonium rearranging to an amide, and found evidence of this possibility for both inter and intra chain locations.

While the above examples used synthetic biocidal agents, Glinel *et al* incorporated magainin I, a naturally occurring antimicrobial peptide, into polymer brushes[237]. The brushes consisted of 2-(2-

methoxyethoxy)ethyl methacrylate (MEO_2MA) and hydroxyl-terminated OEGMA repeat units. The peptide was attached at the hydroxyl group of the OEGMA units. The system proved biocidally active when exposed to two gram-positive bacterial strains, as seen in **Figure 2.27**.

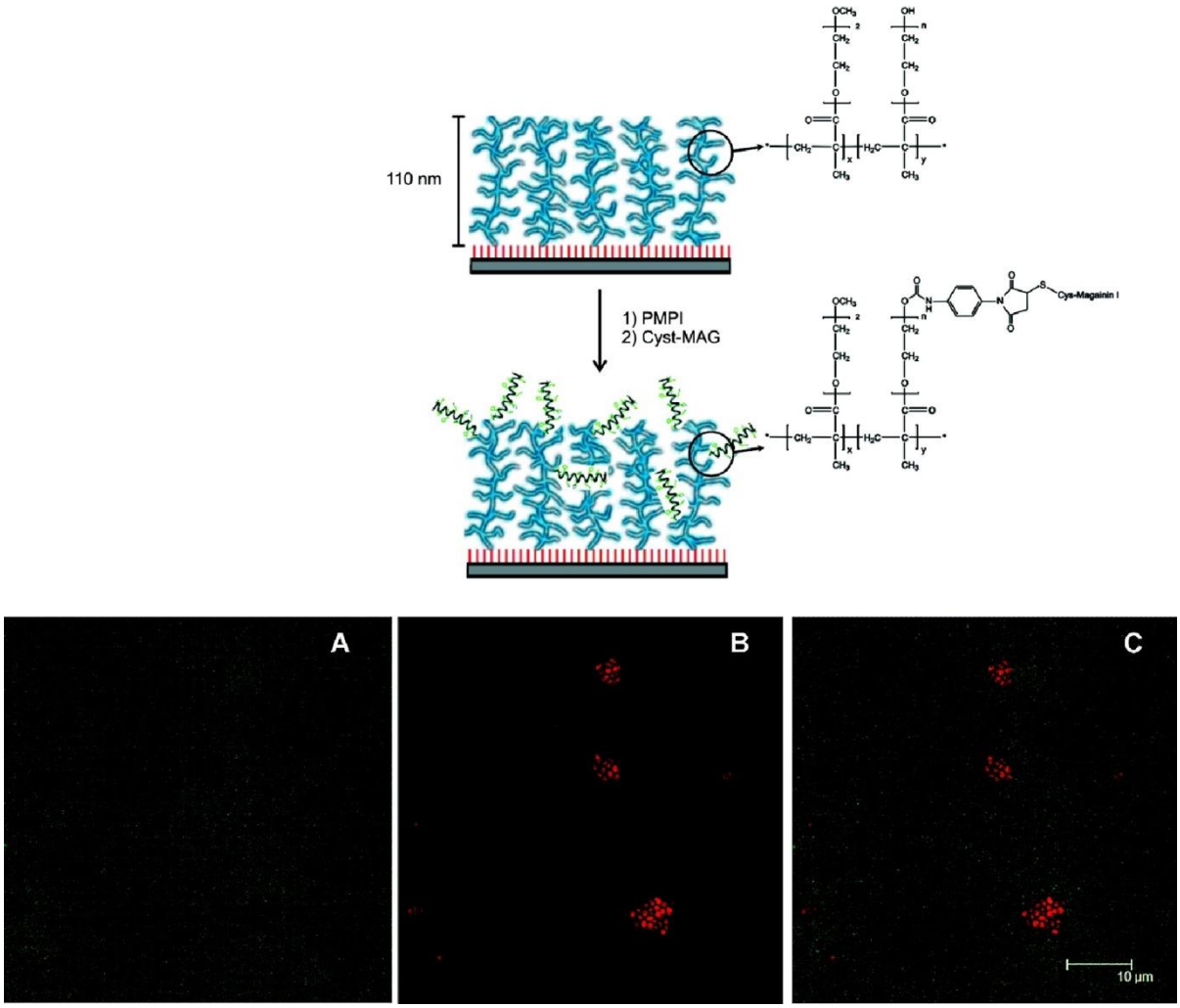

Figure 2.27. (top panel) Oriented Grafting of MAG-Cys Derivative on Poly(MOE_2MA-*co*-HOEGMA) Brushes via a PMPI heterolinker. (bottom panel) CLSM images of MAG-Cys-functionalized poly(MEO_2MA-*co*-HOEGMA) [33:67] brush incubated in the presence of *L. ivanovii* and subsequently stained with the LIVE/DEAD viability kit: (A) green channel image corresponding to alive stained bacteria; (B) red channel image corresponding to dead bacteria; (C) overlay image built from (A) and (B). Reproduced with permission from the American Chemical Society[237].

In an effort to examine antibacterial brushes on a more practical surface, Ignatova *et al* grew polycation macromolecules on stainless steel using both "grafting from" and "grafting to" approaches[238]. In the case of grafting from, an ATRP macroinitiator eletropolymerized to a stainless steel electrode provided a site to subsequently grow poly(ethyleneimine) (PEI) using ATRP. The grafting to approach utilized the facile derivatization of poly(N-succinimidyl) chains electrografted to the electrode to introduce PEI into the brush. The resulting brushes demonstrated that PEI completely suppressed growth of bacterial colonies. Furthermore, fluorination did not have a notable impact on bacterial resistance. This point suggests that the generation of hydrophobic, antibacterial surfaces is feasible. Yuan *et al* also reported the synthesis of quaternary ammonium polymer brushes on stainless steel surfaces[239]. In a similar vein, Lee *et al* grew PDMAEMA brushes on glass and paper (filter) surfaces, followed by quaternization of the amine group using ethyl bromide[240]. The paper-based platform proved more effective than the glass, killing approximately 10^9 and 10^7 *E. Coli* cells within one hour.

2.3.5.2 Tissue Engineering

Tissue engineering has emerged as an important field of research over the past decade and it promises to revolutionize medical treatment[241]. Polymer brushes have played a pivotal role in bringing the potential of tissue engineering technology to fruition[242]. As seen in the examples below, that role will likely increase in importance going forward.

One current problem this field faces involves finding appropriate scaffolds for the tissues *in vivo*. In an effort to advance Si-based scaffolds for human implants, Xu *et al* grew brushes of PHEMA on Si wafers, then derivatized the brushes with collagen[243]. Attachment occurred either exclusively at the active halide site at the end terminus of the PHEMA chains, or at the hydroxyl pendant groups following its replacement with a halide. For both cases, the collagens primary amine provided the subsequent linkage. After 8 hours of reaction time, the brushes had grown to thicknesses up to ≈40 nm. However, as verified by XPS, longer reaction times reduced the number of active halide end groups, likely due to disproportionation reactions. The collagen-modified brushes demonstrated a marked increase in cell proliferation of 3T3 fibroblasts. Interestingly, thicker brushes showed less cell adhesion even for collagen-modified surfaces. PHEMA brushes first modified with pendant halide groups displayed more cell adhesion than the unmodified PHEMA brush.

Another example related to tissue scaffolding involved modifying hydrogels after polymerization with amine functionalities connected with a range of spacer lengths in order to improve corneal epithelial cell attachment. Specifically, Rimmer *et al* copolymerized laurylmethacrylate (LMA), ethyleneglycol dimethacrylate (EGDMA), glycercol monomethacrylate (GM) and glycidylmethacrylate (GMA) at various relative concentrations[244]. Two cases contained all four monomers, while one case excluded the hydrophobic LMA. After producing the hydrogel, diamines of varying spacer length (1 to 5) reacted with and modified the surface of the scaffolds. Interestingly, spacer length did not have a significant impact on the quantity of amines that appeared on the surface, and the spacer length did not affect the amount of water these hydrogels could contain at equilibrium (equilibrium water content, EWC). In terms of cell viability, the authors determined amine content and spacer length to have the most significant effect on cell viability, with longer spacer lengths improving cell growth. Since spacer lengths of 1, 4, 5 are fully ionized (2 and 3 have reduced basicity due to proximity of the two amines), surface charge may play a significant role.

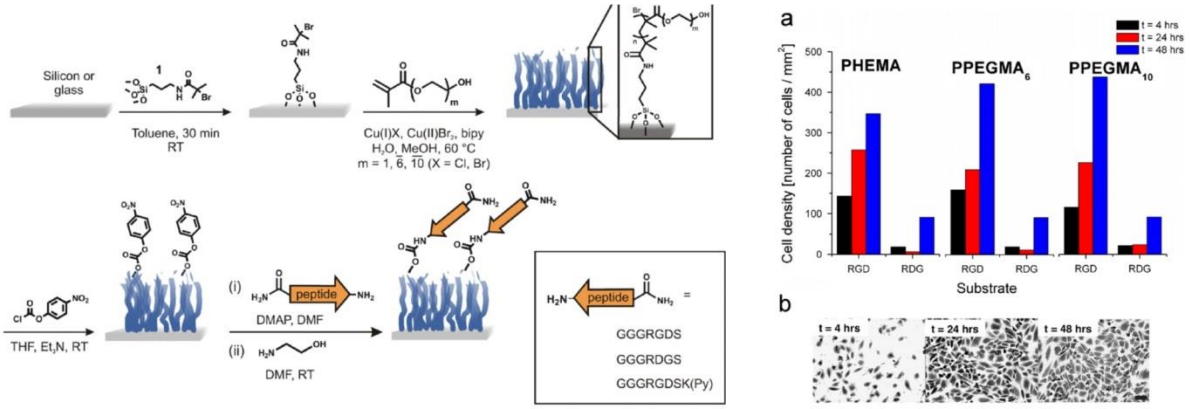

Figure 2.28. (left panel) Schematic of brush functionalization with peptides. (right panel) Proliferation of HUVECs on GGGRGDS and GGGRDGS functionalized 20 nm thick PHEMA, $PPEGMA_6$ and $PPEGMA_{10}$ brushes. (a) HUVEC density 4, 24 and 48 h post-seeding. (b) Photomicrographs of HUVECs on a 20 nm thick $PPEGMA_{10}$ brush 4, 24 and 48 h post-seeding. The peptide concentration in the functionalization solution was 1 mm. Scale bar: 50 μm. Reproduced with permission from Elsevier[246].

Patrucco *et al* made use of P(GM-*co*-DMAEMA) brushes to tune cellular adhesion for tissue substrates[245]. The researchers modified tissue culture PS (TCPS) with a macroinitiator, then grew the

copolymers in varying composition ratios. PGM prevents cell adhesion, creating a non-fouling surface, while DMAEMA will promote cell adhesion at physiological pH values. Their results demonstrate that PGM homopolymer is a non-toxic and non-adhesive material for cell growth. Unfortunately, the group could not determine the composition of the P(GM-*co*-DMAEMA) copolymers. Nonetheless, the cells show morphologies similar to ones that have come in contact with an adhesive after exposure to the copolymer brushes.

Tugulu *et al* modified brushes of PHEMA or poly(poly(ethylene glycol)methacrylate) (PPEGMA) with peptide ligands bearing Arginine-Glycine-Aspartic Acid (RGD) sequences in an effort to promote endothelial cell adhesion to a substrate[246]. The results demonstrate a clear improvement over neat polymer brushes, as depicted in **Figure 2.28**. The group has since reported the synthesis of these RGD-bearing PPEGMA brushes on polyethylene, which is a non-biofouling surface and widely used in the biotechnology industry[247].

Navarro *et al* further explored the effect of spatial arrangement of RGD in the polymer brush on cell adhesion[248]. They grew brushes of PMAA and incorporated RGD sequences using EDC/NHS. Some of these substrates were used as is, while some had an extension of the PMAA brush grown from the terminal end of the brush. The substrates were then exposed to human osteoblast cells and characterized. While the samples did not lead to differences in cell adhesion, differences in cell morphology were observed. Substrates with RGD sequences located at the surface led to higher cell spreading, with adhesion points at the periphery of the cytoplasm, as seen in **Figure 2.29**.

A number of groups have taken advantage of thermoresponsive polymer brushes to tune cellular adhesion. Notably, the Okano group has employed this approach to develop free-standing cellular sheets that do not require a scaffold[249]. By seeding cells onto a PNIPAAm layer above its LCST (hydrophobic surface), then harvesting the cells below its LCST (hydrophilic surface), the need for enzymatic treatment to release the cells is avoided. This approach preserves the extracellular matrix and the cells form a continuous sheet upon release, which is depicted schematically in **Figure 2.30**. The group has achieved homogenous and patterned cellular sheets with this technique[250]; these sheets can then be assembled into stacks to form 3-D structures[251]. Xu *et al* have also taken advantage of the LCST of PNIPAAm to tune cellular adhesion[252].

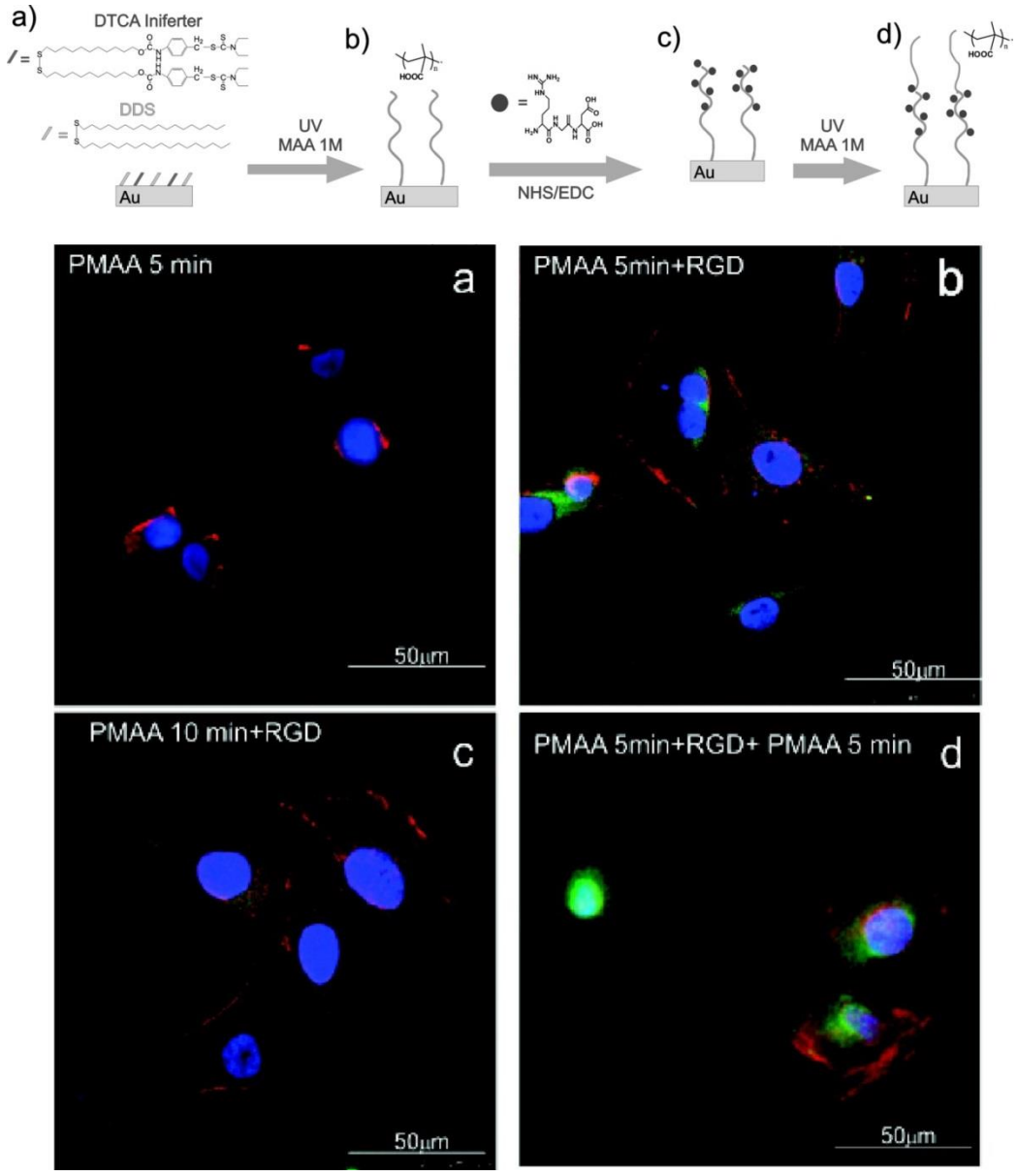

Figure 2.29. (top panel) Preparation of RGD-modified polymer brushes grafted from immobilized precursors on gold by photopolymerization: (a,b) Photografting of PMAA brushes from immobilized photoiniferter DTCA/ODT SAMs; (c) immobilization of RGD peptides; and (d) chain extension via photografting of a top PMAA brush layer. (bottom panel) Immunofluorescence images of MG63 cells on the studied surfaces: (a) PMAA, (b,c) PMAA−RGD, and (d) PMAA−RGD−PMAA after 6 h of contact. Reproduced with permission from the American Chemical Society[248].

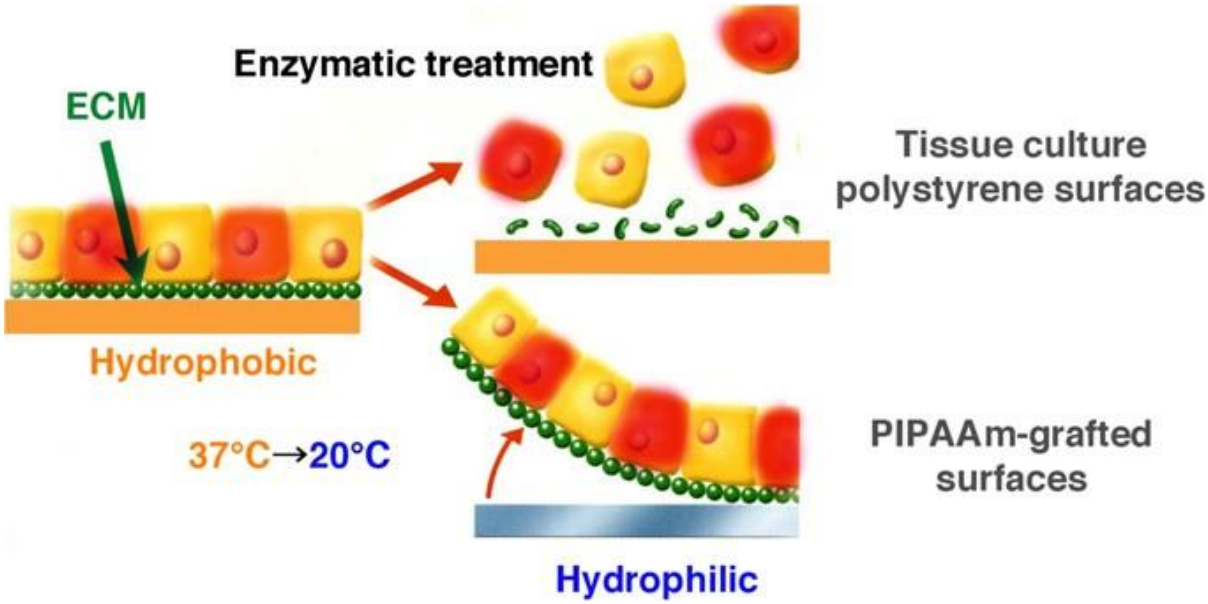

Figure 2.30. Schematic showing the approach pioneered by the Okano group to create continuous cellular sheets. By employing a thermoresponsive polymer coating, cells can be released from the substrate without enzymatic treatment, preserving the ECM and structure of the sheet. These sheets offer a scaffold-free approach to tissue engineering and therapy. Reproduced with permission by IOP Publishing[249].

2.4 Summary and outlook

The examples mentioned and discussed in this review highlight the diverse applications PPM of surface-anchored polymers. From responsive surfaces to *in situ* particle formation to protein functionalized surfaces, the relatively brief union of polymer brushes and PPM reactions has already yielded significant technological advances and appears destined to play an important role in technology development going forward.

In spite of tremendous progress during the past few years, several outstanding questions remain unanswered in this area of research. In particular, a solid understanding of the spatial distribution of modified repeat units within the polymer brush remains elusive. Other issues pertaining to establishing the spatial distributions of larger penetrants (*i.e.*, nanoparticles, proteins, chain modifiers) remain unresolved and ripe for investigation. A simple thought exercise leads to the conclusion that surface-anchored polymeric grafts with lower grafting density and molecular weight, and using smaller modifying agents will lead to more uniform distributions of modified sites. The

interplay between these parameters has not been thoroughly sorted out; work underway in several labs hopes to provide further insight.

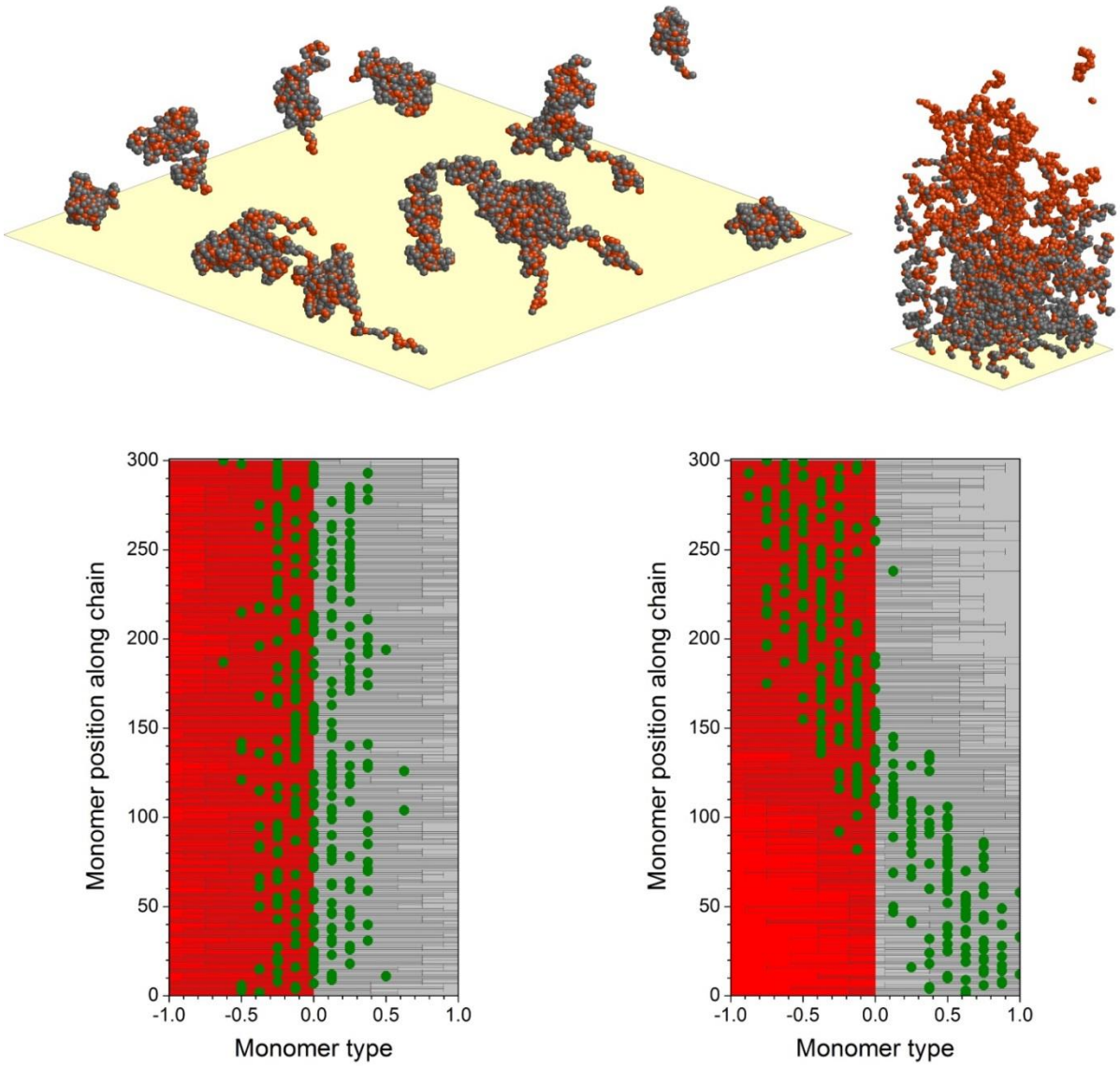

Figure 2.31. Position along $A_{0.5}B_{0.5}$ 300-mers as a function of monomer type (B = -1, A = +1) tethered at surface densities $\rho = 0.001$ (left panel) and 0.010 (right panel) polymers/area for $kT/|\varepsilon_{AA}| = 6.0$ and $R_{BA} = 5.0$. Typical chain conformations are shown for each case in the upper part (A = grey, B = red). Reproduced with permission from the American Chemical Society[263].

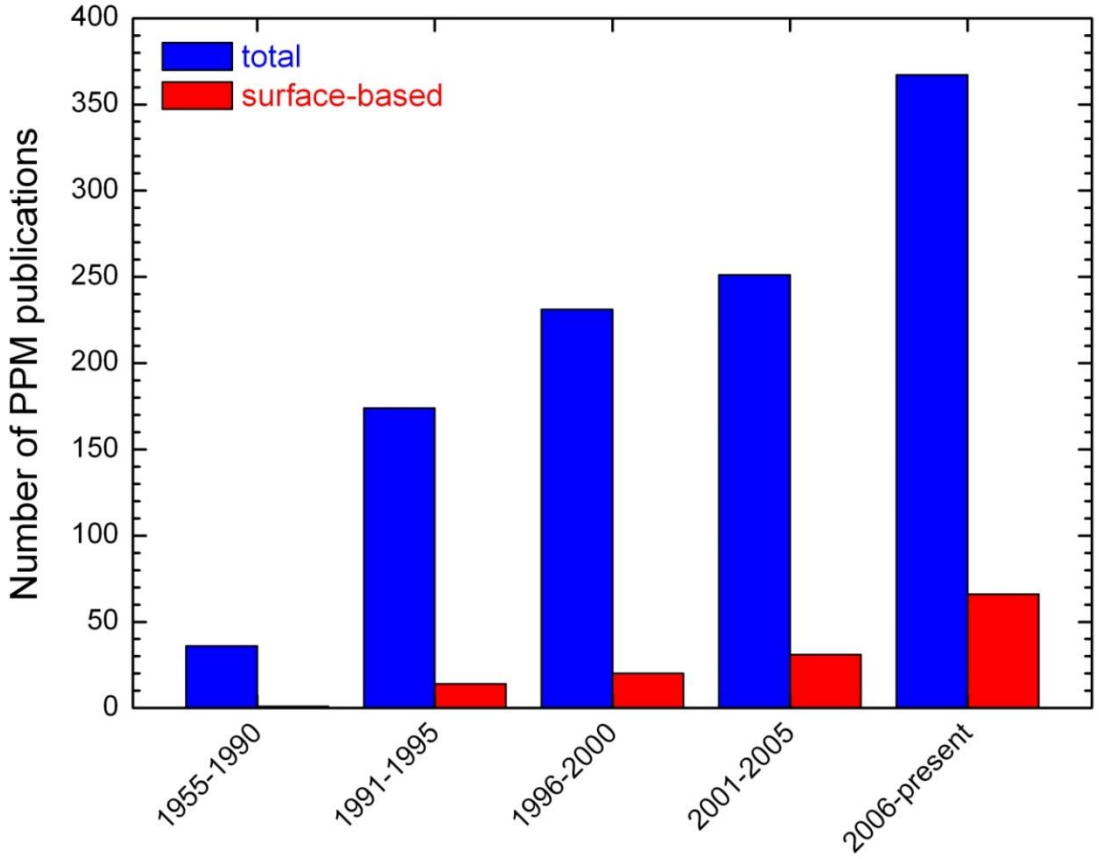

Figure 2.32. Number of peer-reviewed publications describing the PPM process.

These issues are not merely academic; they are vital for addressing some outstanding issues of polymer physics with immediate impact to many technological applications, *i.e.*, adsorption of proteins in polymer brushes[253]. Furthermore, the limited ability of reactants to penetrate into a brush may prove crucial for developing unique brush systems. Controlling the final sequence distribution of monomers in synthetic heteropolymers has received significant attention recently[64,254–261], and promises to emerge as a noteworthy research topic. The Genzer group has employed a theory first suggested by Khokhlov[258,259]. This scheme was later explored further experimentally and by computer simulations by modifying homopolymer under different solvent conditions[80,260–264]. While brominating polystyrene in a good solvent, in which the polymer chains are expanded, produced random copolymers, brominating polystyrene in a poor solvent, with collapsed chains, generated

samples with a "random-blocky" distribution of brominated species, as determined by an analysis of the Kerr constants of the resulting polymer samples[261] and retention times using interaction chromatography[265]. This concept has proven successful in brush systems examined using computer simulations[262,263] (*cf.* **Figure 2.31**), and is currently under further experimental investigation. More details describing this "chemical coloring" method and sub-topics related to the properties of copolymers with disordered monomer sequence distributions can be found in a recent book chapter[266].

While rather young, the field of PPM of surface-anchored polymers has grown very rapidly. More exciting and stimulating findings with important insight remain to be seen (and hopefully understood) in the immediate future. As highlighted by this review, these results will prove valuable in a variety of technologies across a number of fields. The growing number of publications related to polymer analogous reactions or post-polymerization modification provides evidence of this field's rapid growth (*cf.* **Figure 2.32**). Perhaps even more exciting is the steady increase in citations each year, suggesting the foundational nature of this field of research. The authors hope this review will help to explain why this trend has developed and appears likely to continue in the future.

2.5 Acknowledgement

The authors thank the National Science Foundation and the Office of Naval Research for support. CJG acknowledges the support of a National Science Foundation EAPSI Fellowship. JG thanks the Deutsche Forschungsgemeinschaft for providing a Mercator Fellowship at the University of Freiburg, Germany, where a portion of this review was written. The authors thank Dr. Richard A. Vaia for reading the manuscript and providing fruitful suggestions.

2.6 Glossary of used abbreviations and symbols

ATRP	atom transfer radical polymerization
Boc-AEMA	butoxycarbonylaminoethylmethacrylate
BSA	bovine serum albumin
C_7	heptane
C16	hexadecane
C8F15	pentadecylfluoro octane
DEA	diethylamine
DMAP	dimethylaminopyridine
DOBEMA	2-(2-diazo-3-oxo-butyrloxy)ethyl methacrylate
DSC	N,N'-disuccinimidyl carbonate
ECM	extracellular matrix
EDC	1-Ethyl-3-[3-dimethylaminopropyl]carbodiimide hydrochloride
EGDMA	ethyleneglycol dimethacrylate
EIS	electrochemical impedance spectroscopy
Est	esterase
EWC	equilibrium water content
FBZ	pentafluorobenzoyl chloride
GM	glycercol monomethacrylate
GMA	glycidyl methacrylate
GOx	glucose oxidase
h	dry brush thickness
HEMA	2-hydroxyethylmethacrylate
HPLC	High-performance liquid chromatography
ITC	isothermal titration calorimetry
ITO	indium tin oxide
LCST	lower critical solution temperature
LMA	laurylmethacrylate
MALDI-MS	Matrix-assisted laser desorption/ionization – mass spectrometry
MEO_2MA	2-(2-methoxyethoxy)ethyl methacrylate
M_n	number average molecular weight
MPC	2-methacryloyloxyethyl phosphorylcholine
MW	molecular weight
N_A	Avogadro’s number
NHS	N-hydroxysuccinimide
NMP	nitroxide-mediated polymerization
NP	nanoparticle
PAA	poly(acrylic acid)
PDHPA	poly-*N*-(2,3-dihydroxypropyl) acrylamide
PDMAEMA	poly(2-dimethylaminoethyl methacrylate)
PDMDOMA	poly-*N*-[(2,2-dimethyl-1,3-dioxolane)methyl]acrylamide
PDMS	poly(dimethylsiloxane)
PEG	poly(ethylene glycol)
PEI	poly(ethyleneimine)
PGM	poly(glycercol monomethacrylate)

PHEMA	poly(2-hydroxyethylmethacrylate)
PM	poly(methylene)
PMAA	poly(methyacrylic acid)
PMEP	poly(methacryloyloxyethyl phosphate)
PMES	poly(2-(methacryloyloxy)ethyl succinate)
PML	poly(methacryloyl-L-lysine)
PNB	polynorborene
PNIPAAm	poly(N-isopropyl acrylamide)
POEGMA	poly(oligo(ethylene glycol) methacrylate)
PPEGMA	poly(poly(ethylene glycol)methacrylate)
PPM	post-polymerization modification
PS	polystyrene
PtBA	poly(*tert*-butyl acrylate)
PTFE	poly(tetrafluoro ethylene)
P2VP	poly(2-vinylpyridine)
P4VP	poly(4-vinylpyridine)
RAFT	reversible addition-fragmentation chain transfer
R_g	radius of gyration
RGD	Arginine-Glycine-Aspartic Acid
S-Glc	sulfonated glycosaminoglycan
SP	“strong” (or quenched) polyelectrolytes
TCPS	tissue culture polystyrene
TEM	transmission electron microscopy
TMSPMA	3-(trimethyoxysilyl)propyl methacrylate
Ur	urease
WP	“weak” (or annealed) polyelectrolytes
σ	grafting density

2.7 References

(1) Boaen, N. K.; Hillmyer, M. a. *Chem. Soc. Rev.* **2005**, *34*, 267–275.

(2) Barbey, R.; Lavanant, L.; Paripovic, D.; Schüwer, N.; Sugnaux, C.; Tugulu, S.; Klok, H.-A. *Chem. Rev.* **2009**, *109*, 5437–5527.

(3) Gauthier, M. A.; Gibson, M. I.; Klok, H.-A. *Angew. Chem. Int. Ed. Engl.* **2009**, *48*, 48–58.

(4) Pollino, J. M.; Weck, M. *Chem. Soc. Rev.* **2005**, *34*, 193–207.

(5) Fleer, G.; Cohen Stuart, M.; Scheutjens, J. M. H. M.; Cosgrove, T.; Vincent, B. *Polymers at Interfaces*; Chapman & Hall: New York, NY, 1993.

(6) Ducker, R.; Garcia, A.; Zhang, J.; Chen, T.; Zauscher, S. *Soft Matter* **2008**, *4*, 1774.

(7) Genzer, J.; Bhat, R. R. *Langmuir* **2008**, *24*, 2294–2317.

(8) Hoffmann, M.; Lu, Y.; Schrinner, M.; Ballauff, M.; Harnau, L. *J. Phys. Chem. B* **2008**, *112*, 14843–14850.

(9) Homenick, C. M.; Lawson, G.; Adronov, A. *Polym. Rev.* **2007**, *47*, 265–290.

(10) Karaiskos, E.; Bitsanis, I. A.; Anastasiadis, S. H. *J. Polym. Sci. Part B Polym. Phys.* **2009**, *47*, 2449–2461.

(11) Merlitz, H.; He, G.-L.; Wu, C.-X.; Sommer, J.-U. *Phys. Rev. Lett.* **2009**, *102*, 1–4.

(12) Sheiko, S. S.; Sumerlin, B. S.; Matyjaszewski, K. *Prog. Polym. Sci.* **2008**, *33*, 759–785.

(13) Toomey, R.; Tirrell, M. *Annu. Rev. Phys. Chem.* **2008**, *59*, 493–517.

(14) Xie, M.; Dang, J.; Han, H.; Wang, W.; Liu, J.; He, X.; Zhang, Y. *Macromolecules* **2008**, *41*, 9004–9010.

(15) Bhat, R. R.; Tomlinson, M. R.; Wu, T.; Genzer, J. *Adv. Polym. Sci* **2006**, *198*, 51–124.

(16) Currie, E. P. K.; Norde, W.; Cohen Stuart, M. A. *Adv. Colloid Interface Sci.* **2003**, *100-102*, 205–265.

(17) Edmondson, S.; Osborne, V. L.; Huck, W. T. S. *Chem. Soc. Rev.* **2004**, *33*, 14–22.

(18) Gao, C.; Yan, D. *Prog. Polym. Sci.* **2004**, *29*, 183–275.

(19) Ionov, L.; Zdyrko, B.; Sidorenko, A.; Minko, S.; Klep, V.; Luzinov, I.; Stamm, M. *Macromol. Rapid Commun.* **2004**, *25*, 360–365.

(20) Jennings, G. K.; Brantley, E. L. *Adv. Mater.* **2004**, *16*, 1983–1994.

(21) *Surface-Initiated Polymerization I*; Jordan, R., Ed.; Advances in Polymer Science; Springer Berlin Heidelberg: Berlin, Heidelberg, 2006; Vol. 197.

(22) *Surface-Initiated Polymerization II*; Jordan, R., Ed.; Advances in Polymer Science; Springer-Verlag: Berlin/Heidelberg, 2006; Vol. 198.

(23) Rühe, J.; Ballauff, M.; Biesalski, M.; Dziezok, P.; Gröhn, F.; D; Rühe, J. *Adv. Polym. Sci* **2004**, *165*, 79–150.

(24) Senaratne, W.; Andruzzi, L.; Ober, C. K. *Biomacromolecules* **2005**, *6*, 2427–2448.

(25) Ayres, N. *Polym. Chem.* **2010**, *1*, 769.

(26) De Gennes, P. G. *Macromolecules* **1980**, *13*, 1069–1075.

(27) Gast, A. P. *Langmuir* **1996**, *12*, 4060–4067.

(28) Husseman, M.; Malmström, E. E.; McNamara, M.; Mate, M.; Mecerreyes, D.; Benoit, D. G.; Hedrick, J. L.; Mansky, P.; Huang, E.; Russell, T. P.; Hawker, C. J. *Macromolecules* **1999**, *32*, 1424–1431.

(29) Milner, S. T. *Science* **1991**, *251*, 905–914.

(30) Milner, S. T.; Witten, T. a.; Cates, M. E. *Macromolecules* **1988**, *21*, 2610–2619.

(31) Netz, R.; Andelman, D. *Phys. Rep.* **2003**, *380*, 1–95.

(32) Rühe, J.; Knoll, W. *Polym. Rev.* **2002**, *42*, 91–138.

(33) Zhao, B.; Brittain, W. J. *Prog. Polym. Sci.* **2000**, *25*, 677–710.

(34) Zhou, F.; Huck, W. T. S. *Phys. Chem. Chem. Phys.* **2006**, *8*, 3815.

(35) Brittain, W. J.; Minko, S. *J. Polym. Sci. Part A Polym. Chem.* **2007**, *45*, 3505–3512.

(36) Wu, T.; Efimenko, K.; Genzer, J. *J. Am. Chem. Soc.* **2002**, *124*, 9394–9395.

(37) Prucker, O.; Rühe, J. *Macromolecules* **1998**, *31*, 592–601.

(38) Prucker, O.; Rühe, J. *Macromolecules* **1998**, *31*, 602–613.

(39) Braunecker, W. A.; Matyjaszewski, K. *Prog. Polym. Sci.* **2007**, *32*, 93–146.

(40) Cheng, N.; Azzaroni, O.; Moya, S.; Huck, W. T. S. *Macromol. Rapid Commun.* **2006**, *27*, 1632–1636.

(41) Coessens, V.; Pintauer, T.; Matyjaszewski, K. *Prog. Polym. Sci.* **2001**, *26*, 337–377.

(42) Huang, W.; Kim, J.-B.; Bruening, M. L.; Baker, G. L. *Macromolecules* **2002**, *35*, 1175–1179.

(43) Kaiser, A.; Dutz, S.; Schmidt, A. M. *J. Polym. Sci. Part A Polym. Chem.* **2009**, *47*, 7012–7020.

(44) Kong, X.; Kawai, T.; Abe, J.; Iyoda, T. *Macromolecules* **2001**, *34*, 1837–1844.

(45) Matyjaszewski, K.; Miller, P. J.; Shukla, N.; Immaraporn, B.; Gelman, A.; Luokala, B. B.; Siclovan, T. M.; Kickelbick, G.; Vallant, T.; Hoffmann, H.; Pakula, T. *Macromolecules* **1999**, *32*, 8716–8724.

(46) Matyjaszewski, K.; Tsarevsky, N. V.; We, P.; States, U. *Nat. Chem.* **2009**, *1*, 276–288.

(47) Perruchot, C.; Khan, M. a.; Kamitsi, a.; Armes, S. P.; von Werne, T.; Patten, T. E. *Langmuir* **2001**, *17*, 4479–4481.

(48) Pyun, J.; Kowalewski, T.; Matyjaszewski, K. *Macromol. Rapid Commun.* **2003**, *24*, 1043–1059.

(49) Pyun, J.; Matyjaszewski, K. *Chem. Mater.* **2001**, *13*, 3436–3448.

(50) Rowe, M. D.; Hammer, B. A. G.; Boyes, S. G. *Macromolecules* **2008**, *41*, 4147–4157.

(51) Teare, D. O. H.; Barwick, D. C.; Schofield, W. C. E.; Garrod, R. P.; Ward, L. J.; Badyal, J. P. S. *Langmuir* **2005**, *21*, 11425–11430.

(52) Wu, T.; Efimenko, K.; Genzer, J. *Macromolecules* **2001**, *34*, 684–686.

(53) Fristrup, C. J.; Jankova, K.; Hvilsted, S. *Soft Matter* **2009**, *5*, 4623.

(54) Baum, M.; Brittain, W. J. *Macromolecules* **2002**, *35*, 610–615.

(55) Chiefari, J.; Chong, Y. K. (Bill); Ercole, F.; Krstina, J.; Jeffery, J.; Le, T. P. T.; Mayadunne, R. T. A.; Meijs, G. F.; Moad, C. L.; Moad, G.; Rizzardo, E.; Thang, S. H. *Macromolecules* **1998**, *31*, 5559–5562.

(56) Favier, A.; Charreyre, M.-T. *Macromol. Rapid Commun.* **2006**, *27*, 653–692.

(57) Gruendling, T.; Dietrich, M.; Barner-Kowollik, C. *Aust. J. Chem.* **2009**, *62*, 806.

(58) Lowe, A. B.; McCormick, C. L. *Prog. Polym. Sci.* **2007**, *32*, 283–351.

(59) Moad, G.; Rizzardo, E.; Thang, S. H. *Aust. J. Chem.* **2005**, *58*, 379.

(60) Moad, G.; Rizzardo, E.; Thang, S. H.; Front, R. *Aust. J. Chem.* **2006**, *59*, 669.

(61) Moad, G.; Rizzardo, E.; Thang, S. H. *Polymer.* **2008**, *49*, 1079–1131.

(62) Brinks, M. K.; Studer, A. *Macromol. Rapid Commun.* **2009**, *30*, 1043–1057.

(63) Hawker, C. J.; Bosman, A. W.; Harth, E. *Chem. Rev* **2001**, *101*, 3661–3688.

(64) Wang, L.; Broadbelt, L. J. *Macromolecules* **2009**, *42*, 7961–7968.

(65) Bartholome, C.; Beyou, E.; Bourgeat-Lami, E.; Chaumont, P.; Zydowicz, N. *Macromolecules* **2003**, *36*, 7946–7952.

(66) Turgman-Cohen, S.; Genzer, J. *Macromolecules* **2010**, *43*, 9567–9577.

(67) Genzer, J. *Macromolecules* **2006**, *39*, 7157–7169.

(68) Sumerlin, B. S.; Vogt, A. P. *Macromolecules* **2010**, *43*, 1–13.

(69) Iha, R. K.; Wooley, K. L.; Nyström, A. M.; Burke, D. J.; Kade, M. J.; Hawker, C. J. *Chem. Rev.* **2009**, *109*, 5620–5686.

(70) Nebhani, L.; Barner-Kowollik, C. *Adv. Mater.* **2009**, *21*, 3442–3468.

(71) Barner-Kowollik, C.; Inglis, A. J. *Macromol. Chem. Phys.* **2009**, *210*, 987–992.

(72) Kolb, H. C.; Finn, M. G.; Sharpless, K. B. *Angew. Chem. Int. Ed. Engl.* **2001**, *40*, 2004–2021.

(73) Evans, R. A. *Aust. J. Chem.* **2007**, *60*, 384.

(74) Golas, P. L.; Matyjaszewski, K. *Chem. Soc. Rev.* **2010**, *39*, 1338–1354.

(75) Orski, S. V; Poloukhtine, A. A.; Arumugam, S.; Mao, L.; Popik, V. V; Locklin, J. *J. Am. Chem. Soc.* **2010**, *132*, 11024–11026.

(76) Hoyle, C. E.; Lowe, A. B.; Bowman, C. N. *Chem. Soc. Rev.* **2010**, *39*, 1355–1387.

(77) Kade, M. J.; Burke, D. J.; Hawker, C. J. *J. Polym. Sci. Part A Polym. Chem.* **2010**, *48*, 743–750.

(78) Hensarling, R. M.; Doughty, V. A.; Chan, J. W.; Patton, D. L. *J. Am. Chem. Soc.* **2009**, 3–5.

(79) Jaeger, W.; Bohrisch, J.; Laschewsky, A. *Prog. Polym. Sci.* **2010**, *35*, 511–577.

(80) Jhon, Y. K.; Semler, J. J.; Genzer, J. *Macromolecules* **2008**, *41*, 6719–6727.

(81) Kambour, R. P.; Bendler, J. T.; Bopp, R. C. *Macromolecules* **1983**, *16*, 753–757.

(82) Tran, Y.; Auroy, P. *J. Am. Chem. Soc.* **2001**, *123*, 3644–3654.

(83) Miyaura, N.; Yamada, K.; Suzuki, A. *Tetrahedron Lett.* **1979**, 3437–3440.

(84) Suzuki, A. *J. Organomet. Chem.* **1999**, *576*, 147–168.

(85) Böker, A.; Herweg, T.; Reihs, K. *Macromolecules* **2002**, *35*, 4929–4937.

(86) Groll, J.; Amirgoulova, E. V; Ameringer, T.; Heyes, C. D.; Röcker, C.; Nienhaus, G. U.; Möller, M. *J. Am. Chem. Soc.* **2004**, *126*, 4234–4239.

(87) Hensarling, R. M.; Rahane, S. B.; LeBlanc, A. P.; Sparks, B. J.; White, E. M.; Locklin, J.; Patton, D. L. *Polym. Chem.* **2011**, *2*, 88.

(88) Hirao, A.; Sugiyama, K.; Yokoyama, H. *Prog. Polym. Sci.* **2007**, *32*, 1393–1438.

(89) Hansen, N.; Jankova, K.; Hvilsted, S.; Journal, E. P. *Eur. Polym. J.* **2007**, *43*, 255–293.

(90) Murata, H.; Prucker, O.; Rühe, J. *Macromolecules* **2007**, *40*, 5497–5503.

(91) Walters, K. B.; Hirt, D. E. *Macromolecules* **2007**, *40*, 4829–4838.

(92) Lokitz, B. S.; Messman, J. M.; Hinestrosa, J. P.; Alonzo, J.; Verduzco, R.; Brown, R. H.; Osa, M.; Ankner, J. F.; Kilbey, S. M. *Macromolecules* **2009**, *42*, 9018–9026.

(93) Cullen, S. P.; Mandel, I. C.; Gopalan, P. *Langmuir* **2008**, *24*, 13701–13709.

(94) Kawai, T.; Saito, K.; Lee, W. *J. Chromatogr. B* **2003**, *790*, 131–142.

(95) Matrab, T.; Hauquier, F.; Combellas, C.; Kanoufi, F. *Chemphyschem* **2010**, *11*, 670–682.

(96) Rastogi, A.; Paik, M. Y.; Tanaka, M.; Ober, C. K. *ACS Nano* **2010**, *4*, 771–780.

(97) Steenackers, M.; Sharp, I. D.; Larsson, K.; Hutter, N. A.; Stutzmann, M.; Jordan, R. *Chem. Mater.* **2010**, *22*, 272–278.

(98) Lenhardt, J. M.; Ong, M. T.; Choe, R.; Evenhuis, C. R.; Martinez, T. J.; Craig, S. L. *Science* **2010**, *329*, 1057–1060.

(99) Bünsow, J.; Kelby, T. S.; Huck, W. T. S. *Acc. Chem. Res.* **2010**, *43*, 466–474.

(100) Huang, H.; Chung, J. Y.; Nolte, A. J.; Stafford, C. M. *Chem. Mater* **2007**, *19*, 6555–6560.

(101) Azzaroni, O.; Trappmann, B.; van Rijn, P.; Zhou, F.; Kong, B.; Huck, W. T. S. *Angew. Chem. Int. Ed. Engl.* **2006**, *45*, 7440–7443.

(102) Lee, H.; Pietrasik, J.; Sheiko, S. S.; Matyjaszewski, K. *Prog. Polym. Sci.* **2010**, *35*, 24–44.

(103) Liu, F.; Urban, M. W. *Prog. Polym. Sci.* **2010**, *35*, 3–23.

(104) Stuart, M. A. C.; Huck, W. T. S.; Genzer, J.; Müller, M.; Ober, C.; Stamm, M.; Sukhorukov, G. B.; Szleifer, I.; Tsukruk, V. V; Urban, M.; Winnik, F.; Zauscher, S.; Luzinov, I.; Minko, S. *Nat. Mater.* **2010**, *9*, 101–113.

(105) Kozlovskaya, V.; Kharlampieva, E.; Erel, I.; Sukhishvili, S. A. *Soft Matter* **2009**, *5*, 4077.

(106) Tokarev, I.; Motornov, M.; Minko, S. *J. Mater. Chem.* **2009**, *19*, 6932.

(107) Zhao, B.; Zhu, L. *Macromolecules* **2009**, *42*, 9369–9383.

(108) Luzinov, I.; Minko, S.; Tsukruk, V. V. *Soft Matter* **2008**, *4*, 714.

(109) Crespy, D.; Rossi, R. M. *Polym. Int.* **2007**, *56*, 1461–1468.

(110) Ballauff, M. *Prog. Polym. Sci.* **2007**, *32*, 1135–1151.

(111) Ballauff, M.; Borisov, O. *Curr. Opin. Colloid Interface Sci.* **2006**, *11*, 316–323.

(112) Minko, S. *J. Macromol. Sci. Part C Polym. Rev.* **2006**, *46*, 397–420.

(113) Schmaljohann, D. *Adv. Drug Deliv. Rev.* **2006**, *58*, 1655–1670.

(114) Gil, E. S.; Hudson, S. M. *Prog. Polym. Sci.* **2004**, *29*, 1173–1222.

(115) Luzinov, I.; Minko, S.; Tsukruk, V. *Prog. Polym. Sci.* **2004**, *29*, 635–698.

(116) Sidorenko, A.; Minko, S.; Schenk-Meuser, K.; Duschner, H.; Stamm, M. *Langmuir* **1999**, *15*, 8349–8355.

(117) Wu, T.; Gong, P.; Szleifer, I.; Vlček, P.; Šubr, V.; Genzer, J. *Macromolecules* **2007**, *40*, 8756–8764.

(118) Treat, N. D.; Ayres, N.; Boyes, S. G.; Brittain, W. J. *Macromolecules* **2006**, *39*, 26–29.

(119) Biesalski, M.; Johannsmann, D.; Rühe, J. *J. Chem. Phys.* **2002**, *117*, 4988.

(120) Dai, X.; Zhou, F.; Khan, N.; Huck, W. T. S.; Kaminski, C. F. *Langmuir* **2008**, *24*, 13182–13185.

(121) Biesalski, M.; Rühe, J. *Macromolecules* **1999**, *32*, 2309–2316.

(122) Schepelina, O.; Zharov, I. *Langmuir* **2008**, *24*, 14188–14194.

(123) Biesalski, M.; Ruhe, J. *Macromolecules* **2003**, *36*, 1222–1227.

(124) Sanjuan, S.; Tran, Y. *J. Polym. Sci. Part A Polym. Chem.* **2008**, *46*, 4305–4319.

(125) Sanjuan, S.; Tran, Y. *Macromolecules* **2008**, *41*, 8721–8728.

(126) Biesalski, M.; Ruhe, J. *Macromolecules* **2002**, *35*, 499–507.

(127) Biesalski, M.; Ruhe, J. *Macromolecules* **2004**, *37*, 2196–2202.

(128) Plamper, F. A.; Schmalz, A.; Penott-Chang, E.; Drechsler, M.; Jusufi, A.; Ballauff, M.; Müller, A. H. E. *Macromolecules* **2007**, *40*, 5689–5697.

(129) Plamper, F. a.; Ruppel, M.; Schmalz, A.; Borisov, O.; Ballauff, M.; Müller, A. H. E. *Macromolecules* **2007**, *40*, 8361–8366.

(130) Ayres, N.; Boyes, S. G.; Brittain, W. J. *Langmuir* **2007**, *23*, 182–189.

(131) Ayres, N.; Cyrus, C. D.; Brittain, W. J. *Langmuir* **2007**, *23*, 3744–3749.

(132) Sanjuan, S.; Perrin, P.; Pantoustier, N.; Tran, Y. *Langmuir* **2007**, *23*, 5769–5778.

(133) Choi, E.-Y.; Azzaroni, O.; Cheng, N.; Zhou, F.; Kelby, T.; Huck, W. T. S. *Langmuir* **2007**, *23*, 10389–10394.

(134) Rodrı, M. J.; Gassa, L. M.; Azzaroni, O.; Gervasi, C. A.; Rodríguez Presa, M. J. *Anal. Chem.* **2009**, *81*, 7936–7943.

(135) Combellas, C.; Kanoufi, F.; Sanjuan, S.; Slim, C.; Tran, Y. *Langmuir* **2009**, *25*, 5360–5370.

(136) Bantz, M. R.; Brantley, E. L.; Weinstein, R. D.; Moriarty, J.; Jennings, G. K. *J. Phys. Chem. B* **2004**, *108*, 9787–9794.

(137) Brantley, E. L.; Holmes, T. C.; Jennings, G. K. *J. Phys. Chem. B* **2004**, *108*, 16077–16084.

(138) Brantley, E. L.; Holmes, T. C.; Jennings, G. K. *Macromolecules* **2005**, *38*, 9730–9734.

(139) Arifuzzaman, S.; Ozçam, A. E.; Efimenko, K.; Fischer, D. A.; Genzer, J. *Biointerphases* **2009**, *4*, FA33–44.

(140) Deng, X. M.; Castillo, E. J.; Anderson, J. M. *Biomaterials* **1986**, *7*, 247–251.

(141) Khoo, C. G. L.; Lando, J. B.; Ishida, H. *J. Polym. Sci. Part B Polym. Phys.* **1990**, *28*, 213–232.

(142) Zou, Y.; Rossi, N. A. A.; Kizhakkedathu, J. N.; Brooks, D. E. *Macromolecules* **2009**, *42*, 4817–4828.

(143) Husemann, M.; Morrison, M.; Benoit, D.; Frommer, J.; Mate, C. M.; Hinsberg, W. D.; Hedrick, J. L.; Hawker, C. J. *J. Am. Chem. Soc.* **2000**, *122*, 1844–1845.

(144) Brown, A. A.; Azzaroni, O.; Fidalgo, L. M.; Huck, W. T. S. *Soft Matter* **2009**, *5*, 2738.

(145) Brown, A. A.; Azzaroni, O.; Huck, W. T. S. *Langmuir* **2009**, *25*, 1744–1749.

(146) Liu, Z.; Liu, J.; Hu, H.; Yu, B.; Chen, M.; Zhou, F. *Phys. Chem. Chem. Phys.* **2008**, *10*, 7180–7185.

(147) Lim, H. S.; Lee, S. G.; Lee, D. H.; Lee, D. Y.; Lee, S.; Cho, K. *Adv. Mater.* **2008**, *20*, 4438–4441.

(148) Azzaroni, O.; Brown, A. A.; Huck, W. T. S. *Adv. Mater.* **2007**, *19*, 151–154.

(149) Döbbelin, M.; Arias, G.; Loinaz, I.; Llarena, I.; Mecerreyes, D.; Moya, S. *Macromol. Rapid Commun.* **2008**, *29*, 871–875.

(150) Spruijt, E.; Choi, E.-Y.; Huck, W. T. S. *Langmuir* **2008**, *24*, 11253–11260.

(151) Samanta, S.; Locklin, J. *Langmuir* **2008**, *24*, 9558–9565.

(152) Fries, K.; Samanta, S.; Orski, S.; Locklin, J. *Chem. Commun.* **2008**, 6288–6290.

(153) Bai, D.; Habersberger, B. M.; Jennings, G. K. *J. Am. Chem. Soc.* **2005**, *127*, 16486–16493.

(154) Bai, D.; Hardwick, C. L.; Berron, B. J.; Jennings, G. K. *J. Phys. Chem. B* **2007**, *111*, 11400–11406.

(155) Bai, D.; Ibrahim, Z.; Jennings, G. K. *J. Phys. Chem. C* **2007**, *111*, 461–466.

(156) Berron, B. J.; Payne, P. A.; Jennings, G. K. *Ind. Eng. Chem. Res.* **2008**, *47*, 7707–7714.

(157) Yu, B.; Hu, H.; Wang, D.; Huck, W. T. S.; Zhou, F.; Liu, W. *J. Mater. Chem.* **2009**, *19*, 8129.

(158) Tam, T. K.; Pita, M.; Motornov, M.; Tokarev, I.; Minko, S.; Katz, E. *Electroanalysis* **2010**, *22*, 35–40.

(159) Motornov, M.; Tam, T. K.; Pita, M.; Tokarev, I.; Katz, E.; Minko, S. *Nanotechnology* **2009**, *20*, 434006.

(160) Motornov, M.; Sheparovych, R.; Katz, E.; Minko, S. *ACS Nano* **2008**, *2*, 41–52.

(161) Tam, T. K.; Pita, M.; Trotsenko, O.; Motornov, M.; Tokarev, I.; Halámek, J.; Minko, S.; Katz, E. *Langmuir* **2010**, *26*, 4506–4513.

(162) Tam, T. K.; Ornatska, M.; Pita, M.; Minko, S.; Katz, E. *J. Phys. Chem. C* **2008**, *112*, 8438–8445.

(163) Tam, T. K.; Zhou, J.; Pita, M.; Ornatska, M.; Minko, S.; Katz, E. *J. Am. Chem. Soc.* **2008**, *130*, 10888–10889.

(164) Calvo, A.; Yameen, B.; Williams, F. J.; Soler-Illia, G. J. A. A.; Azzaroni, O. *J. Am. Chem. Soc.* **2009**, *131*, 10866–10868.

(165) Yameen, B.; Ali, M.; Neumann, R.; Ensinger, W.; Knoll, W.; Azzaroni, O. *Nano Lett.* **2009**, *9*, 2788–2793.

(166) Yameen, B.; Ali, M.; Neumann, R.; Ensinger, W.; Azzaroni, O.; Knoll, W. *Chem. Commun. (Camb).* **2010**, *46*, 1908–1910.

(167) Li, Y.; Benicewicz, B. C. *Macromolecules* **2008**, *41*, 7986–7992.

(168) Segalman, R. a. *Mater. Sci. Eng. R Reports* **2005**, *48*, 191–226.

(169) Shenhar, R.; Norsten, T. B.; Rotello, V. M. *Adv. Mater.* **2005**, *17*, 657–669.

(170) Haryono, A.; Binder, W. H. *Small* **2006**, *2*, 600–611.

(171) Kinge, S.; Crego-Calama, M.; Reinhoudt, D. N. *Chemphyschem* **2008**, *9*, 20–42.

(172) Ofir, Y.; Samanta, B.; Rotello, V. M. *Chem. Soc. Rev.* **2008**, *37*, 1814–1825.

(173) Wang, Y.; Angelatos, A. S.; Caruso, F. *Chem. Mater.* **2008**, *20*, 848–858.

(174) Boyes, S. G.; Akgun, B.; Brittain, W. J.; Foster, M. D. *Macromolecules* **2003**, *36*, 9539–9548.

(175) Lu, Y.; Mei, Y.; Walker, R.; Ballauff, M.; Drechsler, M. *Polymer.* **2006**, *47*, 4985–4995.

(176) Gupta, S.; Agrawal, M.; Conrad, M.; Hutter, N. A.; Olk, P.; Simon, F.; Eng, L. M.; Stamm, M.; Jordan, R. *Adv. Funct. Mater.* **2010**, *20*, 1756–1761.

(177) Azzaroni, O.; Brown, A. a.; Cheng, N.; Wei, A.; Jonas, A. M.; Huck, W. T. S. *J. Mater. Chem.* **2007**, *17*, 3433.

(178) Zhang, M.; Liu, L.; Wu, C.; Fu, G.; Zhao, H.; He, B. *Polymer.* **2007**, *48*, 1989–1997.

(179) Yu, B.; Zhou, F.; Bo, Y.; Hou, X.; Liu, W. *Electrochem. Commun.* **2007**, *9*, 1749–1754.

(180) Ye, Q.; Wang, X.; Hu, H.; Wang, D.; Li, S.; Zhou, F. *J. Phys. Chem. C* **2009**, *113*, 7677–7683.

(181) Choi, W. S.; Koo, H. Y.; Kim, J. Y.; Huck, W. T. S. *Adv. Mater.* **2008**, *20*, 4504–4508.

(182) Llarena, I.; Romero, G.; Ziolo, R. F.; Moya, S. E. *Nanotechnology* **2010**, *21*, 055605.

(183) Yu, K.; Wang, H.; Han, Y. *Langmuir* **2007**, *23*, 8957–8964.

(184) Gupta, S.; Uhlmann, P.; Agrawal, M.; Lesnyak, V.; Gaponik, N.; Simon, F.; Stamm, M.; Eychmüller, A. *J. Mater. Chem.* **2008**, *18*, 214.

(185) Liu, X.; Chang, H.; Li, Y.; Huck, W. T. S.; Zheng, Z. *ACS Appl. Mater. Interfaces* **2010**, *2*, 529–535.

(186) Proch, S.; Mei, Y.; Villanueva, J. M. R.; Lu, Y.; Karpov, A.; Ballauff, M.; Kempe, R. *Adv. Synth. Catal.* **2008**, *350*, 493–500.

(187) Schrinner, M.; Proch, S.; Mei, Y.; Kempe, R.; Miyajima, N.; Ballauff, M. *Adv. Mater.* **2008**, *20*, 1928–1933.

(188) Cho, W. K.; Kang, S. M.; Kim, D. J.; Yang, S. H.; Choi, I. S. *Langmuir* **2006**, *22*, 11208–11213.

(189) Tugulu, S.; Barbey, R.; Harms, M.; Fricke, M.; Volkmer, D.; Rossi, A.; Klok, H.-A. *Macromolecules* **2007**, *40*, 168–177.

(190) Tokareva, I.; Minko, S.; Fendler, J. H.; Hutter, E. *J. Am. Chem. Soc.* **2004**, *126*, 15950–15951.

(191) Gupta, S.; Uhlmann, P.; Agrawal, M.; Chapuis, S.; Oertel, U.; Stamm, M.; Simon, F. *Macromolecules* **2008**, *41*, 8152–8158.

(192) Gupta, S.; Agrawal, M.; Uhlmann, P.; Simon, F.; Oertel, U.; Stamm, M. *Macromolecules* **2008**, *41*, 8152–8158.

(193) Gupta, S.; Agrawal, M.; Uhlmann, P.; Simon, F.; Stamm, M. *Chem. Mater.* **2010**, *22*, 504–509.

(194) Koh, S. J. *Nanoscale Res. Lett.* **2007**, *2*, 519–545.

(195) Bhat, R. R.; Tomlinson, M. R.; Genzer, J. *Macromol. Rapid Commun.* **2004**, *25*, 270–274.

(196) Kim, J.; O'Shaughnessy, B. *Phys. Rev. Lett.* **2002**, *89*, 2–5.

(197) Diamanti, S.; Arifuzzaman, S.; Elsen, A.; Genzer, J.; Vaia, R. A. *Polymer.* **2008**, *49*, 3770–3779.

(198) Yu, K.; Wang, H.; Xue, L.; Han, Y. *Langmuir* **2007**, *23*, 1443–1452.

(199) Canalle, L. a; Löwik, D. W. P. M.; van Hest, J. C. M. *Chem. Soc. Rev.* **2010**, *39*, 329–353.

(200) Krishna, O. D.; Kiick, K. L. *Biopolymers* **2010**, *94*, 32–48.

(201) Jain, P.; Baker, G. L.; Bruening, M. L. *Annu. Rev. Anal. Chem.* **2009**, *2*, 387–408.

(202) Xu, F. J. J.; Neoh, K. G. G.; Kang, E. T. T. *Prog. Polym. Sci.* **2009**, *34*, 719–761.

(203) Kim, M.; Khang, G.; Lee, H.; Suk, M.; Bang, H. *Prog. Polym. Sci.* **2008**, *33*, 138–164.

(204) Bo, H. G.; Lutz, J.; Borner, H. *Prog. Polym. Sci.* **2008**, *33*, 1–39.

(205) Bayramoglu, G.; Yavuz, E.; Senkal, B. F.; Arica, M. Y. *Colloids Surfaces A Physicochem. Eng. Asp.* **2009**, *345*, 127–134.

(206) Henzler, K.; Haupt, B.; Ballauff, M. *Anal. Biochem.* **2008**, *378*, 184–189.

(207) Goto, M.; Okubo, T.; Kawakita, H.; Uezu, K.; Tsuneda, S.; Saito, K.; Tamada, M.; Sugo, T. *Biochem. Eng. J.* **2007**, *37*, 159–165.

(208) Ito, H.; Nakamura, M.; Saito, K.; Sugita, K.; Sugo, T. *J. Chromatogr. A* **2001**, *925*, 41–47.

(209) Sun, L.; Dai, J.; Baker, G. L.; Bruening, M. L. *Chem. Mater.* **2006**, *18*, 4033–4039.

(210) Jain, P.; Dai, J.; Baker, G. L.; Bruening, M. L. *Macromolecules* **2008**, *41*, 8413–8417.

(211) Gautrot, J. E.; Huck, W. T. S.; Welch, M.; Ramstedt, M. *ACS Appl. Mater. Interfaces* **2010**, *2*, 193–202.

(212) Liu, Z.; Khan, N.; Hu, H.; Yu, B.; Liu, J.; Chen, M.; Zhou, F. *Macromol. Rapid Commun.* **2008**, *29*, 1937–1943.

(213) Chen, L.; Rengifo, H. R.; Grigoras, C.; Li, X.; Li, Z.; Ju, J.; Koberstein, J. T. *Biomacromolecules* **2008**, *9*, 2345–2352.

(214) Reichhart, C.; Czeslik, C. *Langmuir* **2009**, *25*, 1047–1053.

(215) De Vos, W. M.; Biesheuvel, P. M.; de Keizer, A.; Kleijn, J. M.; Cohen Stuart, M. a; Vos, W. M. De; Keizer, A. De; Stuart, M. A. C. *Langmuir* **2008**, *24*, 6575–6584.

(216) Henzler, K.; Haupt, B.; Lauterbach, K.; Wittemann, A.; Borisov, O.; Ballauff, M. *J. Am. Chem. Soc.* **2010**, *132*, 3159–3163.

(217) Wilson, D. S.; Nock, S. *Angew. Chem. Int. Ed. Engl.* **2003**, *42*, 494–500.

(218) Angenendt, P.; Glökler, J.; Sobek, J.; Lehrach, H.; Cahill, D. J. *J. Chromatogr. A* **2003**, *1009*, 97–104.

(219) Tugulu, S.; Arnold, A.; Sielaff, I.; Johnsson, K.; Klok, H.-A. *Biomacromolecules* **2005**, *6*, 1602–1607.

(220) Waichman, S.; Bhagawati, M.; Podoplelova, Y.; Reichel, A.; Brunk, A.; Paterok, D.; Piehler, J. *Anal. Chem.* **2010**, *82*, 1478–1485.

(221) Trmcic-Cvitas, J.; Hasan, E.; Ramstedt, M.; Li, X.; Cooper, M. A; Abell, C.; Huck, W. T. S.; Gautrot, J. E. *Biomacromolecules* **2009**, *10*, 2885–2894.

(222) Yun, J.; Jung, C.-H.; Kim, D.; Hwang, I.; Choi, J.-H.; Ganesan, R.; Kim, J.-B. *J. Mater. Chem.* **2010**, *20*, 2007.

(223) Meier, H.; Zeller, K.-P. *Angew. Chemie Int. Ed. English* **1975**, *14*, 32–43.

(224) Zou, Y.; Yeh, P.-Y. J.; Rossi, N. a a; Brooks, D. E.; Kizhakkedathu, J. N. *Biomacromolecules* **2010**, *11*, 284–293.

(225) Cullen, S. P.; Liu, X.; Mandel, I. C.; Himpsel, F. J.; Gopalan, P. *Langmuir* **2008**, *24*, 913–920.

(226) Zhang, Z. B.; Yuan, S. J.; Zhu, X. L.; Neoh, K. G.; Kang, E. T. *Biosens. Bioelectron.* **2010**, *25*, 1102–1108.

(227) Iwata, R.; Satoh, R.; Iwasaki, Y.; Akiyoshi, K. *Colloids Surf. B. Biointerfaces* **2008**, *62*, 288–298.

(228) Iwasaki, Y.; Omichi, Y.; Iwata, R. *Langmuir* **2008**, *24*, 8427–8430.

(229) Wong, V. N.; Fernando, G.; Wagner, A. R.; Zhang, J.; Kinsel, G. R.; Zauscher, S.; Dyer, D. J. *Langmuir* **2009**, *25*, 1459–1465.

(230) Ayres, N.; Holt, D. J.; Jones, C. F.; Corum, L. E.; Grainger, D. W. *J. Polym. Sci. A. Polym. Chem.* **2008**, *46*, 7713–7724.

(231) Gabriel, G. J.; Som, A.; Madkour, A. E.; Eren, T.; Tew, G. N. *Mater. Sci. Eng. R. Rep.* **2007**, *57*, 28–64.

(232) Noimark, S.; Dunnill, C. W.; Wilson, M.; Parkin, I. P. *Chem. Soc. Rev.* **2009**, *38*, 3435.

(233) Ramstedt, M.; Cheng, N.; Azzaroni, O.; Mossialos, D.; Mathieu, H. J.; Huck, W. T. S. *Langmuir* **2007**, *23*, 3314–3321.

(234) Shchukarev, A. V; Bucht, A.; Ramstedt, M.; Ekstrand-hammarstro, B.; Welch, M.; Huck, W. T. S.; Lars, O.; Ekstrand-Hammarström, B.; Osterlund, L. *Biomaterials* **2009**, *30*, 1524–1531.

(235) Huang, J.; Koepsel, R. R.; Murata, H.; Wu, W.; Lee, S. B.; Kowalewski, T.; Russell, A. J.; Matyjaszewski, K. *Langmuir* **2008**, *24*, 6785–6795.

(236) Madkour, A. E.; Dabkowski, J. M.; Nüsslein, K.; Tew, G. N.; Nusslein, K. *Langmuir* **2008**, *25*, 1060–1067.

(237) Glinel, K.; Jonas, A. M.; Jouenne, T.; Galas, L.; Huck, W. T. S.; Leprince, J. *Bioconjug. Chem.* **2009**, *20*, 71–77.

(238) Ignatova, M.; Voccia, S.; Gabriel, S.; Gilbert, B.; Cossement, D.; Jérôme, R.; Jérôme, C.; Je, R.; Je, C. *Langmuir* **2008**.

(239) Yuan, S. J.; Pehkonen, S. O.; Ting, Y. P.; Neoh, K. G.; Kang, E. T. *ACS Appl. Mater. Interfaces* **2009**, *1*, 640–652.

(240) Lee, S. B.; Koepsel, R. R.; Morley, S. W.; Matyjaszewski, K.; Sun, Y.; Russell, A. J. *Biomacromolecules* **2004**, *5*, 877–882.

(241) Langer, R. *Tissue Eng.* **2007**, *13*, 1–2.

(242) Raynor, J. E.; Capadona, J. R.; Collard, D. M.; Petrie, T. a.; García, A. J. *Biointerphases* **2009**, *4*, FA3.

(243) Xu, F. J.; Zhong, S. P.; Tong, Y. W.; Kang, E. T.; Neoh, K. G.; Yung, L. Y. L. *Tissue Eng.* **2005**, *11*, 1736–1748.

(244) Rimmer, S.; Johnson, C.; Zhao, B.; Collier, J.; Gilmore, L.; Sabnis, S.; Wyman, P.; Sammon, C.; Fullwood, N. J.; MacNeil, S. *Biomaterials* **2007**, *28*, 5319–5331.

(245) Patrucco, E.; Ouasti, S.; Vo, C. D.; De Leonardis, P.; Pollicino, A.; Armes, S. P.; Scandola, M.; Tirelli, N. *Biomacromolecules* **2009**, *10*, 3130–3140.

(246) Tugulu, S.; Silacci, P.; Stergiopulos, N.; Klok, H.-A. *Biomaterials* **2007**, *28*, 2536–2546.

(247) Lavanant, L.; Pullin, B.; Hubbell, J. a; Klok, H.-A. *Macromol. Biosci.* **2010**, *10*, 101–108.

(248) Navarro, M.; Benetti, E. M.; Zapotoczny, S.; Planell, J. A.; Vancso, G. J. *Langmuir* **2008**, *24*, 10996–11002.

(249) Hannachi, I. E.; Yamato, M.; Okano, T. *Biofabrication* **2009**, *1*, 022002.

(250) Tsuda, Y.; Kikuchi, A.; Yamato, M.; Nakao, A.; Sakurai, Y.; Umezu, M.; Okano, T. *Biomaterials* **2005**, *26*, 1885–1893.

(251) Tsuda, Y.; Shimizu, T.; Yamato, M.; Kikuchi, A.; Sasagawa, T.; Sekiya, S.; Kobayashi, J.; Chen, G.; Okano, T. *Biomaterials* **2007**, *28*, 4939–4946.

(252) Xu, F. J.; Zhong, S. P.; Yung, L. Y. L.; Tong, Y. W.; Kang, E.-T.; Neoh, K. G. *Biomaterials* **2006**, *27*, 1236–1245.

(253) Genzer, J.; Arifuzzaman, S.; Bhat, R. R.; Efimenko, K.; Ren, C.; Szleifer, I. *Langmuir* **2012**, *28*, 2122–2130.

(254) Badi, N.; Lutz, J.-F. *Chem. Soc. Rev.* **2009**, *38*, 3383–3390.

(255) Lutz, J.-F. *Polym. Chem.* **2010**, *1*, 55–62.

(256) Hartmann, L.; Börner, H. G. *Adv. Mater.* **2009**, *21*, 3425–3431.

(257) Zaremski, M. Y.; Kalugin, D. I.; Golubev, V. B. *Polym. Sci. Ser. A* **2009**, *51*, 103–122.

(258) Khokhlov, A.; Khalatur, P. *Phys. Rev. Lett.* **1999**, *82*, 3456–3459.

(259) Khalatur, P. G.; Khokhlov, A. R. In *Advances in Polymer Science*; 2006; pp. 1–100.

(260) Semler, J. J.; Genzer, J. *J. Chem. Phys.* **2006**, *125*, 014902.

(261) Semler, J. J.; Jhon, Y. K.; Tonelli, A.; Beevers, M.; Krishnamoorti, R.; Genzer, J. *Adv. Mater.* **2007**, *19*, 2877–2883.

(262) Strickland, L. A.; Hall, C. K.; Genzer, J. *Macromolecules* **2009**, *42*, 9063–9071.

(263) Strickland, L. A.; Hall, C. K.; Genzer, J. *Langmuir* **2010**, 1–38.

(264) Jhon, Y. K.; Semler, J. J.; Genzer, J.; Beevers, M.; Gus'kova, O. a.; Khalatur, P. G.; Khokhlov, A. R. *Macromolecules* **2009**, *42*, 2843–2853.

(265) Han, J.; Jeon, B. H.; Ryu, C. Y.; Semler, J. J.; Jhon, Y. K.; Genzer, J. *Macromol. Rapid Commun.* **2009**, *30*, 1543–1548.

(266) Genzer, J.; Khalatur, P. G.; Khokhlov, A. R. In *Polymer Science: A Comprehensive Reference*; Matyjaszewski, K.; Moller, M., Eds.; Elsevier: Amsterdam, 2012; Vol. 6, pp. 689–723.

3. Degrafting of Polyelectrolyte Brushes from Solid Substrates in Aqueous Environments

3.1 Introduction

Polymer brushes have received increased interest in the soft matter research community over the past decade[1]. These assemblies, which for this Chapter we will define as polymer chains covalently tethered to a solid substrate, offer two distinct advantages as surface coatings. First, through the scheme of post-polymerization modification[2,3], the side-chain chemistry of the macromolecules can be tuned to include a variety of functional groups. Since polymer brushes extend away from the substrate, the density of these functional groups is significantly higher than a monolayer assembly. In the case of polyelectrolytes and polyzwitterions, electrostatic charges are produced as a by-product of the modification reaction. These systems have emerged in recent years as platforms for anti-microbial and anti-fouling coatings, respectively[2], and offer a system with rich physics to study theoretically, experimentally and with simulations.

The second advantage of these structures is a permanency due to the covalent graft between the polymer chains and the substrate. However, the field of mechano-chemistry has demonstrated recently the severing of carbon-carbon single bonds in polymer chains through purely physical forces[4–7]. The systems required to generate forces capable of appreciably changing the lifetime of a covalent bond (≈ 100 pN) are not exotic or rare, and include densely grafted polymer brushes[8]. Moreover, theory has shown a three order of magnitude increase in tension (pN → nN) can occur in tethered polymer chains by adding bulkier pendant groups[8]. Indeed, some reports of tethered polymer chains degrafting from substrates have appeared in the literature[9,10]. Even if outright bond scission does not occur, additional tension can activate certain functional groups, such as ester bonds[7], to more readily undergo chemical transformation. We emphasize the importance of ester groups here because of their prevalence in polymerization initiator molecules, notably Rühe's initiator for free radical polymerization[11] and BMPUS, the standard initiator for atom transfer radical polymerization (ATRP)[12]. Prior work has suggested these functional groups are particularly liable to degrafting[13].

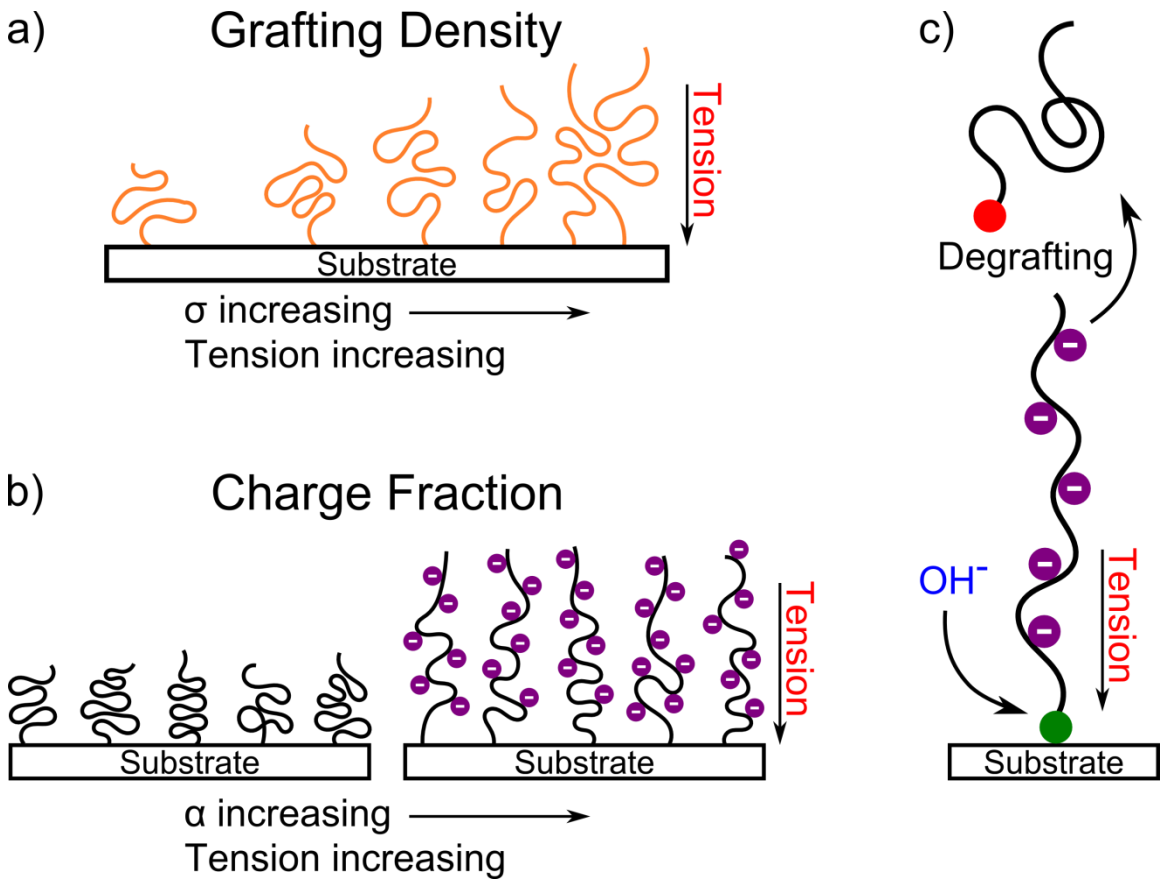

Figure 3.1. a) Influence of σ on tension generated along chain backbone. b) Influence of α on tension generated along chain backbone. Cartoon is drawn for a polyacid (*e.g.*, PMAA). Counterions not depicted for clarity. c) Proposed degrafting mechanism where tension generated along chain backbone activates grafting chemistry for hydrolysis by hydroxyl ions. Neighboring chains, counterions and charges on degrafted chain not depicted for clarity. Cartoons not drawn to scale.

One factor affecting the tension present in a surface grafted polymer film is the grafting density (σ) of chains at the surface[8]. As σ increases, the tethered chains will extend away from the surface due to excluded volume effects[14], as suggested in **Figure 3.1a**. This extension generates tension along the polymer chain backbone beyond the inherent tension in a free polymer. A second factor is repulsion between electrostatic charges in the polymer side chain. As the charge fraction, α, of the polymer brush increases, the chains will stretch away from the substrate[15], generating additional tension along the polymer backbone. This concept is depicted schematically in **Figure 3.1b**. The level of α in a weak polyelectrolyte will depend on solution pH and on σ. Since the

proposed degrafting mechanism involves hydrolysis by hydroxyl ions in solution (*cf.* shown in **Figure 3.1c**) brush degrafting from the substrate will exhibit a complex interplay among these three parameters. This Chapter explores the influence of α, σ and pH in the degrafting of weak polyelectrolyte brushes comprising poly(methacrylic acid) (PMAA) or poly(2-(dimethylamino)ethyl methacrylate) (PDMAEMA), leveraging gradient techniques to demonstrate the interplay of these parameters. Additional findings are also presented showing the influence of these three parameters on the surface morphology of PDMAEMA brushes.

3.2 Experimental

3.2.1 General Methods and Materials

Ethanol, dimethylsulfoxide (DMSO), (dimethylamino)ethyl methacrylate (DMAEMA), *tert*-butyl methacrylate (tBMA), N,N,N',N',N''-pentamethyldiethylenetriamine (PMDETA), 2,2'-bipyridyl, CuCl, trifluoroacetic acid (TFA), dichloromethane (DCM) and inhibitor remover packing were purchased from Sigma-Aldrich and used as received. Monosodium phosphate and disodium phosphate were purchased from Fisher Scientific and used as received. *n*-Octyltrichlorosilane (OTS) was purchased from Gelest and used as received. 0.5 mm thick, 100 mm diameter silicon wafers were purchased from Silicon Valley Microelectronics.

3.2.2 Sample Preparation

3.2.2.1 Initiator Deposition

[11-(2-bromo-2-methyl)propionyloxy] undecyltrichlorosilane (BMPUS) was synthesized according to the method of Matyjaszewski and coworkers[12]. Silicon wafers measuring 4.5 cm x 5 cm were sonicated in methanol, dried with a stream of N_2 gas, and treated in a UV-Ozone apparatus for 20 minutes. Wafers were then placed perpendicular to a well containing a mixture of OTS in mineral oil (1:4) for 7 minutes. After OTS deposition, the wafer was immediately placed into a solution of 30 μL of 5 vol % BMPUS in anhydrous toluene and 30 mL of anhydrous toluene and incubated at -20^{o} C overnight. The wafer was then removed from solution, rinsed with ethanol, dried with a stream of N_2 gas, then sonicated in ethanol for 20 minutes and dried with a stream of N_2 gas. The wafer was then immediately analyzed by contact angle using deionized (DI) H_2O as a probing liquid, then dried with a stream of N_2 gas before polymerization.

3.2.2.2 PMAA Brush Synthesis

The polymerization solution comprised 45 mL of tBMA (purified by passing through a column containing inhibitor remover), 45 mL of DMSO, 40 μL of PMDETA, and 0.058 g of CuCl. This solution was degassed by bubbling with N_2 gas for 30 minutes, then charged using a degassed glass syringe to a custom-built glass reactor containing an initiator-modified wafer. The polymerization proceeded for one hour, at which point the reactor was opened and the wafer removed. The wafer was rinsed thoroughly with ethanol, then sonicated in ethanol for 20 minutes, followed by drying with a stream of N_2 gas. The PtBMA brush was then characterized using ellipsometry, followed by hydrolysis for a total of 40 minutes by a 50 vol % solution of TFA in DCM to yield the PMAA brush.

3.2.2.3 PDMAEMA Brush Synthesis

The polymerization solution comprised 50 mL of DMAEMA (purified by passing through a column containing inhibitor remover), 50 mL of DMSO, 3.1251 g 2,2'-bipyridyl, and 0.9339 g of CuCl. This solution was degassed by bubbling with N_2 gas for 30 minutes, then charged using a degassed glass syringe to a custom-built glass reactor containing an initiator-modified wafer. The polymerization proceeded for three hours, at which point the reactor was opened and the wafer removed. The wafer was rinsed thoroughly with ethanol, then sonicated in ethanol for 20 minutes, followed by drying with a stream of N_2 gas.

3.2.3 Incubation Experiments

Buffer solutions with strengths of 10 mM were prepared using sodium phosphate salts and adjusted to pH 4, 7.4 and 9 using minute quantities of HCl and KOH. The pH of each buffer was measured to ± 0.02 using an Accumet AB15 pH meter (Fisher Scientific) equipped with a platinum pH electrode. Periodic measurement of the buffer solutions were done to ensure no pH drift occurred. The parent polymer brush samples were segmented into 1 cm wide samples and placed individually into glass vials containing buffer solution that had been filtered using 0.2 μm syringe filters. The vials were then sealed and stored in the dark at room temperature for the duration of the incubation. After a certain incubation time (*i.e.*, 24 or 120 hours), the samples were removed, rinsed briefly with DI H_2O and dried with a stream of N_2 gas and stored for further characterization.

3.2.4 Characterization Techniques

3.2.4.1 Spectroscopic ellipsometry

Measurements were performed on a Variable Angle Spectroscopic Ellipsometer (J.A. Woollam) controlled by WVASE32 (J.A. Woollam). For brush thicknesses > 30 nm, data were collected at incidence angles of 65°, 70° and 75° from wavelengths of 400 to 1000 nm. These data were fit to a model comprising a Si substrate, SiO_x layer (thickness 1.5 nm) and a Cauchy layer. The Si and SiO_x layers used material files supplied with the WVASE32 software. The Cauchy layer was fit using thickness, A_n and B_n. For thicknesses < 30 nm, the thickness and Cauchy parameters cannot be independently fit. Thus, data were collected at 632.8 nm over a range of incidence angles from 60° to 80° in 1° increments. These data were fit to a model comprising a Si substrate, SiO_x layer (thickness 1.5 nm) and a Cauchy layer. The Cauchy parameters were held constant using values obtained at the thickest part of the brush. Only thickness was used as a fitting parameter.

3.2.4.2 Infrared Variable Angle Spectroscopic Ellipsometry (IR-VASE)

Measurements were performed on an IR-VASE (J.A. Woollam) controlled by WVASE-IR software (J.A. Woollam) at a 50° angle of incidence with a resolution of a 4 cm^{-1}. The data were fitted using the WVASE32 software package (J.A. Woollam) to a model comprising a Si substrate, SiO_x layer (thickness 1.5 nm) and a general oscillator layer. These layers used material files supplied with the WVASE32 software. The absorption peaks in the ellipsometric data associated with chemical functional groups were modeled by Gaussian oscillators. The amplitude, width and location of these peaks were fit to the ellipsometric data over a range of 1000 cm^{-1} to 4000 cm^{-1}. The peaks near 1550 cm^{-1} and 1720 cm^{-1} were fit for each sample, and the ratio of the amplitudes of these peaks (A_{1550} and A_{1720}, respectively) used to calculate $\beta = A_{1550}/A_{1720}$.

3.2.4.3 Atomic Force Microscopy

Surface topography measurements were made in air using an Asylum MFP-3D system (Asylum Research) in tapping mode using Si tips (Model AC160TS; Asylum Research) with a resonance frequency of 300 kHz and spring constant of 42 N/m. Scans were collected over an area of 4 μm x 4 μm at a scan rate of 1.0 Hz and resolution 512 lines/scan. Data were analyzed in the Gwyddion software package[16] (http://gwyddion.net).

3.3 Results and Discussion

3.3.1 Dense PMAA Brush Degrafting

In order to investigate the influence of polymer chain grafting density (σ) and pH on the stability of surface-grafted polymer chains, samples expressing a gradient in initiator (BMPUS) fraction were prepared using a method reported previously[14]. The BMPUS fraction at a given location on the wafer was determined from water contact angle (WCA) measurement data analyzed by the Cassie-Baxter equation. Polymerizing these BMPUS gradient samples with *tert*-butyl methacrylate (tBMA) leads to surface-anchored PtBMA assemblies that express a gradient in σ as a function of position on the substrate. Poly(methyacrylic acid) (PMAA) brushes were derived from the PtBMA gradient sample using a post-polymerization modification (PPM) strategy, in which the pendant *t*-butyl groups were hydrolyzed with trifluoroacetic acid (TFA). This sample was then segmented into three samples 1 cm in width and 4 cm long for further incubation in pH buffer solutions.

The thicknesses of the PtBMA brushes as a function of substrate position are plotted in **Figure 3.2a-c** as the black data. A smooth variation in thickness as a function of position on the sample is seen in each sample, and is consistent with the variation in BMPUS fraction on the substrate prior to polymerization. Assuming that the MW of the grafted polymer chains is comparable along the substrate (*i.e.*, the polymerization rate does not depend dramatically on the density of the initiator centers), the differences in thickness of the PtBMA brush originate from differences in σ and ultimately from the variation in BMPUS fraction on the substrate.

The thickness maximum at 1.5 cm is a real feature based on visual inspection of the samples. A darker coloration consistent with a thicker polymer brush is visible just after the gradient region (position < 1.5 cm) compared to the lighter coloration in the homogeneous portion of the brush (position > 2.0 cm). We do not have a clear explanation for this result at this time. The thicker brush in this region suggests that the sample is somehow more densely grafted assuming a constant MW of the grafted chains as a function of σ. One possibility is that the slight dilution of initiating sites at this point on the substrate (BMPUS fraction ≈ 0.95) leads to a higher initiating efficiency as a result of a reduction in interference from neighboring chains. The efficiency of surface-grafted initiators is known to be low (≈10 %)[17–19], so a relative increase in efficiency at an intermediate grafting density—due to a reduction in blocking of initiators—could lead to a higher chain grafting density,

even if the initiator fraction is lower. Our data does not provide sufficient information to prove or disprove this claim, which would require careful control of initiation and polymerization kinetics.

The red data in **Figure 3.2a-c** depict the thickness of the PMAA samples derived by hydrolyzing the PtBMA brushes with TFA. For all samples, the shape of the PMAA thickness profile replicates that of the original PtBMA brush, in which thickness of the chains increases with increasing wafer position. The reduction in thickness stems from the removal of the bulky *t*-butyl group from the polymer side chain. The red data in **Figure 3.2d-e** show the thickness of the PMAA samples normalized by the PtBMA brush thickness. The homogeneous portion of the samples (*i.e.*, little variation in σ; position > 2.0 cm) shows a consistent reduction in thickness for all three samples to ≈ 0.58. The gradient portion of the samples (position < 1.5 cm) follows a less consistent pattern, and does not indicate a clear trend in behavior. Note that these samples were not exposed to aqueous solution prior to the measurements from which these data are derived. While two of the samples show a smaller thickness reduction in the gradient region compared to the homogeneous region, the other sample shows a greater thickness reduction. The origin of these differences is not apparent from the data.

Following hydrolysis of the PtBMA brushes to PMAA brushes, the samples were incubated in phosphate buffer solutions at pH 4, 7.4 or 9 (all 10 mM of total salt) for 24 hours. After incubation, the samples were removed from the buffer solutions, dried by a stream of nitrogen gas, and characterized by ellipsometry. The blue data in **Figure 3.2a-c** plots the resulting thickness of the brush as a function of substrate position. The sample incubated at pH 4 shows no significant change in thickness, consistent with the pK_a value of PMAA brushes[20] of ≈ 7.0. At pH 4, the polymer brush will be largely uncharged and thus will swell only marginally. In contrast, the samples incubated at pH 7.4 and pH 9 show an increase in thickness at 24 hours of incubation over the entire range of substrate positions. The blue data in **Figure 3.2d-f** depict the thickness of PMAA at 24 hours of incubation normalized by the initial PMAA thickness.

For all three pH levels, the sparsest region of the brush shows no significant increase in thickness. The sample incubated at pH 4 shows a slight increase within the gradient, and essentially no swelling in the homogeneous portion of the substrate. In contrast, the samples incubated at pH 7.4 and pH 9 show a trend of increasing swelling with increasing wafer position. Furthermore, the sample at pH 9 exhibits a higher swelling factor than the pH 7.4 sample. This finding is consistent with charging within the brush. As the charge fraction (α) of the brush increases with increasing pH,

the brush thickness increases as well due to repulsion among changes within the brush. This leads to water retention within the brush, even after drying under a stream of nitrogen gas, and accounts for the observed increase in thickness. This point will be considered in further detail later in this chapter.

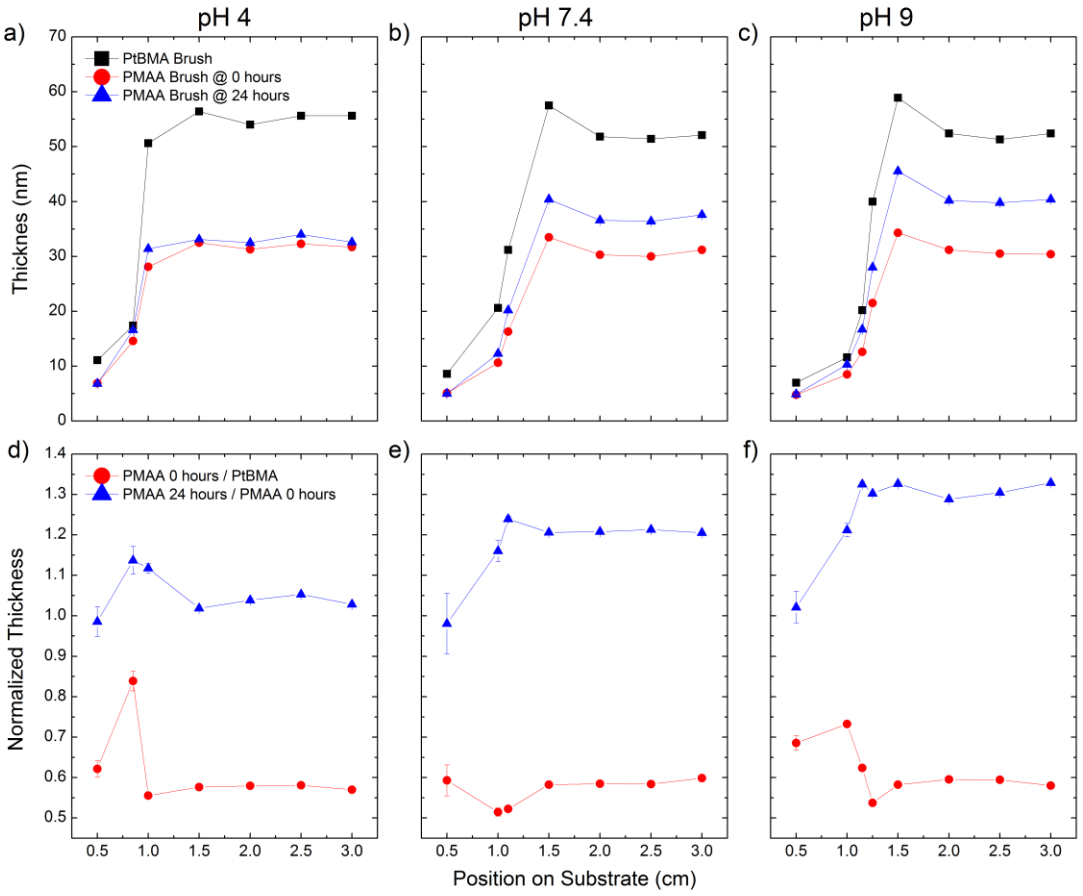

Figure 3.2. a-c) Thickness profiles as a function of position on the substrate for PtBMA brushes (black squares) and PMAA brushes at 0 and 24 hours of incubation (red circles and blue triangles, respectively) in buffer solutions at pH 4 (a), 7.4 (b) or 9 (c). d-f) Data from panels a-c comprising PMAA at 0 hours normalized by PtBMA thickness (red circles) and PMAA at 24 hours normalized by PMAA at 0 hours incubation (blue squares) for buffer solutions at pH 4 (d), 7.4 (e) or 9 (f).

The samples were further incubated in identical pH buffer solutions for 120 hours or more followed by characterization with ellipsometry. Focusing on the point of highest σ for each sample (sample position = 3.0 cm; BMPUS fraction > 0.99), the thickness at this point is plotted as a function

incubation time in **Figure 3.3a**. The thicknesses after 24 hours of incubation show a larger increase with a higher pH, as noted in the prior paragraph. With increasing incubation time, the thickness of the sample incubated at pH 4 remains relatively constant. In contrast, the samples incubated at pH 7.4 and 9 show decreasing thickness values over the entire range of incubation times. After approximately 350 hours, the samples at pH 7.4 and pH 9 exhibit thicknesses that are lower than that corresponding to the specimen incubated at pH 4. After 550 hours, the samples incubated at pH 7.4 and pH 9 have thicknesses lower than their initial, pre-incubation level. The thickness data in **Figure 3.3b** are normalized to the thickness values at 24 hours. This normalization reveals that the reduction in thickness follows the pH level of the incubating solution, such that higher pH levels lead to greater reductions in thickness.

Figure 3.3c plots $\beta = A_{1550}/A_{1720}$, as determined from IR-VASE spectra, the ratio of peak amplitudes associated with charged carboxylate groups (*i.e.*, COO^-; A_{1550}) to uncharged carboxylic groups (*i.e.*, COOH; A_{1720}). Note that β is not a direct measure of α in the brush; rather, it is used here to assess qualitative differences between the samples incubated at different pH levels. The magnitude of β increases with increasing pH, consistent with other observations, which suggest that α increases with increasing pH. Furthermore, over the entire incubation range, β remains constant within error, suggesting that α does not change appreciably during the measurement periods of these experiments. The large error bars associated with the data point for pH 9 at 554 hours stems from the relatively large error associated with determining the height of the carboxylic peak. Propagation of the large relative error in this peak leads to the large error bars, even though the absolute size of the carboxylic peak is small compared to the carboxylate peak.

We can now return to the thickness increase observed after 24 hours incubation, and how water can remain in the brush despite drying extensively with a stream of nitrogen gas. The data in **Figure 3.3c** suggest that water trapped in the brush is not H_2O, but H_3O^+ that is acting as a counterion to the dissociated carboxylic group, COO^-, in the polymer side chain. Alternatively, sodium ions from the phosphate buffer are acting as the counterion. Either way, the implication is that the increase in brush thickness after the initial incubation is due to a chemical transformation of the carboxylic acid groups in the side chain, and not from H_2O physically trapped in the film.

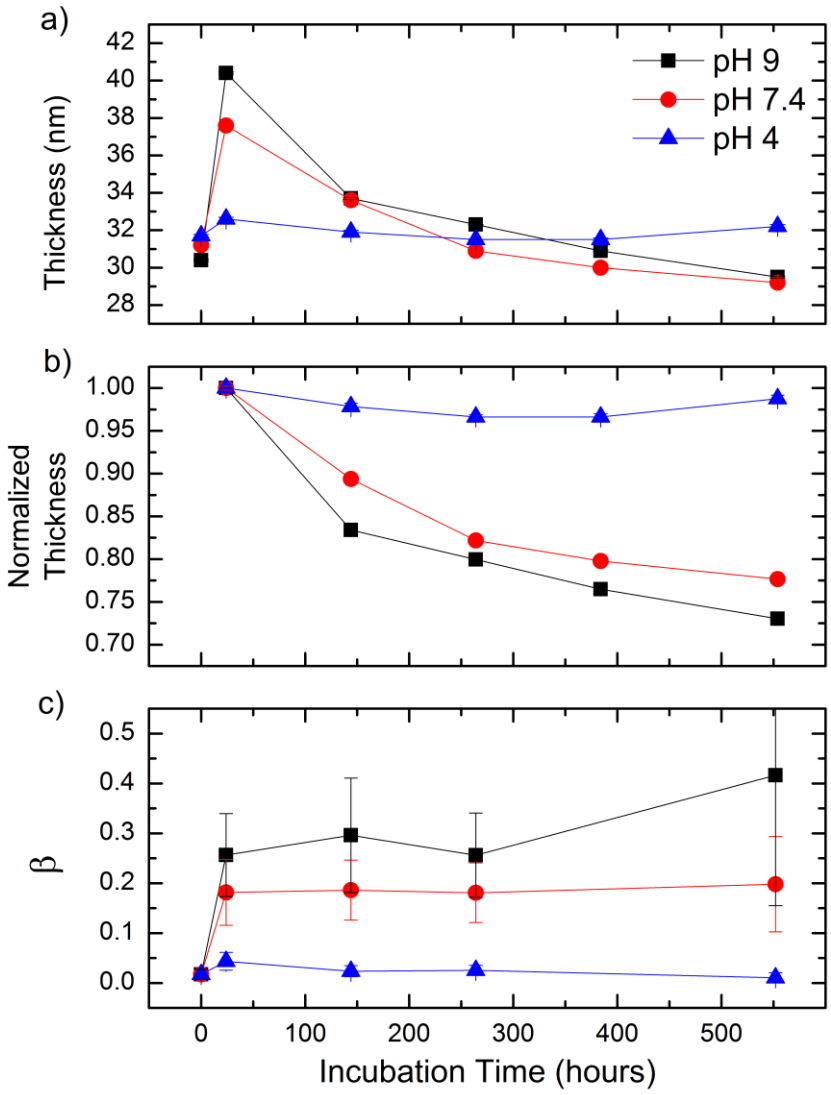

Figure 3.3. a) Thickness of PMAA brushes measured at a wafer position of 3.0 cm (densest σ) plotted as a function of incubation time for samples incubated at pH 9 (black squares), pH 7.4 (red circles) and pH 4 (blue triangles). b) The data in panel a) incubated by the thickness measured at 24 hours incubation. c) Calculated values of β derived from IR-VASE data (see text).

From the data in **Figure 3.2** and **3.3**, we conclude, as others have done previously[13], that the mechanism of degrafting in densely-grafted, weak polyelectrolyte brushes requires tension generated along the polymer chain backbone due to electrostatic repulsion (*cf*. **Figure 3.1c**). This tension

focuses at the chains grafting point, *i.e.*, the initiator, and leads to activation of either the ester group in BMPUS[13] or the siloxane bonds[9,10] at the initiator/substrate interface (or both) by mechanical force. Hydroxyl groups in the incubation solution then hydrolyze these activated bonds, leading to chain degrafting. While both of these locations have been suggested as the point of degrafting, the data in this chapter do not unambiguously confirm which is the primary point of hydrolysis. Under this scenario, the degrafting should increase with increasing pH for a weak polyacid like PMAA, since α and [OH^-] both increase with pH, leading to increased electrostatic repulsion and hydrolysis. That hypothesis is confirmed by the data in **Figure 3.3**.

3.3.2 Sparse PMAA Brush Degrafting

As described in the previous section, degrafting of densely-grafted, weak polyelectrolyte brushes requires mechanical tension generated from electrostatic repulsion. This tension acts in addition to that generated by densely grafting chains on to a solid substrate. Achieving high σ values leads to the extension of the chains away from the substrate due to excluded volume effects[14]. Like electrostatic repulsion inducing tension along the chain backbone, extension of the chains due to high σ will also generate tension that can activate the liable function groups. Therefore, σ will influence the degrafting behavior of a polymer brush. In particular, one expects that polymer assemblies with higher σ will be more liable towards degrafting due to higher osmotic swelling relative to brushes with lower σ.

Figure 3.4 plots the incubated thicknesses, normalized by the thickness at 24 hours incubation, for the three samples described in **Figure 3.2** as a function of PtBMA thickness on the lower abscissa. While not a direct measure of σ without prior knowledge of the system, the PtBMA thickness is an accessible and appropriate proxy based on the gradient thickness profiles in **Figure 3.2**. Using PtBMA thickness as the abscissa variable reveals indirectly trends in the stability of PMAA brushes due to variations in σ. Measuring σ by non-destructive means remains an open issue in the field of polymer science and is beyond the scope of this study. An estimate of σ is provided along the upper abscissa by assuming a value of 0.45 chains/nm^2 at the densest region of the brush[21], and scaling the sparser regions according to a mass balance assuming constant MW of grafted chains along the gradient. In general, increasing pH level leads to greater reductions in thickness regardless of PtBMA thickness (*i.e.*, σ value). The data for pH 4 suggest no clear trend with incubation time, and remain within 80 % of the initial thickness. In contrast, the samples incubated at pH 7.4 and pH 9

show continuous reductions in thickness with time. That finding is in line with the observations in **Figure 3.3**, where higher pH levels lead to greater thickness reduction.

For pH 7.4 and pH 9 incubations, the data develop a distinct minimum at intermediate PtBMA thickness, which correspond to σ levels of ≈ 0.10 - 0.15 chains/nm^2. Comparing the data at these minima between the two pH levels, there is a rapid decrease in thickness for pH 9 after 144 hours, followed by a relatively stable thickness. In contrast, the sample at pH 7.4 shows a slower reduction in thickness at this minimum. This difference in degrafting rate may stem from different levels of α within the brush. The higher α at pH 9 would lead to higher rates of activation of the bonds liable to hydrolysis compared to pH 7.4, leading to a more rapid loss of chains from the surface. After a certain reduction in σ due to the loss of these chains, the tension generated by chain crowding would diminish, leading to a reduction in the rate of degrafting. The sample at pH 9 may have reached that point by 264 hours, while the sample at pH 7.4 has not.

There is no clear explanation at the moment for this minimum at intermediate σ values. One possibility is that the grafted chains provide less protection of the substrate from the incubation solution at lower σ. As a result, hydroxyl ions are better able to reach the grafting chemistry and hydrolyze the grafted bond. This increased accessibility would lead to an increase in hydroxyl concentration at the brush/initiator linkage point. The higher concentration may offset the lower levels of tension at lower σ, leading to higher rates of degrafting. In a similar vein, the sparser brush may experience a different pH at the interface than the dense brush due to a reduction in concentration of carboxylic groups. In areas of high σ, the buffering agents may not be able to access the interface due to steric exclusion. The pH of the solution at the interface would then be markedly different from bulk solution, and presumably would shift to lower pH levels due to the high concentration of acidic carboxylic moieties. As σ decreases, the areal density of carboxylic groups would decrease, while the interface would become more accessible to buffering agents. That combination would result in higher pH levels at the interface, and thus higher rates of degrafting at an intermediate σ.

In the case of weak polyelectrolyte brushes, σ will influence α due to charge regulation[15]. Charge regulation in polymer brushes occurs when the brush achieves a lower α than expected from the solution pH. Due to the high entropy cost of grafting and chain extension, the polymer chain is less likely to form an additional ionic group, which would lead to further chain extension and reduced entropy. A reduction in σ may lead to an increase in α since the entropic restrictions on the brush will

decrease. We have shown earlier that a higher α leads to higher rates of degrafting (*cf.* **Figure 3.3**). That would also lead to an increased degrafting at an intermediate σ. Finally, the increased reductions in thickness may be related to a change in grafting regime of the brush at intermediate σ. As noted before, in a polymer brush the chains extend away from the substrate due to crowding from neighboring chains. As chains are removed due to degrafting, σ decreases, which, in turn, leads to a reduction in measured film thickness. Depending on σ, the grafted chains may be in a true brush regime (highest σ), a mushroom regime (lowest σ) or some transition regime between these two end points[22]. The rate of thickness change with σ is not necessarily constant in these different regimes. Thus, the points at intermediate BMPUS may exhibit a greater relative thickness change because they are changing regimes.

Careful examination of the data in **Figure 3.4** shows certain unexpected trends, wherein the thickness of the brush increases from the prior thickness level. The observation of thickness increases occur at intermediate σ levels for pH 7.4 and pH 9. In both cases, these increases occur after 385 hours of cumulative incubation, followed by apparent resumption of the downward trend at 554 hours. Regions of higher and lower σ exhibit decreasing thickness levels over this period. One additional feature of note in the pH 9 data for the teal data set is the constant thickness from 24 hours to 144 hours, over which period all other BMPUS fractions exhibited a decline in thickness. These observations of non-monotonic thickness decreases at intermediate σ are perplexing, and insufficient data exists currently to determine if they are in fact real features. Should further experiments continue to document such trends, a first hypothesis to test is if reducing σ in weak polyelectrolyte brushes can lead to an increase in α as a result of reduced charge regulation[23], especially if a new scaling regime is accessed.

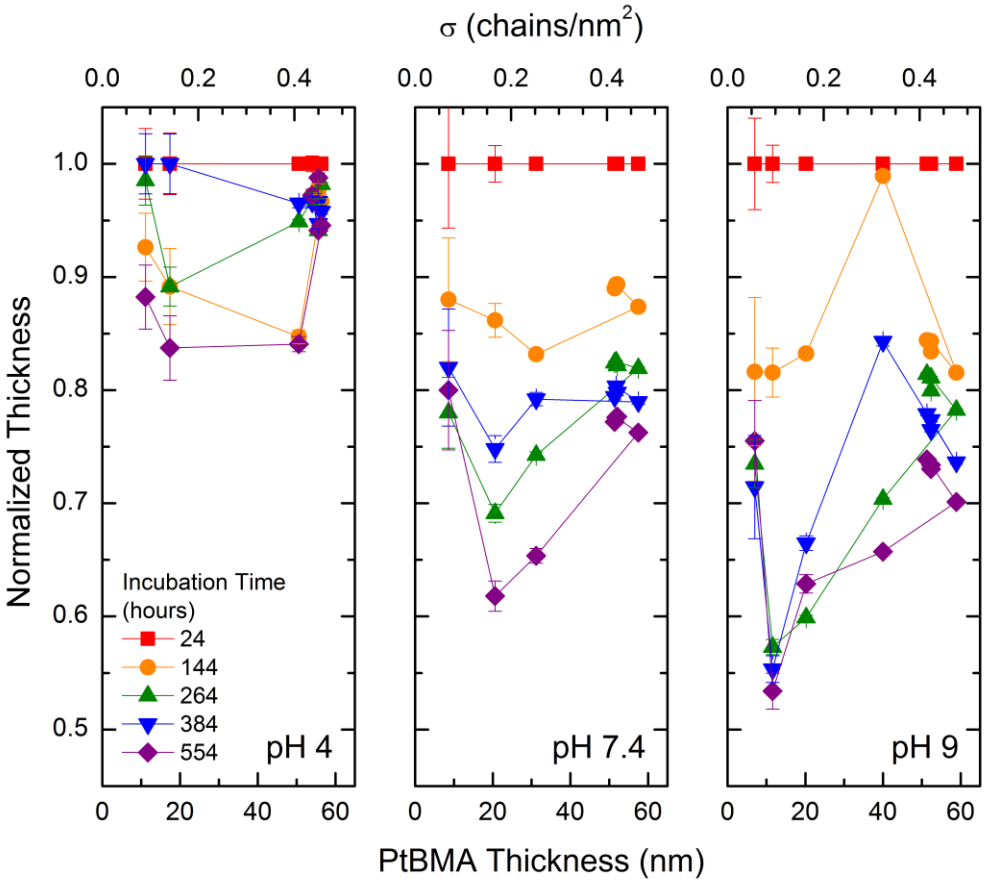

Figure 3.4. Thickness of PMAA brushes normalized by the thickness measured at 24 hours incubated in buffers at pH 4, pH 7.4 and pH 9.

3.3.2 PDMAEMA Brush Degrafting

In the case of a weak polyacid brush, specifically PMAA, the data indicate increasing levels of degrafting with increasing pH, since increasing pH led to a combination of increasing α in the brush and increasing hydroxyl ion concentration in solution. These factors both contribute to increasing degrafting based on the hypothesis described earlier in this chapter, in which mechanical tension induced by electrostatic repulsion activates either the ester group in BMPUS or the siloxane bond at the initiator/substrate interface for hydrolysis by hydroxyl ions. In this section, we consider the behavior of a weak polybase brush comprising poly(2-(dimethylamino)ethyl methacrylate) (PDMAEMA).

In PDMAEMA brushes, α increases with decreasing pH due to protonation of the tertiary amines in the polymer side-chain, which increases with decreasing solution pH. Unlike PMAA, in which α and hydroxyl concentration both increase with pH, PDMAEMA presents a system where these two parameters are diametrically opposed. Prior work has observed that this leads to greater degrafting at an intermediate pH[13]. If the pH is high (*e.g.*, pH 9), the hydroxyl ion concentration is high, but α is low. With a low α, insufficient tension exists along the chain backbone to activate the grafting chemistry for hydrolysis mechano-chemically. Conversely, if the pH is low (*e.g.*, pH 4), then α will be higher and generate sufficient tension to activate the grafting chemistry for hydrolysis. However, the lower concentration of hydroxyl ions in solution will reduce the likelihood of hydrolysis. At an intermediate pH (*e.g.*, pH 7.4), neither α nor hydroxyl concentration are maximized, but their combined effect leads to greater degrafting.

As noted previously, mechanical tension necessary for degrafting of polymer brushes originates from increased osmotic pressure inside the brush that leads to extension of the chains away from the substrate. For a chain with contact MW, this phenomenon can be caused by either increasing α, increasing σ or both. In order to explore how the interplay of pH and σ determines the stability of PDMAEMA brushes, samples expressing a gradient in σ were prepared in the same way as the PMAA discussed previously. **Figure 3.5a-c** plots the thickness profile of the PDMAEMA gradient samples prior to incubation (black data) as a function of substrate position. Examination of the initial PDMAEMA thickness profiles reveals they are uniform across the three samples. Furthermore, the smooth variation in thickness again mimics the variation in BMPUS fraction in the organosilane monolayer attached to the substrate, with increasing thickness levels in regions of increasing BMPUS fraction. As in the case of the PMAA gradient brushes, we assign this variation in thickness to variations in σ due to the variation in BMPUS on the substrate.

Depending on pH and σ, the thickness after 24 hours of incubation at pH 4, 7.4 or 9 (**Figure 3.5a-c** blue data) either increased or decreased. This point is emphasized in **Figure 3.5d-f**, which plots the thickness at 24 hours of incubation normalized by the initial thickness. Looking first at the high σ regions (position > 3.0 cm), this region follows a trend of increasing normalized thickness with decreasing pH. The samples incubated at pH 4 or pH 7.4 show an increase in thickness, while the sample at pH 9 shows a decrease in thickness from the initial thickness levels. This finding is in contrast to the PMAA brushes, which exhibits an increase in thickness for all pH levels after 24 hours incubation. Shifting focus to the gradient region (between 1.5 cm and 2.5 cm), this region exhibits a

trend of larger thickness increases with increasing pH, which is the opposite trend as the high σ region. The samples at pH 7.4 and pH 9 show maxima in thickness increase for all σ values (*i.e.*, substrate positions), while the pH 4 sample shows a minimum in thickness increase in this region. Finally, the sparse region of the gradient samples (position < 1.0 cm) shows for pH 7.4 and pH 9 decreasing normalized thicknesses with wafer position, while pH 4 shows an increase in normalized thickness.

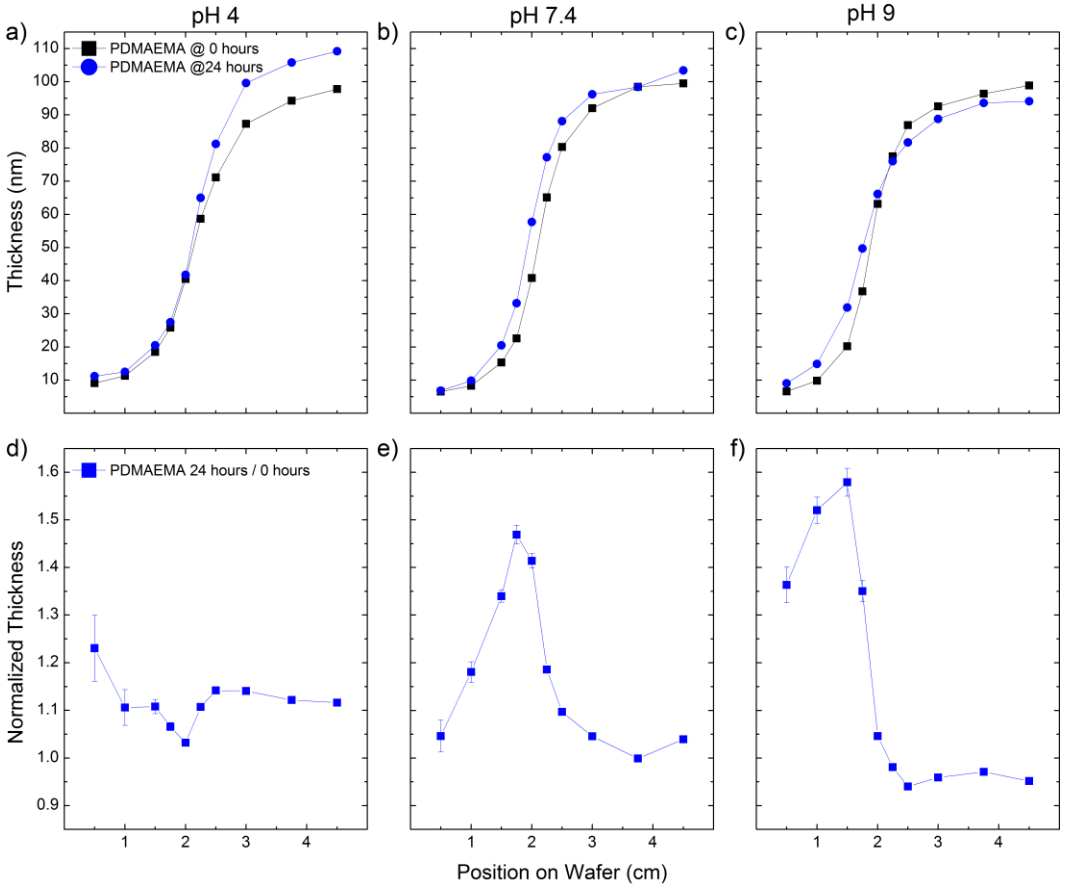

Figure 3.5. a-c) Thickness profiles as a function of position on the substrate for PDMAEMA brushes at 0 and 24 hours of incubation (black squares and blue circles, respectively) in buffer solutions at pH 4 (a), 7.4 (b) or 9 (c). d-f) Data from panels a-c comprising PDMAEMA thickness at 24 hours normalized by thickness at 0 hours incubation (blue squares) for buffer solutions at pH 4 (d), 7.4 (e) or 9 (f).

Following the logic developed in the PMAA section, the increase in thickness observed for pH 4 and pH 7.4 after 24 hours stems from an increase in α in the brush. This increase in α leads to the incorporation of counterions into the brush, which leads to the observed thickness increase. The greater increase in thickness at pH 4 in the densest part of the brush is consistent with this explanation. Unexpectedly, the sample incubated at pH 7.4 shows a greater increase than the pH 4 sample at intermediate σ levels. The data provides no clear explanation for this observation. The increase at low σ for the sample at pH 9 presumably originates with counterion uptake, as well. PDMAEMA is soluble in water in both its protonated and unprotonated state[24]. As a result, water is able to swell the brush. Even though little charging is expected to occur in the system, some protonation will still occur and produce the thickness increase observed after 24 hours. The reduction in thickness seen at higher σ values apparently stems from degrafting. Tension induced by σ alone, coupled with the high hydroxyl concentration, may provide enough activation of the liable bonds to induce degrafting. At lower σ, insufficient tension exists to activate the liable bonds for hydrolysis.

Data acquired after further incubation of the samples for a cumulative total of 168 hours is plotted in **Figure 3.6** as a function of initial PDMAEMA thickness (lower abscissa). This choice of abscissa variable is based on the same logic as used for **Figure 3.4**. The upper abscissa is an estimated σ value based on an assumed value of 0.45 nm^{-2} at the densest region of the brush (thickest initial value)[21], and scaled by a mass balance assumed constant MW of the grafted chains along the gradient. The thickness levels determined at 168 hours were normalized by 24 hours to observe the change in thickness after initial exposure to the buffer solutions, as performed in the PMAA section. The dashed black line at a value of unity indicates the level in which thickness does not change from 24 hours to 168 hours. Above this line, the brush thickness continued to increase. Below this line, the brush thickness decreased. Starting with pH 9, the data show a consistent reduction in thickness as a function of initial thickness. The sample at pH 7.4 also shows a consistent reduction in thickness, with a greater magnitude in reduction than pH 9. For both of these samples, the sparsest region of the brush measured (lowest initial thicknesses) recorded an increase in thickness, in contrast to the dense regions of these samples.

The sample incubated in pH 4 buffer solution reveals a different trend, in which the densest region of the brush shows a reduction in thickness, while the sparsest region shows an increase in thickness. There is a smooth transition from these two extremes over the gradient region of the brush. Depending on σ (*i.e.*, initial thickness), the sample at pH 4 exhibits either more, less or about the

same degree of thickness reduction as the samples at pH 7.4 and pH 9. The samples at pH 7.4 and pH 9 both show a greater reduction in thickness than the sample incubated at pH 4 for initial thicknesses below 60 nm, which corresponds to a σ value of ≈ 0.27 nm^{-2}. Between 60 and 75 nm initial thicknesses (σ ≈ 0.27 to 0.34 nm^{-2}), the pH 4 sample exhibits a thickness reduction between pH 9 and pH 7.4. The pH 4 sample shows the greatest reduction in thickness above 75 nm (σ ≈ 0.34 to 0.45 nm^{-2}).

These data point to the complex interplay between σ, α, and hydroxyl concentration in the degrafting mechanism of a polybase brush like these PDMAEMA samples. There appears to be sufficient concentration of hydroxyl ions in solution to drive degrafting over the entire range of σ for pH 7.4 and pH 9. The greater reduction for pH 7.4 compared to pH 9 may point to the role that tension induced by electrostatic repulsion—due to a greater α—plays in activating the bonds liable to hydrolysis. In the case of the pH 4 sample, there are insufficient hydroxyl ions in solution to induce degrafting below a critical σ value, at least for the measurement times concerned here. Furthermore, electrostatic repulsion at pH 4 alone cannot activate these bonds sufficiently for these levels of hydroxyl ions, even though this pH is expected to induce the greatest α. For degrafting to occur at pH 4, there must be tension due to chain crowding brought on by high σ. Given that pH 7.4 and pH 9 samples show a fairly constant profile over the entire σ range (within a pH), this parameter plays a secondary role at these pH levels.

These observations ultimately stem from macroscopic measurements, and do not account for a detailed picture of the physics that occur inside of the brush layer. It is known that the pH of the microenvironment inside of a polymer brush will differ from that of the bulk solution[25], and this variation will depend on the depth inside the brush. Furthermore, the influence of external ions has not been rigorously considered in these experiments. Buffer solutions were used to ensure a constant pH over the entire incubation period. This constancy comes at the price of incorporating buffering agents into solution. While an attempt was made to minimize the variation between samples by using the same buffering agent for all pH levels (phosphate) at the same concentration (10 mM), the relative concentration of mono-, di- and trivalent phosphate ions will vary with pH[26]. At pH 4, there is ≈100 % $H_2PO_4^-$ in solution; at pH 7.4, there is ≈20 % $H_2PO_4^-$ and ≈80 % $H_2PO_4^{2-}$; at pH 9 there is ≈5 % $H_2PO_4^-$ and 95 % $H_2PO_4^{2-}$. Thus, there are only monovalent ions present at pH 4, and a prevalence of divalent ions present at pH 7.4 and pH 9. The interactions between PDMAEMA and ionic species is

known to depend on the valency of the ions[27], and this point may account for some of the unexplainable observations.

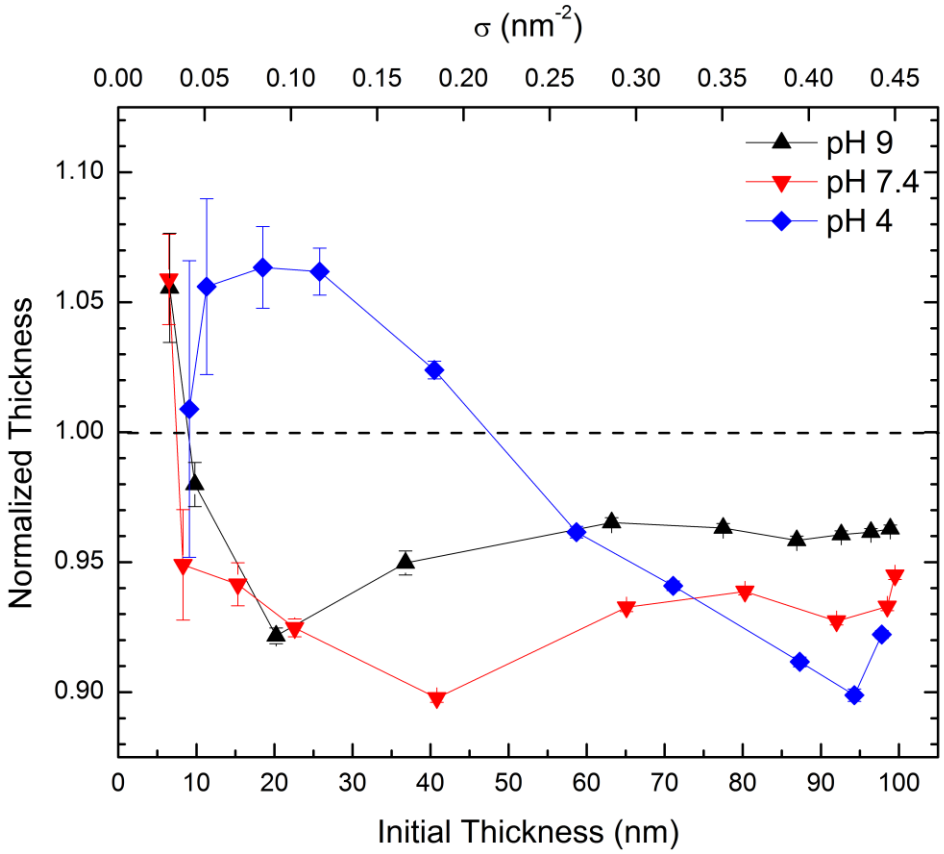

Figure 3.6. Thickness of PDMAEMA brushes at 168 hours of incubation normalized by the thickness measured at 24 hours in buffers at pH 9 (black up-triangles), pH 7.4 (red down-triangles) and pH 4 (blue diamonds).

Moreover, the ionic strength of the three buffer solutions changes as a result of these different ratios of ion species in solution, and introduces an uncontrolled degree of freedom. While identical buffer solutions were used for the PMAA samples, the counterion will be Na^+, so changing valency of the phosphate salts will not influence the PMAA incubations as strongly. Comparison to prior data[13] looking at PDMAEMA brush degrafting is also complicated by this issue, since those experiments

used phosphate buffer saline (PBS) solutions adjusted to a given pH, and thus contain approximately 140 mM of NaCl. Therefore, the conclusions reached above serve only to point the way toward further experiments, including a rigorous accounting of all ionic species in solution. Given the prevalence of ionic species in the human body, this understanding is not only of fundamental, but practical interest as well.

3.3.4 PDMAEMA Brush Morphology

After incubation in buffer solutions and drying by a stream of N_2 gas, both PDMAEMA and PMAA brushes exhibited a change in "dry" thickness that depends on pH. The cases where an observed thickness increase occurred imply incorporation of counterions into the polymer brush and possible retention of water (or dissociated ions). In order to further characterize the effect that the presence of these ions has on the "dry" brush, the surface morphology of PDMAEMA brushes described above were examined using atomic force microscopy (AFM) after incubating in solution for 24 hours. A second set of identical samples (*i.e.*, prepared at the same time) were incubated for 120 hours and also analyzed by AFM. This second set served as a control for these morphology studies. **Figure 3.7** shows AFM micrographs from these samples measured at a substrate position of 3.75 cm. The micrographs are all 4 μm x 4 μm scan size and the color range is over 15 nm for each sample (the absolute range was chosen to emphasize morphology). The surface morphology of the samples shows a clear dependence on solution pH, while within each pH the morphologies are consistent. The samples incubated in pH 9 buffer solution possess a morphology comparable to the morphology prior to incubation. In contrast, the samples at pH 7.4 present a smoother surface with some fine texturing. Finally, the samples incubated at pH 4 exhibit a distinctly different morphology featuring hole-like structures. These holes are at least as deep as the penetration depth of the AFM probe as their coloration is at the lowest end of the color scale.

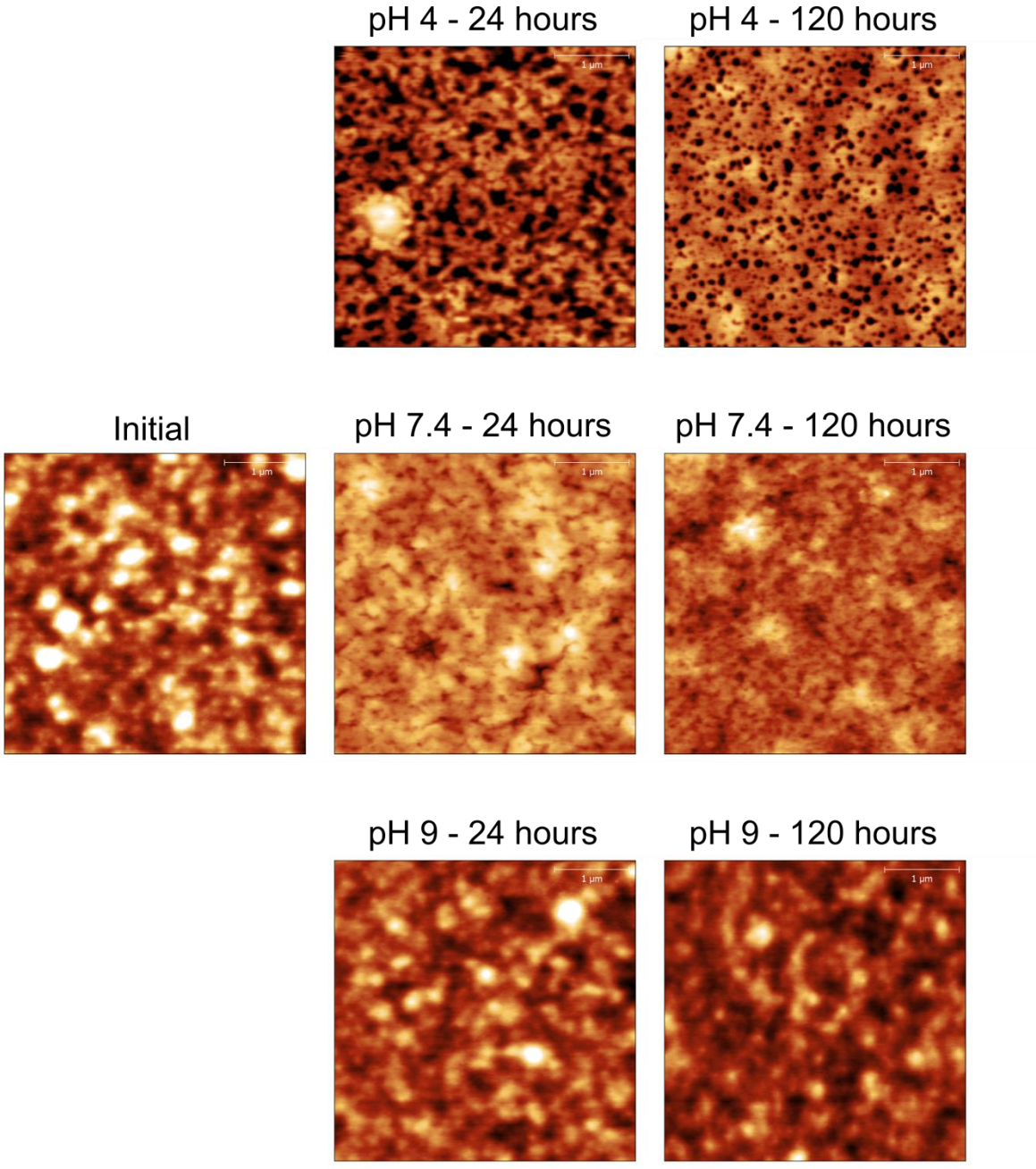

Figure 3.7. AFM micrographs depicting surface topography of PDMAEMA brushes measured at a substrate position of 3.75 cm (dense α) following incubation for 24 hours (center column) or 120 hours (right column) in buffer solutions at pH 4 (top row), pH 7.4 (middle row) or pH 9 (bottom row). Micrographs are 4 μm x 4 μm. Scale bars are 1 μm. Color varies over a range of 15 nm; absolute range values chosen to emphasize morphology.

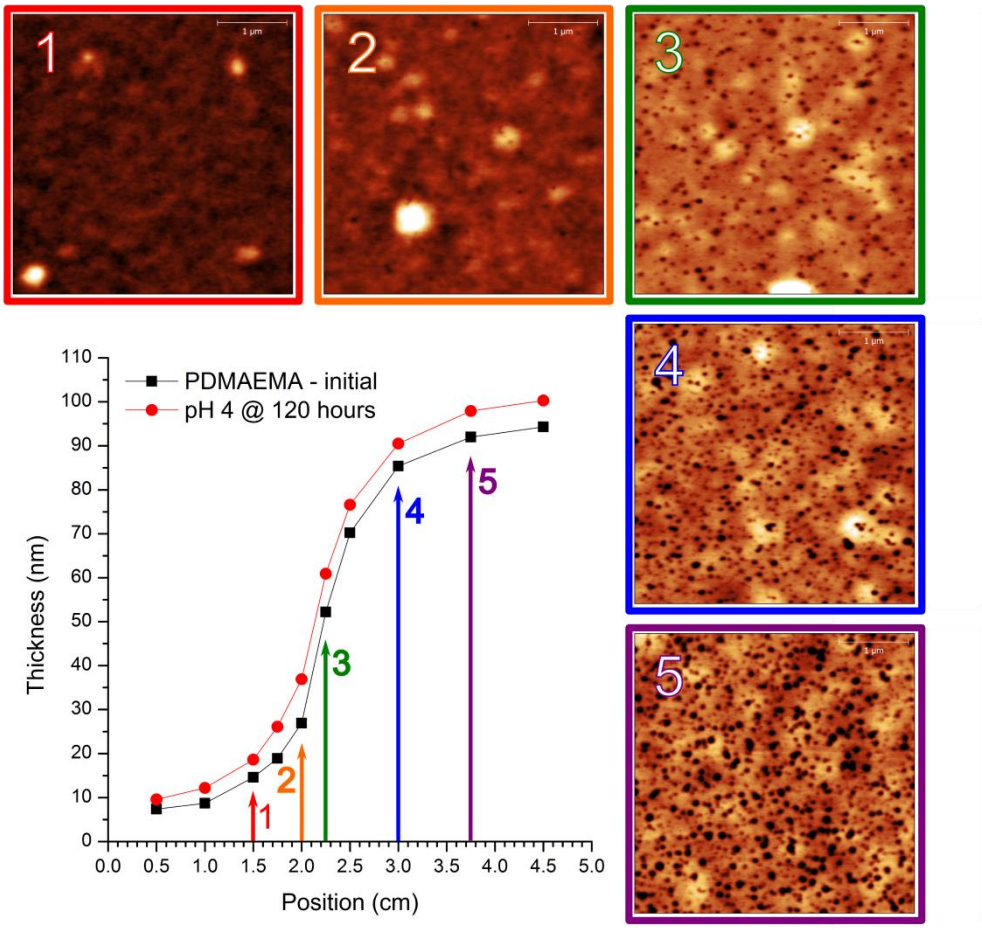

Figure 3.8. AFM micrographs depicting surface topography of a PDMAEMA brush expressing a gradient in σ incubated in a pH 4 buffer for 120 hours measured at various points on the substrate. The plot shows the initial thickness and thickness after incubation (to which the micrographs correspond). Color-coded numbered positions correspond to location of the AFM micrograph. Micrographs are 4 μm x 4 μm. Scale bars are 1 μm. Color varies over a range of 15 nm; absolute range values chosen to emphasize morphology.

The sample incubated at pH 4 for 120 hours was further analyzed along the gradient in σ, the results of which are shown in **Figure 3.8**. Note that the image at point 5 (position 3.75 cm) is the same for pH 4 at 120 hours in **Figure 3.7**. As in **Figure 3.7**, the color scale of the micrographs in **Figure 3.8** is over a range of 15 nm, although the absolute range values were chosen to emphasize the morphology. The plot shows the initial thickness and thickness after incubation for 120 hours and

subsequent drying with a stream of N_2 gas. For all points measured (and the entire gradient), there is a thickness increase at 120 hours incubation. Moving from high σ regions (*i.e.*, thickest part of the brush) to low σ regions results in a reduction of hole density. Careful examination of measurement point 2 (position 2.0 cm) shows some holes. There is no obvious hole formation at measurement point 1 (position 1.5 cm). For all measurement points, the surface morphology is remarkably smooth except for the location of the holes.

Based on **Figure 3.7** and **Figure 3.8**, the surface morphology of PDMAEMA brushes that have been incubated in aqueous solutions and then dried depends on α and σ, which has been predicted theoretically[28]. The mechanism underlying the formation of the holes at pH 4 is not apparent from the studies conducted here, although similar features have been predicted[29] and observed in spuncast block copolymer systems[30]. Perhaps the residual moisture retained by the protonated tertiary amines leads to a dewetting process during the nitrogen drying step. As excess moisture is removed by the nitrogen gas, the charged repeat units attempt to maximize exposure to residual moisture, leading to a segregation of chains to regions that are moisture-rich locally. This segregation results in a depletion of chains in moisture-deficient regions, producing the hole-structure morphology.

3.4 Conclusion

This chapter presented experimental data documenting the effect of α and σ on the stability of weak polyelectrolyte brushes in aqueous environments. For PMAA brushes (weak polyacid), chain degrafting at high σ occurred with increasing α and increasing pH. This trend confirmed the hypothesis that the degrafting mechanism involves electrostatic repulsion generating tension along the chain backbone that activates the grafting chemistry for hydrolysis by hydroxyl ions in solution. Surprisingly, these PMAA brushes showed maximum degrafting at an intermediate σ level, suggesting a higher α at intermediate σ due to charge regulation. PDMAEMA brushes (weak polybase) exhibited the complex interplay between σ and α in generating the tension necessary to induce degrafting. For example, PDMAEMA incubated at pH 4 showed a strong dependence on σ. At high σ, this sample showed degrafting to a greater extent than the samples incubated at pH 7.4 and pH 9. At low σ, that trend was reversed, with the sample at pH 4 showing an increase in thickness compared to a decrease in thickness for the other samples. Finally, this Chapter also presented evidence for the strong dependence of PDMAEMA brush surface morphology on α and σ. These

findings point to the rich set of physical behavior these systems offer for study, and the need to understand more deeply the stability of these systems for long term applications.

3.5 References

(1) Barbey, R.; Lavanant, L.; Paripovic, D.; Schüwer, N.; Sugnaux, C.; Tugulu, S.; Klok, H.-A. *Chem. Rev.* **2009**, *109*, 5437–5527.

(2) Galvin, C. J.; Genzer, J. *Prog. Polym. Sci.* **2012**, *37*, 871–906.

(3) Gauthier, M. a; Gibson, M. I.; Klok, H.-A. *Angew. Chem. Int. Ed. Engl.* **2009**, *48*, 48–58.

(4) Sheiko, S. S.; Sun, F. C.; Randall, A.; Shirvanyants, D.; Rubinstein, M.; Lee, H.; Matyjaszewski, K. *Nature* **2006**, *440*, 191–194.

(5) Garcia-manyes, S.; Liang, J.; Szoszkiewicz, R.; Kuo, T.; Ferna, J. M. **2009**, *1*.

(6) Bünsow, J.; Kelby, T. S.; Huck, W. T. S. *Acc. Chem. Res.* **2010**, *43*, 466–474.

(7) Schmidt, S. W.; Kersch, A.; Beyer, M. K.; Clausen-Schaumann, H. *Phys. Chem. Chem. Phys.* **2011**, *13*, 5994–5999.

(8) Sheiko, S. S.; Panyukov, S.; Rubinstein, M. *Macromolecules* **2011**, *44*, 4520–4529.

(9) Tugulu, S.; Klok, H.-A. *Biomacromolecules* **2008**, *9*, 906–912.

(10) Borozenko, O.; Godin, R.; Lau, K. L.; Mah, W.; Cosa, G.; Skene, W. G.; Giasson, S. *Macromolecules* **2011**, *44*, 8177–8184.

(11) Prucker, O.; Rühe, J. *Macromolecules* **1998**, *31*, 592–601.

(12) Matyjaszewski, K.; Miller, P. J.; Shukla, N.; Immaraporn, B.; Gelman, A.; Luokala, B. B.; Siclovan, T. M.; Kickelbick, G.; Vallant, T.; Hoffmann, H.; Pakula, T. *Macromolecules* **1999**, *32*, 8716–8724.

(13) Bain, E. D.; Dawes, K.; Evren, A. O.; Hu, X.; Gorman, C. B.; Jir, S.; Genzer, J. **2012**.

(14) Wu, T.; Efimenko, K.; Genzer, J. *J. Am. Chem. Soc.* **2002**, *124*, 9394–9395.

(15) Wu, T.; Genzer, J.; Gong, P.; Szleifer, I.; Vlcek, P. In *Polymer Brushes*; Advincula, R. C., Ed.; Wiley-VCH Verlag GmbH, P. O. Box 10 11 61, Weinheim, D-69451, Germany,, 2004; pp. 287–315.

(16) Nečas, D.; Klapetek, P. *Cent. Eur. J. Phys.* **2011**, *10*, 181–188.

(17) Shah, R. R.; Merreceyes, D.; Husemann, M.; Rees, I.; Abbott, N. L.; Hawker, C. J.; Hedrick, J. L. *Macromolecules* **2000**, *33*, 597–605.

(18) Kim, J.; Bruening, M. L.; Baker, G. L. *J. Am. Chem. Soc.* **2000**, *122*, 7616–7617.

(19) Liu, Y.; Klep, V.; Zdyrko, B.; Luzinov, I. *Langmuir* **2004**, *20*, 6710–6718.

(20) Dong, R.; Lindau, M.; Ober, C. K. *Langmuir* **2009**, *25*, 4774–4779.

(21) Tomlinson, M. R.; Genzer, J. *Langmuir* **2005**, *21*, 11552–11555.

(22) Brittain, W. J.; Minko, S. *J. Polym. Sci. Part A Polym. Chem.* **2007**, *45*, 3505–3512.

(23) Zhulina, E. B.; Birshtein, T. M.; Borisov, O. V. *Macromolecules* **1995**, *28*, 1491–1499.

(24) Bütün, V.; Armes, S.; Billingham, N. *Polymer (Guildf).* **2001**, *42*, 5993–6008.

(25) Gong, P.; Wu, T.; Genzer, J.; Szleifer, I. *Macromolecules* **2007**, *40*, 8765–8773.

(26) Schrödter, K.; Bettermann, G.; Staffel, T.; Wahl, F.; Klein, T.; Hofmann, T. Phosphoric acid and phosphates. *Ullmann's Encyclopedia of Industrial Chemistry*, 2012, 679–724.

(27) Wang, X.; Liu, G.; Zhang, G. *Langmuir* **2011**, *27*, 9895–9901.

(28) Tagliazucchi, M.; de la Cruz, M. O.; Szleifer, I. *Proc. Natl. Acad. Sci. U. S. A.* **2010**, *107*, 5300–5305.

(29) Sing, C. E.; Zwanikken, J. W.; Olvera de la Cruz, M. *Nat. Mater.* **2014**, *13*, 694–698.

(30) Stewart-Sloan, C. R.; Olsen, B. D. *ACS Macro Lett.* **2014**, *3*, 410–414.

4. Swelling of Polyelectrolyte and Polyzwitterion Brushes by Humid Vapors

4.1 Introduction

While swelling of surface-grafted polyelectrolyte assemblies in liquids has received extensive attention[1,2], their behavior in aqueous and organic vapors remains a largely underexplored concept. Nonetheless, the performance of these assemblies in humid and vapor-enriched environments has considerable reach, such as a model for biological structures[3] or in manufacturing active layers for gas separation technologies[4]. Swelling induced by a vapor phase is distinctly different from that by a liquid phase of the same molecule, providing new avenues of polymer physics to explore. When solvent vapors interact with a polymer film, three components must be considered, *i.e.*, air, solvent, and polymer, compared to just solvent and polymer in the liquid phase. The interactions among these three components govern the partitioning of solvent vapor into the polymer and thus the swelling behavior of the polymer chains.

Swelling in humid environments occurs with a relatively low concentration of water in the ambient. Even at 100 % relative humidity (RH), there is only ≈2 wt % water present in the air at room temperature. Therefore, vapor measurements can probe the behavior of polymer brushes with low concentrations of water molecules, which are acting as solutes in a solvent of hydrophobic air. The lack of a condensed solvent phase prohibits certain phenomena observed in liquid swelling of polyelectrolyte systems, such as dissociation of counterions[5] and structuring of "liquid-like" water at a polyelectrolyte interface[6]. The implication of these findings is that a polyelectrolyte exposed to water vapor does not necessarily act as a typical polyelectrolyte in aqueous solution. Any observed thermodynamic behavior instead results from the presence of a condensed counterion. In contrast, polysulfobetaines, the class of polyzwitterions considered in this work, do not bear a counterion. As a result, the electrostatic charges present in the side-chain can form intra- and intermolecular complexes[7,8] even without "bulk" solvent present.

Polymer brushes differ from other untethered, polymer thin film assemblies (*e.g.*, spuncast layers) in important ways when considering swelling behavior. In the true polymer brush regime[9] for flat substrates, when the grafting density of chains (σ) is sufficiently high, polymer chains swell in the direction normal to the substrate[2]. In contrast, chains in an untethered thin film swell uniformly in all directions (except those at the substrate/polymer or polymer/air interface). Polymer brush assemblies also offer an avenue to tune σ and produce a gradient in concentration of chains in the film[10]. Controlling this parameter is not possible in untethered assemblies, which comprise a film of uniform density. Exploring the swelling behavior in polymer assemblies featuring a gradient in σ on the same

sample enables one to decouple the effect of polymer crowding and RH. One can thus explore concurrently the performance of systems featuring both low and high concentration of polymer under a given RH level.

In this work we probe the swelling behavior of polyelectrolyte and polyzwitterion polymeric grafts on flat impenetrable substrate in humid environments using a combination of neutron reflectivity (NR), X-ray reflectivity (XR) and spectroscopic ellipsometry (SE). A post-polymerization modification (PPM) strategy[11,12] is employed to generate strong polyelectrolyte and polyzwitterion brushes from a weak polyelectrolyte brush "parent" of poly(2-(dimethylamino)ethyl methacrylate) (PDMAEMA). This PPM approach ensures differences in swelling behavior of the resulting samples stems from differences in side-chain chemistry. We demonstrate that though polyelectrolytes do not experience charge repulsion, their swelling behavior depends strongly on the presence of condensed counterions and the overall hydrophobicity of the side-chain moiety. Polyzwitterion brushes exhibit a more complex swelling behavior that suggests the formation of intermolecular complexes at high σ and intramolecular complexes at low σ.

4.2 Experimental Section

4.2.1 General Methods and Materials

Acetonitrile, (dimethylamino)ethyl methacrylate (DMAEMA), methyl iodide (MeI), propyl iodide (PrI), 1,3-propanesultone (PS), dimethylsulfoxide (DMSO), ethanol, 2,2'-bipyridyl, CuCl and inhibitor remover packing were purchased from Sigma-Aldrich[13] and used as received. The ATRP initiator, [11-(2-bromo-2-methyl)propionyloxy] undecyltrichlorosilane (BMPUS), was synthesized following a previously published procedure[14]. 0.5 mm thick, 100 mm diameter silicon wafers were purchased from Silicon Valley Microelectronics[13]. 5 mm thick, 3" diameter silicon wafers were purchased from El-cat Inc[13]. IR spectra were collected on a Nicolet iN 10 MX microscope (Thermo Scientific[13]) in reflection mode using a liquid nitrogen cooled MCT detector with an aperture of 300 μm^2 and resolution of 4 cm^{-1}.

4.2.2 Sample Preparation

4.2.2.1 PDMAEMA brush synthesis

A silicon wafer measuring 4.5 cm x 5 cm was sonicated in methanol, dried with a stream of N_2 gas, and treated in a UV-ozone chamber for twenty minutes. This wafer was then placed normal to a reservoir containing a 4:1 mixture of mineral oil:n-octyltrichlorosilane (OTS; Gelest[13]) for 7 minutes in an enclosed, plastic Petri dish. After OTS deposition, the wafer was immediately placed into a solution of 30 μL of 5 vol % BMPUS in anhydrous toluene and 30 mL of anhydrous toluene and incubated at -20^o C overnight. The wafer was then removed from solution, rinsed with ethanol, dried with a stream of N_2 gas, then sonicated in ethanol for 20 minutes and dried with a stream of N_2 gas. The wafer was then immediately analyzed by contact angle using deionized (DI) H_2O as a probing liquid, then dried with a stream of N_2 gas before immersion into a custom-built glass reactor containing the polymerization solution. The polymerization solution comprised 50 mL of DMAEMA (purified by passing through a column containing inhibitor remover), 50 mL of DMSO, 3.1251 g 2,2'-bipyridyl, and 0.9339 g of CuCl. An identical approach, without the OTS deposition step, was used to synthesize a PDMAEMA brush for reflectivity measurements on a 5 mm thick, 3" silicon wafer.

4.2.2.2 PDMAEMA brush modification

The PPM reactions were carried out using 0.1 M solutions of MeI, PrI or PS in acetonitrile at 40^o C for 48 hours in an orbital shaker[15,16]. Modified samples were rinsed extensively with acetonitrile and THF, then dried under a stream of N_2 gas prior to further experiments.

4.2.3 Characterization Techniques

4.2.3.1 X-ray reflectivity

Measurements were performed using an X-ray reflectometer (Bruker, D8 Advance) employing Cu K_α radiation at National Institute of Standards and Technology (NIST) Center for Neutron Research (NCNR) (Gaithersburg, MD). The copper source was operated at 40 kV and 40 mA, and the wavelength was 0.154 nm. The beam width was 10 mm and the beam height was 0.1 mm.

4.2.3.2 Neutron reflectivity

Measurements were performed at NG7 horizontal reflectometer at NCNR/NIST. NR was measured using a fixed wavelength of 0.475 nm and varying the incidence angle of the neutrons. During the measurement the sizes of the collimating and detector slits were increased to keep a constant footprint and a relative q resolution, $\Delta q/q$, of 0.04, where $q_z = 4\pi\sin\theta/\lambda$, and θ is the incident and final angle with respect to the surface of the film. For measurements under a humid atmosphere the sample was enclosed in an aluminum chamber with saturated salt solution source to achieve the desired humidity within the chamber.

4.2.3.3 Reflectivity data analysis

Reduction and analysis of the XR and NR data were done using REFLPAK suite[17]. First the off-specular scattering from the sample was subtracted from the raw data and then it was normalized against the slit scan to obtain absolute reflectivity. During a reflectivity measurement the phase information is lost so in general it is not possible to directly invert reflectivity data to a real space scattering length density (SLD) profile. Instead a candidate model is assumed for the structure of the sample and then the reflectivity is calculated from this model by using optical matrix formalism. The thickness and SLD of each layer, and roughness at each interface are varied until the calculated profile agrees sufficiently well with the experimental reflectivity curve. The roughnesses between the layers are characterized using an error function.

4.2.3.4 Spectroscopic ellipsometry

Measurements were performed on a Variable Angle Spectroscopic Ellipsometer (J.A. Woollam[13]) controlled by WVASE32 (J.A. Woollam) using a liquid cell with windows fixed at an incidence angle of 70^o. Contained within the cell were two inverted vial caps (1 cm diameter) holding either pure KOH or a saturated aqueous solution of K_2SO_4. SE measurements were performed every 5 minutes using the Dynamic Scan feature in the WVASE32 software at an incidence angle of 70^o from 400 to 1000 nm. The duration of each measurement was 3 minutes. A custom methacrylate lid with a single opening was used to allow access for the RH-temperature probe (Omega Engineering). The probe connected via USB to a computer that recorded temperature and RH level every 5 minutes at the start of each measurement. The final RH level inside the cell during a measurement was calculated as $RH_{t=0} + (3/5)*(RH_{t=1} - RH_{t=0})$, using the assumption that the

increase in RH was linear over the measurement period. The approximation was found to be accurate within 1 % RH. Note that above ≈85 % RH, the change in RH during a measurement is below 1 %. The plots in **Figures 1, 2** and **3** were constructed using the average RH level, calculated as the average of the initial and final RH levels, with the error bars showing the initial and final RH levels.

4.2.3.5 SE data fitting

The data collected by SE measurements at ≈10 % RH were fit to a model comprising a Si substrate, SiO_x layer (thickness 1.5 nm) and a Cauchy layer. The Si and SiO_x layers used material files supplied with the WVASE32 software. The Cauchy layer was fit using thickness, A_n and B_n. All other data at higher RH levels were fit to a similar layer, except that the polymer brush was modeled as an effective medium approximation (EMA) between the Cauchy film and H_2O, which used a material file supplied with the WVASE32 software. The A_n and B_n values obtained at 10 % RH were used for the Cauchy film and held constant. The thickness and volume fraction of H_2O of the EMA were fit and used to construct plots in **Figures 1**, **2** and **3**.

4.2.4 PPM conversion calculations

Calculations were performed as reported previously[18]. Briefly, we start from a mass balance of the polymer brush:

$$h = \frac{M_n * \sigma}{\rho * N_A} \tag{4.1}$$

where *h* is brush thickness, M_n is the number average molecular weight of the grafted chains, σ is the grafting density of the brush, ρ is the density of the grafted chains, and N_A is Avogadro's number. Assuming a constant σ before and after brush modification (*i.e.*, no chains degrafting during the PPM), the conversion of the modification reaction can be estimated from the change in brush thickness. Values for molecular weight and density were taken from Sigma-Aldrich.

4.2.5 Reduced grafting density (Σ) calculation:

The grafting density (σ) of the dense brush (3.5 cm) was assumed to be 0.45 chains/nm^2 based on a prior investigation[19]. We estimated σ at the other measured points as $\sigma(x) = 0.45 * h_x/h_{3.5cm}$,

where h_x is the thickness at the measured point at a coordinate x and $h_{3.5cm}$ is the thickness (90.0 nm) at 3.5 cm. The molecular weight of the high σ PDMAEMA brush was approximated as h * 1350 Da/nm = 90 nm * 1350 Da/nm = 121.5 kDa. That implies a degree of polymerization of ≈774. Assuming the size of a monomer is 0.3 nm (calculated as $[MW_{DMAEMA}/\rho_{DMAEMA}]^{1/3}$), R_g^2 of the grafted polymer chains is ≈11.6 nm^2. We then calculated $\Sigma(x) = 11.6*\pi*\sigma(x)$.

4.3 Results and Discussion

We employed neutron reflectivity (NR) to examine the uptake of D_2O vapor into a poly(2-(dimethylamino)ethyl methacrylate) (PDMAEMA) brushes grown from a silicon wafer by a surface-initiated atom-transfer radical polymerization (ATRP)[14]. The RH level within the sample chamber was controlled using aqueous, saturated salt solutions (53 ~ 95 % relative humidity, RH) or pure KOH (10 % RH). The initial PDMAEMA "KOH" thickness (*i.e.*, thickness measured at 10 % RH) was ≈30 nm. **Figure 4.1** plots the NR profiles of the PDMAEMA brush at each RH level. The shapes of and distances between fringes in the NR profiles change with increasing RH level, implying that the ambient moisture level influences the structure of the PDMAEMA brushes.

Figure 4.2a shows the scattering length density (SLD) profiles (solid lines) derived from fitting the reflectivity data (black lines in **Figure 4.1**). We identify three key features of these SLD profiles. First, as the RH level increases, the location of the polymer/air interface extends away from the substrate. There is a simultaneous increase in the SLD value of the polymer away from the substrate/polymer interface. Since D_2O has a higher SLD than the polymer layer, the data demonstrate that the PDMAEMA brush is swelling due to an uptake of D_2O vapor. From 10 to 53 % RH, there is only a small change in SLD value and thickness of the film. In contrast, the SLD value and thickness both increase significantly at 75 % RH, and continue to do so up to 95 % RH. The second feature is a small peak present at the substrate/polymer interface for all but the lowest RH level. Since the peak indicates a region of higher SLD, there is an apparent enrichment of D_2O at the substrate/polymer brush interface[20].

Finally, an enrichment of D_2O at the polymer/air interface exists for all RH levels. We have defined this feature as the region where the SLD profile deviates from the dotted lines indicating a constant "bulk" SLD and thus constant water level content within the brush. The shape of this peak appears similar from 10 to 75 % RH. At 85 % RH, the peak becomes shallower compared to the constant "bulk" SLD value, and starts to extend deeper into the brush. This trend continues to 95 %

RH, where the peak extends deeply into the film, and is not as prominent compared to the constant "bulk" SLD value. It is noteworthy that a similar feature was not observed in NR measurements of a poly(methacrylic acid) brush in ambient humidity[21]. Furthermore, the suggested brush structure—a homogeneous "box" with a solvated interface—differs from the smooth, decreasing profile found for PDMAEMA brushes in aqueous solutions grown from silicon[22] and gold[23,24] substrates.

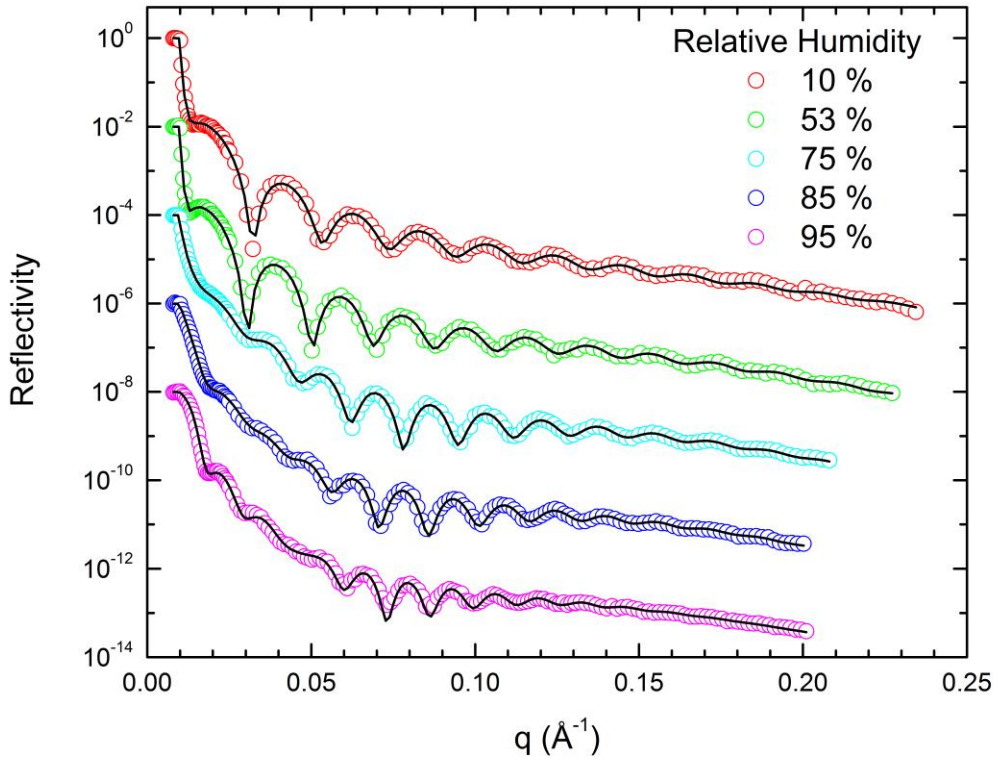

Figure 4.1. Neutron reflectivity profiles of PDMAEMA brush at different RH levels (open circles) showing fits (solid lines) used to derive the SLD profiles in **Figure 4.2a**. The data for RH higher than 10% have been shifted vertically downward for clarify.

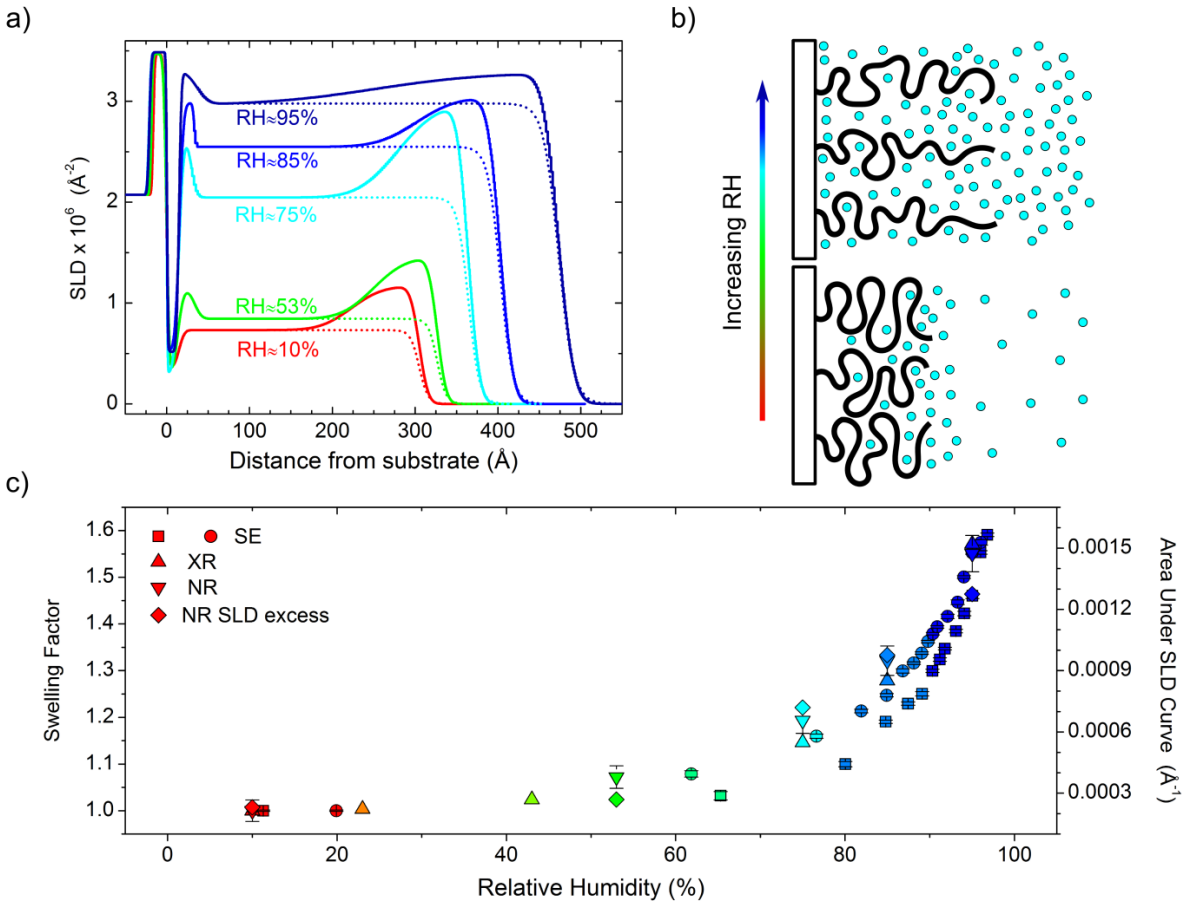

Figure 4.2. a) SLD profiles at various RH levels derived from fitting NR data in **Figure 4.1**. b) Illustration of proposed D_2O enrichment at polymer/air interface at low RH (bottom), leading to more uniform hydration and chain stretching at higher RH (top). c) Compilation of swelling factors calculated from thickness values derived from SE data (squares and circles), XR data (upward triangle) and NR data (downward triangle). The right ordinate (diamonds) depicts the integrated area under the solid lines in the SLD profiles in **Figure 4.2a.**

Figure 4.2b depicts pictorially the situations that resemble the partitioning of D_2O inside the PDMAEMA brushes. At low humidity levels (≈10 % RH), insufficient potential exists to drive D_2O vapor deep into the brush, resulting in an enrichment peak at the polymer/air interface, but no peak at the substrate/polymer interface. As more moisture is added to the air, more water molecules can sorb into and solvate the brush, leading to polymer brush swelling. That increased sorption facilitates, in turn, a deeper penetration of additional water molecules into the polymer brush, thus increasing the

SLD level away from the polymer/air interface. This finding holds significant implications for the evaluation of surface properties of brushes by scanning probe techniques, which may be influenced by this enrichment.

From the data in **Figure 4.2**, it appears that at some critical RH value (≈70% RH) sufficient water content exists inside the brush to swell the brush considerably, thus facilitating acceleration in moisture uptake with increasing RH. This is evident from the data plotted in **Figure 4.2c**, which depicts the swelling factor (*i.e.*, swollen thickness normalized by thickness at 10 % RH) on the ordinate determined from thickness values for the same sample using neutron and X-ray reflectivity (NR and XR, respectively). The close agreement between swelling factors derived from NR and XR measurements, the latter of which was done with H_2O, suggests that the deuterated and hydrogenated solvents swell PDMAEMA in a similar way. The right ordinate denotes the area under the SLD profiles (solid lines) shown in **Figure 4.2a**. Both thickness and SLD profile area follow an exponential-like trend with increasing RH, confirming acceleration in moisture uptake.

Figure 4.2c also plots swelling factors derived from spectroscopic ellipsometry (SE) measurements for a PDMAEMA homopolymer brush ("dry" thickness 90 nm) exposed to H_2O vapor. SE enables the simultaneous fitting of film thickness and solvent fraction (φ), making it a practical substitute for reflectivity measurements. We performed SE measurements while ramping RH levels inside an enclosed sample chamber fitted with a probe capable of recording concurrently temperature and RH. The humidity was adjusted using either dry KOH or saturated aqueous solutions of K_2SO_4. Prior work using a similar technique found that the swelling of a polymer film corresponded precisely with changes in RH[25]. We found that KOH attains an equilibrium RH level of ≈10 % in our chamber, while K_2SO_4 reaches ≈96 %. Since we measure the RH level inside the chamber, we can track the response of the polymer brushes to the changing environment during equilibration. We are thus not limited to the equilibrium RH value of the saturated salt solution. All measurements were performed at ambient lab temperature of 23.5 ± 0.5 ^{o}C. We deliberately maintained the RH level below 96 % to ensure no condensation occurred within the chamber. The comparable results obtained between the different experimental techniques serve to confirm our experimental observations, as well as validating the use of SE in analyzing polymer brush swelling in humid environments.

Using a post-polymerization modification (PPM) strategy[11], we synthesized a series of polymer brushes derived from the same PDMAEMA homopolymer parent brush. By using samples from this parent polymer brush, we can ensure similar degrees of polymerization (DP) and grafting

densities (σ) between samples, assuming no chains are cleaved from the substrate during the PPM reaction. The resulting sample library consists of the neat PDMAEMA, two quaternized samples with a methyl (PDMAEMA-MeI) or propyl (PDMAEMA-PrI) alkyl chain and iodide counterions, and a sample betainized with PS (PDMAEMA-PS), producing a polyzwitterion. These side-chain chemistries are depicted in **Figure 4.3**. Note that betainization does not produce a counterion, instead yielding unshielded charges. This library provides a means to study systematically the effect of introducing permanent charges, hydrophobic moieties and zwitterions into the polymer side-chain on swelling in humid environments. By monitoring how these materials swell over a wide, smoothly varying range of RH levels, we illustrate how side-chain chemistry influences the sorption behavior of water vapor.

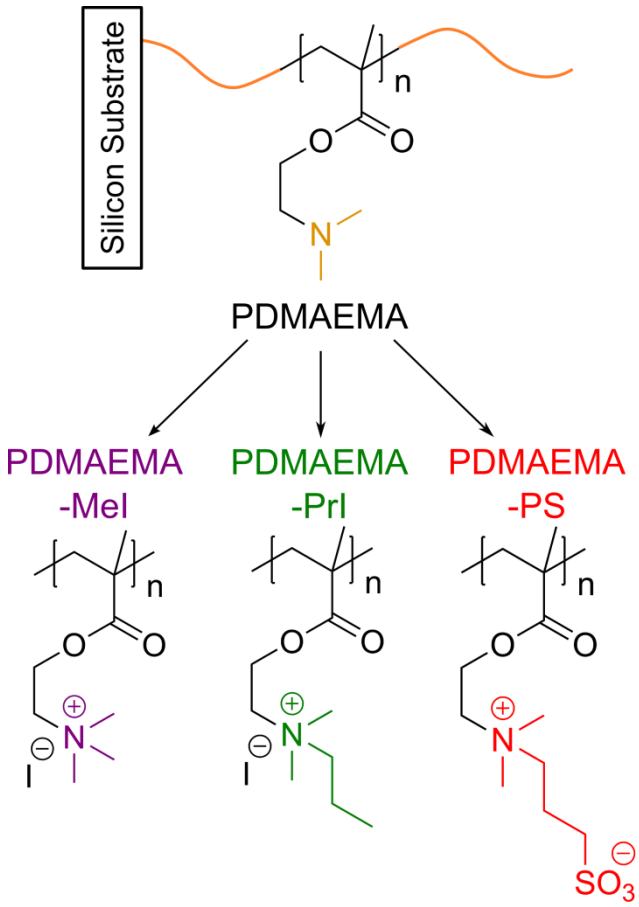

Figure 4.3. Polyelectrolyte and polyzwitterion brushes derived from PPM reactions.

Thicknesses of the initial and modified samples at low RH (≈10 %, termed "KOH" thickness) are listed in **Table 4.1**, along with an estimated conversion based on a mass balance using a methodology reported previously[18]. This estimate provides an upper limit, as there is likely still some residual moisture in these brushes even at 10 % RH.

Table 4.1: Selected properties of polymer brush samples prepared by PPM

Sample name	"KOH" thickness (nm)	Thickness after PPM / "KOH" thickness	Implied Conversion
PDMAEMA	90.0 ± 0.2	N/A	N/A
PDMAEMA-MeI	122.9 ± 0.1	1.37	0.99
PDMAEMA-PrI	138.2 ± 1.0	1.54	0.97
PDMAEMA-PS	183.0 ± 5.6	2.03	1.4 (see text)

Characterization of the samples with infrared spectroscopy, the spectra of which are plotted in **Figure 4.4**, suggests a quantitative conversion of the tertiary amine to the respective modified structures. Carbonyl peaks at 1730 cm^{-1} indicate the presence of polymer after PPM reactions. Signals associated with tertiary amine in PDMAEMA[22] appear as sharp peaks in the unmodified sample at ≈2850 cm^{-1} and ≈2750 cm^{-1}. Disappearance of these peaks provides a qualitative measure of conversion extent. In all cases, residual peaks are on the order of detector noise, consistent with the conversion levels calculated in **Figure 4.5** . PDMAEMA-PS exhibits a sharp peak at 1050 cm^{-1} that is associated[26] with the sulfonate group in the zwitterion side-chain. All modified samples show significant water peaks near 3500 cm^{-1}.

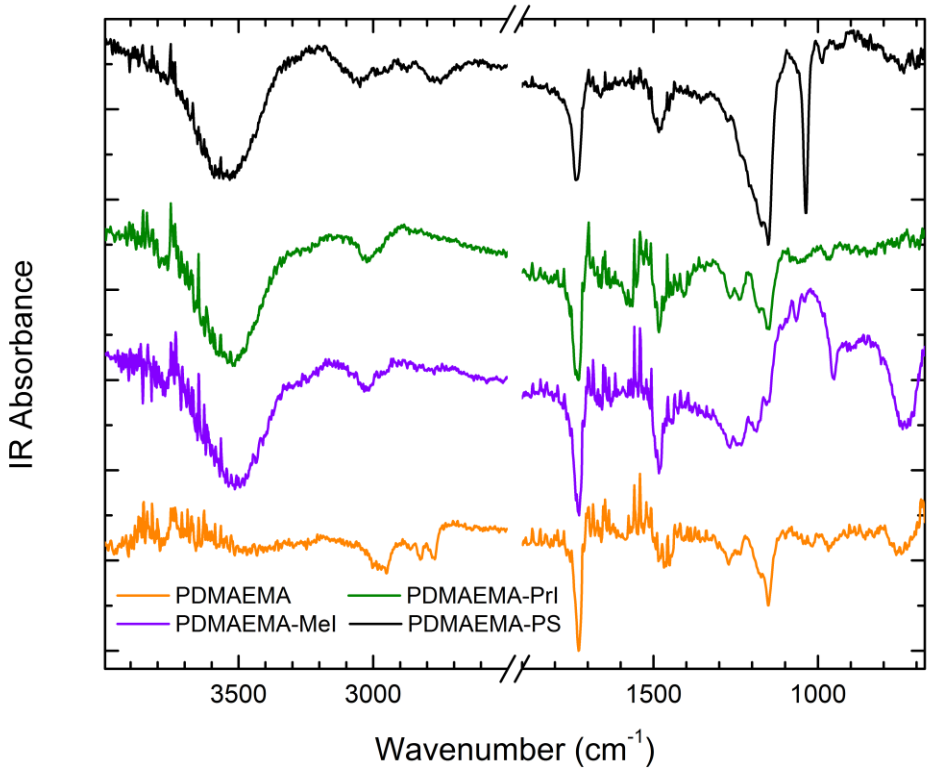

Figure 4.4. FT-IR data of polymer brush samples collected at ambient conditions (≈45 % RH). Orange = PDMAEMA; Purple = PDMAEMA-MeI; Green = PDMAEMA-PrI; Black = PDMAEMA-PS. Noise at ≈1500 cm^{-1} and ≈3750 cm^{-1} originates from atmospheric water due to the open setup of the FT-IR microscope. A break in the abscissa has been inserted to omit peaks associated with CO_2 that result from the open setup of the FT-IR microscope.

The implied conversions from IR spectroscopy are consistent with the calculations for PDMAEMA-MeI and PDMAEMA-PrI, as shown in **Figure 4.5**. Calculations for PDMAEMA-PS predict a conversion greater than 100 %, which, we believe, results from an incorrect assumption that the density of the modified polymer represents a weighted average of the density of PDMAEMA and the PS modifying agent. Our measurements imply that the density of the modified repeat unit is closer to 0.8 g/cm^3, compared to an anticipated value of 1.09 g/cm^3 (see dashed black line in **Figure 4.5**). This lower density would lead to a thicker brush at a given modification, and possibly stems

from charge repulsion due to the unshielded charges present in PDMAEMA-PS. While the repeat units of modified PDMAEMA-PS are overall neutral, the very tip of the side-chain bears an anionic sulfonate group. Repulsion between sulfonate groups would lead to stretching of the brush even in air. Since the quaternized samples bear condensed counterions that shield neighboring charges, no repulsion is present in air. As a result, the quaternized samples behave like uncharged systems in air, and their modified thickness is well-predicted by a mass balance.

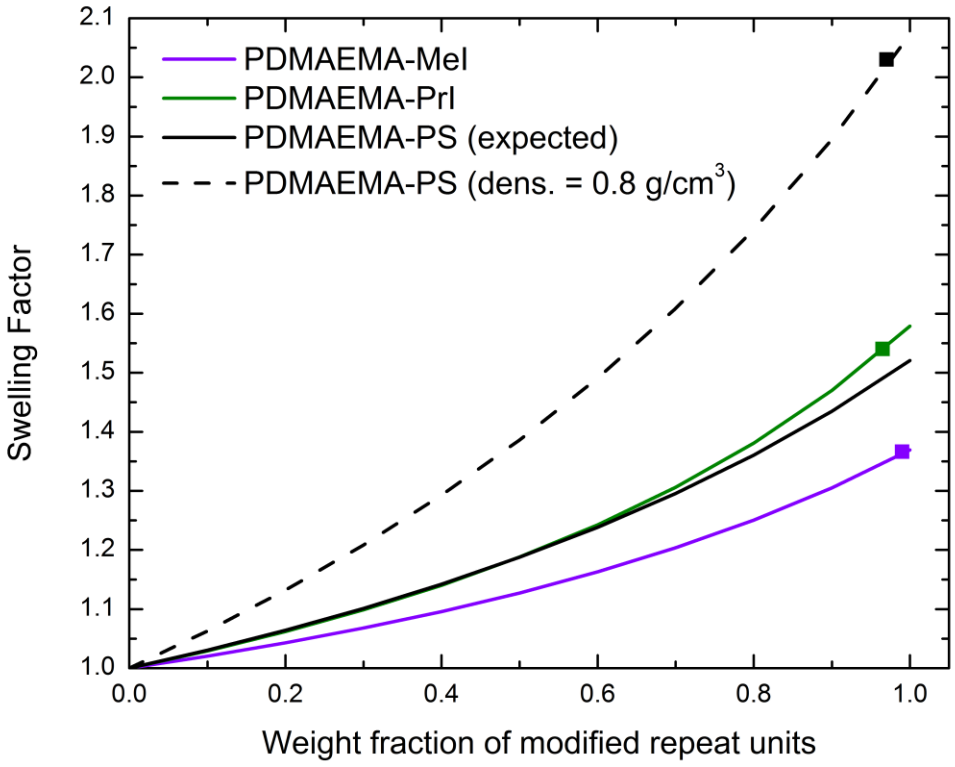

Figure 4.5. Solid lines denote predicted swelling factors as a function of the weight fraction of modified repeat units. Purple = PDMAEMA-MeI; Green = PDMAEMA-PrI; Black = PDMAEMA-PS. These lines are calculated following a previously described procedure[18]. The solid symbols represent measured swelling factors. The quaternized samples are well-described by this model. PDMAEMA-PS follows a trend requiring a lower density.

Figure 4.6a plots swelling factor of the unmodified and quaternized samples versus the average RH level over the duration of the SE measurement for two measurements of the same sample. Note that the PDMAEMA data are the same as in **Figure 4.2**. We observe a strong influence of side-chain chemistry of the modified samples on the extent of swelling. Of the three samples, PDMAEMA-MeI exhibits the largest extent of swelling over the entire measurement range. While PDMAEMA exhibits initially the least swelling, the polymer brush swells rapidly at RH > 75 %. Overall, PDMAEMA-PrI swells more than PDMAEMA at lower RH levels, but much less than PDMAEMA at higher RH levels. The data in **Figure 4.6b** illustrate the relationship between solvent fraction and swelling factor derived from the SE data. PDMAEMA, PDMAEMA-MeI and PDMAEMA-PrI follow the expected relationship, $\varphi=1-1/\text{swelling factor}$ (black line in **Figure 4.6b**). From this trend we conclude that the swelling observed in the data in **Figure 4.6a** is due to uptake of H_2O, since increasing thickness is correlated, as expected, with increasing φ. This finding implies that charge repulsion is not contributing to the swelling process, in line with prior observations[5].

These results illustrate the interplay between the ammonium salt of the quaternized samples and the relative length of the attached alkyl chain. Through ≈50 % RH, the presence of the ammonium salt leads to an increased uptake of water in the quaternized samples compared to PDMAEMA. Eventually, the quaternized samples deviate from one another, and PDMAEMA-MeI swells appreciably more than PDMAEMA-PrI due to the difference in hydrophobicity between the methyl and propyl group. The onset of this deviation may occur when most of the available sites near the condensed counterion are occupied by water molecules.

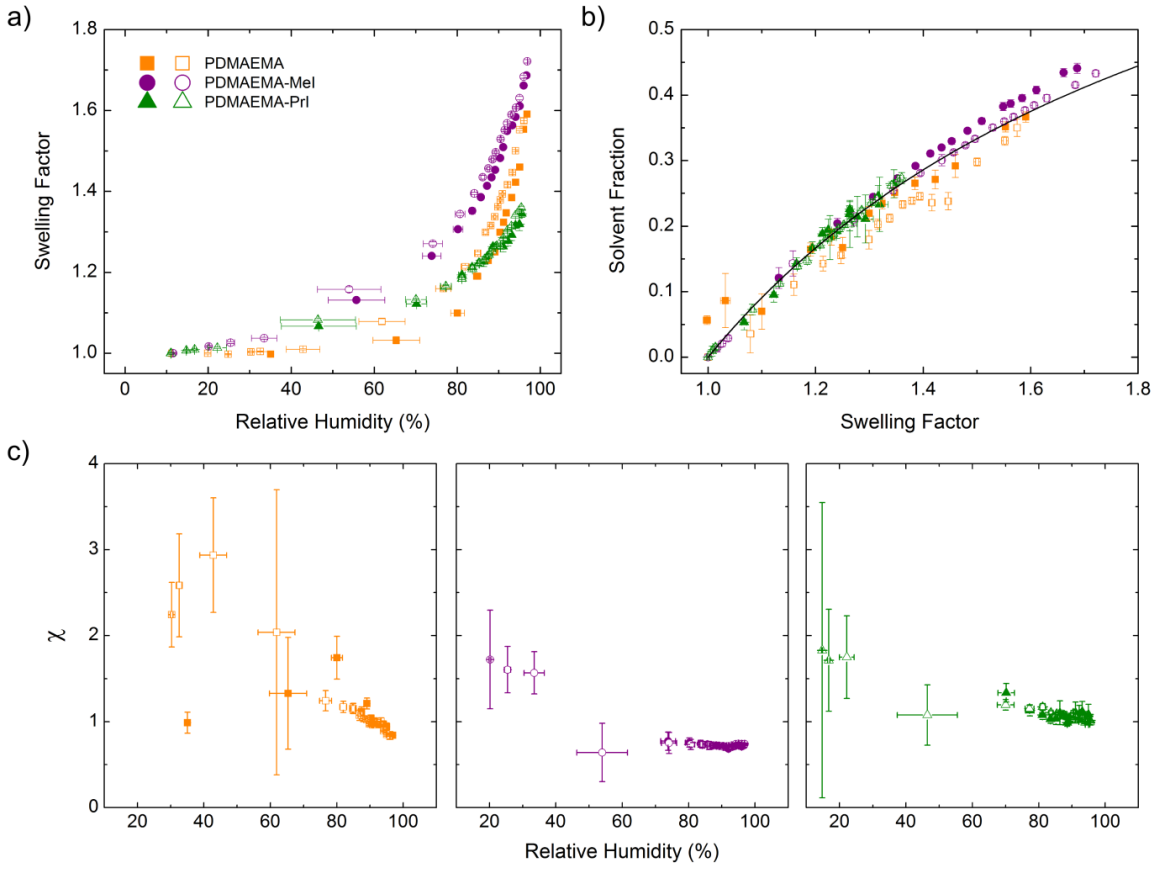

Figure 4.6. a) Swelling factor for PDMAEMA (squares), PDMAEMA-MeI (circles), and PDMAEMA-PrI (triangles) calculated from thickness values derived from fitting the SE data. Closed and open symbols represent results from different runs on the same sample. b) Solvent fraction of the polymer brush determined by fitting the SE data. Closed and open symbols represent results from different runs on the same sample. c) Flory-Huggins χ parameter values calculated from the data in 2B. Closed and open symbols correspond to results from different runs on the same sample. The error bars on the abscissa represent the range of RH levels inside the cell during a measurement for all panels.

Further insight can be gained by analyzing these data in the context of Flory-Huggins theory. We calculated the interaction parameter, χ, as[27]:

$$\chi = \frac{\ln\left(\frac{RH/100}{\phi}\right)+\phi-1}{(1-\phi)^2} \tag{4.1}$$

and plot the resultant values of χ in **Figure 4.6c**. The large error bars at lower RH levels stem from the large relative error associated with φ values. For example, $\varphi = 0.02 \pm 0.01$ is a small amount of moisture overall, but represents 50 % error; propagating this error to a value on the order of 2 leads to error bars of ± 1. At higher RH levels, φ values are larger, while error values remain about the same on an absolute basis, resulting in significantly lower relative error. We note this issue as a limitation of SE measurements on these types of samples. Nonetheless, data at lower RH levels reveal a notable trend. Regardless of the side-chain chemistry, all the samples have higher χ values at lower RH levels. Recalling that air is a hydrophobic medium, we reason that the polymer chains have arranged themselves to minimize exposure of any hydrophilic groups with the air. Interestingly, PDMAEMA-MeI and PDMAEMA-PrI both have χ values in the range of 1.5 to 1.75 at $\approx$20 % RH, while PDMAEMA is $\approx$2.5. This difference may stem from the presence of the ammonium salt. Since the two quaternized samples have comparable values, the length of the alkyl chains studied here may not contribute meaningfully at these RH levels.

The trends in χ at higher RH levels reveal that PDMAEMA grows increasingly hydrophilic with increasing RH, with χ moving from $\approx$1.25 to 0.85, confirming a result found for solvent-cast PDMAEMA films[28]. This decreasing χ value suggests that the polymer grafts are being solvated by the present water molecules, providing a mechanism for the observations seen in **Figure 4.2**. As the enrichment zone extends deeper into the brush, the overall χ value for the polymer film decreases, as seen in the data in **Figure 4.6**. The quaternized samples, PDMAEMA-MeI and PDMAEMA-PrI, exhibit χ values of $\approx$0.7 and $\approx$1.05, respectively, which remain constant within error. These χ values quantify the effect of the more hydrophobic propyl chain in PDMAEMA-PrI relative to the methyl moieties present in PDMAEMA-MeI. Furthermore, the fact that these χ values are constant suggests that these films are not hydrated in the same way as the unmodified PDMAEMA.

Finally, we consider the behavior of the polyzwitterion sample, which comprised a gradient in σ of polymer assemblies prepared using a strategy developed earlier[10]. **Figure 4.7a** plots the swelling factor for points measured along the gradient. The legend names indicate the distance of the measured point from the silane reservoir used in the gradient deposition, such that zero cm indicates the end of the silicon wafer immediately adjacent to the reservoir. Note that the unmodified and quaternized samples described above were taken from the homogeneous portion of the same σ gradient sample. The sample at 3.5 cm is the PDMAEMA-PS specimen described in **Table 1**. The inset shows the "KOH" thickness of the samples (left ordinate) as a function of position on the sample

(lower abscissa) and initiator fraction (upper abscissa) as determined from water contact angle measurements prior to polymerization. As one moves along the wafer from position 1.5 cm to position 3.5 cm, the initiator fraction increases. Assuming that no significant variation in M_n occurs along within the sample, the change in thickness with initiator fraction results from extension of the chains away from the substrate/polymer interface due to increased σ. By assuming σ = 0.45 chains/nm^2 for the thickest region of the brush[19], we estimate the σ values for the other regions of the brush (right ordinate in the inset to **Figure 4.7a**). In the discussion that follows we will refer to the brush at 3.5 cm as "high σ" (≈0.45 chains/nm^2), at 2.25 and 2.0 cm as "medium σ" (≈0.35 chains/nm^2) and at 1.5 cm as "low σ" (≈0.13 chains/nm^2). The term "brush" is used for simplicity, even if the grafted assembly may not be in a true brush regime.

Compared to the unmodified and quaternized samples, the high and medium σ regions of PDMAEMA-PS swell to the greatest extent. The high and medium σ regions show similar swelling factors, while the low σ region swells considerably less. The extent of interaction between neighboring chains can be described using reduced grafting density (Σ), defined as $\Sigma = \sigma\pi R_g$, where R_g is the radius of gyration of the polymer chain. Based on values for the unmodified PDMAEMA gradient, this measurement point has a value Σ of ≈5.6 (see Experimental section for calculation), suggesting the low σ region is in the weakly interacting regime[9]. In contrast, the medium and high σ regions have Σ values of ≈13.6 and ≈16.4, respectively, placing them very close to or in the brush regime. Since the low σ chains are less confined, they are able to swell laterally to a certain extent. In contrast, the chains at the high and medium σ regions swell primarily in the direction normal to the substrate. As a result, these regions have a higher swelling factor. For the measurements at 1.5 cm, there is an apparent shift in trend at 75 RH %. We hypothesize that the origin of this feature is related to a change in the brush's regime as a result of increased interactions between chains due to swelling.

Figure 4.7b plots the same relationship between φ and swelling factor as in **Figure 4.6b**. While the high and medium σ regions exhibit similar swelling behavior, their uptake of solvent differs markedly. The medium σ region follows the expected trend (solid black line), confirming that the increased thickness is due to an uptake of H_2O vapor. In contrast, the data for the high σ brush deviate markedly from this trend at a swelling factor of ≈1.4 (≈75 % RH). The sample at 1.5 cm follows the expected relationship for φ. For comparison, recall that the unmodified and quaternized samples, which have comparable σ follow this trend. We conclude that the shift in trend for

PDMAEMA-PS at high σ density is due to sufficient proximity between chains to enable interactions between the unshielded charges in the brush side chains.

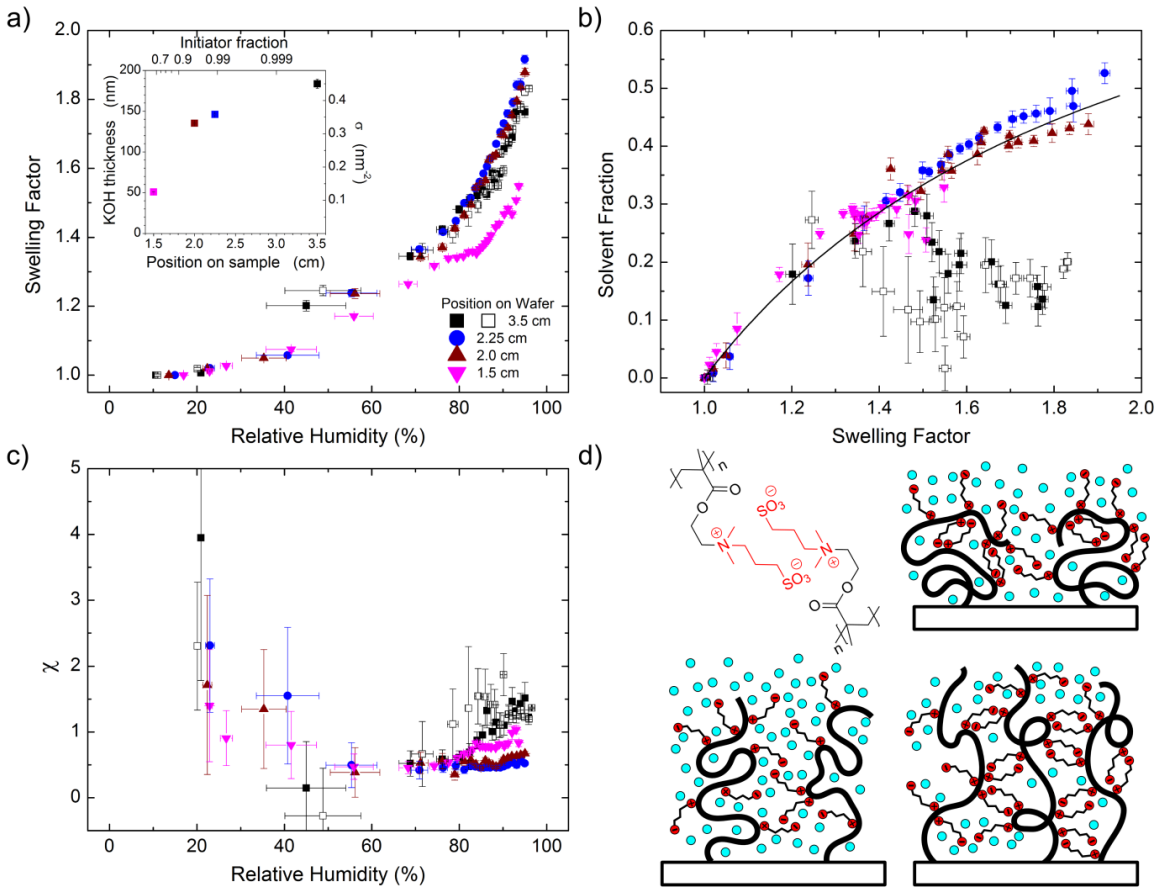

Figure 4.7. a) Swelling factor values calculated from brush thicknesses obtained by fitting SE data. Inset: Thickness of brush at ≈10 % RH (KOH thickness) and PDMAEMA-PS brush grafting density (σ) plotted against position on the substrate and the initiator fraction on the substrate determined by water contact angle measurements. b) Solvent fraction inside PDMAEMA-PS brush determined by fitting SE data plotted against swelling factor values in **3a**. Black line is the expected trend (see text). c) Values of Flory-Huggins interaction parameter, χ, calculated from data in **3b**. d) Clockwise from upper left: illustration of zwitterion complex; low σ region forming predominantly intramolecular complexes; high σ region forming predominantly intermolecular complexes; medium σ region unable to form complexes.

The expected trend plotted in **Figure 4.6b** and **Figure 4.7b** assumes a constant polymer density throughout the swelling process (*i.e.*, the solvent and polymer volumes are additive). In order for PDMAEMA-PS to continue swelling while maintaining a constant H_2O volume fraction, the volume of polymer in the system must change to compensate for the increased volume of water vapor in the film. Since only PDMAEMA-PS exhibits this behavior, we conclude that the presence of opposite, unshielded charges (*i.e.*, no counterions) accounts for our observations. Specifically, the anionic charge of one side-chain can interact with the cationic charge of a nearby side-chain, and vice versa[29]. The resulting complexes will possess an overall higher density, since two interacting side-chains will occupy less volume than two non-interacting or repulsive side-chains. Based on a mass balance, increasing the polymer density would actually lead to a reduction in film thickness (see conversion calculations in PPM Calculations in the Experimental section). Therefore, in order for complexes to form while the brush continues to swell, these complexes are able to break and reform dynamically in response to forces induced by increasing osmotic pressure from increased vapor in the brush.

Figure 4.7c plots the χ parameter for the PDMAEMA-PS gradient. As before, we observe higher χ values at lower RH levels, consistent with the idea that hydrophobic moieties are preferentially exposed to the air. At higher RH levels, the samples converge to a χ value of 0.5 near 70 RH %. With increasing RH, the regions of highest and lowest σ show an increasing χ parameter, while the medium σ regions remain essentially constant at 0.5. An increasing χ value implies the brush is becoming more hydrophobic, and has been observed in thin films of PDMAEMA-PS[30]. Complexing within PDMAEMA-PS will compensate the charges in the zwitterion, reducing the interaction with water vapor[31], and result in a relatively hydrophobic environment comprising propyl spacers and hydrocarbon backbones. It appears that intermolecular zwitterion complexes form at the highest σ. In contrast, the increase in χ value at the lowest σ may stem from intramolecular zwitterion complexes. Between these two extremes, polymer chains at medium σ do not appear to form significant complexes because the solvent fraction follows the expected dependence on the swelling factor. Likely, polymer grafts at these locations on the substrate do not have high enough σ to form intermolecular complexes, but are too dense to allow the chain to coil back on itself and form intramolecular complexes. This scenario is illustrated in **Figure 4.3d**.

The reason humidity can induce the formation of these complexes is not completely clear from our data. One possibility is that the moisture solvates the polymer chains, affording the betaine

moieties enough mobility to form complexes. Below a critical humidity level, the system has insufficient mobility to do so. The moisture may also screen repulsion between neighboring sulfonate groups, lowering the energy barrier for a complex to form. Regardless of the mechanism by which these complexes form, our findings illustrate the significant differences in physical behavior that can result from processing conditions of the underlying brush. Care must be taken to account for differences in brush parameters like σ when comparing across experimental results[9]. The use of gradient samples proves invaluable in this regard, since they provide an internal reference and smooth variation in parameter space.

4.4 Conclusion

We have demonstrated the strong influence that side-chain chemistry has on the swelling of polyelectrolyte and polyzwitterion brushes. Weak polyelectrolyte brushes of PDMAEMA are hydrated heterogeneously due to solvation of the polymer/air interface. While incorporating a condensed counterion into a polymer brush through quaternization tends to increase moisture uptake at lower humidity levels, the hydrophobicity of the modified side-chain can result in overall less swelling compared to the unmodified polymer brush. Furthermore, charge repulsion does not influence film swelling due to the presence of a condensed counterion. In contrast, incorporation of zwitterion chemistry into the side-chain produces complex moisture uptake behavior. The extent of moisture uptake appears to depend on the extent of zwitterion complex formation, which can occur as both intermolecular and intramolecular interactions. The implication from our results is that the most hydrophilic polysulfobetaine brush occurs at an intermediate grafting density that minimizes the formation of these complexes.

4.5 Acknowledgement

The work was supported by the National Science Foundation through Grant No. DMR-0906572.

4.6 References

(1) Rühe, J.; Ballauff, M.; Biesalski, M.; Dziezok, P.; Gröhn, F.; D; Rühe, J. *Adv. Polym. Sci* **2004**, *165*, 79–150.

(2) Toomey, R.; Tirrell, M. *Annu. Rev. Phys. Chem.* **2008**, *59*, 493–517.

(3) Button, B.; Cai, L.-H.; Ehre, C.; Kesimer, M.; Hill, D. B.; Sheehan, J. K.; Boucher, R. C.; Rubinstein, M. *Science* **2012**, *337*, 937–941.

(4) Grajales, S. T.; Dong, X.; Zheng, Y.; Baker, G. L.; Bruening, M. L. *Chem. Mater.* **2010**, *22*, 4026–4033.

(5) Biesalski, M.; Rühe, J. *Langmuir* **2000**, *16*, 1943–1950.

(6) Uosaki, K.; Noguchi, H.; Yamamoto, R.; Nihonyanagi, S. *J. Am. Chem. Soc.* **2010**, *132*, 17271–17276.

(7) Bredas, J.; Chance, R.; Silbey, R. *Macromolecules* **1988**, *21*, 1633–1639.

(8) Schlenoff, J. B. [Online early access]. DOI: 10.1021/la500057j. Published online April 22, *Langmuir* **2014**.

(9) Brittain, W. J.; Minko, S. *J. Polym. Sci. Part A Polym. Chem.* **2007**, *45*, 3505–3512.

(10) Wu, T.; Efimenko, K.; Genzer, J. *J. Am. Chem. Soc.* **2002**, *124*, 9394–9395.

(11) Galvin, C. J.; Genzer, J. *Prog. Polym. Sci.* **2012**, *37*, 871–906.

(12) Günay, K. A.; Theato, P.; Klok, H.-A. *J. Polym. Sci. Part A Polym. Chem.* **2013**, *51*, 1–28.

(13) Commercial materials, instruments and equipment are identified in this paper to specify the experimental procedure as completely as possible. In no case such identification imply a recommendation or endorsement by the National Institute of Standards an.

(14) Matyjaszewski, K.; Miller, P. J.; Shukla, N.; Immaraporn, B.; Gelman, A.; Luokala, B. B.; Siclovan, T. M.; Kickelbick, G.; Vallant, T.; Hoffmann, H.; Pakula, T. *Macromolecules* **1999**, *32*, 8716–8724.

(15) Jaeger, W.; Bohrisch, J.; Laschewsky, A. *Prog. Polym. Sci.* **2010**, *35*, 511–577.

(16) Lowe, A. B.; McCormick, C. L. *Chem. Rev.* **2002**, *102*, 4177–4190.

(17) Kienzle, P. A.; O'Donovan, K. V.; Ankner, J. F.; Berk, N. F.; Majkrzak, C. F. No Title http://www.ncnr.nist.gov/reflpak/.

(18) Arifuzzaman, S.; Ozçam, A. E.; Efimenko, K.; Fischer, D. A.; Genzer, J. *Biointerphases* **2009**, *4*, FA33–44.

(19) Tomlinson, M. R.; Genzer, J. *Langmuir* **2005**, *21*, 11552–11555.

(20) Vogt, B. D.; Soles, C. L.; Jones, R. L.; Wang, C.-Y.; Lin, E. K.; Wu, W.; Satija, S. K.; Goldfarb, D. L.; Angelopoulos, M. *Langmuir* **2004**, *20*, 5285–5290.

(21) Deodhar, C.; Soto-Cantu, E.; Uhrig, D.; Bonnesen, P.; Lokitz, B. S.; Ankner, J. F.; Kilbey, S. M. *ACS Macro Lett.* **2013**, *2*, 398–402.

(22) Sanjuan, S.; Perrin, P.; Pantoustier, N.; Tran, Y. *Langmuir* **2007**, *23*, 5769–5778.

(23) Jia, H.; Wildes, A.; Titmuss, S. *Macromolecules* **2012**, *45*, 305–312.

(24) Rauch, S.; Uhlmann, P.; Eichhorn, K.-J. *Anal. Bioanal. Chem.* **2013**, *405*, 9061–9069.

(25) Mukherjee, M.; Souheib Chebil, M.; Delorme, N.; Gibaud, A. *Polymer (Guildf).* **2013**, *54*, 4669–4674.

(26) Lin-Vien, D.; Colthup, N. B.; Fateley, W. G.; Grasselli, J. G. *The Handbook of Infrared and Raman Characteristic Frequencies of Organic Molecules*; Academic Press: San Diego, CA, 1991.

(27) Flory, P. J. *Principles of Polymer Chemistry*; Cornell University Press: Ithaca, NY, 1953; p. 672.

(28) Arce, A.; Fornasiero, F.; Rodriguez, O.; Radke, C. J.; Prausnitz, J. M. *Phys. Chem. Chem. Phys.* **2004**, *6*, 103 – 108.

(29) Cheng, N.; Brown, A. A.; Azzaroni, O.; Huck, W. T. S. *Macromolecules* **2008**, *41*, 6317–6321.

(30) Galin, J.; Galin, M. *J. Polym. Sci. Part B Polym. Phys.* **1992**, *30*, 1113–1121.

(31) Kondo, T.; Nomura, K.; Murou, M.; Gemmei-Ide, M.; Kitano, H.; Noguchi, H.; Uosaki, K.; Ohno, K.; Saruwatari, Y. *Colloids Surf. B. Biointerfaces* **2012**, *100*, 126–132.

5. Polyelectrolyte Brush Swelling by Water and Alcohol Vapors

5.1 Introduction

Despite extensive work related to swelling of surface-grafted polymer chains in liquid solvents[1,2], the swelling behavior of these macromolecular assemblies in vapor environments remains an underexplored frontier. These assemblies, often referred to as polymer brushes, show promise in vapor-based technologies, such as analyte sensing[3] and gas separations[4]. Furthermore, grafted macromolecular structures in humid environments play key roles in biological systems[5]. Thus, understanding the behavior of polymer brushes in vapor environments is of both practical and fundamental interest.

Key physico-chemical characteristics of polymer brushes[6] include the grafting density (σ) on the substrate and molecular weight (MW), and the chemistry of the grafted chains. These characteristics are depicted schematically in **Figure 5.1**. In order to apply polymer brushes in existing and emerging applications, the effect of these physico-chemical characteristics on the vapor swelling must be understood. Prior work[7] examining the effect of side chain chemistry on swelling and solvent uptake behavior of a weak polyelectrolyte brush employed poly(2-(dimethylamino)ethyl methacrylate) (PDMAEMA) and analog brushes prepared by post-polymerization modification (PPM). These analogs consisted of PDMAEMA brushes quaternized by methyl iodide (PDMAEMA-MeI) and propyl iodide (PDMAEMA-PrI) and betainized by propane sultone (PDMAEMA-PS). Side chain chemistry strongly influenced the swelling and solvent uptake behavior, and led to the formation of zwitterionic complexes in PDMAEMA-PS (*cf.* **Chapter 4**).

This chapter further documents the effect deposition mode (*i.e.*, physical deposition vs. surface grafting) and for the grafted chains the role of σ, MW on the swelling behavior of polymers comprising PDMAEMA, PDMAEMA-MeI, PDMAEMA-PrI and poly(2-(diethylamino)ethyl methacrylate) (PDEAEMA), which bears two ethyl groups on its side chain amine. The structures of these repeat units are shown in **Figure 5.2**. Spectroscopic ellipsometry (SE) is utilized to characterize the swelling and solvent uptake of a PDMAEMA brush expressing a gradient in σ exposed to water vapor. These results are discussed in combination with findings of a PDMAEMA-PS σ gradient sample. A comparison is then made between PDMAEMA and PDMAEMA-MeI brushes and spuncast films on bare silicon wafers that those that have been modified by depositing a self-assembled monolayer comprising n-octyltrichlorosilane (OTS). The role of amine-substituent chemistry is further examined by characterizing the behavior of PDEAEMA in the presence of

humidity. Finally, the swelling behavior of the unmodified and quaternized brush samples in methanol and ethanol vapors is explored.

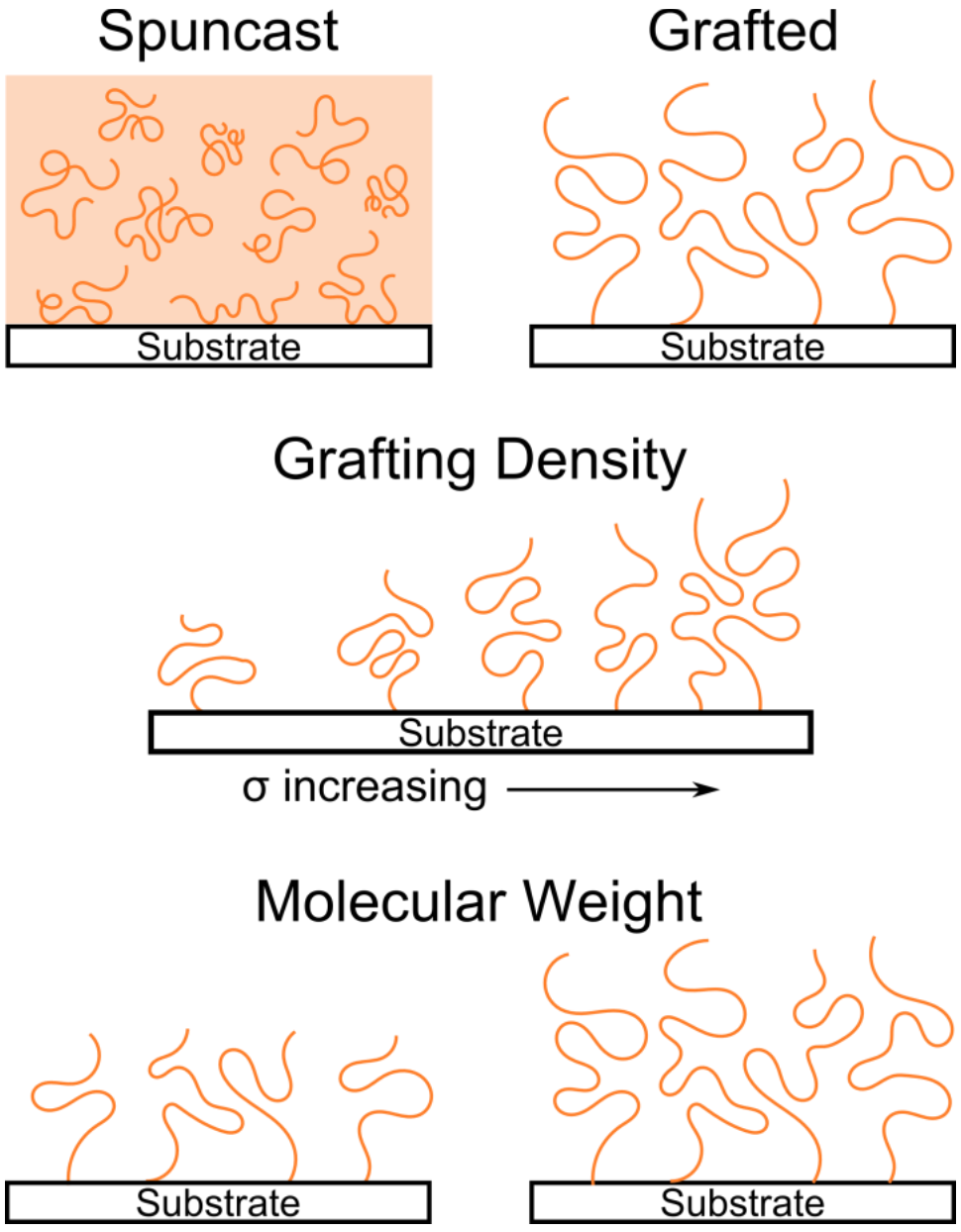

Figure 5.1. Schematic illustrations of polymer parameters considered in vapor swelling experiments. The upper row depicts a spuncast polymer film (left) and a grafted polymer film (right) on the substrate. The center row illustrates a grafted polymer assembly expressing a gradient in σ, which leads to a variation in film height. The bottom row shows two grafted assemblies comprising chains of lower (left) or higher (right) molecular weight. The cartoons are not drawn to scale.

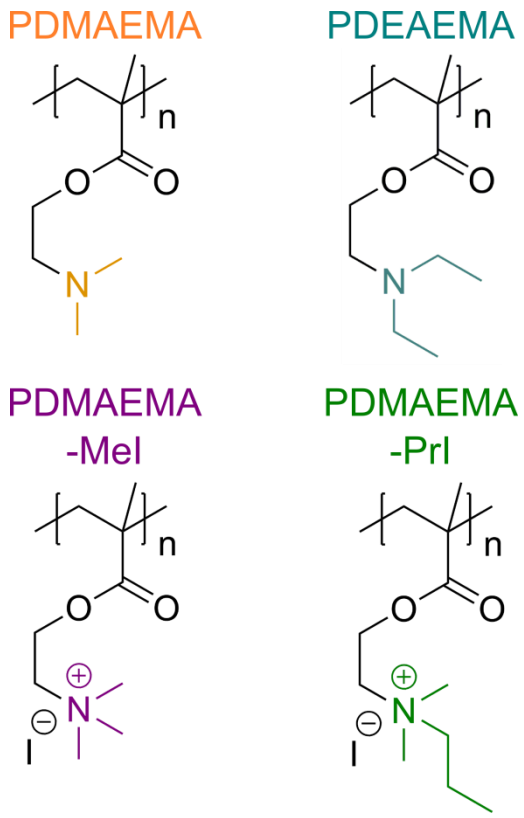

Figure 5.2. Chemical structures of the polymer chains used in vapor swelling experiments.

5.2 Experimental

5.2.1 General methods and materials

Acetonitrile, (dimethylamino)ethyl methacrylate (DMAEMA), methyl iodide (MeI), propyl iodide (PrI), 1,3-propanesultone (PS), dimethylsulfoxide (DMSO), methanol, ethanol, tetramethylene ethylenediamine (TMED), 2,2'-bipyridyl, CuCl and inhibitor remover packing were purchased from Sigma-Aldrich and used as received. n-octyltrichlorosilane (OTS) was purchased from Gelest and used as received. The ATRP initiator, [11-(2-bromo-2-methyl)propionyloxy] undecyltrichlorosilane (BMPUS), was synthesized following a previously published procedure[8]. Silicon wafers (0.5 mm thick, 100 mm diameter) were purchased from Silicon Valley Microelectronics.

5.2.2 Sample Preparation

5.2.2.1 PDMAEMA brush synthesis

A silicon wafer measuring 4.5 cm x 5 cm was sonicated in methanol, dried with a stream of N_2 gas, and treated in a UV-ozone chamber for 20 minutes. This wafer was then placed normal to a reservoir containing a 4:1 mixture of mineral oil:OTS for 7 minutes in an enclosed plastic Petri dish. After OTS deposition, the wafer was immediately placed into a solution of 30 μL of 5 vol % BMPUS in anhydrous toluene and 30 mL of anhydrous toluene and incubated at -20°C overnight. The wafer was then removed from solution, rinsed with ethanol, dried with a stream of N_2 gas, sonicated in ethanol for 20 minutes and dried with a stream of N_2 gas. The sample was then immediately analyzed by contact angle measurement using deionized (DI) H_2O as a probing liquid, then dried with a stream of N_2 gas before immersion into a custom-built glass reactor containing the polymerization solution. The polymerization solution comprised 50 mL of DMAEMA (purified by passing through a column containing inhibitor remover), 50 mL of DMSO, 3.1251 g 2,2'-bipyridyl, and 0.9339 g of CuCl. The reaction was allowed to proceed for 3 hours. Following polymerization, the sample was removed, rinsed extensively with ethanol and sonicated in ethanol for 20 minutes before being dried under a stream of N_2 gas.

5.2.2.2 PDMAEMA brush modification

The PPM reactions were carried out using 0.1 M solutions of MeI, PrI or PS in acetonitrile at 40°C for 48 hours in an orbital shaker[9,10]. Modified samples were rinsed extensively with acetonitrile and THF and then dried under a stream of N_2 gas prior to further experiments.

5.2.2.3 PDEAEMA brush synthesis

An identical procedure was employed for PDEAEMA brush synthesis, except without the OTS deposition step in order to produce a polymer brush with homogeneous σ. The PDEAEMA polymerization solutions contained 45 mL of DMSO, 45 mL of DEAEMA (purified by passing through a column containing inhibitor remover), 2.813 g 2,2'-bipyridyl and 0.8394 g CuCl. The polymerization lasted for 4 hours, after which point the sample was removed, rinsed extensively with ethanol, sonicated in ethanol for 20 minutes, and finally dried with a stream of N_2 gas.

5.2.2.4 PDMAEMA bulk polymer synthesis

10 mL of DMAEMA monomer was purified by passing through a column with inhibitor remover. 9.2 mg of AIBN was dissolved into bulk monomer while degassing solution by bubbling with N_2 for one hour in a Schlenk flask. The flask was sealed and immersed in oil bath at 90^o C. The reaction was allowed to proceed for 4 hours, after which the flask was opened and the content dissolved in THF and precipitated in hexanes. Repeated precipitation from THF into hexanes recovered a white solid.

5.2.2.5 PDMAEMA spuncast film preparation

1.5 cm x 1.5 cm silicon wafer segments were sonicated in ethanol, dried by a stream of N_2 and treated in a UV-ozone chamber for 20 minutes. Bulk PDMAEMA was dissolved in THF to create either 1 wt % or 2 wt % solutions. PDMAEMA solution was pipetted onto clean wafers and spuncast at 2000 rpm for 60 seconds with a 500 rev/sec ramp. For OTS-based samples, clean wafers were first inverted over pure OTS in an enclosed plastic vessel for 10 minutes. These OTS-modified substrates were sonicated in ethanol for 20 minutes, then dried under a stream of N_2 gas, and characterized by ellipsometry. PDMAEMA solution was pipetted onto the OTS-modified substrate and spuncast at 2000 rpm for 60 seconds with a 250 rev/sec ramp.

5.2.2.6 Spuncast PDMAEMA modification

A silicon wafer supporting a PDMAEMA spuncast film was incubated in an enclosed glass vial containing 100 μL for 48 hours. The sample was then removed and exposed to a stream of N_2 gas.

5.2.3 Characterization Techniques

5.2.3.1 Spectroscopic ellipsometry (SE) – Humidity Measurements

Measurements were performed on a Variable Angle Spectroscopic Ellipsometer (J.A. Woollam) controlled by WVASE32 software (J.A. Woollam) using a liquid cell with windows fixed at an incidence angle of 70°. Contained within the cell were two inverted vial caps (1 cm diameter) holding either pure KOH or a saturated aqueous solution of K_2SO_4. SE measurements were performed every 5 minutes using the "dynamic scan" option in the WVASE32 software at an incidence angle of 70° from 400 to 1000 nm. The duration of each measurement was 3 minutes. A

custom poly(methyl methacrylate) lid with a single opening was used to allow access for the RH-temperature probe (Omega Engineering). The probe was connected via USB to a computer and recorded temperature and RH level every 5 minutes at the start of each measurement. The final RH level inside the cell during a measurement was calculated as $RH_{t=0} + (3/5)*(RH_{t=1} - RH_{t=0})$, using the assumption that the increase in RH was linear over the measurement period. The approximation was found to be accurate within 1 % RH. Note that above ≈85 % RH, the change in RH during a measurement is below 1 %. Plots in the Results and Discussion section were constructed using the average RH level, calculated as the average of the initial and final RH levels, with the error bars showing the initial and final RH levels.

5.2.3.2 SE – Organic Solvents

Measurements were performed on a Variable Angle Spectroscopic Ellipsometer (J.A. Woollam) controlled by WVASE32 software (J.A. Woollam) using a liquid cell with windows fixed at an incidence angle of 70°. Contained within the cell were two inverted vial caps (1 cm diameter) holding either pure methanol or ethanol. The vessel was sealed with a steel lid fitted with an o-ring to prevent vapor escape. SE measurements were performed every 5 minutes using the "dynamic scan" option in the WVASE32 software at an incidence angle of 70° from 400 to 1000 nm. The duration of each measurement was 3 minutes.

5.2.3.3 SE data fitting

For humidity measurements, the data collected by SE measurements at ≈10 % RH were fit to a model comprising a Si substrate, SiO_x layer (thickness 1.5 nm) and a Cauchy layer. The Si and SiO_x layers used material files supplied with the WVASE32 software. The Cauchy layer was fit using thickness, A_n and B_n. All other data at higher RH levels were fit to a similar layer, except that the refractive index of the polymer brush layer was modeled by employing an effective medium approximation (EMA) between the Cauchy film and H_2O, which used a material file supplied with the WVASE32 software. The A_n and B_n values obtained at 10 % RH were used for the Cauchy film and held constant. A similar model was used for alcohol measurements, including identical A_n and B_n values for the Cauchy film, with material files constructed from literature values for methanol[11] and ethanol[12]. The thickness and volume fraction of H_2O, methanol or ethanol of the EMA were fit and used to construct plots below.

5.2.3.4 Infrared Variable Angle Spectroscopic Ellipsometry (IR-VASE)

Measurements were performed on an IR-VASE (J.A. Woollam) controlled by WVASE-IR software (J.A. Woollam) at a 50° angle of incidence with a resolution of a 4 cm^{-1}. Samples were exposed to the ambient environment during measurements.

5.3 Results and Discussion

5.3.1 PDMAEMA Gradient Brush Swelling

We examined the swelling behavior and uptake of solvent by a polymer brush comprising poly(2-(dimethylamino)ethyl methacrylate) (PDMAEMA) in humid environments using spectroscopic ellipsometry (SE). The PDMAEMA sample expressed a gradient in grafting density (σ) created using an organosilane vapor deposition technique described previously[13] that generated a gradient in the surface-grafted ATRP initiator. Prior to polymerization, the water contact angle (WCA) of points along this initiator gradient were measured and analyzed by the Cassie-Baxter equation to determine initiator fraction as a function of position on the substrate. Following polymerization, the thickness of the polymer brush at various substrate positions can be mapped to the calculated initiator fraction. The thickness of the PDMAEMA brush increased with increasing initiator fraction, as seen in the inset of **Figure 5.3a**. Assuming that the molecular weight (MW) of the grafted chains does not depend strongly on the initiator fraction, we assign this variation in brush thickness to variation in brush σ, brought about by the underlying variation of initiator fraction in the organosilane monolayer gradient.

This sample was incubated in a closed cell for *in situ* ellipsometric measurements that contained the sensing end of a relative humidity (RH) probe. The RH level inside the cell was controlled using saturated aqueous solutions of potassium sulfate (K_2SO_4) (for high humidity) or pure KOH (for low humidity). As the RH level changed, SE data was collected simultaneously. This facilitated the correlation of brush thickness and solvent fraction, φ, in the brush as a function of the average RH level over the duration of the SE measurement. Measurements were made at different positions along the sample to probe the effect of σ on the swelling behavior and solvent uptake, the results of which are plotted in **Figure 5.3a** and **5.3b**, respectively. The legend in **Figure 5.3a** corresponds to all panels of **Figure 5.3**, and indicates the position on the substrate measured, with higher positions (*e.g.*, 3.5 cm) exhibiting higher σ and lower positions (*e.g.*, 1.5 cm) exhibiting lower

σ. Hereafter, the region at 3.5 cm will be termed "high σ", the region encompassing 2.0 cm and 1.75 cm will be termed "intermediate σ" and the region at 1.5 cm will be termed "low σ". Note that these descriptors are relative and qualitative.

Two sequential measurements were made at a position of 3.75 cm to account for potential issues related to conditioning the sample since this position was measured first. Examination of the orange data reveals a possible hysteretic effect in the swelling factor, with the lower values corresponding to the first measurement cycle. This finding is somewhat surprising, since the sample is exposed to moderate humidity levels prior to incubation due to transport around the laboratory environment. For all σ levels, the swelling factors plotted in **Figure 5.3a** increase with increasing RH level. The same trend is observed in the φ data in **Figure 5.3b**. Considered together, this finding indicates that the PDMAEMA brush thickness swells due to the incorporation of water vapor into the brush. As more water vapor enters the ambient environment, more water vapor segregates into the brush.

Plotting the swelling factor against the φ in the brush, as done in **Figure 5.3c**, confirms that the correlation between φ and swelling factor is consistent for all σ levels within experimental error. The solid black line in **Figure 5.3c** represents the expected swelling trend based on the relationship, φ=1–1/swelling factor. There is a systematic deviation from this expected trend, wherein the experimental data fall below the trend line. The data do not provide any insight into why this deviation from the trend exists. Considering that PDMAEMA is a weak polyelectrolyte, some of the tertiary amine moieties could potentially be protonated by water molecules that have adsorbed into the brush. In that case, electrostatic repulsion would lead to increased swelling for a given φ. Additional investigation is required to make any definitive claim for or against this hypothesis.

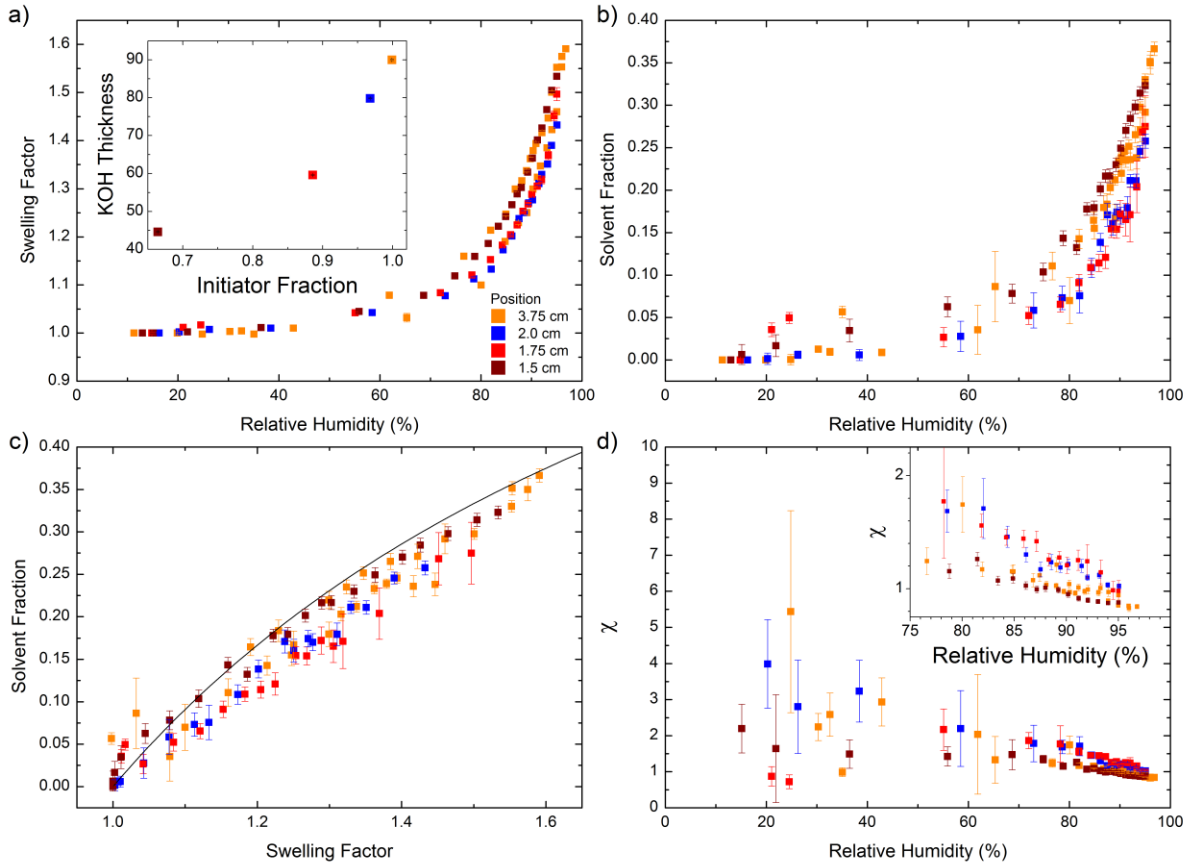

Figure 5.3. a) Swelling factor calculated from thickness values derived from fitting SE data for a PDMAEMA brush expressing a gradient in σ. Legend indicates different measurement points on the substrate, and colors are consistent in all panels. Inset: Thickness of brush at ≈10 % RH for each measurement point, plotted as a function of the initiator fraction calculated from WCA measurements. b) Solvent fraction inside the PDMAEMA brush at each measurement point determined by fitting SE data. c) Solvent fraction data from **Figure 5.3b** plotted against swelling factor data from **Figure 5.3a**. Black line is the expected trend (see text). d) Values of Flory-Huggins interaction parameter, χ, calculated from data in **Figure 5.3b**. Inset: Detail of plot from 75 % RH to 100 % RH.

The data in **Figure 5.3a** cluster into two sets at humidity levels above 75 % RH, with the high and low σ regions exhibiting similar swelling factors, and the two intermediate σ data sets exhibiting similar swelling factors. This clustering occurs in the φ data plotted in **Figure 5.3a** as well. Therefore, the lower swelling factor at intermediate σ originates from a lower uptake of water vapor into the brush. This trend in the data suggests that σ may play a role in the extent of solvent uptake in

the brush. To gain further insight into this possibility, the Flory-Huggins χ parameter was calculated[14] for each data point as:

$$\chi = \frac{\ln\left(\frac{RH/100}{\phi}\right)+\phi-1}{(1-\phi)^2} \quad (5.1)$$

with the resulting χ values plotted in **Figure 5.3c** as a function of RH level. The large error bars at low humidity result from the large relative error associated with small absolute values of φ. For example, φ = 0.03 ± 0.02 is a small amount of moisture uptake overall, but translates to 66 % error. When this relative error value is propagated to χ values of order 2, the resulting error bars are ± 1.3. Nonetheless, χ values for PDMAEMA at the low RH (< 75 % RH) at all σ levels are generally well above unity, implying the polymer brush is hydrophobic. As humidity levels increase above 75 % RH, the χ parameter decreases for all σ levels to a value close to unity. The inset to **Figure 5.3d** plots just the data above 75 % RH to more clearly demonstrate the observed trends in χ for various σ as a function of RH. Consistent with the swelling factor and φ data, the system at intermediate σ exhibits a higher χ value, suggesting a more hydrophobic brush than the highest and lowest σ regions.

The grouping in these trends of high and low σ together and distinct from the intermediate σ regions is unexpected and counterintuitive. Care must be taken to not rely too heavily on one characterization technique when deciding how substantial these differences are. Nonetheless, prior work using identical (*i.e.*, derived from the same parent sample) PDMAEMA σ gradients betainized with propane sultone (PDMAEMA-PS) exhibited a distinct dependence on σ of swelling behavior[7]. As in the case of the parent PDMAEMA sample, the behavior of the betainized PDMAEMA σ samples exhibited a division between the high and low σ regions compared to the intermediate σ regions. Unlike the parent PDMAEMA sample, the PDMAEMA-PS sample showed a more hydrophilic behavior at the intermediate σ regions compared to the high and low σ regions. In other words, the unmodified PDMAEMA sample behaves in the exact opposite fashion from the PDMAEMA-PS sample.

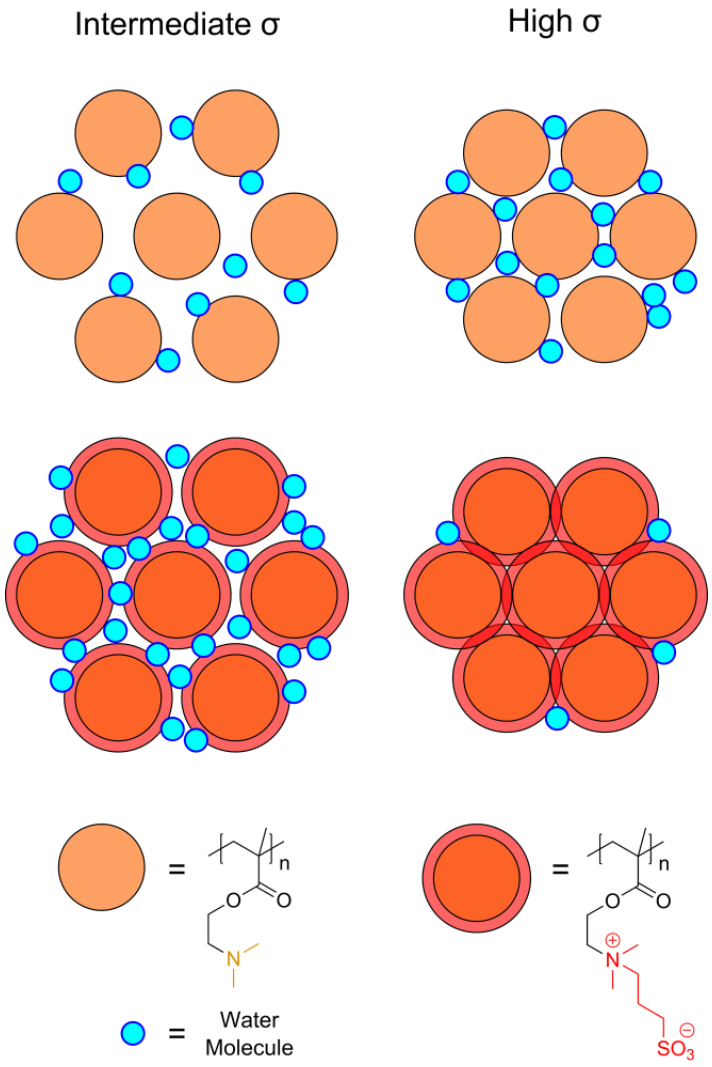

Figure 5.4. Top-down schematic of the projected area of a grafted polymer chain (large orange circles) and the resulting interstitial void space being filled with water molecules (small blue circles). The unmodified PDMAEMA brush (top row) has more void space at intermediate grafting densities (σ) than at high σ, resulting in a more hydrophobic brush environment. The betainized PDMAEMA brush (PDMAEMA-PS; bottom row) expresses a hydrophilic zwitterionic side chain chemistry (red corona) that extends into the void space. At intermediate σ, neighboring chains cannot form zwitterionic complexes, resulting in a hydrophilic environment. At high σ, the side chains in PDMAEMA-PS can form zwitterionic complexes (overlapping red corona regions) that compensate the hydrophilic charges and result in a more hydrophobic brush environment.

When considering what mechanism may underlie these observations, it is important to consider the role of the ambient air, in addition to the polymer chains and water vapor. As σ changes,

the ability of the polymer chains to fill void space will change due to changes in distance between grafted chains. This idea is depicted schematically in **Figure 5.4**. At high σ, the chains exist in close proximity to each other and extend away from the substrate due to crowding from neighboring chains. This proximity may allow chains to fill void spaces created by neighboring chains when collapsed. Since these voids contain primarily air, reducing the fraction of void spaces within the brush will increase the hydrophilicity of the brush. At the lowest σ levels, chains exist in isolation from each other and will collapse in the dry state without crowding by neighboring chains. The flexibility of PDMAEMA, which has a T_g near room temperature[15–17], may allow these isolated or nearly isolated chains to effectively fill their own void spaces. In contrast, chains at intermediate σ are neither as crowded as at high σ nor as isolated as those as low σ. Therefore, the two potential mechanisms of void filling described may not be accessible to chains at intermediate σ, and the brushes will possess a higher void fraction. As a result, the brushes will exhibit a more hydrophobic behavior.

When betaine moieties are incorporated into the PDMAEMA brush, the proximity of neighboring chains at high σ facilitates the creation of intermolecular zwitterionic complexes. At low σ levels, the lower confinement allows the chains space to form intramolecular complexes. Since these complexes will shield the electrostatic charges from water vapor in the brush, complex formation leads to a more hydrophobic brush. Intermediate σ levels appear to frustrate the process of forming both intermolecular and intramolecular complexes. There is simultaneously insufficient proximity to neighboring chains for significant intermolecular complexing, and insufficient space to facilitate rearrangement for intramolecular complexing.

5.3.2 Grafted Versus Spuncast Films

Tethering polymer chains to a substrate by covalent bonding results in a stable film. However, the grafting introduces a significant reduction in entropy. This system is in contrast to a polymer film that has been spuncast or solvent cast onto a substrate. In this latter system, the chains are not necessarily confined to a specific point within the film, as in an end-tethered film. While chain confinement still exists within these spuncast films due to the short distance between the polymer/substrate and polymer/air interface, the chains away from these interfaces are less restricted in the conformations they can adopt. Thus, identifying differences in vapor swelling behavior as a result of grafting the chains to a substrate represents a basic and important question to answer, with implications for developing and improving technologies using grafted systems.

To address this question, a series of PDMAEMA brush samples and a series of PDMAEMA spuncast films were exposed to humid environments and the swelling and solvent uptake analyzed by SE. Both sets of samples contained two thicknesses of comparable magnitude, including 90 nm (orange squares) and 180 nm (black squares) samples for the brush series, and 80 nm (blue circles) and 193 nm (pink circles) samples for the spuncast series. A third sample comprised a brush (purple squares) or spuncast film (cyan circles) quaternized with methyl iodide (PDMAEMA-MeI). The post-polymerization modification (PPM) of the PDMAEMA-MeI brush was described previously[7] (*cf.* **Chapter 4**). For the spuncast PDMAEMA-MeI sample, **Figure 5.5** presents ellipsometric Ψ data collected using an IR-VASE for spuncast PDMAEMA and PDMAEMA-MeI. The peaks in Ψ correspond precisely with infrared (IR) spectroscopy peaks associated with specific functional groups. Comparison of the data for PDMAEMA and PDMAEMA-MeI reveals the disappearance of peaks associated with conversion of the tertiary amine to a quaternary ammonium group[18] and the appearance of a peak associated with water[19] after exposure to MeI vapors, suggesting successful quaternization of the spuncast PDMAEMA film. A final spuncast sample with a thickness of 86 nm was made after first depositing a layer of octyltrichlorosilane (OTS) on the silicon substrate (green circles).

The swelling factors and φ values determined from the SE data for these samples are plotted in **Figures 5.6a** and **5.6b**, respectively. The 90 nm and quaternized brush sample data are the same set from **Chapter 4** and are presented again here for reference. In general, the brush samples exhibit significantly higher swelling factors and solvent uptake. We reason, then, that the increased swelling of the grafted samples stems from their increased uptake of water vapor. Remarkably, the unmodified PDMAEMA brushes swell to a greater extent and take up a greater fraction of water vapor than even the quaternized spuncast film. The OTS-based spuncast film exhibits the lowest swelling factor and φ level of any of the samples, providing evidence that the substrate chemistry plays an important role in the swelling behavior of these samples. This point is considered in more detail below.

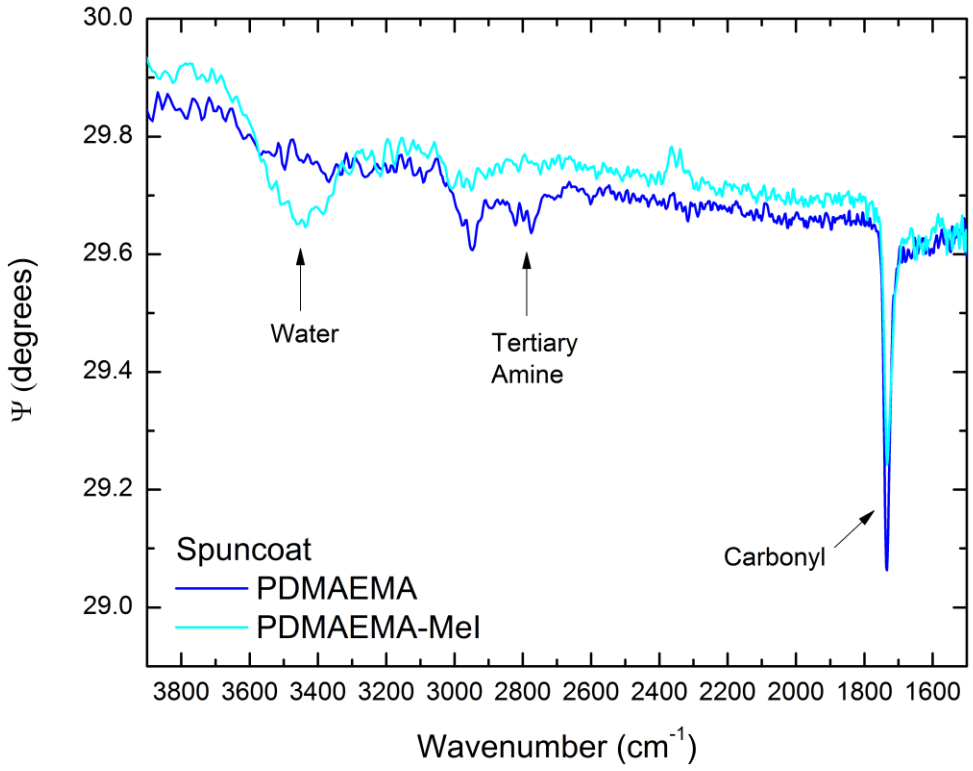

Figure 5.5. IR-VASE data collected at an incidence angle of 50° with a resolution of 4 cm^{-1} for a spuncast PDMAEMA film (blue) and an identical film after exposure to MeI vapors for 48 hours (cyan). The disappearance of peaks at 2750 cm^{-1} and 2800 cm^{-1} is associated with the conversion of side chain tertiary amines to quaternary ammonium groups in PDMAEMA[18]. Following quaternization, a peak at 3450 cm^{-1} associated with water[19] appears in the PDMAEMA-MeI sample.

Solvent fraction is plotted against swelling factors in **Figure 5.6c**. As in the case of the PDMAEMA σ gradient discussed above, the unmodified PDMAEMA samples show a slight deviation below the expected trend line (solid black line). Comparison of the unmodified PDMAEMA brush and spuncast film data shows the thinner spuncast film and OTS-based spuncast film deviate strongly and fall below the brush samples and the thicker spuncast film. These latter three samples exhibit comparable trends. In contrast, both the quaternized brush and quaternized spuncast film follow the trend very closely, even exceeding it for the quaternized brush at large swelling factors.

The trend of the unmodified brush may be explained as before by the possible protonation of the tertiary amine side chain moieties, resulting in electrostatic repulsion. That explanation does not account for the quaternized samples. In fact, the implication of this mechanism for the quaternized samples is that they behave as neutral polymer films, despite bearing cationic quaternary ammonium groups and anionic iodide counterions. While these charged moieties lead to a greater uptake of water vapor overall, they do not appear to dissociate and induce electrostatic repulsion. Indeed, by exhibiting a tendency to deviate above the expected trend line, the quaternized brush sample appears to accommodate more water vapor in the grafted film than expected from the swelling factor. If that is in fact the case, this excess water uptake may be due to a mechanism similar to the void space model developed in the previous section. That is, water is able to penetrate these void spaces to maximize exposure to the ammonium salt in the side chain.

The Flory-Huggins χ parameter for each sample are calculated from **Equation 5.1** above and plotted as a function of RH level in **Figure 5.6d**. The unmodified PDMAEMA brush and spuncast film samples follow a similar trend, wherein the χ parameters are higher at lower RH levels than at higher levels. The large error bars for data at lower RH levels occur for the same reason as described in the previous section. Above $\approx$ 75 RH % the χ values decrease with increasing RH. The reduction in χ values appears to originate from the solvation of the brush by an increasing amount of water vapor[7] (*cf.* **Chapter 4**). It is noteworthy that both the brush and spuncast films exhibit this reduction in χ value. Therefore, the mechanism by which it occurs is likely the same in both series of samples. Nonetheless, the brush samples exhibit consistently lower χ values than the spuncast films in this region. Within each set the thicker samples exhibit a lower χ parameter, consistent with the swelling factor and φ data. Moreover, the OTS-based spuncast film exhibits a higher χ parameter despite being functionally identical to the other spuncast films.

The quaternized brush and quaternized spuncast films produce lower χ values than the unmodified brush and spuncast samples, respectively. However, the quaternized spuncast film still displays a higher χ value than the PDMAEMA brushes, suggesting that water finds the unmodified brush samples more favorable than a quaternized spuncast film. Furthermore, the two quaternized samples show very different behavior from each other. The quaternized brush shows an essentially constant χ value of $\approx$ 0.6 above $\approx$ 50 RH %. The quaternized spuncast film shows a smoothly decreasing χ value that starts near 2.25 at $\approx$ 50 RH % and reaches $\approx$ 1.0 at the highest humidity level. The reason for this difference in behavior is not immediately clear from the data. One possibility is

that the chains in the quaternized brush sample can more easily rearrange due the presence of void space between the chains, as discussed in the preceding section.

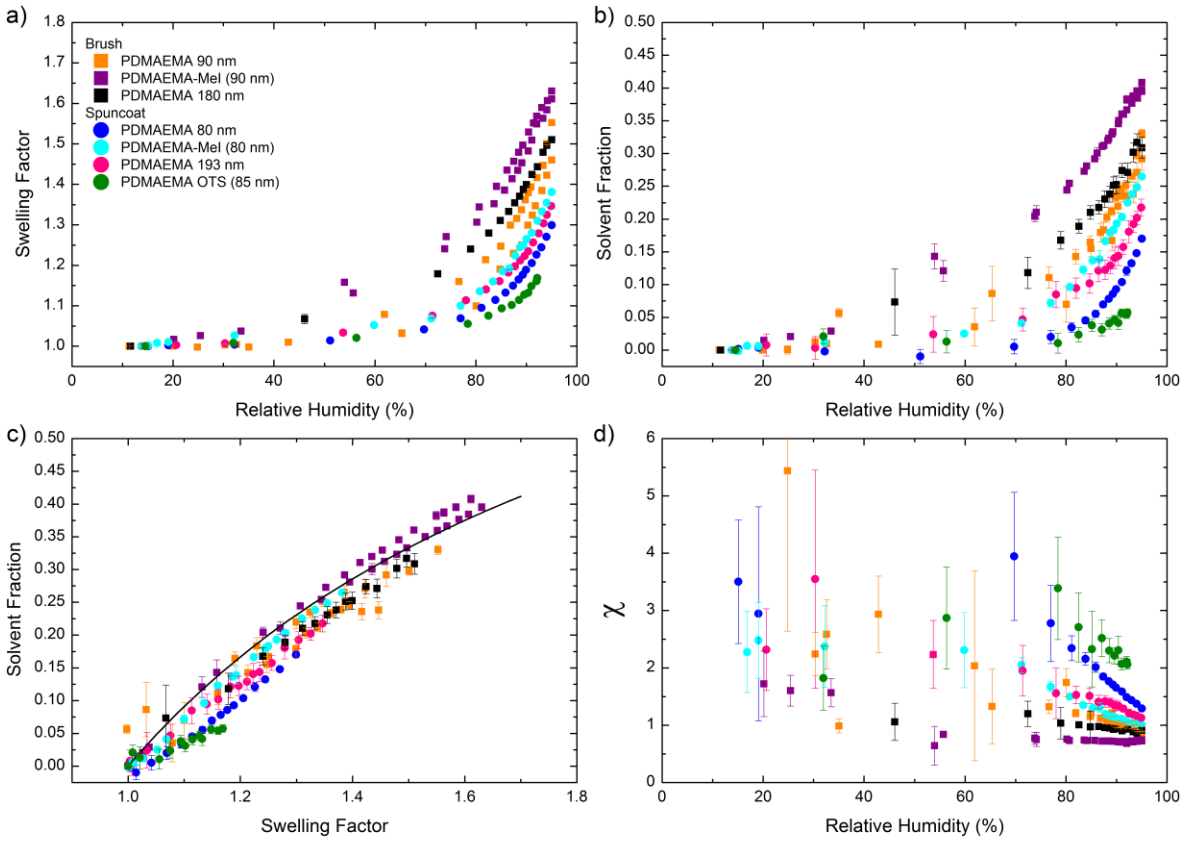

Figure 5.6. a) Swelling factor calculated from thickness values derived from fitting SE data for PDMAEMA and PDMAEMA-MeI brushes and spuncast films. b) Solvent fraction inside the PDMAEMA brushes and spuncast films determined by fitting SE data. c) Solvent fraction data from **Figure 5.6b** plotted against swelling factor data from **Figure 5.6a**. Black line is the expected trend (see text). d) Values of Flory-Huggins interaction parameter, χ, calculated from data in **Figure 5.6b**.

For both the brush samples and the spuncast samples, there is an apparent dependence of swelling factor and φ on the thickness of the polymer film. The thicker samples tend to exhibit a higher swelling factor and solvent uptake level. This difference is more pronounced in the spuncast

films and exists over the entire RH range. The brush samples show a more pronounced difference in the middle of the RH range, from ≈ 40 % RH to ≈ 80 %. At higher RH levels, the swelling factors and φ levels of the thicker and thinner samples begin to converge. Since the thickness dependence appears in both the grafted and non-grafted systems, this finding suggests this phenomenon originates from a surface effect. It is necessary to emphasize that the brush samples and spuncast samples have an important difference between them. The initiator layer first deposited on the substrate for the brush samples creates a molecular barrier between the polymer chains and the silicon oxide (SiO_x) at the substrate interface. This barrier is not present in two of the spuncast films, which are deposited directly onto the silica layer at the interface of the silicon substrate. The OTS-based spuncast film provides an analog to the initiator layer in the brush. Importantly, the initiator layer (WCA ≈ 78^o) is more hydrophilic than the OTS layer (WCA ≈ 105^o). Thus, the mechanism by which the thickness difference appears may be different between the sample sets.

In the case of the brush samples, neutron reflectivity measurements performed on an unmodified PDMAEMA brush[7] (*cf.* **Chapter 4**) provide a starting point for understanding the origin of the thickness effect. The sample used in these experiments had a thickness of ≈ 30 nm. Those experiments revealed that D_2O vapor did not homogeneously solvate the polymer brush. Rather, an enrichment of D_2O appeared at the polymer/air interface that suggested greater solvation of the chains compared to the "bulk" film between the polymer/air and polymer/substrate interfaces. With increasing RH level, this enrichment zone extended deeper into the brush toward the polymer/substrate interface. At the highest RH level examined (95 %) the enriched region had just reached the polymer/substrate interface.

Perhaps this heterogeneous distribution of D_2O within the brush can result in variation of swelling factor and vapor sorption with brush thickness. By increasing the thickness of the brush, the absolute size of the enrichment zone (as measured by penetration depth) can be larger since the polymer/substrate interface is further away from the polymer/air interface, allowing for a greater absolute uptake of water vapor. Since the box-like model applied in the SE modeling will effectively average the vapor uptake over the entire film thickness, increasing the absolute size of the enrichment may result in a higher average φ. At the highest RH levels, the enrichment zone may be penetrating to the polymer/substrate interface for all thicknesses considered in these studies, and thus the swelling factors and φ values converge. NR measurements of thicker polymer brushes can confirm or discredit

this hypothesis. If discredited, then the explanation offered for the spuncast films below may offer an alternative mechanism.

The origin of the thickness effect on swelling factor and φ in spuncast films may be the same as the brush, and NR measurements on spuncast films of PDMAEMA would aid in revealing any sort of enrichment zone at the polymer/air interface. Alternatively, the tertiary amine side chain functionalities in the PDMAEMA chains close to the polymer/substrate interface may be interacting physically with the SiO_x layer that is covered by the initiator layer in the grafted samples. By interacting with the SiO_x layer, the side chain amines are less available to interact with the water vapor that has penetrated into the spuncast film. As a result, the brush may take up less water vapor and exhibit lower swelling factors and φ values than polymer brushes of comparable thickness. Surprisingly, the OTS-based spuncast film exhibits a markedly more hydrophobic response than the other spuncast films directly on silicon. Since the SiO_x interface is passivated by deposition of the inert OTS molecules, the PDMAEMA chains at the polymer/substrate interface are presumably no longer interacting with the SiO_x layer. As reasoned above, the chains in the polymer brush samples do not interact directly with the SiO_x layer either due to the presence of the initiator layer. Thus, it appears the difference in swelling and solvent uptake of the various films originates to some extent with the hydrophobicity of the polymer/substrate interface.

While the initiator layer in the polymer brush samples is more hydrophobic than unmodified SiO_x (WCA < 20^o), it still exhibits a WCA (≈ 78^o) that is technically hydrophilic (defined as WCA < 90^o). OTS is defined as hydrophobic, since its WCA (≈105^o) is > 90^o. The NR measurements of the PDMAEMA brush described above (*cf.* **Chapter 4**) reveal the presence of D_2O at the polymer/substrate interface. A similar enrichment of D_2O vapor has been observed in spuncast polymer films[20]. Therefore, water vapor enriches likely the polymer/initiator interface in the polymer brush system, which may lead to swelling of the brush from both the polymer/substrate interface and polymer/air interface. In the case of the films spuncast directly on silicon substrates, the interaction between the polymer chains and SiO_x layer may block the hydrophilic moieties in both the polymer side chain and substrate from interacting with water molecules. As a result, the accumulation of water at the polymer/substrate interface is muted compared to the polymer brush. Thus, the dual interface swelling phenomenon occurs to a lesser extent, and these samples exhibit a lower swelling factor. In contrast, the hydrophobic OTS layer in the OTS-based spuncast film repels effectively water from the polymer/substrate interface, leading to a significantly more hydrophobic response.

Increasing the thickness of the spuncast film will decrease the fraction of the brush that experiences this surface effect. As seen in the NR measurements of the PDMAEMA brush, the polymer/air interface is enriched by D_2O to a greater extent than the polymer/substrate interface. Based on the substrate effect hypothesis described above, this difference would be amplified in the spuncast film. As a result, the thicker spuncast films will appear more hydrophilic than the thinner film, since the thicker film experiences relatively less influence from the polymer/substrate interface. Furthermore, the suggested mechanisms account for the observation that the data for the spuncast films do not converge at the highest RH levels like the brush samples. Since the influence the polymer/substrate interface may exert on the vapor sorption properties of the film does not depend on the ambient conditions, the length scale over which it influences these properties is possibly constant with RH level. Therefore, the effect of thickness on swelling factor and φ will exist over all RH levels.

5.3.3 Influence of Amino Alkyl Chain Length

The preceding sections considered the influence of σ and end tethering on PDMAEMA brushes and samples derived from PDMAEMA brushes by quaternization and betainization reactions. In all of these experiments, one constant factor is the presence of two methyl groups on the side chain amino group. As described in **Chapter 4**, the length of the alkyl chain introduced into a PDMAEMA brush by quaternization influences strongly the swelling behavior and water sorption of the brush. It follows that the length of alkyl chains present in the unmodified brush will also influence strongly the behavior of the brush in humid environments. To explore this influence, brushes comprising poly(2-(diethylamino)ethyl methacrylate) (PDEAEMA) were synthesized and characterized using the SE methods described previously. This polymer is functionally identical to PDMAEMA, except that the two methyl groups are replaced with two ethyl groups.

Research using PDEAEMA brush has already proven this polymer is insoluble in water in its neutral state, in contrast to PDMAEMA, which is soluble in its neutral state[21]. PDEAEMA is soluble in water when in its charged state. Charging PDEAEMA also influences its water vapor sorption properties as shown by experiments that exposed a PDEAEMA brush to DI water before and after exposing the same brush to acidic water vapor and after incubation in DI water with a basic pH[22]. Prior to exposure to acidic water vapor, the brush showed negligible swelling. After exposure to acidic water vapor, exposing the PDEAEMA to DI water vapor produced a marked increase in

thickness. After incubation in basic solution, which deprotonates the side chain tertiary amine, the brush once again showed negligible swelling when exposed to DI water vapor. These experiments did not use SE, and so only thickness could be fit from the ellipsometric data. Furthermore, no attempt was made to vary the RH level inside the measurement chamber.

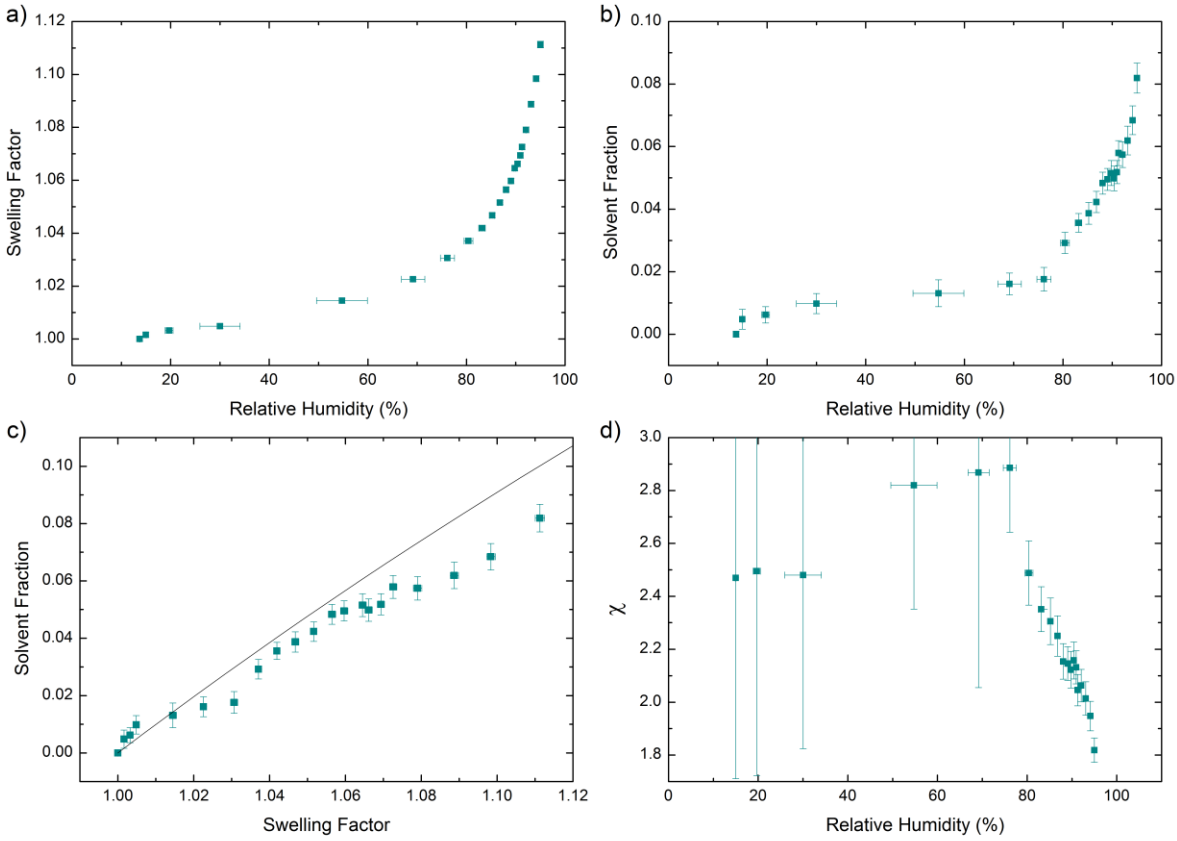

Figure 5.7. a) Swelling factor calculated from thickness values derived from fitting SE data a PDEAEMA brush. b) Solvent fraction inside the PDEAEMA brush determined by fitting SE data. c) Solvent fraction data from **Figure 5.7b** plotted against swelling factor data from **Figure 5.7a**. Black line is the expected trend (see text). d) Values of Flory-Huggins interaction parameter, χ, calculated from data in **Figure 5.7b**.

The swelling factor derived from SE collected while exposing to water vapor a PDEAEMA brush with a thickness of ≈60 nm is plotted in **Figure 5.7a**. The extent of swelling of PDEAEMA is

substantially lower than the PDMAEMA brushes described above. Whereas PDMAEMA reaches a swelling factor of ≈1.6 at the highest RH levels, PDEAEMA only swells by a factor of ≈1.12. Likewise, the φ values plotted in **Figure 5.7b**, which reach a maximum of ≈0.08, are also substantially lower than PDMAEMA, which reaches a maximum of ≈0.30. Therefore, the lower swelling factors observed in PDEAEMA compared to PDMAEMA occur because PDEAEMA takes up less water vapor. While this difference may be due partially to the lower thickness of the PDEAEMA brush (see the previous section), the more likely source is the increased hydrophobicity imparted by the ethyl substituents on the amino group.

Examination of the data in **Figure 5.7a** and **5.7b** reveals what appear to be two distinct regimes in the data. Starting from the lowest RH level, the data first increase then plateau with increasing RH level. Note that the lowest RH data point (≈13 % RH) is arbitrarily set to zero. Above ≈70 % RH, both the swelling factor and φ go through an inflection point and begin to increase precipitously. This latter trend is comparable to that observed in unmodified PDMAEMA brushes. It is possible that the plateauing observed at lower RH levels also occurs in PDMAEMA, but is harder to discern from the data due to the wider range of swelling factor and φ values for PDMAEMA. The clearest evidence of this phenomenon occurring in PDMAEMA is the dataset for 1.5 cm in **Figure 5.3**. Since this inflection in the trend occurs at ≈70~75 % RH for both PDMAEMA and PDEAEMA, this behavior likely stems from the water vapor content reaching a critical ambient value.

Figure 5.7c plots φ versus the swelling factor for the PDEAEMA brush. With increasing RH level, the data show a clear deviation to below the expected trend (solid black line). This behavior is similar to that observed in the PDMAEMA brushes. Close examination of the data in **Figure 5.7c** reveal three regions that exhibit different trends. From a swelling factor of 1.0 to ≈ 1.03 (corresponding to the RH range of ≈13~75 %), the first exceed the expected trend line, then plateau and ultimately cross under the expected trend line. This pattern mimics the plateauing observed in the swelling factor and φ data. From a swelling factor of ≈1.03~1.07 (RH range ≈75~90 %), the data follow the shape of the expected trend line, though the data points fall just below the line. Above a swelling factor of 1.07 (90 % RH), the data diverge below the trend line. A similar trend can be seen in some of the PDMAEMA data sets (*e.g.*, at 1.5 cm in **Figure 5.3**), although the trends are not as clear as in PDEAEMA.

The data in **Figure 5.7b** were used to calculate Flory Huggins χ parameter using **Equation 5.1**; results are plotted in **Figure 5.7d**. In general, the χ values for PDEAEMA are higher than

PDMAEMA, consistent with the increased hydrophobicity associated with the ethyl substituents in PDEAEMA. The χ values at low RH levels are higher than the χ values at higher RH levels. There is a sharp break in the trend at ≈75 % RH, at which point the χ values decrease dramatically, suggesting an increase in the hydrophilicity of the brush. A similar break is seen in the PDMAEMA data sets presented above. When the RH level exceeds 90 %, the PDEAEMA χ values appear to decrease at an increasing rate. These breaks in trend correspond precisely with the three trends observed in **Figure 5.7c**.

This behavior in the PDEAEMA brush can be explained by the same hypothesis presented for PDMAEMA brushes. Specifically, above some critical RH level the tertiary amine in the side chain of PDEAEMA protonates, leading to formation of an electrostatic charge. This charging results in electrostatic repulsion, producing a greater swelling factor than expected from the uptake of water vapor alone. The formation of electrostatic charges would also result in a lower χ value, as observed in PDEAEMA and PDMAEMA. It is important to note that the data presented do not specifically support or discredit this hypothesis, and is presented here only as one possible explanation for the behavior observed in both PDMAEMA and PDEAEMA brushes, but not in the quaternized and betainized brushes derived from these PDMAEMA brushes.

In order to assess the behavior of absorbed water molecules, two types of complementary analyses (Zimm-Lundberg and Brown) were used to calculate the cluster number (N_c) of water molecules that have penetrated into the polymer brushes[23]. N_c provides a measure of whether water molecules inside the brush tend to associate with the polymer chains (lower N_c values) or cluster together with other water molecules (higher N_c). **Figure 5.8** plots N_c against RH level for PDMAEMA (red squares), PDMAEMA-MeI (orange circles), PDMAEMA-PrI (green triangles) and PDEAEMA (purple squares) as calculated by Zimm-Lundberg (closed symbols) and Brown analyses (open symbols). The analysis was restricted to data above 50 % RH in order to focus on behavior around the inflection point observed at ≈75 % RH.

For all four samples, the two approaches yield nearly identical values of N_c. At the lowest RH levels considered, all the samples exhibit N_c values in the range of 1.5~2.5. As RH level increases, the uncharged systems (PDMAEMA and PDEAEMA) and the quaternized samples (PDMAEMA-MeI and PDMAEMA-PrI) appear to follow different trends. PDMAEMA and PDEAEMA stay consistently near a value of 2.5 until ≈75~80 % RH. At this RH level, the samples exhibit an increasing value N_c with increasing RH level. PDMAEMA increases relatively linearly to

a value of ≈5.5 at the highest RH level. PDEAEMA increases at a faster rate than PDMAEMA, and appears to increase at an accelerating rate with increasing RH. At the highest humidity levels, PDEAEMA has an N_c of ≈8.5.

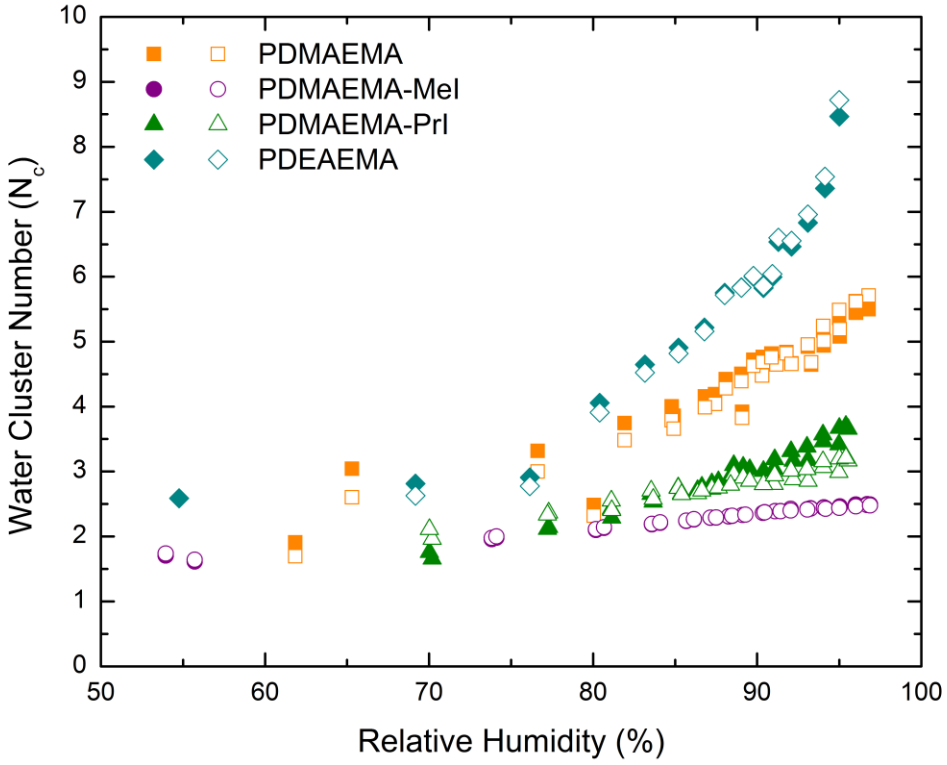

Figure 5.8. Water cluster number (N_c) calculated using Zimm-Lundberg (closed symbols) and Brown (open symbols) analyses plotted as a function of RH % for brushes comprising PDMAEMA (orange data), PDMAEMA-MeI (purple data), PDMAEMA-PrI (green data) and PDEAEMA (dark cyan data).

In contrast, the quaternized samples maintain much lower N_c values over the entire RH range considered. Both PDMAEMA-MeI and PDMAEMA-PrI show N_c levels between 1.5 and 2.0 below 70 % RH. PDMAEMA-MeI reaches an N_c value of 2.5 at the highest humidity level, compared to a

value of ≈3.5 for PDMAEMA-PrI. These lower N_c values imply that water molecules in these quaternized polymer brushes tend to associate with the polymer chains more than in the uncharged PDMAEMA and PDEAEMA brushes. Furthermore, the PDMAEMA-MeI brush presents a more favorable polymer chemistry than PDMAEMA-PrI. This difference stems presumably from the longer alkyl chain introduced into the side chain of PDMAEMA-PrI as a result of quaternization.

As a reminder, the φ levels at the highest humidity levels for these samples order from highest to lowest as PDMAEMA-MeI, PDMAEMA, PDMAEMA-PrI and PDEAEMA (*cf.* **Chapter 4** for PDMAEMA-PrI data). The fact PDMAEMA takes up a greater fraction of water vapor than PDMAEMA-PrI, but exhibits a higher N_c, is surprising. Furthermore, the reverse trend is true for PDEAEMA and PDMAEMA-PrI, wherein PDEAEMA takes up less moisture, but achieves a higher N_c. For both PDMAEMA and PDEAEMA, the increasing value of N_c implies that water molecules penetrating into the brush tend to associate with other water molecules in the brush and not distribute homogeneously throughout the brush itself.

The reason for this tendency to cluster is not clear from these data alone. This finding does fit together with the discussion on deviation from expected swelling behavior for these samples as a result of possible charging within the brush. Perhaps these clusters can accommodate the protonation of a tertiary amine by a water molecule, with other molecules in the cluster solvating the resulting charged moieties (quaternary ammonium and hydroxide counterion) by hydrogen bonding. This hydration could lower the free energy of the charged system, allowing the protonation to persist, which would, in turn, make the brush a more favorable environment for additional water molecules. As these additional water molecules segregate into the brush from the ambient air, they prefer to associate with the charged quaternary ammonium groups over the uncharged tertiary amines. Thus, new water molecules tend to accumulate where water clusters already exist.

This phenomenon would result in a positive feedback loop, with the addition of these new water molecules enabling the hydration of more protonated amines. Evidence of this feedback loop is perhaps best seen in the behavior of N_c for PDEAEMA, where an apparent acceleration in the increase in N_c and decrease in χ is observed at the highest humidity levels. Since PDEAEMA is not soluble in water unless charged, the observed acceleration in N_c and χ may stem from an ever increasing charge fraction within the brush.

It is important to state that this hypothesis is speculative and attempts to draw conclusions of a molecular process from macroscopic measurements. Further evidence is required of how water

molecules interact with the polymer brushes considered here, as well as with other polymer brushes comprising non-polyelectrolytes. A careful set of control experiments, such as with poly(methyl methacrylate) (PMMA) and poly(N-isopropyl acrylamide) (PNIPAAm) brushes, can provide much-needed insight into the validity of the above hypothesis. Furthermore, the interaction of vapor phase molecules with grafted polymer chains is an appealing system for computer simulation work, which can provide molecular-level information about vapor-based solvation.

5.3.4 Swelling by Organic Alcohols

The prior sections discussed the effect that multiple physical and chemical factors of a weak polyelectrolyte brush have on the swelling behavior of that brush by water vapor. Specifically, the effect of σ, thickness and grafting to a substrate were described for PDMAEMA brushes and quaternized PDMAEMA brushes, while a brush comprising PDEAEMA provided insight into the effect of chemical moieties on the side chain tertiary amine. All of these studies employed water vapor in air over a wide range of RH levels as the solvent system. In this final section, the water vapor is replaced with organic alcohols in order to ascertain the effect of solvent vapor chemistry on the swelling behavior of PDMAEMA and PDEAEMA brushes, as well as quaternized PDMAEMA brushes bearing additional methyl and propyl moieties. The alcohols used, *i.e.*, methanol and ethanol, effectively replace a hydrogen atom in water with a methyl or ethyl group. Thus, the swelling behavior of the brushes considered here provides insight into the interplay of the solvent and side chain chemistry.

Figures 5.9a and **5.9c** plot the swelling factors and φ values as a function of time for unmodified PDMAEMA and PDEAEMA brushes, as well as PDMAEMA brushes quaternized by MeI and propyl iodide (PrI), when incubated in the presence of methanol vapors. The measurements were started just after placing vial caps containing liquid methanol into the *in situ* cell and sealing the chamber. The increase in swelling factor and φ with time is due to the increasing vapor pressure of methanol in the chamber as a result of evaporation. The *in situ* cell does not have currently the capability of measuring vapor pressures of organic solvents, thus plots like those used to characterize water vapor swelling cannot be constructed. Furthermore, one important caveat of these measurements is that water vapor is still present in the cell during the organic vapor swelling. The ambient RH level in the room housing the SE system during these measurements was ≈30 % RH. Based on data from water vapor swelling the effect of this ambient humidity is not expected to affect

substantially the measurement results. While these technical points preclude a quantitative assessment of the swelling behavior of these samples, nonetheless, the qualitative trends observed by comparing across solvents systems and polymer brush samples provide useful insight into the behavior of these systems.

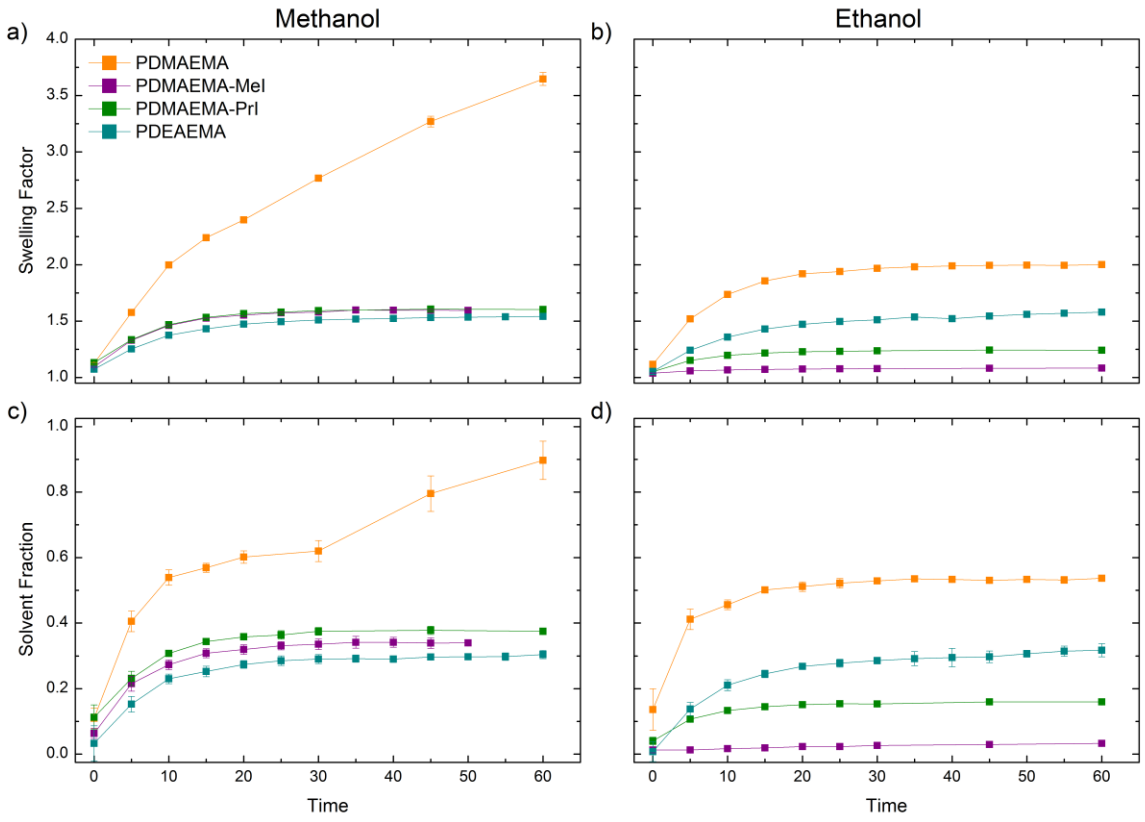

Figure 5.9. a) Swelling factor in methanol calculated from thickness values derived from SE data collected at various incubation times for brushes comprising PDMAEMA (orange data), PDMAEMA-MeI (purple data), PDMAEMA-PrI (green data) and PDEAEMA (dark cyan data). b) Swelling factor in ethanol calculated from thickness values derived from SE data for same samples. c) Methanol fraction inside the polymer brush samples. d) Ethanol fraction inside the polymer brush samples.

As in the case of water vapor, the increasing swelling factor corresponds to an increase in φ. Therefore, the brush swells due to the uptake of solvent vapor. The swelling factors and φ values appear to plateau after ≈ 30 minutes, suggesting that methanol vapor has saturated the cell within this time period, and that any variation in the data between samples is a result of differences in the interaction between methanol and chemistry within the brush. The one exception to the plateauing observation is unmodified PDMAEMA, which does appear to plateau in φ at 30 minutes, but then increases significantly at longer times. This behavior likely stems from condensation of methanol in the brush. Even prior to the point of condensation, PDMAEMA is clearly the most favorable sample for methanol compared to the other samples. Surprisingly, PDMAEMA-MeI, PDMAEMA-PrI and PDEAEMA exhibit very similar swelling factors. The magnitude of these swelling factors is ≈1.5. There is more variation in the φ values of these samples, but even for this parameter the plateau values are quite close. PDMAEMA-PrI exhibits a slightly higher φ values than PDMAEMA-MeI. In both swelling factor and φ, PDEAEMA has the lowest plateau value. Therefore, it appears that in the absence of an electrostatic charge, methanol prefers strongly methyl substituents over ethyl substituents (PDMAEMA vs. PDEAEMA). Upon quaternization, the length of the incorporated alkyl chain matters less than the presence of the counterion, which results in comparable physical behavior of the two quaternized samples when exposed to methanol.

Replacing methanol with ethanol extends the alkyl chain in the solvent vapor by an additional aliphatic carbon. **Figures 5.9b** and **5.9d** plot the swelling thickness and φ values for the same samples exposed to ethanol vapors using an identical experimental methodology. As before, the ambient RH level of the room was ≈30 %, so there is a non-negligible amount of water vapor inside the *in situ* cell. Nonetheless, the samples all appear to reach plateau levels in swelling factor and φ after 30 minutes, as in the case of methanol. Looking at all the samples, swelling factor and φ again correspond precisely, such that a higher swelling factor is observed with a higher φ. Therefore, the brushes swell to varying degrees due to the uptake of varying amounts of solvent vapor.

Unlike for the case of methanol, exposure to ethanol leads to more distinct behavior between the samples. PDMAEMA again exhibits the highest swelling factor and φ level, followed by PDEAEMA. There is a substantial difference between these two samples, with PDMAEMA exhibiting a swelling factor of 2.0 and PDEAEMA a swelling factor of 1.5. The charged samples exhibit substantially lower swelling factors and φ values than the uncharged samples. PDMAEMA-PrI swells to a factor of ≈1.25, while PDMAEMA-MeI shows negligible swelling. For the uncharged

systems, the methyl groups presented by PDMAEMA once again provide a more favorable environment for ethanol than the ethyl groups in the side chain of PDEAEMA. This result is somewhat surprising, since the alkyl chain lengths of the side chain and solvent are more closely matched in the ethanol-PDEAEMA system. Perhaps the increased steric hindrance imparted by the ethyl chains in PDEAEMA frustrates the interaction of the alcohol functional group with the amine. The methyl groups in PDMAEMA would present less steric hindrance and allow better access to the amine group. While care must be taken in comparing the results for methanol and ethanol due to possible differences in partial pressures at saturation, it is worth noting that PDEAEMA exhibits a similar swelling factor in both ethanol and methanol. This finding supports the notion that the ethyl groups on the amine mediate the interactions with the alcohol vapors. In contrast, PDMAEMA swells appreciably less in ethanol. In this case, the longer alkyl chain in ethanol may be imparting a similar steric interference as the ethyl chains in PDEAEMA compared to the methyl group in methanol.

Whereas the length of the alkyl chain incorporated into the polymer side chain by quaternization does not influence strongly swelling methanol vapors, it affects substantially the swelling in ethanol vapors. PDMAEMA-PrI swells to a factor of ≈1.25, while PDMAEMA-MeI shows negligible swelling over the entire incubation period. The additional hydrophobicity imparted to ethanol by the longer alkyl chain appears to make interaction with the quaternary ammonium group unfavorable. The three methyl groups in PDMAEMA-MeI lack sufficient hydrophobicity to accommodate interaction with the ethyl chain in ethanol. Incorporating a propyl chain, as in PDMAEMA-PrI, provides a sufficiently long alkyl group to accommodate hydrophobic interactions. Furthermore, the additional steric hindrance from the longer alkyl chain may better hide the quaternary ammonium group from ethanol, providing an extra measure of hydrophobicity.

While these measurements were not performed in the same way with water vapor due to concerns of condensing the water vapor inside the brush (*cf.* **Figure 5.9c** for methanol in PDMAEMA), the swelling factors obtained at the highest humidity levels observed in **Figure 4.2a** in **Chapter 4** provide a suitable surrogate. These values are likely minimum swelling factors, since the RH levels do not reach full saturation, which appears to be the case of methanol and ethanol. As noted before, differences in absolute partial pressures of water, methanol and ethanol vapor make quantitative comparison of swelling across the solvents difficult. Nonetheless, the qualitative differences between the solvents found for the series of samples used here provide insight into the interplay between polymer brush and solvent chemistry. These orderings are summarized in **Table 1**.

Table 5.1: Relative Magnitudes of Swelling Factors

Sample	Swelling Order of Solvents
PDMAEMA	Methanol > Ethanol > Water
PDEAEMA	Methanol = Ethanol >> Water
PDMAEMA-MeI	Water > Methanol >> Ethanol(negligible)
PDMAEMA-PrI	Methanol > Water > Ethanol

Examination of the trends in the table leads to a notable conclusion. In the vapor phase, the highest swelling is observed typically with methanol. In other words, the presence of a methyl group is more favorable than a hydrogen atom or ethyl chain for PDMAEMA, PDEAEMA and PDMAEMA-PrI. It should be noted that PDEAEMA exhibits a comparable swelling factor for methanol and ethanol. This trend may point to a situation wherein the alcohol functional group orients itself toward the amine and the methyl group associates with the pendant alkyl chains. The exception to this trend is PDMAEMA-MeI, which prefers water to methanol and shows a negligible response to ethanol. PDMAEMA-MeI also possesses the most exposed quaternary ammonium group, suggesting that this feature is the most prominent in determining the extent of solvent uptake. Importantly, this sample still swells in methanol, but there insufficient carbon atoms to shift the microenvironment in favor of methanol, as appears to be the case in PDMAEMA-PrI.

5.4 Conclusion

A systematic investigation into the influence that several physical and chemical parameters have on the swelling behavior in vapor environments of polymer brushes bearing side chain tertiary amine groups. The physical parameters included σ (grafting density), thickness and grafting of the polymer chains to a solid substrate. The chemical parameters included the effect of alkyl chain length of the amine substituents and transformation of the tertiary amine to a quaternary ammonium group by quaternization reaction. Swelling behavior appeared to occur to a lesser extent in water vapor at intermediate σ values, and corroborates the complex effect of this parameter on brush behavior[7] (*cf.* **Chapter 4**). Thicker films and grafted films tend to exhibit more hydrophilic responses, while replacing the methyl groups in PDMAEMA with ethyl groups as in PDEAEMA results in a significant reduction in hydrophilicity. With the exception of PDMAEMA brushes quaternized by

methyl iodide (PDMAEMA-MeI), the samples considered in these studies swelled best in methanol and exhibited evidence of an interplay between the alkyl chains in the solvent and the alkyl chains in the brush.

5.5 References

(1) Rühe, J.; Ballauff, M.; Biesalski, M.; Dziezok, P.; Gröhn, F.; D; Rühe, J. *Adv. Polym. Sci* **2004**, *165*, 79–150.

(2) Toomey, R.; Tirrell, M. *Annu. Rev. Phys. Chem.* **2008**, *59*, 493–517.

(3) McCaig, H. C.; Myers, E.; Lewis, N. S.; Roukes, M. L. *Nano Lett.* **2014**, *14*, 3728–3732.

(4) Grajales, S. T.; Dong, X.; Zheng, Y.; Baker, G. L.; Bruening, M. L. *Chem. Mater.* **2010**, *22*, 4026–4033.

(5) Button, B.; Cai, L.-H.; Ehre, C.; Kesimer, M.; Hill, D. B.; Sheehan, J. K.; Boucher, R. C.; Rubinstein, M. *Science* **2012**, *337*, 937–941.

(6) Barbey, R.; Lavanant, L.; Paripovic, D.; Schüwer, N.; Sugnaux, C.; Tugulu, S.; Klok, H.-A. *Chem. Rev.* **2009**, *109*, 5437–5527.

(7) Galvin, C. J.; Dimitriou, M. D.; Satija, S. K.; Genzer, J. *Submitted* **2014**.

(8) Matyjaszewski, K.; Miller, P. J.; Shukla, N.; Immaraporn, B.; Gelman, A.; Luokala, B. B.; Siclovan, T. M.; Kickelbick, G.; Vallant, T.; Hoffmann, H.; Pakula, T. *Macromolecules* **1999**, *32*, 8716–8724.

(9) Jaeger, W.; Bohrisch, J.; Laschewsky, A. *Prog. Polym. Sci.* **2010**, *35*, 511–577.

(10) Lowe, A. B.; McCormick, C. L. *Chem. Rev.* **2002**, *102*, 4177–4190.

(11) Moutzouris, K.; Papamichael, M.; Betsis, S. C.; Stavrakas, I.; Hloupis, G.; Triantis, D. *Appl. Phys. B* **2013**.

(12) Kedenburg, S.; Vieweg, M.; Gissibl, T.; Giessen, H. *Opt. Mater. Express* **2012**, *2*, 1588.

(13) Wu, T.; Efimenko, K.; Genzer, J. *J. Am. Chem. Soc.* **2002**, *124*, 9394–9395.

(14) Flory, P. J. *Principles of Polymer Chemistry*; Cornell University Press: Ithaca, NY, 1953; p. 672.

(15) Arce, A.; Fornasiero, F.; Rodriguez, O.; Radke, C. J.; Prausnitz, J. M. *Phys. Chem. Chem. Phys.* **2004**, *6*, 103 – 108.

(16) Gao, J.; Zhai, G.; Song, Y.; Jiang, B. *J. Appl. Polym. Sci.* **2008**, *107*, 3548–3556.

(17) Hunley, M. T.; England, J. P.; Long, T. E. *Macromolecules* **2010**, *43*, 9998–10005.

(18) Sanjuan, S.; Perrin, P.; Pantoustier, N.; Tran, Y. *Langmuir* **2007**, *23*, 5769–5778.

(19) Lin-Vien, D.; Colthup, N. B.; Fateley, W. G.; Grasselli, J. G. *The Handbook of Infrared and Raman Characteristic Frequencies of Organic Molecules*; Academic Press: San Diego, CA, 1991.

(20) Vogt, B. D.; Soles, C. L.; Jones, R. L.; Wang, C.-Y.; Lin, E. K.; Wu, W.; Satija, S. K.; Goldfarb, D. L.; Angelopoulos, M. *Langmuir* **2004**, *20*, 5285–5290.

(21) Bütün, V.; Armes, S.; Billingham, N. *Polymer (Guildf).* **2001**, *42*, 5993–6008.

(22) Fielding, L. A.; Edmondson, S.; Armes, S. P. *J. Mater. Chem.* **2011**, *21*, 11773.

(23) Chu, L.-Q.; Mao, H.-Q.; Knoll, W. *Polymer (Guildf).* **2006**, *47*, 7406–7413.

6. Surface-grafted Polymer Assemblies via Grafting-through Polymerization

6.1 Introduction

Surface-grafted polymer assemblies (SGPAs) have enjoyed popularity in the academic research community over the past two decades due to their rich physics and promise to revolutionize technologies ranging from vapor sensors[1] to protein separations[2] to conductive fabrics[3], among others[4]. The development of controlled radical polymerization (CRP) schemes, such as atom-transfer radical polymerization (ATRP)[5] and reversible addition-fragmentation chain transfer (RAFT)[6] polymerization, has enabled access to SGPAs of relatively uniform molecular weight (MW) and architecture by the so-called "grafting from" method[7,8]. In this method a molecule that acts as an initiator (*i.e.*, in ATRP) or transfer agent (*i.e.*, in RAFT) is first deposited on to a solid substrate, which is then immersed in a polymerization solution, and polymer chains grow directly from such modified substrate. This procedure can achieve high polymer grafting densities (σ) of relatively controlled MW dispersity[9,10], and the living nature of the polymer chain ends makes multiblock and gradient copolymers accessible by simply changing the composition of the polymerization solution. For these reasons, the "grafting from" approach has enjoyed immense popularity among many researchers.

While controlled radical polymerization schemes like ATRP and RAFT found immediate adoption in the academic community, these techniques possess certain limitations in an industrial setting, where free radical polymerization (FRP) reigns. Compared to FRP, CRP techniques are complicated, requiring additional ingredients beyond monomer and initiator (*e.g.*, catalyst or transfer agent) that create another degree of freedom, which influences the characteristics of the final product. These additional ingredients further add to cost and necessitate stringent purification to be employed in the technologies which CRP promises to revolutionize. Furthermore, since CRP controls MW dispersity by slowing down the rate of polymerization, CRPs are slower than FRP.

Development of approaches to produce SGPAs that use FRP may be of interest and necessary for a number of industries. One route is through the use of a surface-grafted FRP initiator[11,12]. One drawback of this approach is the need to synthesize the initiator, which requires generally advanced organic chemistry techniques. An alternative approach to create assemblies of polymers tethered to surfaces is to anchor a monomer to a substrate and use a bulk polymerization reaction to link chemically the bulk-generated polymers to the surface-grafted monomers (SGM) via a so-called grafting-through approach[13]. This method has the advantage of being directly applicable to existing bulk polymerization processes (*i.e.*, FRP or CRP). Our work documented here demonstrates that the

thickness of an SGPA obtained by polymerizing through SGMs is completely controllable by bulk parameters, and uniform films on substrates with areas of several cm^2 can be obtained with thicknesses up to several nanometers. These films can either completely or partially cover the SGM layer, presenting a way to tune interfacial properties. We further show that the grafting density (σ) of these films can be adjusted by using a mixture of SGMs and inert molecules.

6.2 Experimental

6.2.1 General methods and materials

1,4-dioxane, 2-(dimethylamino)ethyl methacrylate (DMAEMA), *t*-butyl methacrylate (tBMA), azobisisobutryonitrile (AIBN), toluene and acetonitrile were purchased from Sigma-Aldrich. 11-bromoundecyltrichlorosilane (11-BUTS) and *n*-octyltrichlorosilane (OTS) were purchased from Gelest. Silicon wafers of thickness 0.4 mm were purchased from Silicon Valley Microelectronics. Prior to polymerization, tBMA was passed through a column of inhibitor remover. AIBN was recrystallized from ethanol unless otherwise noted. Toluene was dried over molecular sieves. All other materials were used as received.

6.2.2 Sample Preparation

6.2.2.1 11-BUTS deposition and modification

Silicon wafers were segmented into 1 cm x 3 cm pieces, rinsed and sonicated for 20 minutes in ethanol, then treated in a UV-Ozone chamber for 20 minutes. The wafers were then immediately submerged in a 0.1 vol % solution of 11-BUTS in anhydrous toluene and incubated at -20 °C overnight. Samples were then removed, rinsed with ethanol and dried with a stream of nitrogen gas. The specimens were further cleaned by sonicating in ethanol for 20 minutes and dried with a stream of nitrogen gas before further characterization. For gradient samples, all steps are identical, with the addition of a gas phase OTS gradient deposition procedure prior to immersion of the cleaned silicon wafer into the 11-BUTS toluene solution following a protocol published previously[14]. 11-BUTS-modified silicon wafers were then immersed in a 50 vol % solution of DMAEMA (with inhibitor) in acetonitrile and incubated in an orbital at 40 °C for 24 hours. These samples (11-BUTS/DMAEMA) were removed, rinsed with ethanol and sonicated in ethanol for 20 minutes, then dried with a stream of N_2 gas.

6.2.2.2 Polymerization of surface-bound monomers

Purified tBMA, 1,4-dioxane and AIBN were charged to crimp-top sealable vials with rubber septa caps, and the AIBN was allowed to dissolve at room temperature. Wafers modified with 11-BUTS/DMAEMA were then placed in these vials, which were sealed and degassed by bubbling with nitrogen for one hour. The vials were then placed in a thermocouple controlled oil bath heated to 75 °C for 24 hours. The polymerization solution remained below the level of the heating oil during the entire polymerization to aid in maintaining a more uniform temperature in the polymerization solution. Once the polymerization completed, the vials were opened and the samples removed and sonicated in THF until reaching a constant thickness as determined by ellipsometry (typically within 20 minutes). The polymer solution was saved for further analysis by SEC.

6.2.3 Characterization techniques

Ellipsometry measurements were performed on a Rudolph II ellipsometer operating at an angle of incidence of 70° and wavelength of 633 nm. Data were fit to a model consisting of a silicon substrate, 1.5 nm SiO_x layer (n = 1.462), and a Cauchy film representing the organic film (n = 1.500). Size exclusion chromatography (SEC) was performed on a Waters 2695 chromatography system equipped with a differential refractive index detector (Optilab Rex; Wyatt) using THF at a flow rate of 0.3 mL/min calibrated with PMMA standards. Water contact angle (WCA) measurements were performed using a goniometer (Rame-Hart) with DI H_2O as the probe liquid. WCAs were calculated using automated droplet analysis software provided by the manufacturer. Surface topography measurements were made in air using an Asylum MFP-3D system (Asylum Research) in tapping mode using Si tips (Model AC160TS; Asylum Research) with a resonance frequency of 300 kHz and spring constant of 42 N/m. Scans were collected over an area of 4 μm x 4 μm at a scan rate of 1.0 Hz and resolution of 512 lines/scan. Data were analyzed in the Gwyddion software package[16] (http://gwyddion.net).

6.3 Results and Discussion

6.3.1 Homogeneous Grafting-Through Samples

Figure 6.1 depicts the scheme followed to produce the samples discussed in this Chapter. 11-bromoundecyl trichlorosilane (11-BUTS) was deposited from anhydrous toluene onto silicon

substrates treated in a UV-ozone chamber. This procedure yielded a uniform film of 11-BUTS with a thickness of 1.9 ± 0.1 nm and a static WCA of 83 ± 1.5°. The terminal bromine atom served as a site for attachment of DMAEMA via quaternization reaction, which was carried out in acetonitrile at 40 °C overnight. The resulting surface-grafted monomer (SGM) layer had a thickness of 2.7 ± 0.1 nm and a WCA of 50 ± 1°. The polymerization conditions for the DMAEMA-modified BUTS samples (DMAEMA/11-BUTS) were chosen to illustrate the role of initial FRP parameter values on the final properties of the film. To this end, a series of solutions varying in volume fraction of monomer to solvent as 0, 0.1, 0.25 and 0.5 with approximately constant total volume (20 mL) were prepared with a constant amount of initiator (recrystallized AIBN, 226 mg). These parameters give initial molar ratios of monomer to initiator ([M]/[I]) of 0, 4, 10 and 20, respectively.

Two sets of samples were prepared, but each one has an issue with the experimental method that precludes quantitative assessment of the results. In the case of the first set of samples (sample set 1), the AIBN initiator was not purified by recrystallization, bringing into the question the actual concentration of initiator. The second set of samples (sample set 2) used recrystallized initiator, but due to the effect of acceleration in the hood air flow rate as a result of a reduced sash height, the samples experienced an unknown temperature profile. Specifically, upon removal of the samples at 24 hours, the oil bath had a temperature of 36^{o} C. The cause of this unexpectedly low temperature was investigated using the same hot plate and thermocouple to measure the temperature of a "thermostated" oil bath with the hood sash open to its normal height (18") and closed to approximately 6". At 18", the oil bath maintained the expected temperature. Upon closing the sash, the temperature began to increase at an increasing rate. The experiment was stopped when the temperature appeared to runaway above 100 °C. Therefore, the samples may have experienced extremes in temperature in both directions. The magnitude of these extremes is not known. Fortunately, both of these issues are systematic within each sample set, so only qualitative conclusions can be reached. Furthermore, the resulting samples are still "correct" as far as the behavior of the films is concerned; their actual mechanism of creation simply remains obscured.

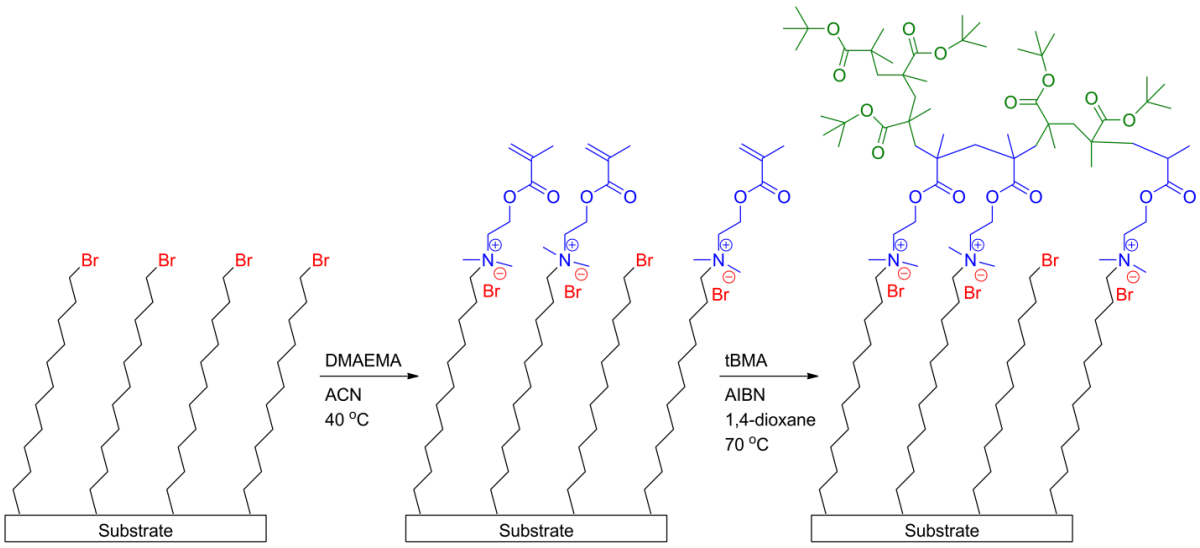

Figure 6.1. Synthesis scheme for grafting-through polymerization using 11-BUTS (black and red molecules), DMAEMA (blue molecules) and tBMA (green molecules).

Looking at only sample set 2 (*i.e.*, the set using recrystallized AIBN), insight into the relationship between the bulk polymerization and surface grafted layer can be obtained by plotting the PtBMA film thickness as a function of the number average MW (M_n) of the bulk polymer, as is done on the left abscissa in **Figure 6.2** (red squares). Note that the film thickness with no free monomer in solution is not zero; the thickness measures 0.30 ± 0.15 nm. A similar value was observed for sample set 1 (0.38 ± 0.12 nm). For these samples, no polymerization can occur, except possibly in-plane polymerization of the SGMs[15]. The observed increase in thickness originates from incorporation of decomposed AIBN moieties into the film by addition to the vinyl bond. While temperature may influence the kinetics of this incorporation, it will not influence the thickness of the final product. Given the comparable thickness increase for the initiator-only samples and the length of the reaction time, it is plausible that the extents of reaction of the initiator-only samples are comparable.

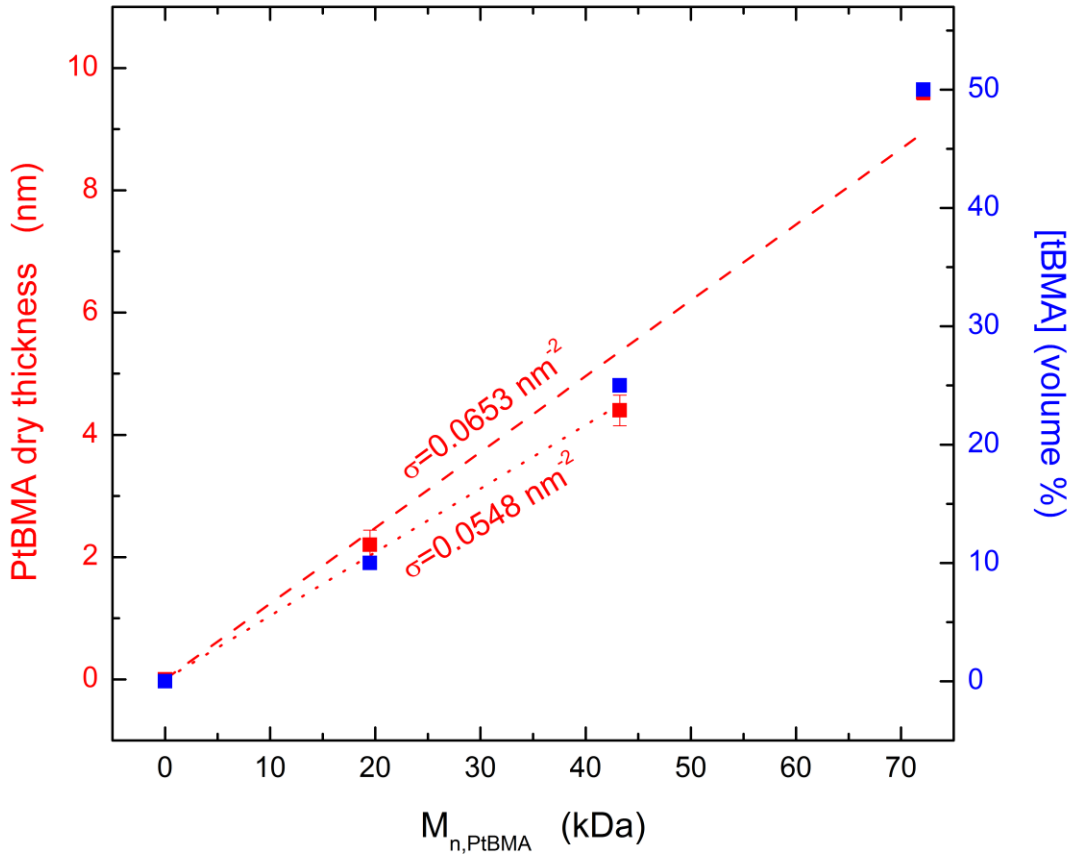

Figure 6.2. The left abscissa shows the relationship between PtBMA film thickness produced by grafting through SGMs (red squares) and M_n of bulk PtBMA recovered from the polymerization solution. The right abscissa shows the correlation between volume % of tBMA monomer in the polymerization solution (blue squares) and M_n of bulk PtBMA recovered from the polymerization solution.

For samples exposed to free monomer, the film thickness increases with M_n. Furthermore, the right abscissa in **Figure 6.2** plots the volume concentration of tBMA ([tBMA]) in the polymerization solutions (blue squares). There is a direct correlation between M_n and [tBMA] that mimics the correlation between PtBMA film thickness and M_n. Thus, we conclude the thickness of the grafted film increases due to an increase in the MW of the grafted polymer chains.

From a mass balance of the film, it is possible to calculate σ of the PtBMA film using the equation:

$$\sigma = \frac{h * \rho * N_A}{M_n} \quad (6.1)$$

where *h* is the film thickness, ρ is the density of the film and N_A is Avogadro's number. The slope of a line fit through the PtBMA film thickness in **Figure 6.2** provides an average σ of the samples. Fitting a line through all the data points reveals a deviation from the linear trend at the highest M_n. For this reason, a similar analysis is applied to the data excluding this highest M_n value. These slopes suggest an average σ of ≈0.065 nm^{-2} and ≈0.055 nm^{-2}, respectively. Care must be taken in interpreting these values and comparing them to systems created by typical "grafting from" and "grafting to" techniques, since in-plane polymerization can occur[15,16]. Nonetheless, these values are much lower than those associated with "grafting from" (0.45 nm^{-2})[9]. This same balance can be applied to the 11-BUTS and DMAEMA/11-BUTS layers and the sample exposed to only AIBN. The results of this calculation, along with values used in the calculation, are listed in **Table 6.1**.

Table 6.1: Physical properties of the SGM and PtBMA grafted films

Sample Name	Thickness (nm)	M_n (g/mol)	ρ (g/cm^3)	σ (nm^{-2})
11-BUTS	1.9 ± 0.09	311	1.26	4.67 ± 0.22
11-BUTS/DMAEMA[a]	0.8 ± 0.05	157	1.1	2.90 ± 0.75
0 % tBMA	0.3 ± 0.15	68[b]	1.1[c]	2.98 ± 1.48
10 % tBMA	2.2 ± 0.24	19505	0.875	≈0.065[d]
25 % tBMA	4.4 ± 0.25	43250	0.875	≈0.065[d]
50 % tBMA	9.6 ± 0.12	72120	0.875	≈0.065[d]

a) Values calculated for only DMAEMA moiety, not DMAEMA modified 11-BUTS molecule.
b) Corresponds to radical produced by AIBN decomposition.
c) Literature value for AIBN, assumed to apply to radical.
d) Value obtained from **Figure 6.2**.

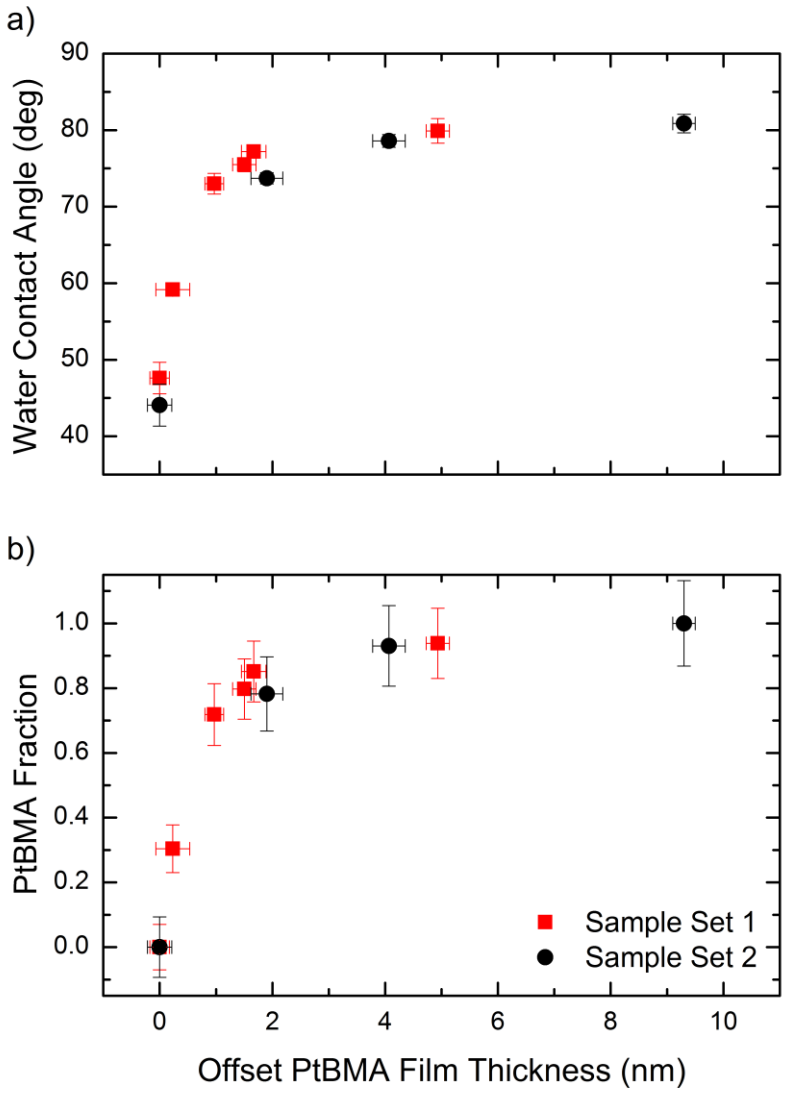

Figure 6.3. a) Dependence of water contact angle (WCA) on PtBMA film thickness for sample sets 1 (red squares) and 2 (black circles). The PtBMA film thickness has been offset by a constant factor for each sample set so that the initiator-only sample has a thickness of zero. b) Calculated Cassie-Baxter fraction of PtBMA from WCA in panel a. See **Equation 6.2** for calculation scheme.

The WCAs of the surfaces following polymerization for both sample sets are plotted against the PtBMA film thickness in **Figure 6.3a**, offset so that the film thickness is equal to zero for the

initiator-only sample. We can calculate the fraction of PtBMA and surface-bound DMAEMA+11-BUTS repeat units from the WCA values using the Cassie-Baxter model[17]:

$$\cos\theta_{obs} = f_{DMAEMA} * \cos\theta_{DMAEMA} + f_{PtBMA} * \cos\theta_{PtBMA} \quad (6.2)$$

where Θ_{obs} is the measured WCA, f_{DMAEMA} is the areal fraction of 11-BUTS/DMAEMA, Θ_{DMAEMA} is the WCA of 11-BUTS/DMAEMA, f_{PtBMA} is the areal fraction PtBMA, and Θ_{PtBMA} is the WCA of PtBMA. The results of this analysis are plotted in **Figure 6.3b** as the fraction of PtBMA against offset PtBMA film thickness. Despite the differences in sample preparation described above, the wetting behavior of the two sample sets is identical. As the PtBMA film thickness increases, the measured WCA increases from a minimum of ≈45° for the initiator-only sample to a maximum WCA of ≈81°. This maximum WCA is reached by a PtBMA thickness of ≈4 nm. Thus, above ≈4 nm of PtBMA film thickness, the water no longer feels the quaternized ammonium group below the polymer film, suggesting a dense film that completely covers the substrate.

AFM topography scans of sample set 2 provide insight into the structure of the film produced by the FRP of bulk monomer with the SGM film. There is a clear morphological change with increasing free monomer concentration in solution, as depicted in **Figure 6.4a-e**. The control sample (**Figure 6.4e**) suggests that some large aggregates may already be present on the surface following quaternization. However, it is not possible to tell at this time whether that is contamination, or unintended polymerization during the quaternization step. Careful inspection of the topography scans reveals the appearance of small features (*i.e.*, the *small* white dots) that increase in concentration and size as the tBMA bulk monomer concentration increases up to 25% tBMA. Between 25 and 50%, the surface structure appears to percolate, with the fine texture becoming a continuous phase. This percolation of the film is in line with the trend in WCA in **Figure 6.3b**, which suggests that above ≈ 3.5 nm the polymer/air interface consists of only PtBMA. A schematic of this explanation is shown in **Figure 6.4f**. The upper image depicts a hypothetical substrate with low MW chains grafted to its surface in such a way that it does not form a continuous film. The lower image is a hypothetical substrate with high MW chains grafted to its surface that can form a continuous film on the surface. To be clear, these illustrations are speculative and intended to suggest an explanation for the qualitative differences observed in the AFM micrographs and WCA measurement profiles.

The evolution of these fine features is revealed by the AFM height distributions shown in **Figure 6.5a**, where curves for 25% tBMA and below have tails skewed to higher thicknesses. With increasing free monomer concentration, the curves grow more symmetrical, culminating in an apparently symmetric curve for 25% and 50% tBMA. Along with increasing symmetry, the peak locations shift to higher values, as plotted on the left ordinate in **Figure 6.5b** as a function of PtBMA film thickness, with calculated RMS values on the right ordinate. The break in trend between PtBMA thickness and RMS, wherein the sample with 50 % tBMA becomes smoother, may support the notion that this structure more evenly covers the surface. As more of the surface is "filled in" by the polymer film due to a presumable increase in MW of the grafted chains, the AFM probe cannot access the space between the polymer "islands" seen in the more dilute samples. One caveat with AFM surface topography measurements of SGPAs in the dry state, such as the samples considered here, is that the chains are collapsed and are not necessarily in their solvated conformations.

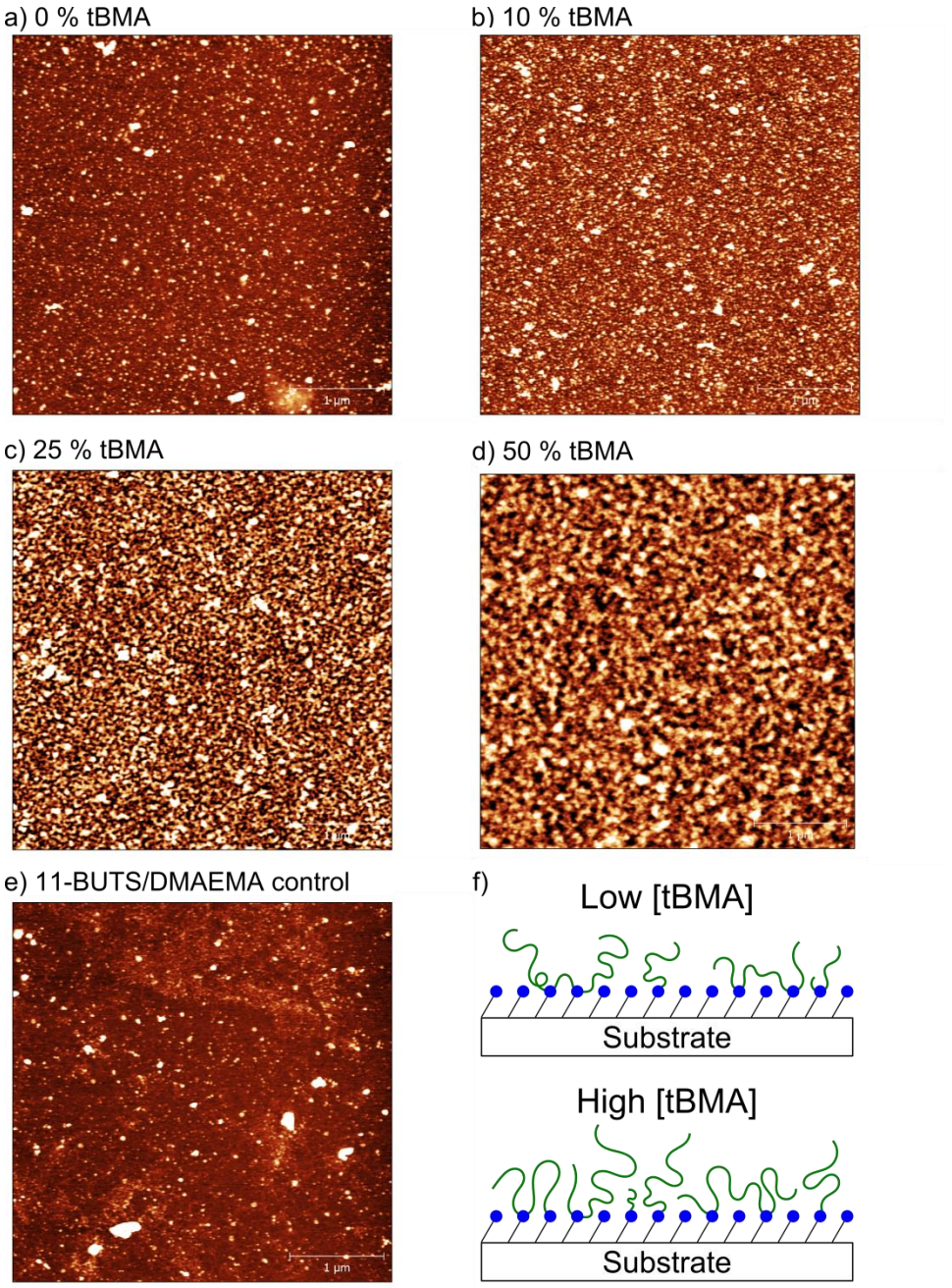

Figure 6.4. a-e) AFM topography micrographs of SGPAs produced by grafting-through SGMs by bulk tBMA monomer. Panel labels indicate concentration of tBMA in polymerization solution. All micrographs are 4 μm x 4 μm. The color scales cover identical ranges (6.0 nm), but over different absolute values (a, b, e = 0~6 nm; c = 2.5~8.5 nm; d = 5~11 nm). These values were chosen to emphasize surface morphology. Scale bars are 1 μm. f) Cartoon depicting possible structures of grafted-through SGPAs produced with a low concentration of free monomer (top) and high concentration of free monomer (bottom).

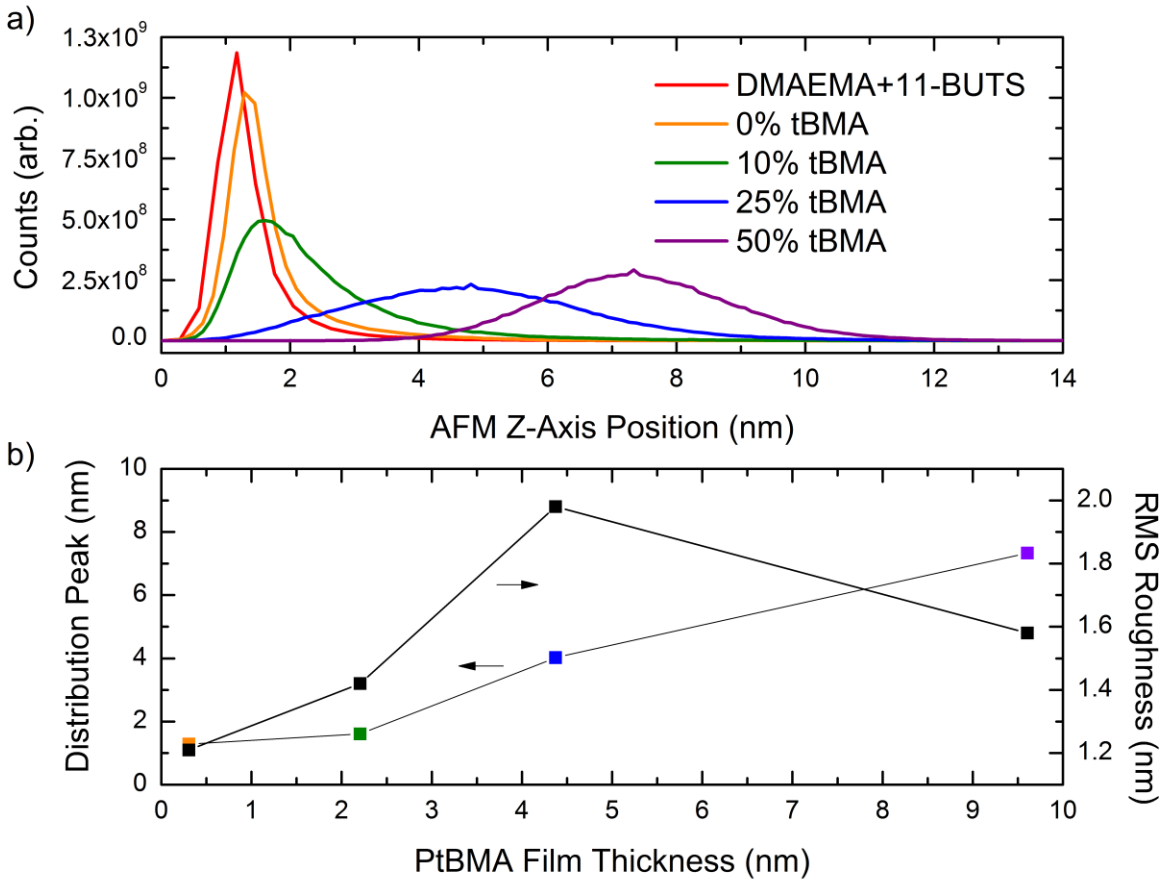

Figure 6.5. a) Distribution of z-axis positions for topography scans in **Figure 6.3a-e**. b) Left abscissa: Peaks of distributions in panel a plotted as a function of PtBMA film thickness. Colors match legend in panel (a). Right abscissa: RMS roughness calculated for topography scans in **Figure 6.4a-d**. Note that **Figure 6.4e** (11-BUTS/DMAEMA control) is not plotted.

6.3.2 Gradient Grafting-Through Samples

While AFM reveals a variation in topography with increasing free monomer concentration, it is not possible to distinguish to what extent σ and MW independently play a role in this topography. Samples expressing a gradient in σ of SGMs should, in theory, produce a gradient in chain grafting density. Since it appears the grafted chains originate in the bulk solution, as suggested by the strong dependence of the grafted film thickness bulk polymer M_n (*cf.* **Figure 6.2**), we can assume that the

MW distribution of the grafted chains is constant over the entire sample and is equal to that of the free polymer whose molecular weight we measure by SEC.

Samples with a gradient in σ of substrate-bound DMAEMA units were prepared by a previously described vapor deposition strategy[14], and backfilled with 11-BUTS in the same solutions as the homogeneous samples in sample set 2. **Figure 6.6a** and **6.6b** plot, respectively, the average ellipsometric thickness and water contact angle as a function of 11-BUTS fraction (determined by **Equation 6.2**) for the 11-BUTS (black data) and 11-BUTS/DMAEMA (red data) modified gradient substrates, as well as the AIBN only sample (0 % tBMA) following incubation. Note that the thickness data represents a cumulative total thickness of the entire organic film. The data for 11-BUTS and 11-BUTS/DMAEMA are averages of measurements over the entire substrate, which measured 4 cm wide by 6 cm long. This parent sample was then broken into four 1 cm wide samples for subsequent polymerization, including the 0 % tBMA sample. The data suggest the gradient is uniform over the entire substrate area, and the shape of the 11-BUTS/DMAEMA modified gradient mirrors that of the11-BUTS gradient.

As the concentration of11-BUTS increases relative to OTS (*i.e.*, increasing the fraction of 11-BUTS in the monolayer), the thicknesses of all three samples increase, as seen in **Figure 6.6a**. Lines have been fit to the four leftmost data points to guide the eye. While11-BUTS thickness does not follow a linear trend in this region, DMAEMA/11-BUTS and the 0 % tBMA sample show a linear thickness increase with11-BUTS fraction ($R^2 > 0.99$). All three samples show a break in trend near a 11-BUTS fraction of 0.95, at which point the thickness increases steeply. This trend change with increased11-BUTS fraction suggests the thicker films derive from better packing of the11-BUTS molecules grafted to the substrate. This better packing leads to more crowding of the moieties introduced in subsequent modifications (*i.e.*, DMAEMA and AIBN fragments), which then extend away from the substrate.

The water contact angles shown in **Figure 6.6b** move smoothly from a maximum in the OTS rich region to a minimum in the 11-BUTS rich regions, consistent with the surface chemistries present in the OTS-BUTS gradient. Modification with DMAEMA results in a decrease in WCA at all points measured in the gradient. While 11-BUTS/DMAEMA and 0 % tBMA have identical WCAs at the sparsest (leftmost) measurement point, 0 % tBMA exhibits a lower WCA over the rest of the gradient. A similar result was obtained for the homogeneous sample described above. Based on these data, the origin of this decrease in WCA does not appear to stem the incorporation of an AIBN-

generated radical into the film. If that were the case, the measurement at the sparsest region should have exhibited a similar decrease in WCA. The current data do not provide an unambiguous explanation for this observation. Chemical analysis of the samples using surface characterization techniques may provide further insight into this observation.

The thickness and σ of the three gradient samples polymerized with free tBMA monomer are plotted as a function of 11-BUTS fraction in **Figure 6.7a** and **6.7b**, respectively. The thickness of all three samples in **Figure 6.7a** increases with increasing11-BUTS fraction, reaching plateau values near the homogeneous samples described above. Assuming there is no significant variation in the MW distribution of grafted chains as a function of 11-BUTS fraction, the increase in thickness is due to an increase in σ. **Figure 6.7b** plots σ as a function of 11-BUTS fraction, calculated using **Equation 6.1**. The M_n values used in this calculation are obtained from the line fit to all of the data points in **Figure 6.2** (*i.e.* the line that produces σ = ≈0.065 chains/nm^2). Given the small number of data points for PtBMA polymerization, this approach was chosen to smooth potential scatter in the M_n measurement data. The σ values for 11-BUTS fractions > 0.8 cluster into the region obtained from **Figure 6.2** (≈0.055 to ≈0.065 chains/nm^2). As the 11-BUTS fraction decreases, the PtBMA σ decreases, consistent with the hypothesis that the bulk polymer chains polymerize through the SGMs. If the σ of SGMs decreases, then the σ of grafted chains should also decrease. There may be an influence of M_n on grafting density in the sparse 11-BUTS regions, wherein the sample polymerized in 50 % tBMA shows a higher σ than the other two samples. Insufficient data is currently available to prove or disprove this observation. A hypothesis built on this trend is presented in **Chapter 7** of this PhD Thesis, along with an experimental approach to test it.

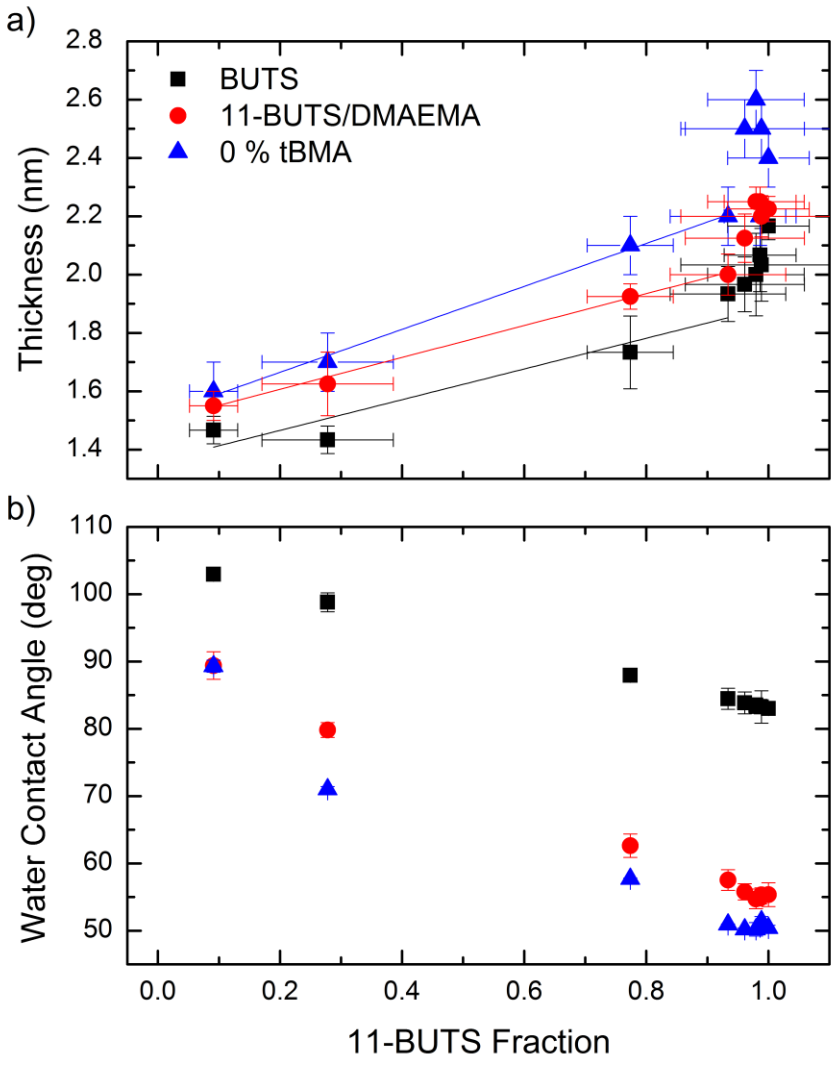

Figure 6.6. a) Thickness of grafted film following 11-BUTS deposition (black squares), DMAEMA quaternization (red circles) and exposure to AIBN (blue triangles) plotted as a function of 11-BUTS fraction on the surface as calculated by **Equation 6.2** for a sample expressing a gradient in 11-BUTS. b) Water contact angle (WCA) data measured after the same synthesis steps as in panel a.

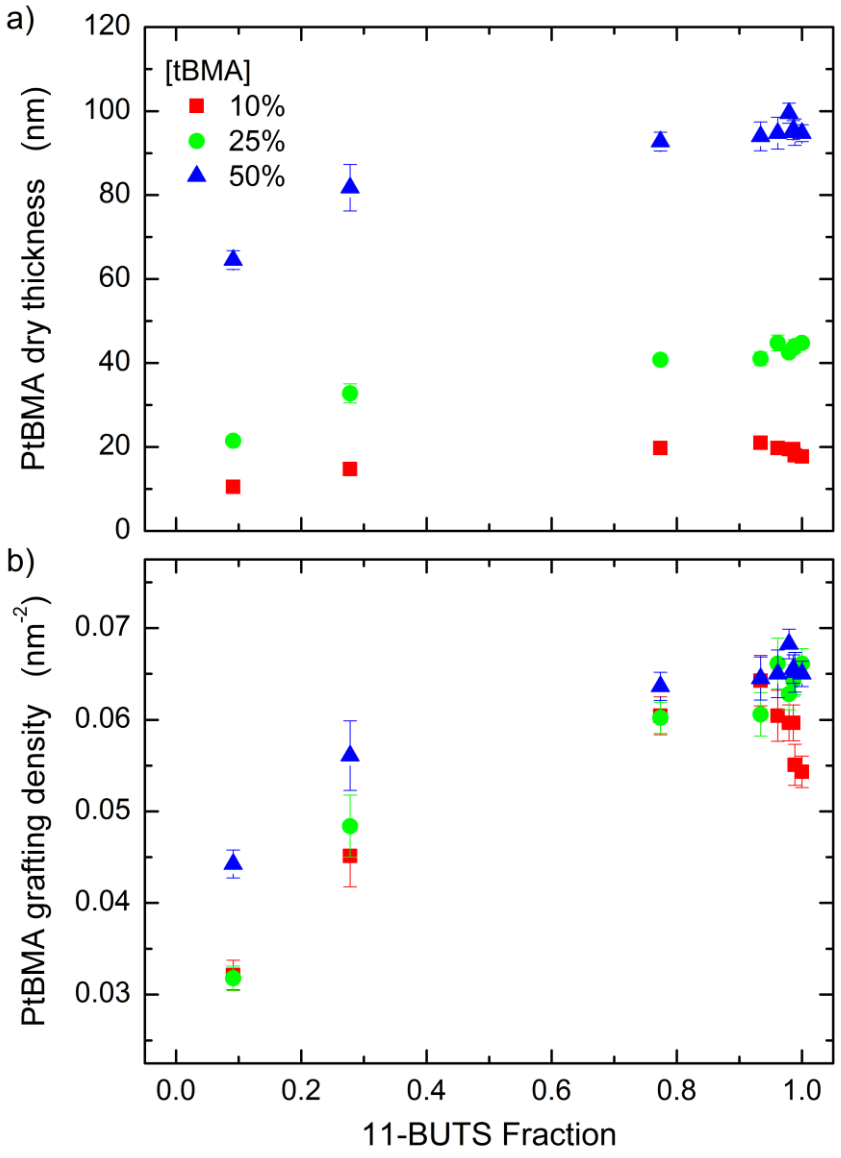

Figure 6.7. a) PtBMA grafted film thickness following polymerization in solutions containing 10 % (red squares), 25 % (green circles) and 50 % (blue triangles) tBMA monomer plotted as a function of 11-BUTS fraction on the surface as calculated by **Equation 6.2** for samples expressing a gradient in 11-BUTS. b) PtBMA grafting density (σ) for samples in panel a calculated using M_n values derived from **Figure 6.2** (see text).

AFM topography scans provide insight into the structure of the grafted films. Careful examination of the trends in **Figure 6.8** reveals a few important findings. First, for a given column (constant σ), a trend emerges that is similar to that seen in the homogeneous topography measurements. That is, fine features (the *small* white dots) develop and increase in apparent size and concentration, ultimately appearing to cover the sample for 50 % tBMA. Moving across the rows suggests two regimes. For samples with tBMA concentrations of 0 and 10 %, there is a maximum in prominence of these fine features at 1.0 cm, which is in the middle of the gradient. In contrast, the samples at 25 and 50 % do not show an intermediate maximum. In fact, the sample at 50 % looks essentially the same for all grafting densities. These trends support the suggestion that the grafted film fully covers the sample at the highest σ and tBMA polymerization concentrations.

Finally, the sample containing 0 % tBMA at the lowest grafting density shows a unique morphology not seen in the other samples. These "finger like" features cannot be caused by free monomer incorporated into the film, as there is none. While, on the one hand, the thickness increase seen for the homogeneous samples exposed to only AIBN suggests incorporation of the initiator into the film, it does not necessarily allow us to conclude in-plane polymerization. On the other hand, these features extend over a distance much longer than a single repeat unit. It is possible that these features result from areas enriched in DMAEMA/11-BUTS, perhaps due to segregation of 11-BUTS during deposition. While an implicit assumption that the OTS and 11-BUTS are homogeneously distributed on the surface is often made, there is no evidence that is actually the case. In fact, others have argued that segregation occurs[18].

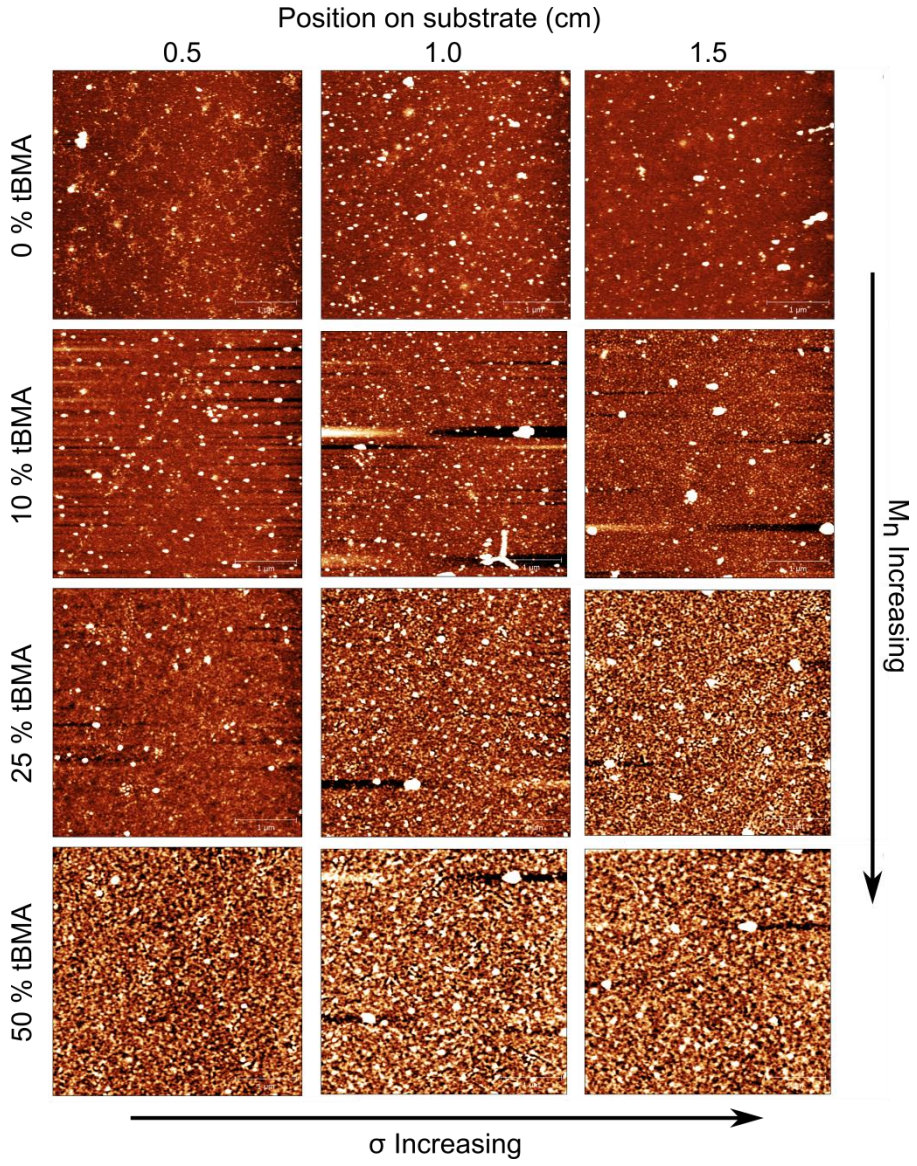

Figure 6.8. AFM topography micrographs of SGPAs produced by grafting-through SGMs by bulk tBMA monomer. Panel labels indicate concentration of tBMA in polymerization solution. All micrographs are 4 μm x 4 μm. The color scales cover identical ranges (6.0 nm; same as **Figure 6.4**), but over different absolute values (ranges similar to **Figure 6.4**). These values were chosen to emphasize surface morphology. Scale bars are 1 μm.

6.4 Conclusion

While "grafting to" and "grafting from" strategies to create SGPAs have been developed extensively over the past two decades, the "grafting through" approach described here offers an alternative. Each of these grafting strategies has benefits and drawbacks. In the case of "grafting through", all of the materials necessary can be purchased, and no complex or difficult organic synthesis is required to produce the SGM layer. While depositing directly a vinyl-bearing silane offers an even easier approach[13] than the two step method used with 11-BUTS and DMAEMA, the latter method offers increased customization of surface chemistry using a very simple chemical reaction (quaternization). By using FRP, the need to add catalysts or other chemical agents is avoided. This simplicity comes at the expense of less control over the grafted chain architecture (*e.g.*, impossible to create diblock copolymers) and grafted MW distribution. The precise mechanism of film formation remains ambiguous, in particular if and to what extent chains graft through multiple SGMs. The answer to that question holds implications for the structure of the grafted films. That structure, in turn, plays an important role in the interfacial properties expressed by the modified-substrate.

6.5 References

(1) McCaig, H. C.; Myers, E.; Lewis, N. S.; Roukes, M. L. *Nano Lett.* **2014**, *14*, 3728–3732.

(2) Jain, P.; Baker, G. L.; Bruening, M. L. *Annu. Rev. Anal. Chem.* **2009**, *2*, 387–408.

(3) Liu, X.; Chang, H.; Li, Y.; Huck, W. T. S.; Zheng, Z. *ACS Appl. Mater. Interfaces* **2010**, *2*, 529–535.

(4) Galvin, C. J.; Genzer, J. *Prog. Polym. Sci.* **2012**, *37*, 871–906.

(5) Matyjaszewski, K.; Miller, P. J.; Shukla, N.; Immaraporn, B.; Gelman, A.; Luokala, B. B.; Siclovan, T. M.; Kickelbick, G.; Vallant, T.; Hoffmann, H.; Pakula, T. *Macromolecules* **1999**, *32*, 8716–8724.

(6) Chiefari, J.; Chong, Y. K. (Bill); Ercole, F.; Krstina, J.; Jeffery, J.; Le, T. P. T.; Mayadunne, R. T. A.; Meijs, G. F.; Moad, C. L.; Moad, G.; Rizzardo, E.; Thang, S. H. *Macromolecules* **1998**, *31*, 5559–5562.

(7) Zhao, B.; Brittain, W. J. *Prog. Polym. Sci.* **2000**, *25*, 677–710.

(8) Barbey, R.; Lavanant, L.; Paripovic, D.; Schüwer, N.; Sugnaux, C.; Tugulu, S.; Klok, H.-A. *Chem. Rev.* **2009**, *109*, 5437–5527.

(9) Tomlinson, M. R.; Genzer, J. *Langmuir* **2005**, *21*, 11552–11555.

(10) Turgman-Cohen, S.; Genzer, J. *J. Am. Chem. Soc.* **2011**, *133*, 17567–17569.

(11) Prucker, O.; Rühe, J. *Macromolecules* **1998**, *31*, 592–601.

(12) Bain, E. D.; Dawes, K.; Evren, A. O.; Hu, X.; Gorman, C. B.; Jir, S.; Genzer, J. **2012**.

(13) Henze, M.; Mädge, D.; Prucker, O.; Rühe, J. *Macromolecules* **2014**, *47*, 2929–2937.

(14) Wu, T.; Efimenko, K.; Genzer, J. *J. Am. Chem. Soc.* **2002**, *124*, 9394–9395.

(15) Ford, J. F.; Vickers, T. J.; Mann, C. K.; Schlenoff, J. B. *Langmuir* **1996**, *12*, 1944–1946.

(16) Datta, P.; Genzer, J. *Macromolecules* **2013**, *46*, 2474–2484.

(17) Cassie, A.; Baxter, S. *Trans. Faraday Soc.* **1944**, 546–551.

(18) Aureau, D.; Ozanam, F.; Allongue, P.; Chazalviel, J.-N. *Langmuir* **2008**, *24*, 9440–9448.

7. Outlook

The work in this Ph.D. Thesis has considered the physical behavior of surface-grafted polymer assemblies (SGPAs) in three distinct ways. **Chapter 3** documented the role that grafting density (σ), charge density (α) and solution pH play in degrafting of polyelectrolyte SGPAs comprising poly(methacrylic acid) (PMAA) and poly(2-(dimethylamino)ethyl methacrylate) (PDMAEMA) in aqueous solutions. **Chapter 4** and **Chapter 5** considered how polyelectrolyte and polyzwitterionic SGPAs derived by post-polymerization modification (PPM) reactions from a common parent SGPA comprising PDMAEMA behave in aqueous and organic alcohol vapors. Finally, **Chapter 6** detailed a method to produce SGPAs from bulk polymerization reactions by grafting-through surface grafted monomers (SGMs) generated from quaternization of DMAEMA monomer to a halogen-terminated surface-grafted monolayer.

While the results of the experiments sufficed to generate a PhD thesis, the advantage of hindsight offers certain improvements in methodology and experimental setup for further investigations based on these results. Furthermore, this work has generated additional lines of inquiry that may be of interest to other researchers in the field of polymer science, in particular succeeding members of the Genzer group. These suggestions and directions are laid out in the following sections, arranged by the general topics of (i) degrafting, (ii) vapor swelling and (iii) grafting-through polymerization.

7.1 Future Work for Polymer Brush Degrafting

The stability in aqueous solutions of SGPAs comprising weak polyelectrolytes was detailed as a function of solution pH, polymer chemistry (*i.e.*, polyacid or polybase) and chain grafting density (σ). The results of these experiments substantiated the proposed degrafting mechanism, in which chain extension by electrostatic repulsion or excluded volume generates tension along the chain backbone that focuses at the grafting point. This tension activates mechanically one of two functional groups—the siloxane bonds at the polymer/substrate interface or the ester group in the surface-grafted initiator—for hydrolysis by hydroxyl ions in solution.

The experiments in **Chapter 3** illustrate the complexity of the systems involved—in particular the weak polybase, PDMAEMA. Initial versions of experiments with PDMAEMA used different buffering systems for each pH, including a zwitterionic buffer for pH 9 (CHES). As a result, the ionic strength of the buffering solutions was not identical. Given the role electrostatics plays in the degrafting mechanism, this parameter is an important degree of freedom to control. The experiments

presented in this Ph.D. Thesis used the same buffering agent, *i.e.*, sodium phosphate, for all the buffers. This choice eliminated a source of experimental variation and allowed a more direct comparison to prior work that used phosphate buffer saline (PBS) solutions titrated to different pH levels[1]. Even this method of standardizing buffer solutions presents an issue, since the relative population of valent states of the phosphate anion changes with pH. At low pH levels, monovalent phosphate is more prevalent than divalent phosphate[2]. Divalent phosphate increases in prevalence with increasing pH. Since these phosphate ions incorporate into the PDMAEMA brush, their valency will influence swelling behavior, and thus the degrafting process. Therefore, choosing zwitterionic buffers may be a better choice, as the ionic strength of the solutions will not change as a result of changing the buffering system[3]. Alternatively, using titrated solutions that have no buffering agents can provide a benchmark for the influence that buffering agents have. One particularly revealing set of experiments would incubate PDMAEMA and PMAA samples in DI water and in buffered solutions of the same pH as the DI water (typically pH 5.5-6.0 due to dissolved CO_2).

This example of how controlling one experimental parameter (pH) can change another relevant experimental parameter (ionic strength) points to the need to consider carefully the experimental design used for these degrafting experiments. None of the parameters considered (*i.e.*, σ, α, pH) are truly independent of each other, and not carefully controlling each of them can influence degrafting in unknown ways. While brush thickness is the most accessible parameter for monitoring degrafting and can be determined accurately with techniques such as ellipsometry, it suffers from ambiguities in terms of identifying molecular scale processes that drive degrafting. Both PDMAEMA and PMAA remain swollen after removing from the incubation solutions and drying, leading to normalization of the data by an arbitrarily chosen time point (*e.g.*, 24 hours incubation thickness). A shorter initial sample incubation time period in the buffer solutions should be used, since it is possible that degrafting processes have started after 24 hours of incubation. One method to choose the initial time period is to incubate a given sample until the *in situ* thickness has plateaued. This plateau is reached relatively quickly (typically within one hour). Once the *in situ* thickness plateaus, the *ex situ* thickness can be measured. These two thickness values provide a natural choice for normalizing thicknesses after subsequent incubation periods. Measuring both *in situ* swollen thickness and *ex situ* "dry" thickness for these subsequent incubation periods will produce additional information that can reinforce any conclusions reached from the data.

The effect of MW of the grafted chains has not been considered in these experiments. The tension exerted on the grafting point of the polymer chain scales with the degree of polymerization of macromolecular grafts[4]. As such, MW is expected to play an important role in the degrafting process. Since increasing MW will also increase brush thickness (for a constant σ), the barrier between the buffer solution and polymer/substrate interface will also increase. Thus, while more tension may be generated at the grafting point, the characteristics of the solution at the polymer/substrate interface may be significantly different from the bulk solution[5]. This ambiguity makes predicting the degrafting behavior as a function of thickness quite challenging. Furthermore, σ is known to influence degrafting, as well as thickness of the brush, further complicating data interpretation. Therefore, samples featuring orthogonal gradients in MW and σ are ideal for probing the interplay between these two parameters[6]. The comprehensive data sets produced by orthogonal gradients will eliminate ambiguity in reaching definite conclusions. Furthermore, these samples can serve a dual purpose for further investigation into the brush morphologies produced by various combinations of pH, σ and MW.

Finally, measuring the stability of a grafted film comprising a weak polybase that is soluble in water when charged, but insoluble in water when neutral, may provide a less ambiguous set of experiments than PDMAEMA. Conveniently, one such polymer species is poly(2-(diethylamino)ethyl methacrylate) (PDEAEMA), which is identical to PDMAEMA, except with two ethyl groups on the amino group instead of two methyl groups. This increase in alkyl chain length and the corresponding increase in hydrophobicity results in the polymer being insoluble when neutral (at high pH levels) and soluble when charged (at lower pH levels)[7]. An example of the effect of this change is seen in the vapor swelling results of PDMAEMA and PDEAEMA in Chapters 4 and 5. This difference in solubility compared to PDMAEMA, which is soluble whether neutral or charged, will magnify the interplay between hydroxyl concentration and electrostatic repulsion in the degrafting mechanism. Since the polymer will be increasingly non-soluble with increasing hydroxyl concentration, the presence of maximum degrafting at an intermediate pH will be easier to confirm. Combined with a σ gradient, PDEAEMA may also prove a good platform for investigating charge regulation. An additional system for such studies would comprise a copolymer brush featuring DMAEMA and a hydrophobic monomer, such as butyl methacrylate (BMA). In this case, the solvation of the grafted chains will be more sensitive to α of the DMAEMA units. Factors such as

copolymer sequence and architecture (*e.g.*, diblock vs. random copolymers) can be varied to induce physical behavior not accessible by homopolymers.

7.2 Future Work for Polymer Brush Vapor Swelling

Chapters 4 and 5 of this Ph.D. Thesis evaluated the impact of side-chain chemistry on the swelling of polymer brushes derived from PDMAEMA in aqueous and organic vapors. The presence or absence of counterions in charged systems (*i.e.*, quaternized or betainized), the hydrophobicity of the side-chain chemistry, and the solvent chemistry led to significant variations in the swelling behavior.

One component not considered in the studies presented in this Ph.D. Thesis is the nature of the counterion. The influence of counterions in the water contact angle (WCA) of polyelectrolyte brushes[8] and swelling of polyelectrolytes gels[9] is well known. Those observations are based on liquid solvents, as opposed to solvent vapors. As documented by this Ph.D. Thesis, the swelling of polyelectrolyte systems by the vapor phase of a solvent can differ markedly from the liquid phase of the same solvent. One important difference with regard to counterions is that a liquid solvent will allow the counterions to dissociate from the polymer side chain. In contrast, dissociation does not appear to occur in non-condensed solvents[10,11]. Since dissociation of the counterions is responsible for the significant swelling exhibited by polyelectrolyte brushes and gels, the response to solvent vapors is likely to be somewhat "muted". Nonetheless, the vapors clearly interact with the counterions, as evidenced by the different responses of the quaternized PDMAEMA brushes to methanol and ethanol. Therefore, exchanging counterions within these brushes enable the ability to tune the interactions between the SGPA and solvent. A strategy of creating gradients in concentration of two counterions can also be used to create regions of varying hydrophilicity[12].

Copolymer brushes offer another avenue for experiments related to vapor phase swelling. In particular, generating brushes that combine hydrophilic and hydrophobic moieties, or anionic and cationic pendant groups in diblock and random copolymer architectures can provide important new insight into molecular interactions within the polymer brush. For example, copolymerizing DMAEMA and methyl methacrylate (MMA) monomers to create P(DMAEMA-co-MMA) copolymer brushes, then betainizing the DMAEMA units would provide an additional system to understand the formation of zwitterion complexes. By diluting with MMA monomers, the concentration of betaine moieties is reduced and may inhibit complex formation. Preventing complex formation will lead to a

more hydrophilic brush based on the work in **Chapter 4**. However, the presence of MMA moieties will reduce the swelling behavior since it is more hydrophobic than PDMAEMA. In a similar vein, copolymerizing DMAEMA and tBMA, followed by quaternization of DMAEMA and hydrolysis of the tBMA to MAA will create a brush with mixed charges. The behavior of the different permutations of this system (*e.g.*, neat or quaternized DMAEMA with tBMA or MAA) can provide insight into the extent of electrostatic interactions[13]. If interactions exist, then the brush will likely exhibit a higher degree of hydrophobicity, as in the polyzwitterion brush in **Chapter 4**.

Finally, vapor pressure offers a way to control the extension of the grafted chains. Subsequently modifying the grafted chains at various swelling factors using a gas phase reaction may result in a way to achieve different modification patterns in the direction normal to the substrate. This concept is based on the notion that the repeat units at the polymer/air interface will change as the brush swells. This idea is depicted schematically in **Figure 7.1**. When collapsed, it is possible that there is a higher likelihood that a repeat unit in the middle of the grafted chain will be at the polymer/air interface and the chain ends will be buried within the brush. As the brush swells, the chain ends will have a higher probability of being at the polymer/air interface and the repeat units in the middle of the chain will be less likely to be at that interface. A macroscopic example of this idea is the snake charmer coaxing the viper out of its basket.

If the vapor phase reactant sorbs into the brush from the polymer/air interface and diffuses toward the substrate, then partially modifying the polymer brush in these different states of swelling will result in different modification patterns in the brush. The choice of reactant will be critical in these experiments. One possibility is using an alkyl halide in the vapor phase (*cf.* **Chapter 5**) that possesses a relatively bulky alkyl chain, such as a hexyl chain. Characterizing the depth profile of these substrates will require rigorous experimental control. Unfortunately, candidates like XPS and TOF-SIMS require high vacuum conditions, which may lead to rearrangement of the functional groups in the SGPA to expose preferentially hydrophobic groups to the polymer/vacuum interface. Neutron reflectivity (NR) does not require high vacuum; high contrast of the modifying agent can be achieved by using a deuterated moiety. However, NR is not sensitive to gradual changes in scattering length density (SLD), which provides insight into the depth profile of deuterated species in the SGPA. One avenue to consider is variations of scanning probe techniques that use the probing tips as antennae for IR radiation[14].

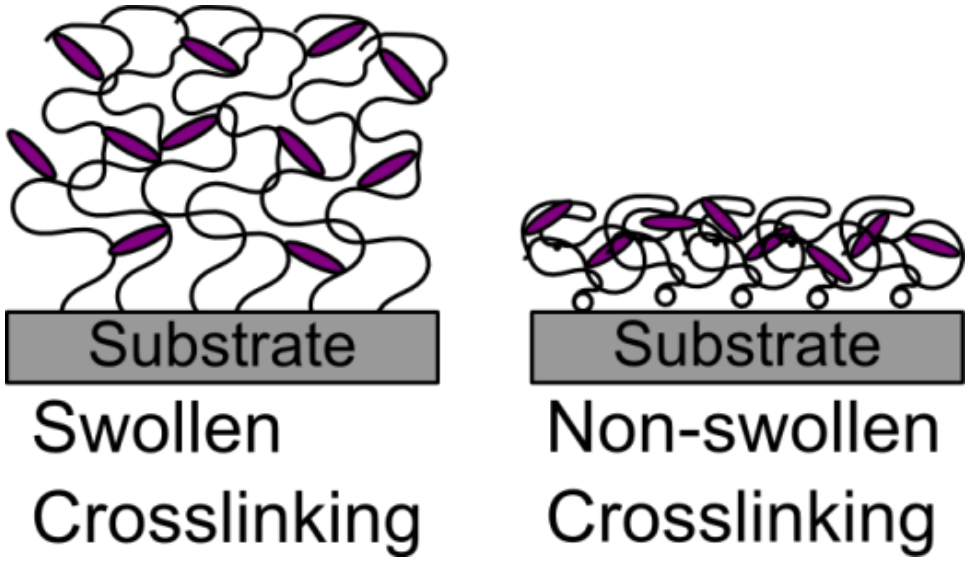

Figure 7.1. Cartoon depicting the different conformations of chains when swollen (left) and collapsed (right). Chemical modification in these different regimes (*e.g.*, crosslinking as shown) may produce different distributions of modifying agent within the brush.

A variation on this set of experiments is to use a modifying agent that can crosslink the polymer brush, such as a dihalide moiety. In this case, an additional constraint is imposed on the polymer brush since the crosslinked brush cannot deswell to their original conformation. This further confinement will likely modify how the brush responds to liquid and vapor environments, in particular the barrier properties of the brush. The mesh structure created by the crosslinking may exhibit some kind of sieving effect, and offer a way to tune both physical and chemical interactions between solvents and the brush.

7.3 Future Work for Grafting-through Polymerization

A variation on the grafting-through process described in **Chapter 6** is developing a system that does not result in a cationic charge. One possibility is to deposit an organosilane agent that bears a terminal group capable of undergoing polymerization. Alternatively, employing a post-deposition modification reaction offers additional versatility in the properties of the surface-grafted monomer (SGM). To that end, starting from the same 11-bromoundecyltrichlorosilane (11-BUTS) precursor offers several opportunities[15], including reaction of the halogen atom with functionalities such as

thiols, nitriles and alcohols. 11-BUTS can also access the popular 1,3-dipolar cyclo addition reactions (*i.e.*, "Click" reaction) by first replacing the bromine atom with an azide group, as suggested in **Figure 7.2**. This azide can then react with alkyne functionalities in efficient and controlled ways[16].

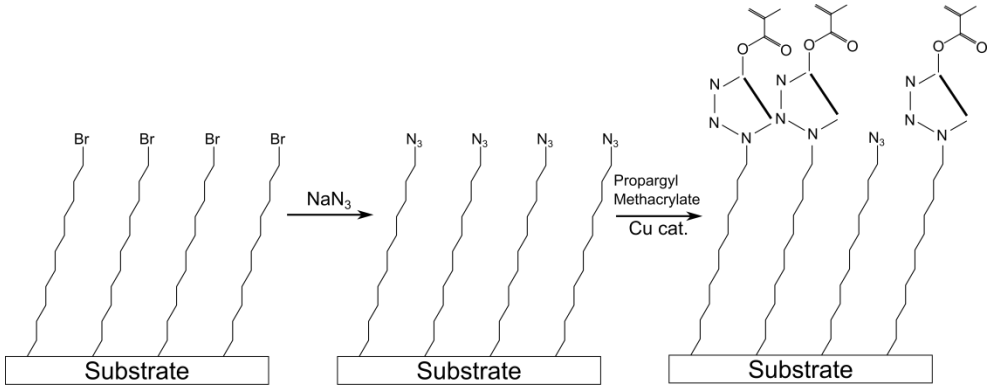

Figure 7.2. Scheme showing the creation of a neutral SGM layer using "Click" chemistry.

A hypothesis related to the mechanism of grafting-through polymerization emerged during the experiments in this Ph.D. Thesis that requires further testing for validation or rejection. Specifically, the grafted-through sample with the highest concentration of bulk monomer has both the highest number average MW (M_n) of bulk chains and highest σ of grafted chains. In this Ph.D. Thesis, we have taken the conservative route and assigned this finding to noise and a limited number of data points, leading us to "smooth" the M_n of bulk chains using an expected value based on data fitting. Even with this smoothing, the gradient samples showed a higher σ for the higher M_n of bulk chains compared to the two lower M_n values in the sparse regions of 11-BUTS on the surface (*cf.* **Figure 6.7** in **Chapter 6**).

If further experimentation reveals that this trend is in fact real, an alternative explanation is required since diffusion and mass balance argument suggest MW and σ of grafted chains are diametrically opposed. A caveat to that point are the different structures realizable in "grafted through" films that do not occur in "grafting from" and "grafting to" methods (*e.g.* loops and trains).

Nonetheless, one possibility is depicted in **Figure 7.3**, in which a growing polymer chain (in red) "polymerizes to" the surface by following a path (dashed line) of free monomer (red circles) to the substrate and subsequently polymerizing through a SGM. By using the addition of free monomer to advance toward to the substrate, the growing chain is able to penetrate through the chains already present at the interface. As a result, both MW and σ of the grafted chains can increase. This mode of reaching the substrate is in contrast to mass diffusion, which would be blocked by chains already present at the surface. The higher the MW, the less likely is the chain to diffuse through the film, and thus MW and σ will be diametrically opposed.

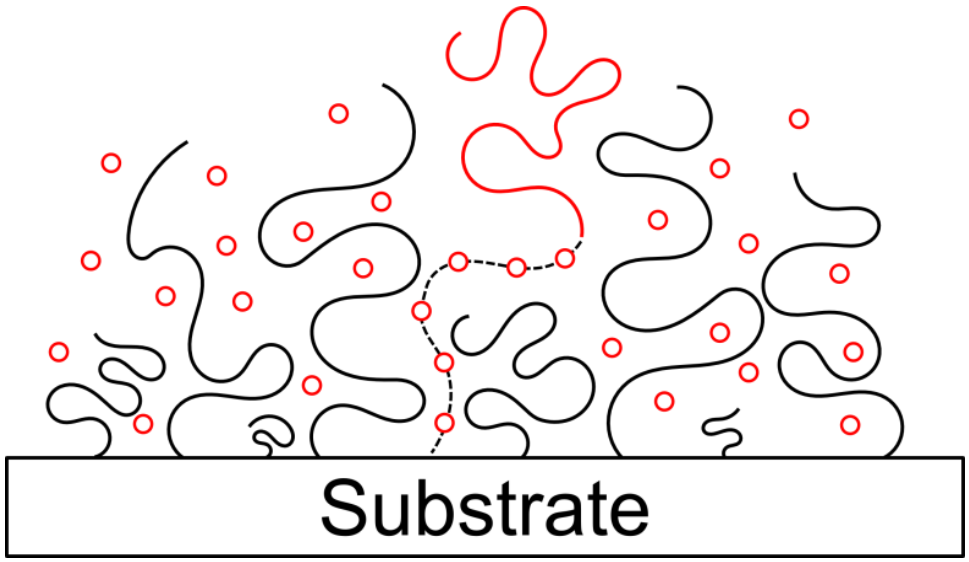

Figure 7.3. Cartoon depiction of a growing polymer (red chain) "polymerizing to" the surface through a grafted film (black chains) using free monomer (red circles).

One way to probe if the growing chains can "polymerize to" the substrate through a grafted polymer film, is to first create a substrate that is decorated with two chemically different silanes. The first organosilane is 11-BUTS, which will be used as in Chapter 6. The second organosilane bears a terminal group that can be reacted with a polymer chain end to create a "grafted to" film. Ideally, a continuous density gradient of these organosilanes can be made using vapor deposition techniques[17]. Alternatively, a series of samples made from solutions with varying concentrations of the two

organosilanes can be used. Creating a film by “grafting to” using an inert polymer, such as poly(methyl methacrylate) (PMMA), will lead to a model system for studying the possibility of “polymerizing to”. This film would comprise the black chains in **Figure 7.3**. Following modification of 11-BUTS with DMAEMA, the samples bearing the “grafted to” polymer film can then be incubated in bulk polymerization solutions with varying concentrations of free monomer (red circles).

The free monomer used in these polymerizations should be chemically different from the “grafted to” chains to generate distinct peaks in infrared spectroscopy (IR spectroscopy) and x-ray photoelectron spectroscopy (XPS). These techniques can then be used to confirm the presence and concentration of the “grafted through” polymer chains (red chain) relative to the “grafted to” polymer chains. Further characterization of thickness and WCA changes of the grafted film, along with MW of the bulk “grafting through” polymer, may provide evidence for or against the existence of “polymerizing to”.

A complementary question to whether “polymerizing to” the surface can happen relates to the kinetics of forming the grafted film. The experiments conducted in Chapter 6 were run for approximately 24. With only one time end point, there is no information on how the film thickness evolves over the duration of the bulk polymerization. Creating a series of “grafted through” samples derived from the same 11-BUTS parent that use the same polymerization conditions with different reactions times can provide insight into how quickly grafted chains populate the surface, and whether the thickness plateaus with polymerization time. Correlating the presence of a plateau thickness (versus a continuously increasing film thickness) with the concentration of free monomer can provide further insight into the “polymerizing to” phenomenon described above.

7.4 References

(1) Bain, E. D.; Dawes, K.; Evren, A. O.; Hu, X.; Gorman, C. B.; Jir, S.; Genzer, J. **2012**.

(2) Schrödter, K.; Bettermann, G.; Staffel, T.; Wahl, F.; Klein, T.; Hofmann, T. Phosphoric acid and phosphates. *Ullmann's Encyclopedia of Industrial Chemistry*, 2012, 679–724.

(3) Stellwagen, E.; Prantner, J. D.; Stellwagen, N. C. *Anal. Biochem.* **2008**, *373*, 407–409.

(4) Sheiko, S. S.; Panyukov, S.; Rubinstein, M. *Macromolecules* **2011**, *44*, 4520–4529.

(5) Wu, T.; Genzer, J.; Gong, P.; Szleifer, I.; Vlcek, P. In *Polymer Brushes*; Advincula, R. C., Ed.; Wiley-VCH Verlag GmbH, P. O. Box 10 11 61, Weinheim, D-69451, Germany,, 2004; pp. 287–315.

(6) Bhat, R. R.; Tomlinson, M. R.; Genzer, J. *J. Polym. Sci. Part B Polym. Phys.* **2005**, *43*, 3384–3394.

(7) Bütün, V.; Armes, S.; Billingham, N. *Polymer (Guildf).* **2001**, *42*, 5993–6008.

(8) Azzaroni, O.; Brown, A. A.; Huck, W. T. S. *Adv. Mater.* **2007**, *19*, 151–154.

(9) Ono, T.; Sugimoto, T.; Shinkai, S.; Sada, K. *Nat. Mater.* **2007**, *6*, 429–433.

(10) Galvin, C. J.; Dimitriou, M. D.; Satija, S. K.; Genzer, J. *Submitted* **2014**.

(11) Biesalski, M.; Rühe, J. *Langmuir* **2000**, *16*, 1943–1950.

(12) Paripovic, D.; Klok, H.-A. *ACS Appl. Mater. Interfaces* **2011**, *3*, 910–917.

(13) Jhon, Y. K.; Arifuzzaman, S.; Özçam, A. E.; Kiserow, D. J.; Genzer, J. *Langmuir* **2012**, *28*, 872–882.

(14) Dazzi, A.; Prater, C.; Hu, Q.; Chase, D.; Rabolt, J.; Marcott, C. *Appl. Spectrosc.* **2012**, *66*, 1365–1384.

(15) Carey, F. *Organic Chemistry*; 7th ed.; McGraw-Hill: New York, New York, USA, 2008.

(16) Kolb, H. C.; Finn, M. G.; Sharpless, K. B. *Angew. Chem. Int. Ed. Engl.* **2001**, *40*, 2004–2021.

(17) Wu, T.; Efimenko, K.; Genzer, J. *J. Am. Chem. Soc.* **2002**, *124*, 9394–9395.